THE STRUCTURE AND OPTICAL ACTIVITY OF TRIS COMPLEXES OF COBALT(III) WITH BIGUANIDE AND WITH 2,4-PENTANEDIONE

A THESIS

Presented to

The Faculty of the Division of Graduate Studies

by

Nadim Chamel Moucharafieh

In Partial Fulfillment

of the Requirements for the Degree

Doctor of Philosophy

in the School of Chemistry

Georgia Institute of Technology

December, 1976

THE STRUCTURE AND OPTICAL ACTIVITY OF TRIS COMPLEXES OF COBALT(III) WITH BIGUANIDE AND WITH 2,4-PENTANEDIONE

Approved:

Donald J. Royer, Chairman

J. Aaron Bertrand

H. R. Hunt, Jr.

Date approved by Chairman: 12/10/76

ACKNOWLEDGMENTS

The author wishes to express his gratitude to the director of this research, Dr. Donald J. Royer, for his guidance, friendship and patience throughout the course of this work. The author wishes to thank the members of the reading committee, Dr. J. Aaron Bertrand and Dr. H. R. Hunt, Jr., for their patience and their helpful suggestions in the preparation of the manuscript for this thesis. Many thanks are due to Dr. P. G. Eller for his help during the crystallographic investigation.

The directors of the School of Chemistry, Dr. W. M. Spicer and Dr. J. A. Bertrand are gratefully thanked for providing a teaching assistanship during the course of this work.

The help of the personnel at the Rich Electronic Computer Center, throughout the lengthy computational work for this project, is gratefully acknowledged.

Mr. Don Lillie, of the glass blowing laboratory, and Mr. Ken Williams, of the machine shop, are duly thanked for their help in the construction of special equipment needed in the course of this work.

TABLE OF CONTENTS

Page

ACKNOWLEDGMENTS ii

LIST OF TABLES v

LIST OF ILLUSTRATIONS vii

SUMMARY xi

Chapter

I. INTRODUCTION 1

II. THEORY 6

Determination of Absolute Configuration
Theoretical Models of Optical Activity

III. EXPERIMENTAL 23

List of Chemicals
Solvents
Preparations and Resolution of Optical Isomers
Biguanide Sulfate
Tris-(biguanidato)cobalt(III) Dihydrate
$(-)_{589}$ Tris-(biguanide)cobalt(III) Bromide Monohydrate
Tris-(2,4-pentanedionato)cobalt(III)
Structural Investigations
$(-)_{546}$ Tris-(2,4-pentanedionato)cobalt(III)
Racemic Tris-(biguanidato)cobalt(III) Dihydrate
$(-)_{589}$ Tris-(biguanide)cobalt(III) Bromide Monohydrate
Spectroscopic Experiments
General Description and Instrumentation
Single Crystal Spectra
Spectra of Powdered Samples in Pressed Salt Discs

IV. RESULTS 85

Structural Data
$(-)_{589}$ Tris-(biguanide)cobalt(III) Bromide Monohydrate

Page

Racemic Tris-(biguanidato)cobalt(III) Dihydrate
Solution Spectra
Absorption Spectra
Optical Rotary Dispersion Spectra
Circular Dichroism Spectra
Powder Spectra
Single Crystal Spectra
Circular Dichroism Spectra
Λ-$Co(C_2N_5H_7)_3Br_3 \cdot H_2O$
Δ-$Co(C_5H_7O_2)_3$
Racemic $Co(C_2N_5H_6)_3 \cdot 2H_2O$
Plane-Polarized Single Crystal Spectra
Λ-$Co(C_2N_5H_7)_3Br_3 \cdot H_2O$
Racemic $Co(C_2N_5H_6)_3 \cdot 2H_2O$
Racemic $Co(C_5H_7O_2)_3$

V. DISCUSSION 161

Structure of Λ-$Co(C_2N_5H_7)_3Br_3 \cdot H_2O$
Structure of $Co(C_2N_5H_6)_3 \cdot 2H_2O$
Correlation of Structures and Spectra

VI. CONCLUSIONS 198

REFERENCES 205

VITA 212

LIST OF TABLES

Table		Page
1.	Intensities for Bijvoet Pairs of Reflections .	12
2.	Final Positional Parameters for Racemic $Co(C_2N_5H_6)_3 \cdot 2H_2O$	47
3.	Final Anisotropic Thermal Parameters for Racemic $Co(C_2N_5H_6)_3 \cdot 2H_2O$	49
4.	List of Structure Factors for Racemic $Co(C_2N_5H_6)_3 \cdot 2H_2O$	50
5.	Final Positional Parameters for $\Lambda Co(C_2N_5H_7)_3 Br_3 \cdot H_2O$	66
6.	Final Anisotropic Thermal Parameters for $\Lambda Co(C_2N_5H_7)_3Br_3 \cdot H_2O$	68
7.	List of Structure Factors for $\Lambda Co(C_2N_5H_7)_3 Br_3 \cdot H_2O$	69
8.	Interatomic Distances for $\Lambda Co(C_2N_5H_7)_3 Br_3 \cdot H_2O$	88
9.	Interatomic Angles for $\Lambda Co(C_2N_5H_7)_3 Br_3 \cdot H_2O$	89
10.	Symmetry-Equivalent Positions for Space-Group $C222_1$	91
11.	Hydrogen Bonds and Short Contacts for $\Lambda Co(C_2N_5H_7)_3Br_3 \cdot H_2O$	92
12.	Equations of the L.S. Planes for the Chelates of $\Lambda Co(C_2N_5H_7)_3Br_3 \cdot H_2O$	93
13.	Values of Some Molecular Parameters for $\Lambda Co(C_2N_5H_7)_3Br_3 \cdot H_2O$	99
14.	Values of Some Molecular Parameters for Racemic $Co(C_2N_5H_6)_3 \cdot 2H_2O$	103
15.	Equations of the L.S. Planes for the Chelates of Racemic $Co(C_2N_5H_6)_3 \cdot 2H_2O$	104

Table		Page
16.	Symmetry Equivalent Positions for Space Group $P2_1/c$	105
17.	Interatomic Distances for Racemic $Co(C_2N_5H_6)_3 \cdot 2H_2O$	106
18.	Interatomic Angles for Racemic $Co(C_2N_5H_6)_3 \cdot 2H_2O$	107
19.	Hydrogen Bonds and Short Contacts for Racemic $Co(C_2N_5H_6)_3 \cdot 2H_2O$	109
20.	Data on Molar Absorbances for Solutions	111
21.	C.D. Spectral Data for Solutions	119
22.	Gaussian Components for Solution C.D. Spectra	120
23.	C.D. Spectra for Powders in KCℓ Discs	127
24.	Gaussian Components for Powder C.D. Spectra	128
25.	Plane-Polarized Single Crystal Spectra	160
26.	Distances and Angles for $\Lambda Co(C_2N_5H_7)_3Br_3 \cdot H_2O$ and $\Delta Co(C_2N_5H_7)_3Cl_3 \cdot H_2O$	161
27.	Some Values for C-N Bond Lengths	162
28.	Co-Distances From Some Ligand Planes	164
29.	Distances and Angles Between Chelate Atoms for $Co(C_2N_5H_6)_3 \cdot 2H_2O$ and $Cr(C_2N_5H_6)_3 \cdot H_2O$	166
30.	Structural Data for Complexes	172
31.	Spectral Data for Complexes	174
32.	Data for the π-Orbitals of the Biguanide Chelate	187
33.	Quadrupole Coupling Constants and Energy Separations for Solid Samples of Complexes	193

LIST OF ILLUSTRATIONS

Figure		Page
1.	Phase Angle Relationships for Two Optical Isomers	8
2.	Components of the Scattering Factor for Two Optical Isomers	8
3.	Molecular Three-Fold Axis	16
4.	Some Molecular Parameters for a Tris-Bidentate	16
5.	Crystals of $Co(C_5H_7O_2)_3$	37
6.	Crystal of $Co(C_2N_5H_6)_3 \cdot 2H_2O$	44
7.	Crystal of $(-)_{589}$ $Co(C_2N_5H_7)_3Br_3 \cdot H_2O$	61
8.	Diagram of Sample Holder for Single Crystal C.D. Spectra	80
9.	Diagram of Salt Press for Powdered Samples	82
10.	Atomic Labeling Scheme for $\Lambda Co(C_2N_5H_7)_3 Br_3 \cdot H_2O$	86
11.	Stereo View of One Molecule of $\Lambda Co(C_2N_5H_7)_3 Br_3 \cdot H_2O$	87
12.	Packing Diagram of Eight Molecules of $\Lambda Co(C_2N_5H_7)_3Br_3 \cdot H_2O$, in a Unit Cell	87
13.	Inclination of the Four Symmetry-Related Three-Fold Axes About the c-Axis Direction	96
14.	Traces of the Four Symmetry-Related Three-Fold Axes on a Plane Parallel to the a and b Axes Directions	96
15.	Illustration of Some Molecular Parameters for a Tris-Bidentate	97
16.	Illustration of Azimuthal Twist Angle for a Tris-Bidentate	97

Figure		Page
17.	Atomic Labeling Scheme for Racemic $Co(C_2N_5H_6)_3 \cdot 2H_2O$	101
18.	Stereo View of One Molecule of Racemic $Co(C_2N_5H_6)_3 \cdot 2H_2O$	102
19.	Packing Diagram of Four Molecules of Racemic $Co(C_2N_5H_6)_3 \cdot 2H_2O$, in a Unit Cell	102
20.	Molar Absorbance of $\Lambda Co(C_2N_5H_7)_3Br_3 \cdot H_2O$ in Water Solution	112
21.	Molar Absorbance of $Co(C_2N_5H_6)_3 \cdot 2H_2O$ in Water Solution	113
22.	Molar Absorbance of $Co(C_5H_7O_2)_3$ in Cyclohexane Solution	114
23.	O.R.D. Spectrum of $\Lambda Co(C_2N_5H_7)_3Br_3 \cdot H_2O$ in Water Solution	116
24.	O.R.D. Spectrum of $\Delta Co(C_5H_7O_2)_3$ in Cyclohexane Solution	117
25.	C.D. Spectrum and Gaussian Components of $\Lambda Co(C_2N_5H_7)_3Br_3 \cdot H_2O$ in Water Solution	122
26.	C.D. Spectrum and Gaussian Components of $\Delta Co(C_5H_7O_2)_3$ in Cyclohexane Solution	123
27.	C.D. Spectrum and Gaussian Component of $\Lambda Co(C_2N_5H_7)_3Br_3 \cdot H_2O$ in Methanol Solution	124
28.	C.D. Spectrum and Gaussian Component of $\Lambda Co(C_2N_5H_6)_3$ in Methanol Solution	125
29.	C.D. Spectrum and Gaussian Components of $\Lambda Co(C_2N_5H_7)_3Br_3 \cdot H_2O$ Powder in KCℓ Disc	129
30.	C.D. Spectrum and Gaussian Components of $\Lambda Co(C_2N_5H_6)_3$ Powder in KCℓ Disc	130
31.	C.D. Spectrum and Gaussian Components of $\Delta Co(C_5H_7O_2)_3$ Powder in KCℓ Disc	131
32.	Single-Crystal C.D. Spectra of $\Lambda Co(C_2N_5H_7)_3 \cdot Br_3 \cdot H_2O$	138

Figure		Page
33.	Resultant Single-Crystal C.D. Spectrum of $\Lambda Co(C_2N_5H_7)_3Br_3 \cdot H_2O$	139
34.	Single Crystal C.D. Spectra of Racemic $Co(C_2N_5H_6)_3 \cdot 2H_2O$	143
35.	Illustration of Light Polarized Parallel to the Direction of the c-Axis of $\Lambda Co(C_2N_5H_7)_3 Br_3 \cdot H_2O$	146
36.	Illustration of Light Polarized Perpendicular to the Direction of the c-Axis of $\Lambda Co(C_2N_5H_7)_3 Br_3 \cdot H_2O$	146
37.	Plane-Polarized Single-Crystal Spectra of $\Lambda Co(C_2N_5H_7)_3Br_3 \cdot H_2O$	151
38.	Inclination of the Two Symmetry-Related Three-Fold Axes From the Direction of the b-Axis for Racemic $Co(C_2N_5H_6)_3 \cdot 2H_2O$	153
39.	Trace of the Plane of the Three-Fold Axes on a Plane Parallel to the a and c Directions for Racemic $Co(C_2N_5H_6)_3 \cdot 2H_2O$	153
40.	Trace of the Planes ECO and SOT on a Plane Parallel to the a and c Directions for Racemic $Co(C_2N_5H_6)_3 \cdot 2H_2O$	154
41.	Illustration of Light Polarized Perpendicular to the Direction of the b-Axis for Spectra Through the (1, 0, 0) Face of Racemic $Co(C_2N_5H_6)_3 \cdot 2H_2O$	154
42.	Plane-Polarized Single-Crystal Spectra of Racemic $Co(C_2N_5H_6)_3 \cdot 2H_2O$	156
43.	Trace of the Plane of the Three-Fold Axes on a Plane Parallel to the a and c Direction for Racemic $Co(C_5H_7O_2)_3$	158
44.	Illustration of Light Polarized Perpendicular to the Direction of the b-Axis for Spectra Through the (1, 0, 0) Face of Racemic $Co(C_5H_7O_2)_3$	158
45.	Plane-Polarized Single-Crystal Spectra of Racemic $Co(C_5H_7O_2)_3$	159

Figure		Page
46.	Labeling of the Atoms of One Chelate	162
47.	Diagramatic Representation of Twist in Tris-Bidentates	167
48.	General Pattern of C.D. Spectra of Λ Tris-Bidentates with Saturated Chelates	181
49.	General Pattern of C.D. Spectra of Λ Tris-Bidentates with Unsaturated Chelates	183
50.	Coefficients of Atomic π-Orbitals in Highest Occupied Level of Biguanide	188
51.	Illustration of a Three-Chelate Ensemble in D3 Symmetry with Parities of Highest Occupied π-Orbitals	188
52.	Consequence of Interaction of Highest Filled Ligand π-Orbitals with Metal d-Orbitals . . .	189
53.	Chelating Agents That May Produce Complexes With Large Distortions from O_h Symmetry . . .	204

SUMMARY

This research was initiated for the purpose of investigating some tris-bidentate metal complexes with rigid chelate rings to better understand and correlate their structural parameters and optical activities.

The absolute configurations and the structural parameters of two Co (III) complexes with biguanide were obtained from crystallographic investigations.

Absorption spectra were measured for $\Lambda Co(C_2N_5H_7)_3Br_3 \cdot H_2O$, $Co(C_2N_5H_6)_3 \cdot 2H_2O$ and $Co(C_5H_7O_2)_3$, and were used in evaluating dipole strengths. C.D. spectra were measured for solutions of $\Lambda Co(C_2N_5H_7)_3Br_3 \cdot H_2O$, $\Delta Co(C_5H_7O_2)_3$ and $\Lambda Co(C_2N_5H_6)_3$. C.D. spectra were also measured for powdered samples of the above complexes, pressed into transparent KCℓ discs, and the data from these spectra were compared with the corresponding data for solutions. C.D. spectra were resolved into Gaussian components to reduce the mutual cancellation of the overlapping bands.

Elaborate single crystal spectra, C.D. and plane-polarized, were used to identify the various transition bands.

Broad line, ^{59}Co n.m.r. spectra were included for crystals of the three materials that were investigated, as evidence for ground state electronic distortions from

octahedral symmetry.

The spectral and structural data for $\Lambda Co(C_2N_5H_7)_3Br_3 \cdot H_2O$, $Co(C_2N_5H_6)_3$ and $Co(C_5H_7O_2)_3$ were compared with data for other available complexes with saturated and unsaturated chelates and no discernible trend was noted between geometric distortions and spectra. All complexes of Λ configuration and saturated chelates had a positive C.D. band at low energy and a negative C.D. band at higher energy, in the region of the $A_1 \rightarrow T_1$ octahedral transition. For complexes with Λ configuration and unsaturated chelate rings the order of transitions was reversed.

A dihedral angle, ψ, is defined to describe the "pitch" of the tris-bidentate, considering a tris-bidentate as a three-blade propeller. $\hat{\psi}$ is the only geometric parameter that correlates with the order of C.D. spectral bands for tris-bidentates with Λ configuration and saturated chelates. No geometric parameter correlates with the order of C.D. bands for the available complexes with unsaturated chelates. A qualitative explanation was offered for the order of the C.D. bands of the latter complexes and their optical activity was discussed in relation with the pertinent theoretical models.

The model of McCaffery and Mason postulates an interaction of metal $d \rightarrow d'$ spectra with the allowed U.V. ligand transitions. This idea is particularly feasible for complexes with unsaturated chelates.

Liehr's model offers the idea of orbital mismatch which is qualitatively in agreement with the estimated orbital orientations for the investigated complexes.

The Mason and Seal model attributes one source of optical activity to the configurational effect of screw dissymmetry in tris-bidentates. The complexes investigated in this thesis derive their optical activity, entirely, from the screw dissymmetry.

It was concluded that the only reliable medium for investigating C. D. spectra is the solid state. Single crystal spectra were seen as the only reliable means for identifying spectral transition bands.

The critical evaluation of the theoretical models of optical activity can not be done until the spectra of complexes spanning the entire range of structural and electronic distortions have been investigated. Some chelating agents were suggested that may produce complexes with such distortions.

CHAPTER I

INTRODUCTION

An optically active material is a substance that can rotate the plane of a linearly polarized light beam passing through it. The phenomenon of optical activity was first observed by Biot (1). Another property of optically active materials is called circular dichroism, C.D. In the region of light absorption for a particular material, the difference between the extinction coefficients for left and right circularly polarized light, $(\varepsilon_\ell - \varepsilon_r)$, gives rise to the circular dichroism spectrum.

There is a great abundance of naturally occurring optically active materials. Sugars, amino-acids and enzymes are well known examples. Werner (2) and Cotton (3) did pioneering works on optically active inorganic materials.

The ability of an optically active material to rotate the plane of linearly polarized light may be due to any one or more of three reasons. When a molecule belongs to a pure rotational symmetry point group such a molecule is dissymmetric and shows optical activity. In addition a crystalline substance may be optically active in the solid state*.

*Ramachandran and Ramaseshan (4) point out the relationships between point group symmetry and optical activity in the solid state. The eleven centrosymmetric point groups do not give rise to optical activity in the solid state. Of the remaining 21 acentric point groups six do not give rise to optical activity while fifteen point groups, some of which possess mirror symmetry, may give rise to optical activity in at least one direction in the solid state.

Examples of such materials are quartz, crystalline potassium chlorate and crystalline nickel sulfate, $NiSO_4 \cdot 6H_2O$ (5). Finally optical activity may be induced in a material by a magnetic field - the Faraday effect. The latter effect finds applications in magnetic circular dichroism, M.C.D. (6, 7). Many discussions of optical activity appear in the literature (5-11).

This investigation is concerned with the optical activity of some inorganic compounds that arises from molecular dissymmetry. The optical activity of Co(III) and Cr(III) complexes in the spectral region of $d \rightarrow d'$ absorption has been a subject of theoretical and experimental interest for some time. Experimental investigations have been concerned with the preparation of various complexes, resolution into optical isomers and the measurement of circular dichroism spectra. With the recent advances in x-ray crystallography the determination of absolute configurations and accurate structural parameters have also become standard procedure in the experimental investigation of optically active metal complexes.

Theoretical investigations of the above materials have been concerned with explaining the origins and magnitudes of their optical activity.

This thesis is concerned with the investigations of the structure and optical activity of some tris-bidentate metal complexes with rigid chelate rings. The chelate rings

in the tris-(biguanide)cobalt(III) ion: $Co(C_2N_5H_7)_3^{3+}$, tris-(biguanidato)cobalt(III): $Co(C_2N_5H_6)_3$ and tris-(2,4-pentanedionato)cobalt(III): $Co(C_5H_7O_2)_3$ contain doubly bonded atoms that secure their geometric structures and prevent them from changing conformation in solution.

The detailed structures of the biguanide complexes and their absolute configurations were determined by x-ray crystallography. Absorption spectra were determined for solutions and single crystals of the above materials whereas C.D. spectra were determined for solutions and for powdered samples pressed into transparent KCℓ discs. The bands corresponding to the various transitions were identified by C.D. and plane polarized single crystal spectra.

Because of the severe overlap and extensive mutual cancellation of bands the various C.D. spectra were resolved into Gaussian components for the individual bands corresponding to the various transitions. Gaussian resolution offers an improvement that aids in the estimation of band areas and positions of absorption maxima. Kuroda and Saito (12) have recently used a somewhat more rigorous technique for obtaining the band areas and peak positions of the various transitions for some metal complexes using single crystal C.D. spectra. Their complexes however, unlike those investigated in this work, have crystallographic three-fold symmetry and are thus ideally suited for single-crystal C.D. spectra. The feasibility of the Kuroda and

Saito technique, for metal complexes in general, is discussed later in this thesis.

The optical activity of tris-bidentate metal complexes has been attributed (11, 13, 14) to various geometric and electronic distortions from octahedral symmetry. To better understand the correlation between optical activity and structure, detailed data sets are presented for a large number of tris-bidentate complexes. Some results from broad-line Co^{59} n.m.r. are utilized to estimate the extent of electronic distortions from octahedral symmetry. A revised description is offered for geometric distortions from octahedral symmetry.

A clear difference is observed between the optical activity of complexes with saturated chelates reported earlier and those having π-bonds on their chelate rings reported here.

In the light of information available to date, transition metal complexes containing saturated chelate rings with Λ absolute configuration usually have similar C.D. spectra with a negative A_2 transition at high energy and a positive E_a transition at lower energy. Complexes with unsaturated chelates and Λ (lambda) absolute configuration also have negative A_2 and a positive E_a transitions. For the latter complexes however the E_a transition occurs at <u>higher</u> energy than the A_2.

The above observations are discussed qualitatively in

relationship to the various theories available. It is concluded that quantitative correlations with theoretical predictions are not possible at present.

Based on the results of this investigation, the relative intensities of the A_2 and E_a transitions of a particular complex are very sensitive to the nature of the solvent, and the ratio of areas under the A and E bands, (IA)/(IE), can be greater or less than unity depending on the medium. In view of this fact, one must refrain from drawing conclusions about the absolute configuration of a complex based on the sign of the net C.D. spectrum.

The only reliable medium for studying intensities is probably the solid state, either in single crystals or, with proper care, in powdered samples pressed into transparent salt (KCℓ) discs. In addition, the only reliable method of identifying the transitions of a C.D. spectrum is by single crystal spectra.

CHAPTER II

THEORY

Determination of Absolute Configuration

The structure factor, for a reflection (hkℓ), is a complex quantity that is expressed in the general case by

$$F(hk\ell) = \Sigma_j(f_j + \Delta f_j' + \Delta f_j'')\exp[2\pi i(hx_j + ky_j + \ell z_j)]$$

where the (f_j) are various terms used to describe the scattering factor of atom (j). From the general expression for F(hkℓ) the following relationships may be written for the structure factors of two reflections (hkℓ) and ($\bar{h}\bar{k}\bar{\ell}$) for two enantiomers*

$$F(hk\ell)(\Lambda) = F(\bar{h}\bar{k}\bar{\ell})(\Delta) \neq F(hk\ell)(\Delta) = F(\bar{h}\bar{k}\bar{\ell})(\Lambda)$$

The intensity, for a reflection (hkℓ) is defined as the product of the corresponding structure factor times its complex conjugate. The relationship between intensities will therefore be,

$$I(hk\ell)(\Lambda) = I(\bar{h}\bar{k}\bar{\ell})(\Delta) \neq I(hk\ell)(\Delta) = I(\bar{h}\bar{k}\bar{\ell})(\Lambda)$$

In the general case the scattering factor of an atom

---

*Two enantiomers have the coordinates of their corresponding atoms related by $x(\Delta) = -x(\Lambda)$, $y(\Delta) = -y(\Lambda)$, and $z(\Delta) = -z(\Lambda)$.

(j) is a complex quantity that is expressed by three terms, f_j, $\Delta f_j'$, and $\Delta f_j''$. Two special cases, that are of particular interest, will be presented below.

When the wavelength of the incident x-ray beam is far removed from the absorption edges of the elements in the crystal the terms $\Delta f_j'$ and $\Delta f_j''$ of the atomic scattering factors are negligible compared to the corresponding f_j. When this condition is encountered the intensities for two reflections $(hk\ell)$ and $(\bar{h}\bar{k}\bar{\ell})$, for a particular crystal, are equal

$$I(hk\ell) = I(\bar{h}\bar{k}\bar{\ell})$$

This is called Friedel's law. When Friedel's law holds the four intensities are equal,

$$I(hk\ell)(\Lambda) = I(\bar{h}\bar{k}\bar{\ell})(\Delta) = I(hk\ell)(\Delta) = I(\bar{h}\bar{k}\bar{\ell})(\Lambda)$$

The structure factors for reflections satisfying Friedal's law are illustrated in Figure 1. Under such conditions the absolute configuration of an optically active molecule can not be determined by x-ray crystallography.

When the wavelength of the incident x-rays is chosen such that it is slightly shorter than the absorption edge of some element, in a crystal having only rotational-translational symmetry, an anomalous dispersion of the x-rays results. For such cases the magnitudes of the $(\Delta f')$ and $(\Delta f'')$ terms of the scattering factors are not negligible

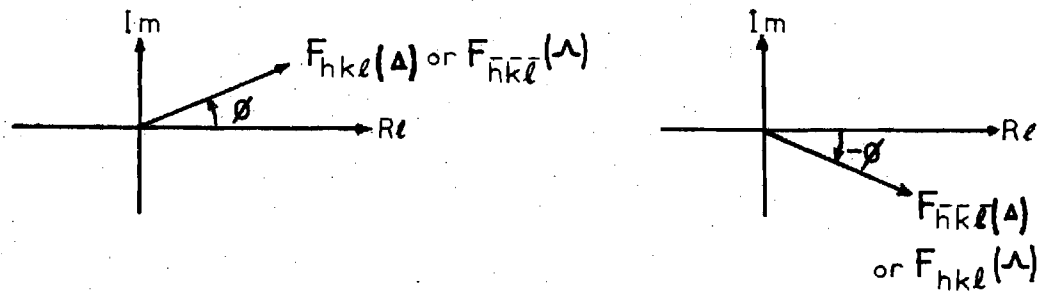

Figure 1. Phase Angle Relationship for Two Optical Isomers.

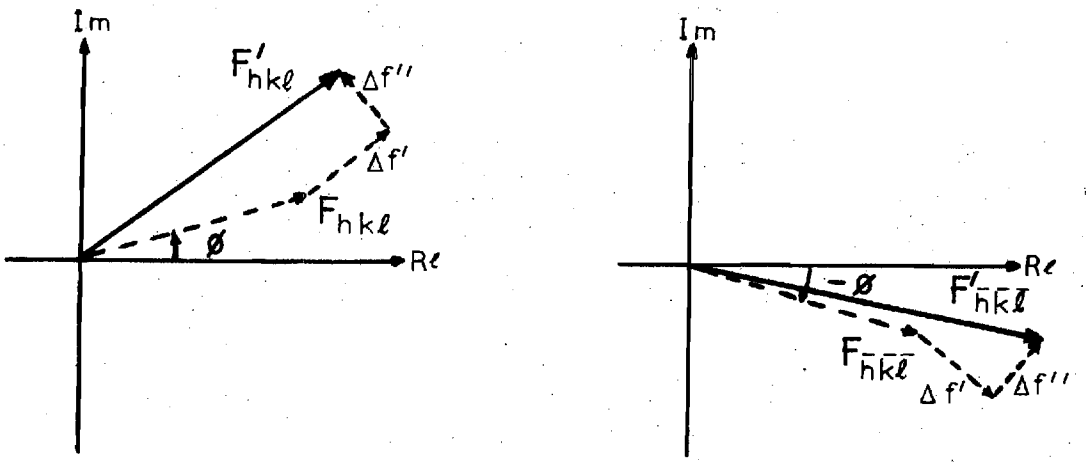

Figure 2. Components of the Scattering Factor for Two Optical Isomers.

compared to the corresponding (f) term. For a particular reflection (hkℓ) the phase of the ($\Delta f_j''$) term is always 90°, or $\pi/2$ radians, ahead of the phase of ($\Delta f_j'$). In Figure 2, $F'(\bar{h}\bar{k}\bar{\ell})$ and $F'(hk\ell)$ are the structure factors of two corresponding reflections which show the effects of anomalous dispersion. In the diagram the magnitudes of ($\Delta f_j'$) and ($\Delta f_j''$) have been slightly exaggerated to clarify the effect. Figure 2 illustrates the following consequences of anomalous dispersion,

$$|\phi' \; hk\ell \; (\Delta)| \neq |\phi' \; \bar{h}\bar{k}\bar{\ell} \; (\Delta)|$$

The angles ϕ and ϕ' are called phase angles.

$$|F' \; hk\ell \; (\Delta)| \neq |F' \; \bar{h}\bar{k}\bar{\ell} \; (\Delta)|$$

and therefore

$$I' \; hk\ell \; (\Delta) \neq I' \; \bar{h}\bar{k}\bar{\ell} \; (\Delta)$$

where the primed quantities indicate that they do incorporate the effects of anomalous dispersion. For the Λ enamtiomer similar relationships may be written. With reference to the four general expressions for intensities and structure factors,

$$\phi' \; hk\ell \; (\Lambda) = \phi' \; (\bar{h}\bar{k}\bar{\ell}) \; (\Delta)$$

$$F' \; hk\ell \; (\Lambda) = F' \; \bar{h}\bar{k}\bar{\ell} \; (\Delta)$$

and

$$I' \; hk\ell \; (\Lambda) = I' \; \bar{h}\bar{k}\bar{\ell} \; (\Delta)$$

Also Figure 1 and Figure 2 illustrate the fact that if

$$I' \; hk\ell \; (\Delta) > I' \; \bar{h}\bar{k}\bar{\ell} \; (\Delta)$$

then

$$I' \; hk\ell \; (\Lambda) < I' \; \bar{h}\bar{k}\bar{\ell} \; (\Lambda)$$

and vice versa.

Clearly when the effects of anomalous dispersion are significant Friedel's law is not obeyed. This fact is made use of in the determination of the absolute configuration of optically active substances by x-ray crystallography.

One method of determining the absolute configuration of an optically active substance by x-ray crystallography is outlined below.

The wavelength of the x-rays is chosen such that it is slightly shorter than the absorption edge of some element in the crystal. The ($\Delta f'$) and ($\Delta f''$) terms for that element will be significant compared to (f), as a consequence of anomalous dispersion. A data set is collected in the usual manner. The structure is solved and refined, assuming one absolute configuration, and the R-factor is noted. The absolute configuration is then reversed, by reversing the signs of the coordinates of all atoms, and the structure is

refined again noting the value of the R-factor. The true absolute configuration should give the better agreement between the observed and the calculated intensities and therefore the lower R-factor. Hamilton (15) has developed a statistical test to evaluate the significance of the choice of absolute configuration based on the differences of the R-values obtained for the two refinements.

Another method for the determination of absolute configuration is to collect accurately the intensities of a set of reflection pairs (hkℓ) and (-h, -k, -ℓ), for which the calculated intensities show maximum differences, along with the collection of the general intensity data. The structure is then solved and refined, assuming one absolute configuration, and the calculated and the measured intensities are noted for the pairs of reflections (h k ℓ) and ($\bar{h}$ $\bar{k}$ $\bar{\ell}$). The structure is refined again with the opposite absolute configuration, where the signs of x, y and z for all atoms are reversed, and the calculated and the measured intensities are noted for the pairs of reflections (h k ℓ) and ($\bar{h}$ $\bar{k}$ $\bar{\ell}$).

The results of the refinements with either enantiomer are compared with the intensities measured for the various pairs of reflections. Table 1 illustrates a set of data for a simple example. From the data in the table it may be deduced that the absolute configuration is Λ.

This was the method used by Bijvoet (16) et. al., to determine the absolute configuration of d-tartaric acid.

Table 1. Intensities for Bijvoet Pairs of Reflections

Reflection	Observed Intensities	Calculated Intensities ΛEnantiomer		ΔEnantiomer	
h k ℓ		$I_{hk\ell}$	$I_{\bar{h}\bar{k}\ell}$	$I_{hk\ell}$	$I_{\bar{h}\bar{k}\ell}$
6, 2, 3	$I_{hk\ell} > I_{\bar{h}\bar{k}\ell}$	301	290	290	301
1, 4, 5	$I_{hk\ell} > I_{\bar{h}\bar{k}\ell}$	98	89	89	98
2, 7, 8	$I_{hk\ell} < I_{\bar{h}\bar{k}\ell}$	99	111	111	99
9, 1, 4	$I_{hk\ell} \approx I_{\bar{h}\bar{k}\ell}$	42	43	43	42
4, 4, 7	$I_{hk\ell} > I_{\bar{h}\bar{k}\ell}$	547	510	510	547

The same method was used by Saito, Nakatsu, Shiro and Kuroya (17) in the first determination of an absolute configuration for an inorganic compound, $Co(en)^{3+}_3$.

Further methods for the determination of the absolute configuration of complexes are reported in a review by Saito (18).

Theoretical Models of Optical Activity

Metal complexes of tris-bidentate goemetry are dissymmetric. A substance having dissymmetric molecules of either configuration displays optical activity. A salient property of optically active compounds is that they have different extinction coefficients for left and right circularly polarized light in the region of their spectral absorption.

The circular dichroism, CD, is a measure of the above

mentioned quantity, $(\varepsilon_\ell - \varepsilon_r)$ for optically active compounds. The rotatory strength, R_{ba} for an optically active substance is the contribution to its optical rotation by an electronic transition from state (a) to state (b). The quantum mechanical expression for R_{ba} is given by Condon (13) as

$$R_{ba} = \mathrm{Im}\{(a|p|b) \cdot (b|m|a)\} \qquad (1)$$

where p and m represent the electric and magnetic dipole operators and the terms $(a|p|b)$ and $(b|m|a)$ are respectively the matrix elements connecting the states b and a of the molecule. Im, indicates the imaginary portion of the product of the two expressions.

In the following discussion, and throughout this thesis, spectral transitions like $A_1 \rightarrow A_2$ and $A_1 \rightarrow E$ have been referred to by their excited states, A_2 and E respectively. R_{ba} in Eq. 1 will be zero if the direct products of the electric and magnetic terms, a x p x b and b x m x a, belong to different irreducible representations in the symmetry group of the particular molecule. R_{ba} may be $\neq 0$ only if the symmetry group of the molecule contains, exclusively, proper rotations.

The d-d´ spectra of octahedral Co(III) complexes show two transitions, $A_{1g} \rightarrow T_{1g}$ at lower energy and $A_{1g} \rightarrow T_{2g}$ at higher energy. For trigonally distorted tris-bidentate molecules the triply degenerate levels, T, from the octaheral parent, split into A and E levels. The T_{1g} level splits into

A_2 and E_a while the T_{2g} level splits into A_1 and E_b. The $A_1 \rightarrow A_2$ transition is observed when incident light is polarized along the direction of the molecular three-fold axis, while the $A_1 \rightarrow E_a$ transition is observed when incident light is polarized in a plane perpendicular to the molecular threefold axis. The discussion that follows will be concerned with the low energy transition $A_{1g} \rightarrow T_{1g}$ of the octahedral "parent" molecule. Tris-bidentate molecules have D_3 or C_3 symmetry yet the six ligating atomsdeviate only slightly from octahedral positions, hence the practice of referring to them by the symmetry terms of the "parent" O_h compound.

The $A_{1g} \rightarrow T_{1g}$ transition is magnetically allowed but is electrically forbidden - (LaPorte forbidden) being a $d \rightarrow d'$ transition, i.e., $a \times p \times b = 0$ and $b \times m \times a \neq 0$.

In the absorption spectra of octahedral molecules the electric transition is assumed to couple with a vibration of odd parity and gives rise to the observed "vibronic" spectra. For the C.D. spectrum the vibronic mechanism is less favorable than for the absorption because coupling with a vibration of odd parity, while helping the electric transition, will render the magnetic transition forbidden.

So that the product in Eq. 1 may be different from zero some mechanism must be found that would "help" the electric transition while still keeping the magnetic transition allowed. The various theories discussed below address

themselves to this problem and to the numerical evaluation of rotatory strengths, R_{ba}. No detailed or comprehensive discussion of these theoretical models is intended here. However, the following treatment will attempt to state briefly the main assumptions and features of each theory and the results obtained therefrom.

The ionic model of Piper and Karipides (19) is an extension of the Moffit (14) treatment incorporating the Sugano (20) correction. In this model the ligating atoms are considered as point-charges or point-dipoles that form a static field of symmetry lower than O_h around the central metal ion. The odd parity needed to make the electric transition allowed is achieved by mixing metal 4p and 4f orbitals into the metal 3d orbitals.

Piper and Karipides allowed for trigonal splitting by small displacements of the ligating atoms from the octahedral positions around the metal. The geometric displacement of the ligands was inferred from the available crystallographic data. By allowing for trigonal distortions, i.e., polar and azimuthal distortions, the one electron rotational strengths obtained for the A_2 and E_a transitions are different from zero. The model gives a correct qualitative description for the A and E components of the C.D. spectrum for $Co(Ox)_3^{3-}$. The rotational strengths obtained are equal and opposite in sign, $R(A_2) = -R(E_a)$, and the predicted net rotation is thus zero, contrary to experimental observation.

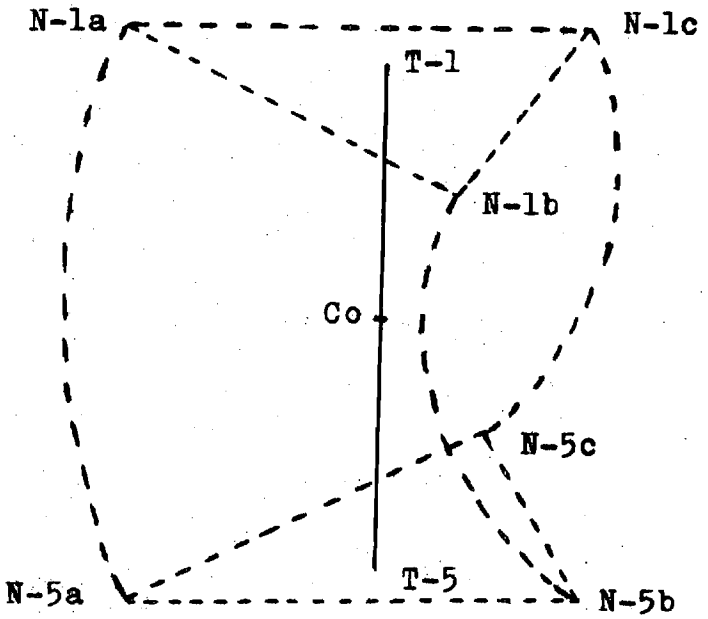

Figure 3. Molecular Three-Fold Axis.

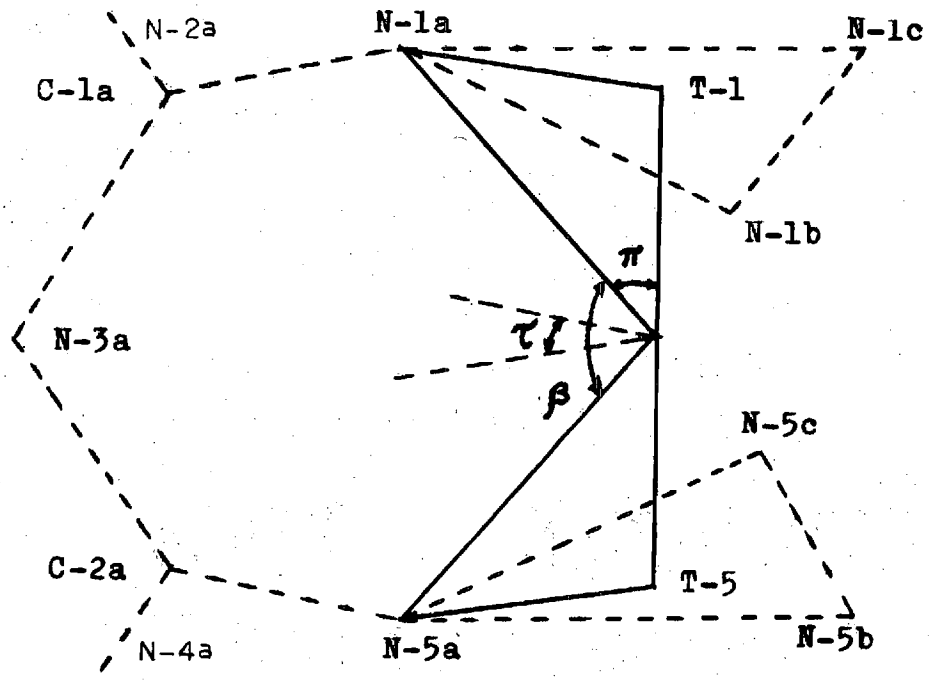

Figure 4. Some Molecular Parameters for a Tris-Bidentate.

The more elaborate molecular orbital model of Karipides and Piper (21) bears some resemblance to the previous ionic model. In this model a twist distortion, $|\hat{\tau}-60°|$, is responsible for rotatory strengths different from zero.

In this model, and in the previous ionic model, the optical activity is attributed solely to the configurational distortion or displacement of the ligating atoms from octahedral symmetry. The conformational effects of the other atoms in the chelate rings are ignored.

In this model the sign of the rotational strength does not depend on the absolute configuration but rather on the signs of the geometric distortions or displacements of the ligating atoms from the octahedral positions. Thus a Δ complex with an azimuthal expansion, $\hat{\tau} > 60°$ and a Λ complex with azimuthal contraction give rise to a positive A_2 and a negative E_a in the C.D. spectrum. For a polar elongation, $\hat{\pi} < 54.74°$, the energy of the E_a transition is predicted to be less than the energy for the A_2 transition. The strengths of the two spectral components are predicted to be equal and opposite in sign, $R(E_a) = -R(A_2)$, and like the ionic model no net rotation is predicted.

The molecular orbital model of Liehr (22) attributes the distortions form octahedral symmetry to a mismatch between the axes of the metal and ligand orbitals participating in the σ-bond. Such distortions may not be noticeable from the geometry of the molecule. The angle of orbital

mismatch, α, is decomposed into σ and π components in two dimensions and into σ, π, and $\tilde{\pi}$ in three dimensions. The σ component is along the straight line joining the nuclei of the two bonded atoms, Liehr's Figures 2, 4, 7, and 19.

Liehr's calculations are complex and lengthy. One expression will be given here to illustrate qualitatively the dependence of R, for the a → e transition, on the geometry of the molecule,

$$R[a_1(t_{2g}) \rightarrow e \pm (e_g)] = A \cdot \sin\alpha$$

where A is a product of constants and two factors for the ligand-metal mixture parameters and the electric dipole moment between the metal and the ligand.

Liehr's model attributes the optical activity of metal complexes solely to the orbital mismatch, between the ligating atoms and the metal, which is a configurational effect. The model does not allow for any contribution by chelate-ring conformation or chirality to the optical activity.

The sign of the rotational strength depends on the sign of the function ($\sin\alpha$). This function is positive for $\alpha > 0$ and negative for $\alpha < 0$. The rotational strength vanishes for $\alpha = 0$.

There seems to be a misrepresentation of the behavior of the function ($\sin\alpha$) in Liehr's discussion, footnote #64, p. 714, (22).

In the sample calculation given by Liehr, pp. 709-713, an initial assumption of $\alpha = 5°$ gave low results for the rotational strengths. The author concludes that for values of the mismatch angle, α, $\approx 15°$ the magnitudes of the rotational strengths obtained are of the order of magnitude observed.

Strickland and Richardson (23), in a recent work, have carried out additional calculations using the M.O. models of Karipides-Piper (21) and Liehr (22). They conclude that these models do provide correct approaches to qualitative predictions about optical activity.

The model of McCaffery and Mason (24) assumes that the electric dipole transition becomes allowed by interaction with the fully allowed transition bands in the U.V. They maintain that the mechanism of 3d - 4p and 3d - 4f mixing, to attain odd parity and render the electric dipole transition allowed, is energetically not favorable. An alternative, and energetically more feasible route, is to assume that the 3d transitions mix with the fully allowed charge transfer or ligand transitions occurring between 3000Å and 2000Å. The metal d-d´ transition of E symmetry couples with the E charge transfer or ligand transition while the A transition couples with an A.

The complex ion $\Lambda(+)$ 589 $Co(en)_3^{3+}$ had been unambiguously identified as having a positive E_a transition at lower energy and a negative A_2 transition at higher energy in the

d-d´ region. The McCaffery and Mason model predicts that a complex with a positive E transition in that region will have a Λ configuration.

The McCaffery and Mason model makes no distinction between the configurational and the conformational contributions to the optical activity.

The M.O. model of Karipides and Piper (21), utilizing the first order ligand field approximation, failed to give any net rotation. Richardson (25) carried the approximation to second order and did obtain a net rotation. The Richardson model assumes a static trigonal field perturbation of an essentailly octahedral ML_6 chromophore. The effects of ring size, substituents and ring puckering on the optical activity are examined. The net observed optical activity is assumed to arise from two simultaneous trigonal field perturbations, one of even parity and the other of odd parity. The effects of d - p mixing and d - f mixing are considered in detail.

Richardson's model, using the second degree perturbation, gave a net rotatory strength due to the conformational puckering of the chelate rings.

Richardson's model may be applied to the configurational as well as the conformational contribution to the optical activity. The author's treatment however is concerned, almost exclusively, with the conformational contribution.

The latest theoretical treatment of the subject is given by the model of Mason and Seal (26). This model retains the idea of the interaction (24) of d-d´ metal transitions with the fully allowed change transfer and ligand transitions in the U.V. The electric dipole moment for the octahedral ($A_{1g} \rightarrow T_{1g}$) transition is expressed, in the first order approximation, as the sum of two pairs of terms. The first two terms form the basis of the one-electron static crystal field theory. The remaining two terms represent the coulombic correlation of the transient electric dipole moment induced in the ligands by the charge distribution of the metal ion and these form the basis for the dynamic coupling model.

Calculations of the rotational strengths of $\Lambda Co(en)_3^{3+}$, for the $A_1 \rightarrow A_2$ and $A_1 \rightarrow E$, gave the same values for the conformational contribution as from conformational and configurational contributions combined.

No expression is given for the configurational contribution to the rotatory strength. However this configurational contribution, due to a screw-dissymmetry, is obtained by subtracting the conformational rotation from the total contribution. The configurational contribution for $Co(en)_3^{3+}$, according to this model, was found to be zero.

Mason and Seal extend their dynamic coupling calculation to the second order approximations and indicate that such extended calculations improve the agreement with experimental values. The calculations for the second order

approximation are even more complex and some of the approximations used lead to a loss of generality.

The effects of correlation with charge transfer and ligand transitions in the U. V. are discussed. The accuracy of the Mason-Seal calculations depends on the availability of accurate spectra in the far U.V. for the materials investigated.

The first order approximation in the above model accounts for the increase in the dipole strength observed when going from the $Co(NH_3)_6^{3+}$ of O_h symmetry to the $Co(en)_3^{3+}$ of D_3 symmetry.

CHAPTER III

EXPERIMENTAL

List of Chemicals

The following is a listing of chemicals utilized. Reagent grade quality was used except when otherwise stated.

Ammonium Chloride (laboratory grade)

Ammonium Hydroxide

Ammonium Sulfate (purified)

Barium Chloride Dihydrate

Barium Bromide Dihydrate (laboratory grade)

Calcium Oxide (technical powder)

Cobaltous Carbonate, Basic

Cobaltous Chloride Hexahydrate

Cuprous Sulfate Pentahydrate

Cyanoguanidine (M.P. 209-211°C)

Dimethyl Sulfoxide

Dimethyl Sulfoxide, d-6 (99.5%)

Heavy Water (99.5% D_2O)

Hydrochloric Acid

Lactose

2,4-Pentanedione (freshly distilled, B.P. 136-139°C)

Potassium Bromide

Potassium Chloride

Sodium Chloride (laboratory grade)

Sodium Bromide

Sodium Bromate

Sodium Iodide (laboratory grade)

Sodium Hydroxide (laboratory grade)

Selenous Acid

Hydrogen Peroxide, 30-volume %

Sulfuric Acid

d-Tartaric Acid

Solvents

The following solvents were utilized during this project. The quality of the material or the extent of purification is stated in each case.

Water. Local tap water is very low in solids and was used for preliminary synthetic work. Distilled, degassed and CO_2-free water was used for all qualitative and quantitative spectral work and for crystallization and purification.

n-Butanol. Reagent grade butanol was dehydrated by stirring with CaO and then distilled. (B.P. 116-117°C)

Diethyl Ether. The anhydrous material was used.

Methanol. The stock material was dehydrated by stirring with CaO, refluxing over Mg turnings and fractionation. (B.P. 64.0-64.1°C)

Benzene, Heptane and Toluene. These solvents were purified by distillation. Their boiling points were 80-81°C, 94-96°C and 113-114°C respectively.

Hexane. The stock material was stirred several times with water to remove a water soluble impurity. It was then dried over $CaCl_2$ and Na-metal and finally distilled. (B.P. 62-63°C)

Cyclohexane. The reagent grade material was used.

Preparations and Resolution of Optical Isomers

Biguanide Sulfate

Several batches of this material were prepared at various times. The procedure of Karipides and Fernelius (27) was followed except for the modifications given below. The following describes a typical preparation.

Cyanoguanidine (25.22g) was slowly fused with ammonium chloride (40.1g) in a 250 ml beaker. The temperature control of the reaction was very critical. The reaction vessel was heated in an oil bath placed on an electric hot plate. The temperatures of the oil bath and the reactants were separately monitored to prevent heating beyond 165°C. Overheating by about 10°C completely destroyed the product. After about 45 minutes of heating and stirring the powdered mixture fused to a jelly. The temperature of the reacting jelly was kept at 160 to 165°C for about 10 minutes, after which the heating was stopped. When the temperature of the solidifying mass dropped below 100°C, a 150 ml volume of boiling water was added and the instructions of Karipides and Fernelius (27) were followed without any further

modifications.

Tris-(biguanidato)cobalt(III) Dihydrate

The method of preparation used was reported by Ray and Dutt (28). Several batches of this material $Co(C_2N_5H_6)_3 . 2H_2O$ (F.Wt. 395.27) were prepared over a period of time. The procedure described below is a typical one.

A solution of cobaltous chloride hexahydrate (5 g in 25 ml water) was added to a strongly basic solution of biguanide sulfate dihydrate (20 g of the material) in a filter flask. The yellow suspension was stirred with a magnetic stirrer while the side arm of the filter flask was attached to an aspirator. A glass tube passed through the stopper on the flask and reached to the bottom. The stirring was started and the aspirator was turned on to let a continuous stream of air bubble through the reaction mixture. A few pellets of sodium hydroxide were added to the system every six to eight hours. The oxidation process was continued for 12 to 24 hours and was complete when the suspended material was bright red in color. The system was then taken apart and the flask with its contents were chilled in ice. The red material was filtered off and washed a few times with small quantitites of ice-cold water and dried in air. The finely divided product slowly loses its hydration upon long standing in air. It was stored in a stoppered flask, without further purification, for use in growing crystals and in preparing the optically active salt form of this (free base) complex.

Identification of the material was done by dehydration of weighed samples of large well formed crystals. Similar crystals were also used in obtaining plane polarized spectra. The large crystals were grown by recrystallizing from dilute (0.08 M) sodium hydroxide solution. A small sample of material was dissolved in the hot dilute base to give a saturated solution at about 50°C. The solution was then decanted to another container, further heated to about 70°C and filtered through a funnel containing a warm, wet filter paper. The filtrate was collected in a 50 ml beaker and this beaker was covered and placed in a large dewar flask half filled with hot water. The dewar flask was then covered and set aside for its contents to cool very slowly. In one or two days, large stable crystals of the material were formed. If the solution in the small beaker was rapidly cooled in air small crystals, suitable for crystallography, were obtained. If the material was crystallized from stronger base solutions (over 0.1 M) the resulting crystals were smaller, lost their water of hydration, turned opaque and developed cracks within a few days of standing in air. When weaker base solutions (under 0.05 M) were used for the recrystallization the product appeared different due probably to the formation of the $CO_3^{=}$ or HCO_3^{-} salt.

Quantitative determination of water was done by dehydration under vacuum. Samples of the well formed crystals were heated to about 150°C, with continuous vacuum

pumping, for 12 to 24 hours. The percentage loss in weight was 9.15(5)%*. The calculated weight percent of water is 9.115%.

Optically active samples of the above material were prepared from the active salt by deprotonation with a base in non-aqueous solvents. Three such methods were tried, by sodium methoxide in methanol, by calcium oxide in methanol and by calcium oxide in diemthyl sulfoxide. The method of calcium oxide in dimethyl sulfoxide, though the most tedious, seemed to give the best results. Enough sample of the optically active powdered salt (preparation and resolution in the next section) was dissolved in a few mls of dimethyl sulfoxide to form a saturated solution at room temperature, solubility is over 0.6 M. To the red-brown solution was added a three or four fold excess of fresh CaO or BaO and the mixture was stirred briskly for about 15 minutes. The excess solid was then completely removed by centrifugation and filtration. The resulting solution was dark red in color. This solution was then slowly added to twice its volume of n-butanol (freshly distilled, CO_2-free, anhydrous) with continuous stirring. A pasty dark red precipitate of the optically active free base complex was formed. The suspension was then cooled in ice and the liquids were decanted. The solid residue was thoroughly washed, several times,

*The quantity in parenthesis, after an experimental measurement, is the standard deviation.

with anhydrous ether to remove all traces of dimethyl sulfoxide and butanol, and the resulting dull red powder was stored in an evacuated dessicator. The finely powdered material, though always kept under vacuum, partially reverted to the salt (protonated) form after several openings of the dessicator. This was probably due to absorption of CO_2 and water through its large surface area.

$(-)_{589}$ Tris-(biguanide)cobalt(III) Bromide Monohydrate

The methods of preparation and resolution of optical isomers utilized were those described by Ray and Dutt (29). Because of the large amounts of the material needed, several batches were prepared and resolved. The procedure described here is for a typical preparation. A sample of the free base complex, $Co(C_2N_5H_6).2H_2O$, weighing 39.5 g was dissolved in enough water to make a saturated solution at 45-50°C. Fifteen g of d-tartaric acid and nine mls of conc. HCℓ (36%-37% by wt., density 1.17 g/mℓ) were dissolved in 250 mls of water. The acid solution was then slowly added to the red solution of the complex, while the mixture was continuously stirred. The resulting solution was then set aside and allowed to evaporate slowly to about one half of the original volume. The resulting crystals were of the less soluble chloride-d-tartrate diastereoisimer*. They were washed with small

*The less soluble chloride-d-tartrate diastereoisomer of the complex was the only one prepared. Only the first crop of crystals was collected. The mother liquor was then treated with sodium hydroxide and recycled into the racemic free base complex. This procedure ensured that only one optical isomer of the material was present.

portions of water and dissolved in enough water to make a saturated solution at 45-50°C. To this solution was added, dropwise, a saturated water solution of ammonium sulfate while the mixture was continuously being stirred. A fine yellow crystalline precipitate of the optically active sulfate salt slowly formed. A second crop of crystals was obtained by adding a slight excess of ammonium sulfate solution to the filtrate and chilling in ice. The product was washed twice with small portions of ice-cold water and dried in air.

The optically active bromide salt was prepared from the sulfate by treatment of the latter with barium bromide. Eleven grams of the sulfate complex, $[Co(C_2N_5H_7)_3]_2(SO_4)_3 \cdot 7H_2O$, were dissolved in enough water to make a saturated solution at 45-50°C. A solution of $BaBr_2 \cdot 2H_2O$ was prepared by dissolving 10 g of the solid in 100 ml of water, thus affording a small excess over the stoichiometric amount needed for preparing the bromide salt of the complex. The barium bromide solution was added slowly to the warm solution of the complex sulfate while the mixture was continuously being stirred. The reaction flask was then set aside for the insoluble barium sulfate to settle down as the solution cooled to room temperature. The precipitate was filtered off and the filtrate was placed in large evaporating dishes and allowed to evaporate in air. When all the solvent had evaporated, reddish brown crystals of the optically active bromide salt were left in the evaporating dishes. The

crystalline residue was redissolved in a minimum amount of water and the solution was filtered and left to crystallize by evaporation. By using a minimum amount of solvent, the less soluble racemic material was easily separated at the beginning of every recrystallization. The crop of crystals formed was removed, before the solution had completely dried, and recrystallized for a second time. The crystals formed were again removed before the solution had completely dried, washed twice with small portions of ice cold water and set to dry in air. By removing the crystals before the solvent was completely dry, excess barium salts, from the preparation stage, were left behind in solution.

Gravimetric analysis for bromide, by precipitation with silver nitrate, yielded 38.67(25)% by wt. bromine. The calculated percentages, by wt., of bromine are 38.665% and 39.822% for the monohydrate and the anhydrous materials respectively. The results of the gravimetric determination of bromide suggested that the material was a monohydrate. No loss in weight, however, resulted when a sample of the material was heated under vacuum at 150°C for 24 hours.

Good quality large crystals of the optically active bromide salt were prepared by allowing a concentrated water solution of the material to evaporate slowly at room temperature. Typical crystallizations ran from three days to a week, without any significant racemization. The large crystals obtained measured around 1 mm x 2 mm x 4 mm, and

selected samples from those were used for single crystal spectra of the material. Smaller crystals, suitable for x-ray structural studies, were grown by allowing a warm saturated solution of the material to cool in air. Essentially complete resolution was obtained. The molecular rotation of the material was found to be -4261° (546 mμ) and -2243° (589 mμ). The corresponding value for the chloride salt of the other enantiomer (30) was reported to be +2287° (589 mμ). The molecular rotation is defined as specific rotation x molecular weight/100.

Tris-(2,4-pentanedionato)cobalt(III)

The method of preparation utilized was reported by Bryant and Fernelius (31). The amounts used were twice those reported therein. The fine dark green crystals were separated by filtration through a buchner funnel, washed several times with small amounts of water and set to dry in air. No analysis or characterization were done on the sample of the dark green material and it was stored, without any further purification, for later use.

Large well formed single crystals of the racemic material were easily obtained by slow evaporation of a benzene or toluene solution. Such crystals were about 1 mm x 2 mm x 4 mm and selected samples of those were used for single crystal spectra.

The cobalt (III) complex with 2,4-pentanedione is water insoluble and electrically neutral. No simple method

of resolution, into optical isomers, is known for such compounds. The resolution was done by chromatography through a column packed with dried lactose. The eluting liquid was a mixture of benzene and hexane in the ratio of one to two by volume. This method is a modification of the procedure described by Collman (32) et. al., (33, 34).

A glass column 230 cm long and 5.2 cm in diameter was used. At the bottom it had a fritted glass disc retainer and a stopcock that was used to adjust the rate of eluant flow. A sample of about three kg of lactose was dried at 110°C for 48 hours, and was mixed with three liters of hexane to form a slurry. The slurry was frequently stirred as it was poured into the column. The stopcock at the bottom of the column was opened periodically during the filling process to allow the hexane to drain off. An electric vibrator was also set against the side of the column and switched on during the entire slurry addition. After about a week of vibration-packing and slurry readdition, the lactose level had settled to about 30 cm from the top, hence it was convenient to start using the column. Eluant level was kept at 15 cm over the lactose level when the column was not in use.

Samples of the racemic material weighing 0.3 g were found to be optimum for a single pass. The racemic samples were dissolved in five milliliters of benzene and added to the column after the eluant was drained to the level of the

packing. When the sample had soaked in, eluant was introduced at the top of the column through a glass syphon from a carboy. The carboy level was adjustable, and was set so that the eluant level over the packing stayed about 25 cm during the entire elution process.

A typical run lasted between 12 and 24 hours, with fractions being collected automatically in test tubes at eight minute intervals. The total number of test tubes per run was about 100 (with about 15 mls in each) of which the last 40 or 50 contained the green material. Absorbances and polarimetric rotations of the eluted samples were determined as a quick check to evaluate the efficiency of the resolution. The negatively rotating enantiomer (546 mμ) eluted first while the positively rotating isomer trailed. Maximum rotation readings were about ±100 millidegrees (@ 546 mμ) in a 5 cm cell while maximum absorbances were about 0.5 in a 1 cm cell, at the absorption peak about 593 mμ. Homorotatory samples were combined and stripped of their solvent in a rotatory evaporator.

A total of about 50 first passes were made through the column and the two partially resolved samples were accumulated. Those partially resolved samples were in turn passed through the column to enhance their optical activities. A special fractional crystallization was then used to separate the bulk of the racemic material from the above samples. These complexes were dissolved in minimal amounts of benzene

in small evaporating dishes. The evaporating dishes were then put inside large funnels that had their stems running into large test tubes immersed in ice in dewar flasks. When the large funnels were covered the solvent evaporated slowly inside the closed systems and condensed inside the ice-cold parts of the test tubes. Within 24 hours the evaporating dishes were dry and the material at the bottom was mainly the less soluble racemic hexagonal crystals. On the sides of the dishes the rough irregular crop of crystals was mainly the optically active part. A second such crystallization of the bottom samples separated the bulk of the racemic material. This simple method allowed the two materials, active and racemic, to crystallize separately in a fairly short time. Crystallization by solvent evaporation in a draft of air was too fast to give any separation while a slower rate of evaporation resulted in total racemization.

The final stage of resolution was done by fractional precipitation. The method used was a modification of the procedure of Fay, et al. (33). The optically active samples were dissolved in minimal amounts of benzene and two to five times those volumes of hexane were added to the benzene solutions. The mixtures were stirred, set aside for a few minutes and the racemic precipitates were filtered off. The filtrates were collected in small clean beakers which were then covered and put inside a large dewar flask containing dry ice. The beakers were held over insulating materials

and made no direct contact with the dry ice. The large dewar flask was covered and set aside for the contents to reach thermal equilibrium overnight. The separation of racemic material occurred by precipitation at room temperature while the slow cooling to dry ice temperature yielded a crystalline product of the optically active material. A second precipitation and crystallization produced crops of well formed pure optically active crystals of the complex tris-(2,4-pentanedionato)cobalt(III). The molecular rotations for the two optical isomers were -25800 and +27700. Reported values were -28920 and +29070 (34) respectively.

The optically active crystalline material showed no racemization when stored at room temperature for over two years. The two diagrams in Figure 5 illustrate the appearance of the optically active and racemic crystals.

Structural Investigations

$(-)_{546}$ Tris-(2,4-pentanedionato)cobalt(III)

The preparation of single crystals of the optically active material and the determination of the absolute configuration had not been reported at the time this study was begun*.

Knowledge of the structure and absolute configuration are essential for the proper interpretation of the bands in

*The short communication (35) by Fay and Von Dreele, on the absolute configuration of the optically active $(-)_{546}$ isomer had not appeared yet in the literature.

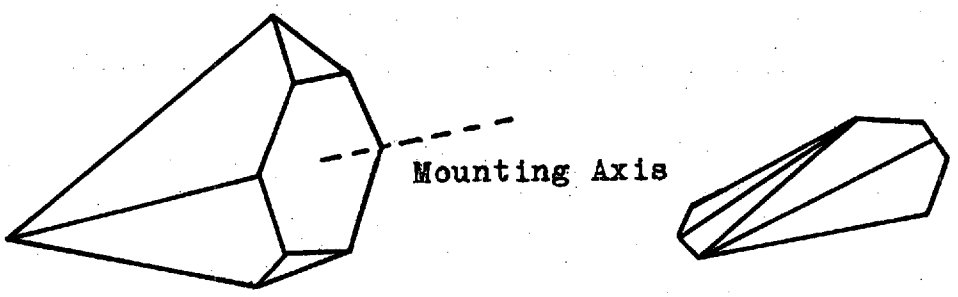

Crystals of the Optically
Active Material.

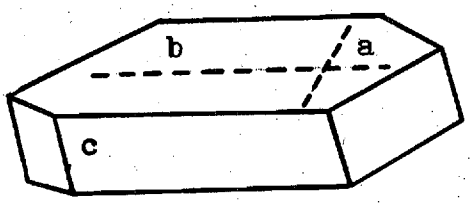

Crystal of the
Racemic Material.

Figure 5. Crystals of $Co(C_5H_7O_2)_3$.

circular dichroism spectra. It was therefore decided to investigate the material by x-ray crystallography.

A crystal of $(-)_{546}$ $Co(C_5H_7O_2)_3$ measuring about 0.3 mm x 0.3 mm x 0.2 mm was mounted along an apparent axis on a small glass fiber and attached to a goniometer head. The goniometer head was then mounted on a Buerger precession camera. Copper radiation was used (Kα, λ = 1.542Å) and the crystal was oriented in the x-ray beam. Two zones with mm symmetry were found at spindle settings 78° 58' apart (β^* = 78° 58'). Zero level photographs at these two settings had odd reflections along the horizontal axis systematically absent. No other systematic absences were observed. First level photographs showed vertical mirror symmetry only. The crystal, thus, belongs to monoclinic space group $P2_1$, #4, (36). The approximate unit cell parameters, calculated from film data, are a = 11.29(3)Å, b = 12.45(4)Å, c = 12.47(4)Å, $\hat{\beta}$ = 101 2'(2') and z = 4. The density of the material, determined by flotation in NaBr solution with traces of soap as a wetting agent, was d_{exp} = 1.36 g/ml and d_{calc} = 1.375 g/ml. Two structural investigations of the racemic material had then been published (37, 38) and the absolute configuration was reported by Fay and Von Dreele (35). The information available from these sources was sufficient for the interpretation of spectral properties and no further structural investigation of the optically active material was performed.

Racemic Tris-(biguanidato)cobalt(III) Dihydrate

A small crystal of this material was mounted on a glass fiber, along its prismatic axis, and set on a goniometer head via a small metal platform. Zero level precession photographs of two zones showed vertical and horizontal mirror symmetry. Odd reflections were systematically absent along the horizontal axis. Upper level photographs at these two settings showed only vertical mirror symmetry. Another crystal was then mounted and oriented such that its prismatic axis was along the direction of the x-ray beam, and a zero level $(h,0,\ell)$ picture confirmed the angle between the two main zones observed before. It also revealed, by comparing the spacings between its rows to the spacings on other zero level picutres, that ($\ell = 2n+1$) reflections were systematically absent. The space group was thus confirmed as $P2_1/c$, #14 (39). Preliminary calculations gave the following data for unit cell parameters, $a = 9.19(3)\mathring{A}$, $b = 9.98(3)\mathring{A}$, $c = 16.79(4)\mathring{A}$, $\hat{\beta} = 103.5(1)°$.

Density determination, by flotation in $CC\ell_4/CH_2I_2$, gave 1.702(2) g/ml. Calculations indicated that there were four molecules per unit cell.

Another crystal of the above material was selected and mounted, as described before, on a eucentric goniometer head. The crystal was approximately oriented on a Buerger precession camera and then it was transferred to a Picker four-circle diffractometer. The mosaicity of the crystal

was checked by ω - scans of two low-angle reflections. The full widths at half maxima for those were 0.12° and 0.18°. These values are within the range for ideally imperfect crystals (40). A working set of unit cell parameters was then obtained by refining the data from 16 individually centered reflections. Those values were, a = 9.190(3)Å, b = 10.037(2)Å, c = 16.567(5)Å and $\hat{\beta}$ = 103.43(1)°. A more accurate set of unit cell parameters was used for the final refinement. Control cards for the diffractometer settings were then generated for two octants of reciprocal lattice space, h = 0 to 10, k = 0 to 12, ℓ = -19 to 19, including those for the systematically absent reflections. Zirconium-filtered molybdenum $K\bar{\alpha}$ radiation was used, λ = 0.7107Å, and the takeoff angle of the x-ray tube was set at an optimum value of 2.8°. Symmetric 2θ scans of 2° around the calculated positions were taken at a rate of 1° per minute. Static background counts, each of 20 seconds duration, were collected at (2θ ± 1)° for every peak. Three axial reflections, (7, 0, 0), (0, $\bar{4}$, 0) and (0, 0, 6) were collected after every 150 reflections to check for crystal orientation and to monitor systematic changes in intensity. Intensity data for a total of 2761 reflections were collected. Those intensities were corrected for background according to the relationship,

$$CI = RI - 3\ (Bkgd_1 + Bkgd_2) \qquad (2)$$

where CI is the corrected intensity, RI is the raw intensity, $Bkgd_1$ and $Bkgd_2$ are the background counts. The factor 3 arises because the total time of collecting background counts is 1/3 the time duration for scanning the reflection.

A least squares linear fit for the net intensitites of the standard reflections collected after every 150 reflections gave a 15% drop over the entire data collection period.

The intensities for all reflections were corrected for background. They were then linearly scaled such that the intensity for the last collected reflection was increased by 15% while the intensity for the reflection measured first was left unchanged. After these two corrections, the reflections were assigned weighting factors, based upon counting statistics, according to the formula,

$$[\sigma(I)]^2 = [RI+4.5+0.25R^2(Bkgd_1+Bkgd_2+9.0) + (PxCI)^2-25] \quad (3)$$

where $\sigma(I)$ is the standard deviation, P is an "ignorance" factor assigned the value of 0.02, R = 6.0 is the ratio of intensity collection time to the time for collecting one background, and the other terms have the same significance as for the previous Eq. 2. Reflections were rejected if their corrected intensitites were less than three times their standard deviation.

A total of 2139 reflections were thus retained. Lorentz and polarization corrections were then applied and a three dimensional Patterson map were calculated using all

2139 reflections. The positions of the cobalt atoms were determined from the Patterson map. A difference electron density map, phased via the cobalt positions, yielded the coordinates of the ligand atoms and the oxygen atoms of the water molecules.

The scattering factors used were those of Cromer and Waber (41). The anomalous dispersion values for the cobalt (and bromine, for the next structure) were from Cromer (42). Scattering factors for the hydrogens were from Stewart and Davidson (43).

Absorption corrections were then applied. The linear absorption coefficient, μ, was calculated according to the relationship (44),

$$\mu = (n/V_c)\Sigma_i(\mu_a)_i \qquad (4)$$

where n is the number of molecules per unit cell (n = 4), V_c is the volume of the unit cell in cm^3 and μ_a is the atomic absorption coefficient, for element (i), for Mo-K$\bar{\alpha}$ radiation (λ = 0.7107Å). The values of the atomic absorption coefficients were obtained from the same source as Eq. 4 (44). The value of μ for $Co(C_2N_5H_6)_3.2H_2O$ was 12.37 cm^{-1}. The relationship for absorption correction for a given reflection was,

$$I_{corr} = A^* \times I_{msd} \qquad (5)$$

where I_{corr} is the intensity, corrected for absorption, I_{msd} is the intensity incorporating all previously mentioned corrections and A* is the absorption correction calculated for the path of the x-ray beam through the crystal. The absorption correction, A*, is the reciprocal of the absorption integral, A. (A) values were computed numerically by summing over a grid of 10 x 10 x 10 points through the crystal volume,

$$A^* = 1/A$$

$$A = (1/_V)\int e^{-\mu\tau} dV$$

where (τ) is the effective thickness through which the x-ray beam travels for a particular reflection hkℓ, (μ) is the linear absorption coefficient and (V) is the crystal volume.

The crystal measured* 0.2 mm x 0.3 mm x 0.5 mm and was bound by the (0, $\bar{1}$, 0), (1, 0, 0), ($\bar{1}$, 0, 0), (0, 0, $\bar{1}$), (0, 0, 1), (0, 2, 1) and (0, 2, $\bar{1}$) faces. The diagram in Figure 6 illustrates the appearance of the crystal.

Stewart's x-ray 70 program (45) was used to evaluate numerically the absorption corrections, A*. The (0, 2, 1) reflection had the maximum value of A*, 1.450, while the (1, 2, $\bar{1}$) reflection had the minimum value of A*, 1.249.

A full matrix least squares refinement was performed with a scale factor, coordinates and anisotropic temperature

*The dimensions of the crystals used for structure determination were measured on a toolmaker's microscope.

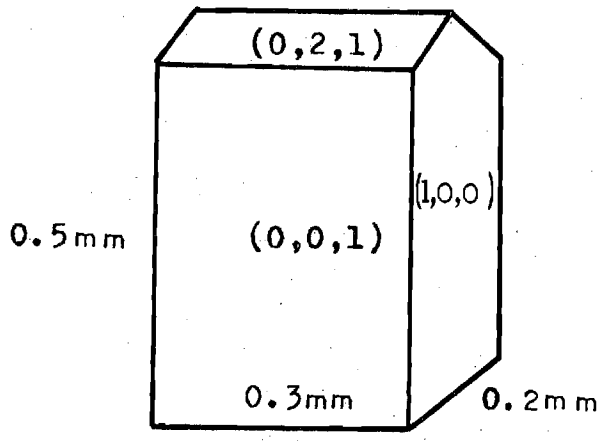

Figure 6. Crystal of $Co(C_2N_5H_6)_3 \cdot 2H_2O$.

factors of all nonhydrogen atoms as variables. The refinement minimized the quantity $\Sigma_i \omega_i (|Fo| - |Fc|)^2$, where $|Fo|$ is the absolute value of the observed structure factor and $|Fc|$ is the corresponding calculated value for a given reflection. The summation is for all reflections (i) with corresponding weighting factors (ω_i), given by the relationship

$$\omega_i = [\sigma(I)^2/I_c] \tag{6}$$

The quantity $\sigma(I)$ is the standard deviation, as defined in Eq. 3 above, and I_c is the corrected intensity for that particular reflection. The refinement was continued until the shifts for all variables were small, $(\Delta/\sigma) << 0.05$, and the values obtained for R and R_w were 0.065 and 0.071 respectively.

$$R = \frac{\Sigma_i |(|Fo|) - (|Fc|)|}{\Sigma_i (|Fo|)}$$

$$R_w = \left[\frac{\Sigma_i \omega_i (|Fo| - |Fc|)^2}{\Sigma_i \omega_i (|Fo|)^2}\right]^{1/2}$$

A difference fourier electron density map was computed at that stage and revealed the positions of the hydrogen atoms. The hydrogens were entered into the refinement with invariant isotropic temperature factors of 4.0 and their positions were refined. From that stage on the refinements were performed in blocks. The scale factor and coordinates of all atoms were varied in one cycle and the scale factor and anisotropic temperature factors were varied in another cycle.

Successive refinements converged to a weighted R-factor of 0.060 and a conventional R-factor of 0.054. At that stage close inspection of the observed and calculated structure factors showed that twenty-one reflections had observed structure factors that were much larger than the calculated ones. Upon checking intensities and scan profiles it was noted that a machine malfunction had doubled the scans and the recorded intensities were double the actual values. Those reflections were removed from the data set and refinement with the remaining 2118 reflections converged to give R = 0.04087 and R_w = 0.03525.

Another crystal of the material was then selected, mounted on a goniometer head, and put on a Syntex $P2_1$ automatic diffractometer equipped with a Mo target x-ray tube

and a graphite monochromator. Fifteen reflections, chosen from a rotation picture, were entered into the minicomputer of the diffractometer for centering and cell refinement. The following were obtained, a = 9.323(1)Å, b = 10.121(1)Å, c = 16.814(2)Å, $\hat{\beta}$ = 103.43(1)°, V = 1543.2(3)Å^3. The calculated density, based on these cell parameters, was 1.701 g/cc, for z = 4, and the measured density was 1.702(2) g/cc.

Refinement was continued with the revised cell parameters. At convergence the following values were obtained, R = 0.04087 and R_w = 0.03525. A final difference electron density map revealed no residual peaks larger than 0.48Å^3 in magnitude. Before any hydrogens were found the strongest peak had a 1.03Å^3 magnitude while the weakest non-hydrogen ligand atom had a peak height of 7.39Å^3 on the first difference electron density map. The first difference electron density map was phased with the refined coordinates of the Co atoms that were obtained from the solution of the Patterson.

Tables 2 and 3 give the coordinates and the temperature factors for all atoms of one formula unit. Table 4 gives the observed and calculated structure factors for the 2118 unique reflections utilized in the final refinement.

$(-)_{589}$ Tris-(biguanide)cobalt(III) Bromide Monohydrate

The techniques utilized during this structural investigation are very similar to those described in the previous section. Only the main differences will be presented here.

Table 2. Final Positional Parameters for Racemic $Co(C_2N_5H_6)_3 \cdot 2H_2O$.

Atom	x	y	z
Co	0.14743(5)	0.06929(4)	-0.17986(3)
N-1a	0.32712(31)	0.13235(25)	-0.20236(17)
N-2a	0.49889(32)	0.17496(28)	-0.27909(19)
C-1a	0.38383(34)	0.10221(28)	-0.26352(20)
N-3a	0.33568(32)	0.00459(26)	-0.31907(18)
C-2a	0.23777(34)	-0.08644(30)	-0.30392(19)
N-4a	0.22030(38)	-0.19268(31)	-0.35529(22)
N-5a	0.16834(29)	-0.08232(25)	-0.24523(16)
N-1b	0.03184(31)	0.15346(25)	-0.27688(16)
N-2b	-0.13711(36)	0.13964(32)	-0.40316(18)
C-1b	-0.09051(37)	0.10508(28)	-0.32151(19)
N-3b	-0.18369(31)	0.01979(26)	-0.29767(16)
C-2b	-0.15647(37)	-0.01880(29)	-0.21725(20)
N-4b	-0.26724(34)	-0.08878(30)	-0.19784(18)
N-5b	-0.03613(32)	0.00435(27)	-0.16231(17)
N-1c	0.13960(32)	0.22232(26)	-0.11292(17)
N-2c	0.15412(40)	0.34798(29)	0.00466(19)
C-1c	0.17871(37)	0.23180(31)	-0.03294(20)
N-3c	0.24119(39)	0.13732(28)	0.02024(18)
C-2c	0.28123(38)	0.01951(33)	-0.00846(21)
N-4c	0.35681(45)	-0.06308(34)	0.05156(18)
N-5c	0.25296(32)	-0.01895(26)	-0.08374(16)
O-1	0.44835(30)	0.39305(24)	-0.11170(17)
O-2	0.46123(31)	-0.28958(28)	-0.04078(18)

Table 2. (Continued)

Atom	x	y	z	B
H-1a	0.3694(51)	0.1944(41)	-0.1747(28)	4.0
H-2a1	0.5454(52)	0.1524(42)	-0.3119(28)	4.0
H-2a2	0.5492(49)	0.2078(41)	-0.2366(28)	4.0
H-4a1	0.2460(50)	-0.1807(40)	-0.4006(28)	4.0
H-4a2	0.1528(53)	-0.2458(41)	-0.3563(27)	4.0
H-5a	0.1141(52)	-0.1614(41)	-0.2463(28)	4.0
H-1b	0.0750(50)	0.2067(40)	-0.3034(28)	4.0
H-2b1	-0.2295(52)	0.1403(43)	-0.4237(28)	4.0
H-2b2	-0.0843(51)	0.1951(40)	-0.4252(28)	4.0
H-4b1	-0.3370(50)	-0.1046(41)	-0.2325(27)	4.0
H-4b2	-0.2556(50)	-0.1162(42)	-0.1424(27)	4.0
H-5b	-0.0374(51)	-0.0320(40)	-0.1157(28)	4.0
H-1c	0.1082(51)	0.2993(43)	-0.1395(28)	4.0
H-2c1	0.1978(50)	0.3629(41)	0.0475(28)	4.0
H-2c2	0.1314(50)	0.4157(41)	-0.0248(27)	4.0
H-4c1	0.3945(49)	-0.0261(42)	0.1006(27)	4.0
H-4c2	0.3960(51)	-0.1255(42)	0.0342(28)	4.0
H-5c	0.2927(49)	-0.0908(41)	-0.0191(27)	4.0
H-1(0-1)	0.3726(51)	0.4449(41)	-0.1319(27)	4.0
H-2(0-1)	0.5080(51)	0.4304(43)	-0.1277(27)	4.0
H-1(0-2)	0.4908(53)	-0.3438(42)	-0.0024(29)	4.0
H-2(0-2)	0.5190(51)	-0.2596(44)	-0.0529(27)	4.0

The isotropic temperature factor of an atom, in $\mathring{A}^2$, is given by the expression, $\exp[-\frac{B}{4}(\frac{2\sin\theta_{hk\ell}}{\lambda})^2]$. Values of B are given in Tables 2 and 5.

Table 3. Final Anisotropic Thermal Parameters for Racemic $Co(C_2N_5H_6)_3 \cdot 2H_2O$ (Parameters x 10^4).

Atom	β_{11}	β_{22}	β_{33}	β_{12}	β_{13}	β_{23}
Co	43(.5)	34(.4)	12(.2)	-00(.4)	4(.2)	-00(.2)
N-1a	49(4)	48(3)	18(1)	-12(2)	3(2)	-4(1)
N-2a	62(4)	61(3)	29(1)	-16(3)	18(2)	-7(2)
C-1a	39(4)	41(3)	18(1)	13(3)	6(2)	6(1)
N-3a	63(4)	61(3)	20(1)	-9(3)	14(2)	-6(2)
C-2a	47(4)	41(3)	18(1)	3(3)	2(2)	-6(2)
N-4a	103(5)	77(3)	33(2)	-32(3)	30(2)	-25(2)
N-5a	56(3)	36(3)	19(1)	1(3)	8(2)	-00(1)
N-1b	55(4)	43(2)	16(1)	-5(2)	6(2)	3(1)
N-2b	72(4)	98(4)	14(1)	-21(3)	-1(2)	10(2)
C-1b	55(4)	35(3)	16(1)	9(3)	11(2)	1(1)
N-3b	59(4)	56(3)	14(1)	-11(3)	5(2)	-2(1)
C-2b	60(4)	36(3)	17(1)	-2(3)	14(2)	-7(2)
N-4b	86(4)	82(3)	17(1)	-37(3)	10(2)	-1(2)
N-5b	60(4)	61(3)	14(1)	-6(3)	8(2)	5(1)
N-1c	58(4)	41(3)	17(1)	7(1)	4(2)	-2(1)
N-2c	121(5)	62(3)	19(1)	20(3)	1(3)	-7(1)
C-1c	53(4)	49(3)	17(1)	-3(3)	8(2)	-2(2)
N-3c	125(5)	57(3)	15(1)	9(3)	8(2)	-2(2)
C-2c	62(4)	61(3)	17(1)	-7(3)	9(2)	4(2)
N-4c	180(6)	78(3)	16(1)	45(1)	6(2)	9(2)
N-5c	67(4)	49(2)	16(1)	11(3)	3(2)	00(1)
0-1	83(3)	70(3)	30(1)	-4(2)	12(2)	9(1)
0-2	87(4)	97(3)	33(1)	7(3)	2(2)	5(2)

The expression for the anisotropic temperature factor of an atom is, $\exp[-(\beta_{11}h^2 + \beta_{22}k^2 + \beta_{33}\ell^2 + 2\beta_{12}hk + 2\beta_{13}h\ell + 2\beta_{23}k\ell)]$. The values of the β-terms for the individual atoms are given in Tables 3 and 6.

Table 4. List of Structure Factors for Racemic $Co(C_2N_5H_6)_3 \cdot 2H_2O$.

H	K	L	F_o	F_c	H	K	L	F_o	F_c	H	K	L	F_o	F_c
0	1	-19	16.3	16.3	2	6	-16	24.3	23.5	5	5	-14	34.1	33.8
1	1	-19	23.2	25.4	3	6	-16	18.7	19.2	6	5	-14	20.8	19.3
3	1	-19	35.6	36.7	4	6	-16	13.6	13.2	0	6	-14	59.7	60.5
4	1	-19	13.7	13.2	5	6	-16	11.2	8.2	1	6	-14	34.6	35.2
5	1	-19	15.1	14.3	2	7	-16	10.5	9.2	3	6	-14	53.4	54.3
2	2	-19	26.3	26.2	0	1	-15	12.8	9.1	4	6	-14	21.5	21.3
3	2	-19	18.0	18.7	1	1	-15	12.2	6.9	5	6	-14	13.7	11.4
4	2	-19	11.3	9.8	2	1	-15	52.8	54.7	6	6	-14	38.2	36.9
3	3	-19	16.7	16.2	3	1	-15	38.6	39.6	7	6	-14	37.4	37.3
1	0	-18	15.4	14.1	4	1	-15	23.6	23.8	0	7	-14	11.7	5.6
3	0	-18	11.2	8.3	5	1	-15	72.3	72.5	2	7	-14	9.6	7.9
5	0	-18	11.5	10.6	6	1	-15	30.1	28.7	4	7	-14	13.8	12.8
6	0	-18	36.1	36.7	7	1	-15	13.4	11.5	0	8	-14	21.6	22.2
1	1	-18	12.9	10.2	8	1	-15	31.6	31.2	1	8	-14	27.8	26.3
2	1	-18	17.9	15.2	0	2	-15	29.5	28.6	2	8	-14	19.6	17.7
3	1	-18	13.2	11.6	1	2	-15	15.7	15.5	3	8	-14	24.0	23.7
4	1	-18	17.9	17.5	3	2	-15	10.5	8.4	4	8	-14	19.7	20.2
1	2	-18	19.4	19.1	4	2	-15	42.4	42.5	1	1	-13	58.3	61.3
2	2	-18	20.9	20.1	5	2	-15	24.5	23.1	2	1	-13	28.5	27.9
5	2	-18	19.4	18.4	7	2	-15	13.0	14.3	3	1	-13	10.7	10.9
6	2	-18	22.6	22.2	8	2	-15	19.8	19.9	4	1	-13	61.2	62.6
0	3	-18	21.6	21.2	0	3	-15	16.6	17.5	5	1	-13	60.4	61.3
1	3	-18	28.1	27.5	3	3	-15	19.3	19.1	7	1	-13	27.3	25.8
3	3	-18	34.3	34.7	5	3	-15	14.2	16.2	8	1	-13	48.6	49.4
4	3	-18	33.3	33.2	7	3	-15	22.9	23.0	0	2	-13	24.9	25.6
3	4	-18	10.9	8.8	0	4	-15	35.9	35.6	1	2	-13	10.0	10.1
0	1	-17	18.7	19.3	1	4	-15	10.4	10.8	2	2	-13	41.4	41.7
2	1	-17	21.1	21.1	2	4	-15	9.5	6.3	3	2	-13	43.1	43.4
3	1	-17	46.0	47.7	3	4	-15	16.2	15.2	4	2	-13	36.4	36.7
4	1	-17	18.5	17.4	4	4	-15	28.6	28.9	5	2	-13	12.5	14.1
5	1	-17	23.0	23.2	5	4	-15	18.8	18.4	6	2	-13	14.0	12.9
6	1	-17	36.8	35.4	6	4	-15	28.7	27.9	7	2	-13	28.0	27.1
7	1	-17	14.2	15.9	7	4	-15	23.1	23.0	9	2	-13	26.3	26.4
0	2	-17	14.9	12.5	0	5	-15	12.8	10.0	0	3	-13	38.4	38.9
3	2	-17	10.5	8.5	1	5	-15	22.1	21.2	1	3	-13	30.7	31.1
4	2	-17	22.6	22.7	2	5	-15	21.2	20.3	2	3	-13	29.3	28.7
5	2	-17	22.7	22.1	4	5	-15	21.5	21.8	3	3	-13	15.5	16.1
6	2	-17	11.7	13.1	6	5	-15	9.0	9.1	4	3	-13	17.9	16.8
0	3	-17	15.7	16.3	7	5	-15	11.9	10.2	5	3	-13	20.0	19.4
4	3	-17	20.1	18.8	0	6	-15	28.9	27.9	6	3	-13	20.6	19.4
0	4	-17	16.0	15.1	1	6	-15	10.8	12.3	7	3	-13	10.0	9.3
1	4	-17	28.0	28.7	2	6	-15	13.2	11.4	9	3	-13	16.6	16.1
2	4	-17	43.2	43.6	3	6	-15	13.7	14.2	0	4	-13	33.7	34.1
3	4	-17	12.5	11.2	4	6	-15	19.8	19.6	2	4	-13	21.8	22.0
4	4	-17	18.9	18.8	6	6	-15	15.9	16.0	3	4	-13	15.0	14.5
5	4	-17	24.9	24.0	0	7	-15	13.6	11.5	4	4	-13	10.0	8.0
2	5	-17	15.0	14.2	1	7	-15	11.5	13.7	6	4	-13	17.9	16.9
3	5	-17	18.3	16.9	2	7	-15	44.4	44.4	7	4	-13	37.6	37.5
5	5	-17	15.9	13.8	3	7	-15	16.9	19.6	0	5	-13	23.2	23.8
0	0	-16	23.2	23.0	5	7	-15	20.9	20.2	3	5	-13	17.6	17.7
1	0	-16	31.9	32.4	0	0	-14	56.8	57.4	4	5	-13	21.2	20.6
2	0	-16	26.9	27.4	1	0	-14	23.9	22.9	5	5	-13	16.3	15.4
3	0	-16	9.7	8.8	2	0	-14	10.5	10.5	7	5	-13	16.7	16.1
4	0	-16	74.9	76.3	3	0	-14	73.2	75.8	8	5	-13	25.3	23.2
5	0	-16	22.8	21.7	4	0	-14	54.6	56.3	0	6	-13	16.8	17.2
6	0	-16	22.1	22.7	6	0	-14	17.1	16.2	2	6	-13	27.7	27.3
7	0	-16	16.2	15.8	7	0	-14	14.8	15.6	3	6	-13	18.4	18.8
8	0	-16	19.9	16.2	0	1	-14	20.5	29.7	4	6	-13	15.5	13.8
2	1	-16	18.6	18.0	1	1	-14	20.7	21.1	6	6	-13	29.1	29.3
3	1	-16	24.0	23.9	2	1	-14	13.7	14.3	7	6	-13	12.9	7.5
5	1	-16	12.2	13.4	4	1	-14	31.6	30.8	0	7	-13	26.1	28.0
6	1	-16	25.0	24.4	5	1	-14	19.9	17.5	1	7	-13	45.9	46.9
7	1	-16	24.1	23.4	6	1	-14	20.9	19.1	2	7	-13	15.2	15.8
0	2	-16	28.6	29.7	9	1	-14	10.3	8.2	4	7	-13	30.8	30.9
1	2	-16	9.8	8.9	0	2	-14	22.8	21.4	5	7	-13	27.8	26.8
3	2	-16	10.1	9.0	1	2	-14	25.3	25.7	0	8	-13	16.9	14.8
4	2	-16	15.3	16.3	2	2	-14	11.6	12.9	2	8	-13	9.4	7.4
5	2	-16	16.3	15.8	3	2	-14	23.9	24.0	5	8	-13	12.6	9.5
6	2	-16	12.6	11.6	4	2	-14	14.3	14.0	1	9	-13	14.7	14.8
0	3	-16	25.0	23.9	7	2	-14	9.3	9.6	2	9	-13	24.8	24.3
1	3	-16	13.9	13.1	9	2	-14	10.8	8.9	1	0	-12	13.7	14.6
2	3	-16	28.6	28.8	0	3	-14	29.9	29.2	2	0	-12	74.1	76.1
3	3	-16	30.9	31.1	2	3	-14	8.9	9.3	3	0	-12	63.6	64.9
5	3	-16	25.2	25.1	3	3	-14	16.2	14.1	5	0	-12	45.7	45.4
6	3	-16	30.5	29.7	4	3	-14	31.4	31.6	6	0	-12	26.3	25.9
7	3	-16	17.4	16.1	5	3	-14	11.0	10.7	8	0	-12	19.6	19.8
0	4	-16	14.3	14.1	6	3	-14	19.4	20.4	9	0	-12	39.2	39.1
1	4	-16	28.6	28.1	8	3	-14	25.2	23.4	10	0	-12	16.4	16.1
2	4	-16	9.8	8.2	0	4	-14	10.3	9.2	0	1	-12	17.5	26.5
3	4	-16	26.2	26.7	2	4	-14	17.1	15.7	2	1	-12	9.3	11.4
5	4	-16	22.9	22.0	3	4	-14	10.4	11.8	3	1	-12	15.1	13.7
6	5	-16	28.9	29.9	4	4	-14	14.4	14.6	4	1	-12	29.8	29.3
2	5	-16	17.1	17.1	6	4	-14	12.5	11.8	6	1	-12	26.4	26.3
3	5	-16	19.5	18.4	7	4	-14	17.0	15.9	7	1	-12	13.5	13.7
4	5	-16	26.7	26.7	0	5	-14	14.7	13.4	0	2	-12	43.8	44.9
6	5	-16	27.9	28.3	1	5	-14	30.4	30.5	1	2	-12	21.2	21.2
0	6	-16	36.5	35.2	3	5	-14	16.2	16.8	3	2	-12	28.3	28.3
1	6	-16	46.5	47.4	4	5	-14	24.4	25.9	4	2	-12	13.9	13.6

Table 4. (Continued)

H	K	L	F_o	F_c
5	2	-12	11.3	10.6
6	2	-12	28.4	28.5
7	2	-12	13.5	14.2
8	2	-12	17.4	16.5
9	2	-12	19.8	18.2
0	3	-12	38.4	37.3
1	3	-12	30.3	30.7
2	3	-12	18.2	19.7
3	3	-12	29.4	30.2
4	3	-12	43.2	42.2
5	3	-12	27.4	26.2
6	3	-12	21.6	22.0
7	3	-12	26.8	26.4
8	3	-12	25.6	26.2
1	4	-12	22.4	21.8
2	4	-12	11.3	12.6
3	4	-12	77.9	79.9
4	4	-12	51.2	51.2
5	4	-12	19.9	21.5
6	4	-12	20.5	21.4
9	4	-12	13.5	11.9
1	5	-12	41.2	42.5
2	5	-12	27.5	28.1
3	5	-12	38.5	38.4
4	5	-12	27.2	27.5
5	5	-12	12.3	12.0
7	5	-12	37.7	37.1
8	5	-12	14.4	15.0
1	6	-12	10.4	9.3
2	6	-12	12.9	12.0
3	6	-12	53.3	54.1
4	6	-12	9.3	10.3
5	6	-12	42.0	41.1
6	6	-12	40.9	40.7
7	6	-12	9.5	6.5
1	7	-12	20.5	20.8
2	7	-12	11.8	13.1
5	7	-12	22.3	22.2
6	7	-12	11.0	8.4
7	7	-12	13.1	10.7
2	8	-12	26.3	25.8
3	8	-12	25.0	26.3
4	8	-12	9.2	8.9
5	8	-12	27.0	26.6
6	8	-12	27.1	25.9
0	9	-12	19.1	20.3
1	9	-12	18.4	18.8
3	9	-12	16.6	17.0
4	9	-12	16.5	17.1
1	1	-11	51.8	51.3
3	1	-11	41.2	41.4
4	1	-11	42.8	42.6
5	1	-11	10.9	11.1
7	1	-11	38.1	38.3
8	1	-11	31.9	32.0
9	1	-11	22.7	23.5
10	1	-11	32.1	31.8
2	2	-11	46.5	47.1
3	2	-11	28.1	26.6
4	2	-11	16.8	16.6
5	2	-11	41.8	41.7
6	2	-11	16.1	14.6
8	2	-11	19.4	18.2
9	2	-11	24.0	23.8
10	2	-11	9.8	10.0
1	3	-11	37.3	35.9
3	3	-11	23.2	22.6
4	3	-11	23.0	24.3
5	3	-11	37.9	37.7
6	3	-11	15.9	15.6
7	3	-11	38.8	38.3
8	3	-11	10.1	8.4
9	3	-11	15.5	14.6
0	4	-11	34.3	34.8
1	4	-11	61.7	62.5
2	4	-11	42.1	42.2
3	4	-11	23.7	24.7
4	4	-11	28.7	28.7
5	4	-11	38.3	39.1
6	4	-11	28.1	28.1
8	4	-11	11.9	11.4
9	4	-11	20.6	20.8
1	5	-11	23.2	23.1
4	5	-11	46.3	45.2
5	5	-11	9.2	11.2
6	5	-11	20.3	21.1
7	5	-11	27.7	26.6
8	5	-11	20.4	20.6
0	6	-11	14.1	17.8
3	6	-11	18.6	17.2
5	6	-11	18.8	17.6
6	6	-11	26.0	25.0
8	6	-11	22.0	20.7
0	7	-11	39.1	39.2
1	7	-11	20.6	18.4
2	7	-11	17.3	16.4
3	7	-11	43.1	42.6
4	7	-11	33.6	34.0
6	7	-11	31.9	31.7
7	7	-11	44.3	43.9
1	8	-11	26.9	27.2
2	8	-11	16.1	16.4
4	8	-11	17.1	15.4
5	8	-11	15.5	15.2
0	9	-11	26.1	26.2
1	9	-11	22.5	23.5
2	9	-11	10.5	11.4
3	9	-11	21.4	22.5
4	9	-11	11.7	10.5
5	9	-11	11.2	13.2
0	0	-10	71.7	70.0
1	0	-10	80.1	79.6
2	0	-10	25.3	28.4
3	0	-10	19.9	20.5
4	0	-10	31.1	31.7
5	0	-10	69.3	69.3
7	0	-10	18.6	17.1
8	0	-10	49.0	48.5
9	0	-10	29.4	30.7
10	0	-10	14.6	15.3
1	1	-10	36.6	34.9
3	1	-10	16.8	17.0
4	1	-10	19.4	17.1
6	1	-10	37.1	35.9
8	1	-10	19.1	17.5
9	1	-10	23.6	23.2
10	1	-10	15.8	14.8
0	2	-10	38.7	36.3
1	2	-10	30.0	28.7
2	2	-10	24.0	23.9
3	2	-10	13.5	14.1
4	2	-10	27.1	26.0
5	2	-10	40.7	40.5
6	2	-10	35.8	36.5
8	2	-10	20.5	20.8
9	2	-10	20.3	18.7
10	2	-10	11.3	10.3
0	3	-10	61.1	61.0
1	3	-10	24.0	24.6
2	3	-10	36.4	36.5
3	3	-10	56.7	57.8
4	3	-10	52.3	51.7
5	3	-10	40.5	40.0
6	3	-10	58.6	59.3
7	3	-10	18.6	19.1
9	3	-10	27.5	27.5
10	3	-10	21.8	21.1
0	4	-10	22.3	23.7
1	4	-10	34.1	34.1
2	4	-10	30.0	30.0
3	4	-10	10.8	11.4
4	4	-10	21.0	20.8
5	4	-10	16.2	17.2
7	4	-10	9.4	8.2
9	4	-10	17.3	17.6
0	5	-10	18.3	19.0
1	5	-10	9.8	8.6
2	5	-10	20.3	20.4
3	5	-10	52.1	52.6
4	5	-10	43.8	43.7
5	5	-10	13.3	13.9
6	5	-10	37.6	37.0
7	5	-10	31.8	31.2
8	5	-10	14.7	13.8
9	5	-10	17.4	15.9
0	6	-10	9.7	7.7
1	6	-10	27.0	26.7
2	6	-10	27.4	27.8
3	6	-10	23.2	23.7
4	6	-10	15.2	15.0
5	6	-10	41.7	41.9
6	6	-10	34.2	35.7
8	6	-10	19.3	20.2
0	7	-10	18.1	17.6
2	7	-10	15.0	15.0
3	7	-10	22.3	22.2
4	7	-10	12.3	10.6
5	7	-10	8.8	6.6
6	7	-10	10.7	7.5
7	7	-10	15.4	12.1
0	8	-10	14.8	12.4
1	8	-10	34.2	34.6
2	8	-10	35.1	36.7
4	8	-10	15.0	15.1
5	8	-10	32.1	32.0
6	8	-10	19.0	18.6
7	8	-10	24.5	25.3
0	9	-10	22.2	22.3
2	9	-10	23.2	23.3
3	9	-10	20.4	21.9
1	10	-10	18.6	16.5
2	10	-10	12.0	10.1
0	1	-9	65.8	65.7
2	1	-9	35.3	32.2
3	1	-9	43.0	43.2
4	1	-9	39.5	38.1
5	1	-9	37.6	35.5
6	1	-9	48.5	48.5
7	1	-9	23.9	23.8
8	1	-9	10.3	12.5
9	1	-9	46.7	45.2
10	1	-9	43.3	43.0
1	2	-9	68.4	67.7
2	2	-9	23.9	24.0
4	2	-9	75.5	75.4
5	2	-9	17.0	16.5
6	2	-9	19.2	18.9
7	2	-9	31.5	31.5
8	2	-9	18.5	17.9
9	2	-9	18.0	17.3
10	2	-9	15.2	14.4
2	3	-9	28.6	28.8
4	3	-9	10.6	6.9
5	3	-9	20.8	20.3
6	3	-9	15.9	14.2
7	3	-9	9.0	7.5
8	3	-9	10.3	8.7
10	3	-9	11.1	10.0
0	4	-9	25.4	25.8
1	4	-9	52.0	51.3
2	4	-9	62.6	62.1
3	4	-9	36.2	36.3
4	4	-9	77.0	76.8
5	4	-9	40.5	40.9
6	4	-9	17.1	15.2
7	4	-9	27.0	25.8
8	4	-9	15.7	14.7
0	5	-9	39.0	41.2
1	5	-9	28.2	27.8
2	5	-9	45.8	45.0
3	5	-9	15.5	15.1
4	5	-9	11.9	10.8
5	5	-9	20.0	20.3
6	5	-9	15.1	13.5
7	5	-9	21.7	21.3
1	6	-9	13.0	12.3
2	6	-9	8.4	9.6
3	6	-9	23.6	24.6
4	6	-9	25.6	25.0
0	7	-9	19.3	17.8
1	7	-9	10.8	10.5
2	7	-9	61.1	61.9
3	7	-9	33.8	34.3
4	7	-9	8.4	7.8
5	7	-9	17.3	17.8
6	7	-9	37.0	36.4
7	7	-9	12.5	13.0
8	7	-9	10.4	11.1
1	8	-9	33.7	34.6
4	8	-9	23.5	23.4
5	8	-9	10.9	11.3
7	8	-9	14.0	10.9
0	9	-9	34.9	36.8
2	9	-9	30.9	30.8
3	9	-9	29.3	31.2
4	9	-9	9.4	8.5
5	9	-9	10.2	4.9
6	9	-9	28.6	27.3
1	10	-9	40.4	40.9
2	10	-9	26.7	26.6
3	10	-9	18.5	20.3
4	10	-9	26.6	25.1
0	0	-8	74.2	72.8
2	0	-8	20.2	18.4
3	0	-8	28.5	25.6
4	0	-8	50.1	50.7
5	0	-8	37.5	37.4
6	0	-8	16.2	16.3
7	0	-8	20.4	20.3
8	0	-8	35.3	34.2
10	0	-8	46.8	45.5
1	1	-8	29.3	28.5
2	1	-8	27.4	25.8
5	1	-8	45.6	43.5
6	1	-8	29.0	27.0
9	1	-8	23.9	22.8
0	2	-8	48.2	46.1
1	2	-8	52.8	53.0
4	2	-8	10.6	11.9
4	2	-8	54.9	50.4
5	2	-8	36.4	34.6
6	2	-8	9.4	8.1

Table 4. (Continued)

H	K	L	F_o	F_c
8	2	-8	29.9	28.7
10	2	-8	18.7	20.3
0	3	-8	40.2	39.9
1	3	-8	19.8	21.2
2	3	-8	74.8	77.2
3	3	-8	27.0	28.1
5	3	-8	63.7	63.5
6	3	-8	63.6	64.8
8	3	-8	28.4	28.0
9	3	-8	43.3	45.0
10	3	-8	19.5	19.9
0	4	-8	17.8	17.1
1	4	-8	10.1	10.1
3	4	-8	11.2	9.4
4	4	-8	23.3	21.0
6	4	-8	15.0	14.8
8	4	-8	17.3	15.1
0	5	-8	31.7	30.6
1	5	-8	17.8	18.2
2	5	-8	98.5	99.2
3	5	-8	33.5	33.4
4	5	-8	13.2	14.2
5	5	-8	38.4	39.3
6	5	-8	31.9	31.5
8	5	-8	35.4	35.3
9	5	-8	26.7	25.5
0	6	-8	43.0	43.7
1	6	-8	66.3	67.8
3	6	-8	43.5	43.7
4	6	-8	23.3	23.6
5	6	-8	22.2	22.2
7	6	-8	23.0	23.0
8	6	-8	26.3	26.6
0	7	-8	28.4	28.6
1	7	-8	7.6	2.4
3	7	-8	26.9	27.6
4	7	-8	19.9	19.9
8	7	-8	12.3	10.8
0	8	-8	33.2	32.0
1	8	-8	31.1	30.4
2	8	-8	9.2	3.7
3	8	-8	27.5	28.7
4	8	-8	25.4	25.2
7	8	-8	37.6	37.5
1	9	-8	36.3	36.6
2	9	-8	40.6	42.0
4	9	-8	14.8	15.2
5	9	-8	12.6	13.4
6	9	-8	16.3	17.1
4	10	-8	12.1	12.4
5	10	-8	9.2	8.8
1	1	-7	14.9	17.2
3	1	-7	15.8	14.6
4	1	-7	60.0	60.9
5	1	-7	78.3	79.4
6	1	-7	49.1	49.7
7	1	-7	28.5	28.1
8	1	-7	22.1	21.3
9	1	-7	32.3	32.1
0	2	-7	80.2	79.8
3	2	-7	60.1	61.9
4	2	-7	53.8	53.3
5	2	-7	12.5	11.9
6	2	-7	71.7	72.6
7	2	-7	27.8	27.6
8	2	-7	17.4	17.3
10	2	-7	24.0	23.3
1	3	-7	9.7	8.4
2	3	-7	25.3	24.8
4	3	-7	14.2	13.5
5	3	-7	17.0	19.0
6	3	-7	18.7	18.5
8	3	-7	21.5	22.5
0	4	-7	88.5	90.5
1	4	-7	43.6	44.3
2	4	-7	37.5	39.3
3	4	-7	50.4	52.8
4	4	-7	53.5	54.9
5	4	-7	20.9	20.1
6	4	-7	37.8	38.3
7	4	-7	41.9	41.5
8	4	-7	12.7	13.7
9	4	-7	18.7	19.7
10	4	-7	35.1	35.7
0	5	-7	14.9	15.6
1	5	-7	8.3	6.7
2	5	-7	56.0	56.6
3	5	-7	29.3	28.9
4	5	-7	30.4	30.5
5	5	-7	19.5	18.1
6	5	-7	9.3	9.3
7	5	-7	19.9	19.2
9	5	-7	20.4	20.8
1	6	-7	28.7	29.2
2	6	-7	29.3	29.4
3	6	-7	35.9	36.3
4	6	-7	7.7	6.1
5	6	-7	11.9	11.1
6	6	-7	10.9	8.4
9	6	-7	13.3	12.8
1	7	-7	32.3	33.9
2	7	-7	54.6	56.6
3	7	-7	10.6	10.4
4	7	-7	12.5	11.7
6	7	-7	8.4	5.0
7	7	-7	9.7	1.8
8	7	-7	27.7	28.9
0	8	-7	17.6	18.3
1	8	-7	12.5	9.4
2	8	-7	24.3	25.8
3	8	-7	10.4	12.2
4	8	-7	23.3	24.8
5	8	-7	30.0	31.0
6	8	-7	10.9	14.1
7	8	-7	20.1	19.5
1	9	-7	24.6	25.2
2	9	-7	32.5	33.1
3	9	-7	18.2	16.4
4	9	-7	22.5	23.5
5	9	-7	10.5	14.0
6	9	-7	14.8	15.1
0	10	-7	23.9	24.6
1	10	-7	23.3	23.9
3	10	-7	21.3	22.4
4	10	-7	38.5	40.1
5	10	-7	11.7	11.6
2	11	-7	9.3	9.8
0	0	-6	86.6	89.3
1	0	-6	75.4	77.3
2	0	-6	104.6	108.3
3	0	-6	23.5	26.4
4	0	-6	8.3	5.7
5	0	-6	20.2	18.3
6	0	-6	37.2	38.3
9	0	-6	13.6	13.0
10	0	-6	14.1	15.3
0	1	-6	65.8	65.2
1	1	-6	77.0	79.1
2	1	-6	6.4	1.4
3	1	-6	23.7	23.3
4	1	-6	69.6	69.9
5	1	-6	37.3	38.5
7	1	-6	16.7	15.6
8	1	-6	16.0	15.9
0	2	-6	58.3	56.5
1	2	-6	46.9	47.9
2	2	-6	50.3	48.4
3	2	-6	19.7	20.4
4	2	-6	26.9	28.0
6	2	-6	44.4	44.1
7	2	-6	30.1	30.3
8	2	-6	19.9	19.8
9	2	-6	12.7	15.0
10	2	-6	19.8	19.7
0	3	-6	35.8	35.5
1	3	-6	94.4	98.6
2	3	-6	72.2	73.8
3	3	-6	34.3	34.1
4	3	-6	69.0	70.9
5	3	-6	82.3	83.3
6	3	-6	14.3	14.6
7	3	-6	27.3	26.2
8	3	-6	60.5	61.7
9	3	-6	38.8	40.2
10	3	-6	12.2	12.1
0	4	-6	15.1	11.8
1	4	-6	31.6	30.4
2	4	-6	29.0	29.6
3	4	-6	42.0	40.9
4	4	-6	29.4	28.6
8	4	-6	13.4	15.3
10	4	-6	11.9	13.4
0	5	-6	32.5	34.6
1	5	-6	43.5	45.6
2	5	-6	24.4	25.3
3	5	-6	14.1	13.9
5	5	-6	12.1	9.8
7	5	-6	12.4	11.1
8	5	-6	36.4	36.8
0	6	-6	20.9	21.3
1	6	-6	27.6	27.8
2	6	-6	49.2	52.1
3	6	-6	63.3	65.7
5	6	-6	18.3	17.1
6	6	-6	17.5	16.6
7	6	-6	11.7	11.3
9	6	-6	18.2	17.9
0	7	-6	12.3	10.8
3	7	-6	22.9	22.2
6	7	-6	26.9	27.6
0	8	-6	24.1	23.2
3	8	-6	46.8	50.8
4	8	-6	8.5	6.6
6	8	-6	22.8	23.1
7	8	-6	30.7	30.9
8	8	-6	9.2	6.6
0	9	-6	13.2	10.9
1	9	-6	21.7	22.6
2	9	-6	19.3	19.6
4	9	-6	20.3	20.9
5	9	-6	17.9	17.3
7	9	-6	24.9	24.3
1	10	-6	8.4	9.8
3	10	-6	18.0	19.0
4	10	-6	9.2	8.3
5	10	-6	12.6	12.8
0	11	-6	27.5	27.7
1	11	-6	31.1	32.1
2	11	-6	25.5	24.7
1	1	-5	58.6	59.0
2	1	-5	13.7	11.3
3	1	-5	50.7	51.7
4	1	-5	69.5	68.6
5	1	-5	79.3	80.1
7	1	-5	67.9	67.3
8	1	-5	11.3	9.6
10	1	-5	20.9	19.7
0	2	-5	10.8	12.0
1	2	-5	16.8	15.1
2	2	-5	30.4	32.7
3	2	-5	21.4	21.7
4	2	-5	26.3	25.4
5	2	-5	20.5	18.8
6	2	-5	49.4	49.7
7	2	-5	30.0	30.5
8	2	-5	8.4	2.2
9	2	-5	18.7	20.5
10	2	-5	15.9	16.1
1	3	-5	33.4	33.2
2	3	-5	63.0	64.6
5	3	-5	58.6	57.6
6	3	-5	11.8	11.7
7	3	-5	28.3	28.2
8	3	-5	21.9	21.3
9	3	-5	23.9	25.3
0	4	-5	78.8	82.7
1	4	-5	58.5	60.1
2	4	-5	85.0	90.0
3	4	-5	87.1	90.8
4	4	-5	27.7	27.6
5	4	-5	33.1	33.7
7	4	-5	21.8	21.4
8	4	-5	34.3	35.8
9	4	-5	44.0	44.7
10	4	-5	22.0	20.6
0	5	-5	68.5	72.7
1	5	-5	16.9	17.0
2	5	-5	13.7	13.0
3	5	-5	46.7	46.9
6	5	-5	27.3	27.9
7	5	-5	24.4	25.2
8	5	-5	28.0	27.7
9	5	-5	10.9	12.4
0	6	-5	4.8	3.7
2	6	-5	37.8	39.8
3	6	-5	7.9	7.3
6	6	-5	18.9	17.8
7	6	-5	17.0	16.8
8	6	-5	22.9	23.3
9	6	-5	19.6	21.1
0	7	-5	31.7	34.7
1	7	-5	47.3	48.5
2	7	-5	16.4	14.8
4	7	-5	28.7	29.1
6	7	-5	15.1	15.1
7	7	-5	27.8	27.6
8	7	-5	17.1	17.6
1	8	-5	14.2	14.3
2	8	-5	12.7	10.8
3	8	-5	22.6	23.1
5	8	-5	9.2	9.4
6	8	-5	18.0	17.5
0	9	-5	17.8	19.5
1	9	-5	37.8	38.8
2	9	-5	7.7	4.7
3	9	-5	9.4	8.6
4	9	-5	35.2	35.7
5	9	-5	14.7	14.8
7	9	-5	13.1	10.5
0	10	-5	12.2	14.0
2	10	-5	28.2	29.8
3	10	-5	36.6	37.2

Table 4. (Continued)

H	K	L	F_o	F_c
4	10	-5	11.6	10.2
1	11	-5	8.9	4.3
5	10	-5	27.1	26.7
2	11	-5	11.4	6.6
3	11	-5	11.5	10.8
0	0	-4	62.9	63.8
1	0	-4	29.2	29.4
2	0	-4	39.5	37.8
3	0	-4	45.4	47.1
4	0	-4	10.1	9.3
5	0	-4	103.1	106.8
7	0	-4	8.4	7.9
8	0	-4	15.9	17.0
9	0	-4	27.5	27.4
10	0	-4	12.2	12.8
1	1	-4	47.7	47.6
2	1	-4	56.5	56.3
3	1	-4	6.7	3.2
4	1	-4	37.0	33.9
7	1	-4	28.0	28.7
9	1	-4	14.5	12.6
10	1	-4	23.6	22.7
1	2	-4	53.1	54.0
2	2	-4	16.2	15.1
3	2	-4	36.4	37.8
4	2	-4	99.6	99.0
5	2	-4	51.0	51.3
6	2	-4	25.9	24.2
7	2	-4	27.0	25.6
8	2	-4	17.7	18.5
0	3	-4	40.7	41.8
1	3	-4	67.2	69.9
2	3	-4	33.6	34.5
3	3	-4	76.2	76.9
4	3	-4	80.4	82.5
6	3	-4	46.6	48.1
7	3	-4	69.5	65.5
8	3	-4	21.1	20.5
9	3	-4	17.6	16.9
10	3	-4	32.5	33.6
0	4	-4	36.3	34.7
1	4	-4	71.2	70.7
2	4	-4	10.3	5.7
3	4	-4	36.8	36.1
4	4	-4	24.6	23.6
5	4	-4	7.2	5.0
6	4	-4	9.2	9.3
8	4	-4	10.5	12.7
0	5	-4	26.8	27.0
1	5	-4	67.3	70.8
2	5	-4	60.4	61.7
3	5	-4	33.8	33.3
4	5	-4	20.9	20.0
5	5	-4	28.5	28.9
6	5	-4	12.6	10.1
7	5	-4	34.6	34.5
8	5	-4	31.5	31.0
0	6	-4	13.8	17.6
1	6	-4	36.9	38.5
2	6	-4	31.4	32.9
3	6	-4	56.3	59.1
5	6	-4	27.0	27.5
6	6	-4	28.8	28.2
8	6	-4	21.9	21.6
9	6	-4	29.8	28.4
0	7	-4	7.8	5.3
2	7	-4	11.1	11.6
5	7	-4	14.5	14.2
0	8	-4	8.4	7.9
1	8	-4	31.4	30.8
2	8	-4	61.3	62.5
3	8	-4	25.3	26.5
4	8	-4	12.2	11.1
5	8	-4	50.8	52.0
6	8	-4	19.2	18.5
7	8	-4	8.8	6.9
8	8	-4	32.7	31.7
0	9	-4	24.4	25.3
1	9	-4	47.8	50.0
2	9	-4	12.7	12.6
3	9	-4	35.7	36.7
4	9	-4	26.9	26.9
6	9	-4	11.7	10.4
7	9	-4	27.5	26.3
1	10	-4	27.5	30.8
6	10	-4	11.4	8.2
0	11	-4	28.8	29.8
1	11	-4	34.1	34.3
2	11	-4	11.7	8.7
3	11	-4	39.5	40.0
4	11	-4	31.2	31.7
1	1	-3	56.4	55.4
3	1	-3	132.7	143.7
4	1	-3	52.9	52.4
5	1	-3	22.8	23.7
6	1	-3	51.8	51.8
7	1	-3	49.5	49.5
8	1	-3	14.8	13.6
9	1	-3	38.9	38.7
10	1	-3	42.2	43.3
0	2	-3	34.6	34.7
1	2	-3	81.2	86.6
2	2	-3	120.4	143.8
3	2	-3	29.8	29.3
4	2	-3	10.3	8.3
5	2	-3	76.-	77.9
6	2	-3	32.3	31.8
7	2	-3	10.9	9.8
8	2	-3	23.3	23.7
9	2	-3	21.8	21.3
0	3	-3	19.7	21.7
1	3	-3	96.0	103.0
2	3	-3	47.1	47.8
3	3	-3	28.3	26.4
4	3	-3	17.3	16.9
5	3	-3	37.3	37.8
6	3	-3	19.6	19.2
8	3	-3	20.6	21.5
10	3	-3	10.0	7.2
1	4	-3	72.8	77.0
2	4	-3	70.7	74.3
4	4	-3	59.8	60.1
5	4	-3	42.4	43.4
6	4	-3	35.8	34.9
7	4	-3	29.5	29.8
8	4	-3	31.3	31.2
9	4	-3	33.7	34.0
10	4	-3	10.2	10.7
0	5	-3	34.8	35.6
1	5	-3	58.5	57.3
2	5	-3	87.4	89.7
3	5	-3	21.7	22.1
4	5	-3	17.5	17.9
5	5	-3	18.6	19.1
6	5	-3	37.0	38.0
7	5	-3	17.8	17.5
8	5	-3	12.6	11.3
9	5	-3	24.4	22.7
0	6	-3	23.4	22.1
1	6	-3	43.4	44.1
2	6	-3	15.0	14.6
3	6	-3	13.9	12.5
4	6	-3	22.4	22.3
5	6	-3	24.2	23.0
8	6	-3	26.4	26.1
9	6	-3	16.3	16.5
0	7	-3	54.0	55.8
1	7	-3	7.6	5.8
2	7	-3	20.1	21.0
3	7	-3	46.3	46.1
4	7	-3	8.6	9.2
6	7	-3	29.1	28.8
7	7	-3	38.7	38.1
8	7	-3	9.9	11.1
0	8	-3	23.4	22.2
1	8	-3	9.5	10.2
2	8	-3	23.7	23.8
6	8	-3	13.4	12.0
7	8	-3	10.7	12.5
0	9	-3	31.1	32.3
2	9	-3	44.6	45.4
3	9	-3	25.4	26.4
4	9	-3	31.7	30.7
5	9	-3	8.9	8.4
6	9	-3	15.7	14.5
7	9	-3	18.0	16.0
1	10	-3	39.8	41.8
2	10	-3	35.2	35.6
3	10	-3	16.6	17.0
4	10	-3	25.3	26.1
5	10	-3	20.0	19.1
0	11	-3	9.8	5.7
3	11	-3	9.0	4.5
4	11	-3	15.3	13.7
2	0	-2	117.2	121.8
3	0	-2	61.1	60.8
4	0	-2	123.4	126.2
5	0	-2	67.1	67.3
6	0	-2	32.3	32.0
7	0	-2	22.1	22.7
8	0	-2	37.1	37.7
10	0	-2	19.5	18.5
0	1	-2	50.5	51.0
1	1	-2	21.3	20.0
2	1	-2	14.5	14.5
3	1	-2	79.3	79.1
4	1	-2	67.9	67.5
5	1	-2	22.5	21.3
6	1	-2	32.6	32.5
8	1	-2	9.8	8.1
9	1	-2	15.8	14.7
10	1	-2	19.0	20.7
0	2	-2	97.4	114.0
1	2	-2	72.8	76.2
3	2	-2	117.7	123.5
4	2	-2	94.0	93.2
5	2	-2	16.8	15.5
6	2	-2	32.7	32.4
7	2	-2	13.2	13.4
10	2	-2	24.0	24.4
0	3	-2	35.6	37.0
1	3	-2	81.3	88.1
2	3	-2	30.5	29.8
3	3	-2	53.1	53.5
4	3	-2	36.3	34.5
5	3	-2	60.8	61.4
6	3	-2	42.8	43.8
7	3	-2	25.7	26.8
8	3	-2	27.6	29.0
9	3	-2	23.6	24.3
10	3	-2	28.3	29.7
0	4	-2	36.7	38.5
1	4	-2	14.7	14.8
3	4	-2	71.5	70.5
4	4	-2	27.6	27.0
5	4	-2	29.3	27.8
6	4	-2	19.3	17.7
7	4	-2	20.9	20.1
9	4	-2	10.5	7.2
10	4	-2	12.7	13.5
0	5	-2	63.0	65.9
1	5	-2	14.2	15.7
2	5	-2	29.0	28.5
3	5	-2	59.7	60.2
4	5	-2	25.2	24.2
5	5	-2	23.3	24.0
6	5	-2	50.9	53.1
7	5	-2	41.7	42.3
8	5	-2	13.7	11.2
9	5	-2	33.3	33.8
0	6	-2	33.8	34.9
5	6	-2	36.2	36.4
6	6	-2	27.3	27.8
7	6	-2	51.3	53.6
8	6	-2	37.9	38.6
0	7	-2	15.6	11.1
1	7	-2	12.2	9.7
2	7	-2	27.4	26.4
6	8	-2	30.4	29.2
1	8	-2	29.4	30.0
2	8	-2	11.5	12.3
3	8	-2	29.4	30.5
4	8	-2	10.0	9.3
5	8	-2	30.2	31.8
7	8	-2	32.0	31.9
8	8	-2	37.5	37.0
0	9	-2	37.3	38.3
2	9	-2	28.4	29.0
3	9	-2	31.1	30.8
5	9	-2	16.0	16.7
6	9	-2	20.1	20.6
7	9	-2	15.3	15.0
0	10	-2	16.5	14.3
1	10	-2	14.4	14.0
2	10	-2	19.6	22.7
5	10	-2	19.2	20.1
0	11	-2	27.2	28.3
2	11	-2	31.1	31.0
3	11	-2	28.6	27.7
4	11	-2	24.0	23.0
1	1	-1	53.5	55.0
2	1	-1	89.7	90.6
3	1	-1	42.8	44.6
4	1	-1	22.0	20.5
5	1	-1	70.2	70.1
6	1	-1	17.7	18.6
7	1	-1	19.3	18.5
9	1	-1	48.4	49.2
10	1	-1	26.4	27.8
1	2	-1	102.3	106.6
2	2	-1	113.6	120.9
3	2	-1	44.6	45.6
4	2	-1	88.7	90.6
5	2	-1	30.8	29.4
6	2	-1	37.1	37.6
7	2	-1	9.9	11.3
8	2	-1	22.6	23.3
1	3	-1	30.2	29.3
2	3	-1	38.7	35.7
3	3	-1	32.1	31.4
4	3	-1	17.1	15.8
6	3	-1	38.9	38.9

Table 4. (Continued)

H	K	L	F_o	F_c
7	3	-1	36.4	37.7
8	3	-1	17.7	17.7
9	3	-1	13.1	13.3
1	4	-1	39.4	41.5
2	4	-1	20.3	19.9
3	4	-1	33.9	34.4
4	4	-1	68.2	69.9
5	4	-1	18.2	18.3
7	4	-1	23.6	22.9
8	4	-1	33.5	32.6
10	4	-1	14.3	14.9
1	5	-1	39.3	39.4
2	5	-1	56.2	54.1
3	5	-1	28.0	28.8
4	5	-1	28.1	28.0
5	5	-1	43.2	44.7
6	5	-1	14.9	13.0
7	5	-1	25.7	24.7
8	5	-1	31.8	32.4
9	5	-1	12.8	11.5
0	6	-1	20.9	19.6
1	6	-1	13.7	16.4
2	6	-1	22.5	22.6
3	6	-1	28.3	27.1
4	6	-1	43.0	43.4
5	6	-1	10.6	9.9
7	6	-1	39.0	39.2
8	6	-1	17.3	15.4
0	7	-1	26.0	24.8
1	7	-1	24.1	23.8
2	7	-1	94.7	96.8
3	7	-1	48.4	48.9
5	7	-1	47.9	48.5
6	7	-1	53.0	54.1
7	7	-1	13.4	15.0
8	7	-1	29.7	30.5
1	8	-1	26.3	25.2
2	8	-1	23.5	21.6
4	8	-1	44.7	44.9
5	8	-1	12.8	13.0
8	8	-1	14.2	13.6
0	9	-1	8.0	6.6
1	9	-1	28.6	29.0
2	9	-1	34.2	34.6
3	9	-1	20.7	20.0
6	9	-1	14.6	13.8
7	9	-1	14.7	10.3
0	10	-1	16.7	15.8
1	10	-1	11.4	9.9
2	10	-1	12.3	13.3
3	10	-1	26.2	25.1
4	10	-1	20.1	20.6
5	10	-1	9.5	7.4
6	10	-1	14.0	13.0
4	11	-1	11.7	11.3
2	0	0	113.9	120.1
3	0	0	147.7	168.2
4	0	0	46.2	48.2
6	0	0	74.9	79.8
7	0	0	57.1	57.8
8	0	0	20.3	28.4
10	0	0	53.9	54.2
2	1	0	38.3	36.4
3	1	0	16.6	16.7
5	1	0	46.5	46.9
6	1	0	12.6	14.3
8	1	0	39.3	39.6
9	1	0	17.6	18.5
1	2	0	50.5	47.4
2	2	0	83.6	86.3
3	2	0	30.1	30.3
4	2	0	41.6	41.4
6	2	0	22.4	21.6
7	2	0	33.2	33.3
9	2	0	15.2	19.6
10	2	0	24.9	26.0
1	3	0	56.9	56.5
2	3	0	8.9	7.2
3	3	0	20.9	23.0
4	3	0	29.7	30.4
5	3	0	16.7	17.5
6	3	0	45.4	47.1
7	3	0	13.8	12.8
8	3	0	31.6	32.7
9	3	0	32.9	34.0
0	4	0	40.8	42.2
1	4	0	8.4	9.6
2	4	0	8.1	7.2
3	4	0	10.1	9.3
4	4	0	12.2	13.0
5	4	0	11.1	8.3
6	4	0	13.9	12.1
1	5	0	18.7	19.7
2	5	0	75.6	76.8

H	K	L	F_o	F_c
3	5	0	26.1	26.1
4	5	0	29.9	29.8
5	5	0	58.8	60.7
6	5	0	45.2	46.6
8	5	0	32.1	33.1
9	5	0	16.2	15.6
0	6	0	28.9	29.4
1	6	0	11.2	13.4
2	6	0	23.4	23.0
3	6	0	56.5	56.2
4	6	0	60.6	61.3
6	6	0	10.2	8.2
7	6	0	30.3	32.4
8	6	0	11.5	12.9
9	6	0	9.7	8.7
1	7	0	17.6	16.7
2	7	0	27.6	28.0
3	7	0	9.1	7.7
4	7	0	20.5	20.3
5	7	0	11.2	12.0
0	8	0	11.1	12.8
1	8	0	12.9	13.6
3	8	0	48.5	49.5
4	8	0	25.2	25.7
6	8	0	21.4	21.0
7	8	0	21.9	20.4
2	9	0	20.2	19.8
3	9	0	18.3	17.5
4	9	0	13.7	12.0
5	9	0	20.3	20.3
6	9	0	16.5	16.1
0	10	0	11.8	9.4
1	10	0	11.5	15.4
3	10	0	10.2	10.8
4	10	0	12.2	12.5
1	11	0	23.9	23.6
2	11	0	40.9	41.8
3	11	0	9.3	8.0
4	11	0	10.7	11.5
1	1	1	96.7	100.5
2	1	1	44.9	42.4
3	1	1	29.5	27.7
4	1	1	9.2	11.1
5	1	1	73.7	74.6
6	1	1	13.2	14.0
7	1	1	23.0	24.2
8	1	1	36.9	38.9
9	1	1	14.8	12.8
0	2	1	96.2	103.6
1	2	1	25.8	24.4
3	2	1	10.2	9.0
4	2	1	69.3	69.1
5	2	1	14.2	14.4
6	2	1	67.8	69.3
7	2	1	27.4	27.9
8	2	1	9.4	9.3
9	2	1	25.2	25.7
10	2	1	15.5	12.7
0	3	1	92.2	103.8
1	3	1	6.2	6.1
3	3	1	34.6	33.9
5	3	1	16.3	16.8
6	3	1	37.0	37.7
1	4	1	56.1	55.8
2	4	1	79.3	80.5
3	4	1	32.6	32.2
4	4	1	74.2	76.3
5	4	1	36.6	37.1
6	4	1	33.6	33.1
7	4	1	25.7	25.4
8	4	1	15.8	15.7
9	4	1	9.6	10.2
1	5	1	10.6	10.6
2	5	1	42.6	40.3
3	5	1	8.9	10.1
4	5	1	42.4	42.2
5	5	1	43.3	43.3
6	5	1	22.0	22.3
7	5	1	15.6	13.4
8	5	1	32.7	32.7
9	5	1	16.8	18.0
0	6	1	19.6	19.6
2	6	1	18.7	18.9
3	6	1	58.3	59.3
4	6	1	17.7	19.0
5	6	1	9.2	8.2
6	6	1	32.6	34.3
9	6	1	9.8	10.3
0	7	1	24.1	24.8
1	7	1	80.1	81.3
2	7	1	77.6	78.1
3	7	1	15.9	14.4
4	7	1	102.2	107.5
5	7	1	43.2	44.6

H	K	L	F_o	F_c
6	7	1	16.1	15.3
7	7	1	23.1	23.3
8	7	1	36.4	36.3
0	8	1	9.0	6.6
2	8	1	18.4	19.3
3	8	1	18.9	18.6
4	8	1	25.7	25.8
5	8	1	9.0	1.6
7	8	1	9.3	9.5
1	9	1	8.3	7.6
2	9	1	51.9	51.6
3	9	1	11.7	12.2
4	9	1	26.5	25.0
6	9	1	12.2	11.2
0	10	1	15.3	15.8
1	10	1	12.4	11.3
3	10	1	27.3	27.9
4	10	1	11.6	10.8
4	11	1	10.9	8.3
2	0	2	100.4	102.3
3	0	2	84.3	88.6
4	0	2	28.1	26.3
5	0	2	72.4	71.8
6	0	2	123.7	130.9
8	0	2	16.9	16.4
9	0	2	36.2	37.3
10	0	2	12.4	10.7
0	1	2	53.0	51.0
2	1	2	93.8	97.4
3	1	2	14.7	13.3
5	1	2	11.9	10.9
7	1	2	24.1	25.0
9	1	2	18.2	19.5
0	2	2	106.5	114.0
1	2	2	36.7	35.0
2	2	2	74.9	70.9
3	2	2	53.9	53.8
4	2	2	12.7	12.4
5	2	2	27.8	27.0
6	2	2	53.2	53.8
7	2	2	33.5	33.5
8	2	2	17.9	18.0
10	2	2	16.3	16.6
0	3	2	37.7	37.0
1	3	2	20.2	20.1
2	3	2	35.2	33.0
3	3	2	13.4	12.8
4	3	2	27.2	27.0
5	3	2	58.4	59.0
6	3	2	21.9	20.9
7	3	2	26.9	26.8
8	3	2	31.8	32.4
9	3	2	18.1	17.4
10	3	2	20.9	19.4
0	4	2	38.6	38.5
1	4	2	25.0	23.6
2	4	2	15.2	11.2
3	4	2	33.0	31.3
7	4	2	14.3	14.6
8	4	2	10.2	9.1
0	5	2	68.8	65.9
1	5	2	76.3	73.3
2	5	2	23.9	22.4
3	5	2	41.1	38.7
4	5	2	67.2	67.5
5	5	2	27.0	27.7
7	5	2	17.3	16.8
8	5	2	28.5	28.2
9	5	2	10.3	6.8
0	6	2	36.9	34.9
1	6	2	9.6	7.8
2	6	2	96.7	96.0
3	6	2	76.0	74.7
4	6	2	7.7	6.8
5	6	2	28.7	28.6
7	6	2	10.2	9.4
0	7	2	12.5	11.1
1	7	2	18.5	17.9
2	7	2	16.9	15.7
3	7	2	16.6	14.8
4	7	2	16.7	16.7
6	7	2	9.6	9.4
0	8	2	30.0	29.2
1	8	2	13.2	8.5
2	8	2	47.8	48.1
3	8	2	62.2	63.3
5	8	2	24.3	24.3
6	8	2	17.7	19.6
7	8	2	12.9	12.8
0	9	2	39.3	38.3
1	9	2	37.4	37.0
2	9	2	10.9	9.6
3	9	2	27.8	27.0
4	9	2	24.5	23.0

Table 4. (Continued)

H	K	L	F_o	F_c
1	10	2	13.9	12.1
0	11	2	29.4	28.3
1	11	2	28.4	27.6
3	11	2	16.2	16.1
1	1	3	115.2	124.6
2	1	3	7.7	8.4
4	1	3	69.9	65.4
5	1	3	29.2	30.5
6	1	3	45.6	45.7
7	1	3	67.0	70.1
8	1	3	17.5	16.9
10	1	3	22.5	23.0
0	2	3	36.7	34.7
1	2	3	140.1	142.3
2	2	3	45.6	45.8
3	2	3	10.2	10.4
4	2	3	38.9	37.9
5	2	3	70.8	72.5
6	2	3	28.5	29.1
8	2	3	20.7	20.9
9	2	3	18.8	18.9
0	3	3	22.4	21.7
1	3	3	10.2	12.3
2	3	3	26.7	24.2
3	3	3	28.0	28.4
4	3	3	24.1	23.1
9	3	3	13.2	14.6
1	4	3	63.0	60.1
2	4	3	57.9	58.8
3	4	3	54.7	51.4
5	4	3	34.9	35.4
6	4	3	27.6	26.3
7	4	3	12.3	10.2
8	4	3	24.7	24.3
9	4	3	23.8	25.1
0	5	3	37.3	35.6
1	5	3	81.2	77.6
2	5	3	35.0	33.8
3	5	3	22.0	22.7
4	5	3	52.8	52.4
5	5	3	27.4	26.3
6	5	3	31.9	32.3
7	5	3	18.2	17.9
8	5	3	13.9	14.7
0	6	3	24.8	22.1
2	6	3	53.2	52.0
3	6	3	13.5	12.6
4	6	3	36.6	35.8
5	6	3	18.1	18.5
7	6	3	9.1	2.9
8	6	3	11.1	9.9
0	7	3	56.9	55.8
1	7	3	31.7	31.6
2	7	3	11.6	9.7
3	7	3	46.0	44.8
4	7	3	53.6	52.4
5	7	3	19.2	20.9
6	7	3	18.9	19.4
7	7	3	37.7	38.0
8	7	3	14.9	15.8
0	8	3	23.5	22.2
1	8	3	28.3	27.6
3	8	3	13.4	12.7
4	3	3	39.4	38.6
7	8	3	17.5	17.7
0	9	3	33.4	32.3
1	9	3	33.0	31.4
3	9	3	30.9	30.7
4	9	3	29.5	29.3
5	9	3	16.3	16.1
6	9	3	12.4	8.6
1	10	3	24.6	24.3
2	10	3	12.4	12.3
3	10	3	19.8	19.9
5	10	3	9.5	8.7
1	11	3	10.2	13.5
1	0	4	36.1	33.9
2	0	4	84.8	81.3
3	0	4	37.9	38.4
4	0	4	44.6	43.8
5	0	4	107.3	110.3
6	0	4	42.9	43.1
7	0	4	16.8	18.4
8	0	4	24.6	24.9
9	0	4	22.8	21.9
1	1	4	48.3	46.4
2	1	4	16.3	14.9
3	1	4	63.4	64.7
5	1	4	36.3	36.9
7	1	4	11.1	12.5
8	1	4	9.3	9.9
1	2	4	12.1	12.1
2	2	4	128.6	127.2
3	2	4	52.9	49.4
4	2	4	38.2	38.6
5	2	4	51.9	52.5
6	2	4	16.4	17.6
7	2	4	9.2	10.6
8	2	4	11.2	13.4
9	2	4	11.7	11.1
0	3	4	44.1	41.8
1	3	4	76.4	71.6
2	3	4	60.1	58.8
3	3	4	68.8	65.7
4	3	4	14.7	15.6
6	3	4	37.9	38.4
7	3	4	20.9	21.5
5	4	4	23.5	24.1
8	3	4	17.0	17.4
9	3	4	9.5	4.9
0	4	4	38.8	34.7
1	4	4	26.8	22.1
2	4	4	15.3	14.0
3	4	4	17.1	15.2
4	4	4	11.5	13.4
6	4	4	10.2	10.5
7	4	4	21.8	22.3
8	4	4	16.3	16.6
0	5	4	28.2	27.6
1	5	4	13.2	11.0
2	5	4	12.3	12.0
3	5	4	56.4	54.7
5	5	4	12.7	14.1
6	5	4	13.0	10.7
7	5	4	18.0	17.5
0	6	4	17.5	17.6
1	6	4	41.6	39.8
2	6	4	62.8	61.5
3	6	4	19.1	18.6
5	6	4	58.6	58.4
6	6	4	10.0	9.6
7	6	4	24.0	25.9
8	6	4	24.3	25.6
1	7	4	21.6	20.7
3	7	4	8.7	8.2
4	7	4	10.1	11.0
5	7	4	10.0	7.8
8	7	4	23.9	23.0
7	7	4	13.3	12.2
0	8	4	9.3	7.9
1	8	4	47.8	46.6
2	8	4	16.2	16.3
3	8	4	16.7	16.8
6	8	4	14.8	14.5
7	8	4	9.9	9.9
0	9	4	27.1	25.3
2	9	4	22.0	22.0
3	9	4	36.4	34.6
4	9	4	13.1	12.5
5	9	4	18.1	17.6
6	9	4	26.9	26.3
0	10	4	11.7	8.8
1	10	4	18.2	19.0
2	10	4	10.3	8.1
4	10	4	16.6	15.9
0	11	4	29.5	29.8
1	11	4	11.3	13.4
2	11	4	13.1	12.6
3	11	4	31.2	29.1
1	1	5	13.4	10.8
2	1	5	31.9	33.3
3	1	5	42.0	41.9
4	1	5	12.9	14.1
5	1	5	32.6	32.2
6	1	5	47.9	49.7
7	1	5	48.9	51.0
9	1	5	26.4	25.6
0	2	5	13.3	12.0
1	2	5	141.3	137.5
2	2	5	44.9	41.2
3	2	5	62.8	58.8
4	2	5	48.5	47.8
5	2	5	12.1	9.5
6	2	5	15.2	15.1
7	2	5	25.4	26.2
1	3	5	33.1	30.0
2	3	5	48.9	45.2
3	3	5	50.6	48.2
4	3	5	8.1	6.7
5	3	5	25.8	26.3
6	3	5	15.1	15.7
7	3	5	12.8	11.8
9	3	5	18.6	17.5
0	4	5	83.7	82.7
1	4	5	142.3	137.5
2	4	5	77.2	74.4
3	4	5	61.1	58.2
4	4	5	37.5	37.1
5	4	5	38.6	34.3
6	4	5	8.3	3.4
7	4	5	23.9	23.1
8	4	5	31.8	32.7
9	4	5	21.2	19.6
0	5	5	74.5	72.7
2	5	5	35.0	32.9
3	5	5	28.6	27.2
4	5	5	29.0	28.6
6	5	5	28.0	28.5
7	5	5	20.3	18.9
8	5	5	12.9	10.8
1	6	5	43.9	42.9
2	6	5	35.1	34.5
4	6	5	43.6	42.6
5	6	5	22.8	22.4
7	6	5	24.0	22.4
8	6	5	30.5	31.1
0	7	5	36.5	34.7
2	7	5	26.9	25.9
3	7	5	50.3	50.3
4	7	5	20.9	20.9
5	7	5	10.0	9.9
7	7	5	17.9	15.6
1	8	5	29.1	28.1
2	8	5	16.7	17.5
4	8	5	15.0	14.8
0	9	5	20.8	19.5
2	9	5	28.5	27.5
3	9	5	28.8	26.9
4	9	5	19.6	20.4
0	10	5	16.5	14.0
1	10	5	18.5	17.5
2	10	5	21.0	20.3
3	10	5	10.4	8.6
4	10	5	26.1	25.4
0	11	5	9.4	6.2
1	11	5	12.6	10.2
0	0	6	84.8	89.3
1	0	6	61.7	62.7
2	0	6	9.3	3.8
3	0	6	31.9	31.1
4	0	6	51.3	53.0
5	0	6	39.7	40.1
6	0	6	13.4	13.3
7	0	6	50.8	50.5
9	0	6	14.9	16.1
0	1	6	67.0	65.2
1	1	6	29.2	27.3
2	1	6	85.7	87.8
3	1	6	30.6	29.4
4	1	6	18.8	19.3
5	1	6	41.2	41.5
6	1	6	34.0	34.6
8	1	6	22.7	23.8
9	1	6	12.7	11.7
0	2	6	61.0	56.5
1	2	6	33.7	31.9
2	2	6	75.5	70.9
4	2	6	25.5	26.2
5	2	6	39.0	38.1
6	2	6	15.4	18.8
7	2	6	22.7	22.5
8	2	6	24.7	24.6
0	3	6	34.7	35.5
1	3	6	75.8	70.4
2	3	6	82.0	79.8
3	3	6	10.5	12.5
5	3	6	38.6	39.6
6	3	6	55.3	55.7
8	3	6	18.8	17.7
9	3	6	23.6	21.7
0	4	6	16.2	11.8
1	4	6	12.0	8.9
2	4	6	26.9	24.5
3	4	6	17.6	16.2
4	4	6	22.3	22.5
5	4	6	43.9	43.1
8	4	6	23.8	23.1
0	5	6	36.2	34.0
1	5	6	18.8	16.8
2	5	6	20.1	19.1
3	5	6	24.4	24.9
5	5	6	31.2	30.3
6	5	6	16.1	15.6
8	5	6	13.5	11.1
0	6	6	19.3	21.8
1	6	6	33.5	31.2
2	6	6	32.4	31.2
4	6	6	23.4	22.4
5	6	6	38.8	37.0
7	6	6	32.1	31.3
0	7	6	12.7	10.8
1	7	6	22.4	21.2

Table 4. (Continued)

H	K	L	F_o	F_c
2	7	6	14.2	13.6
4	7	6	13.3	11.7
7	7	6	20.5	18.8
0	8	6	23.8	23.2
1	8	6	31.3	31.5
2	8	6	12.3	10.8
3	8	6	31.0	29.5
4	8	6	45.8	45.0
0	9	6	14.4	10.9
1	9	6	18.6	17.8
2	9	6	33.0	31.4
3	9	6	28.7	29.8
5	9	6	33.7	32.3
2	10	6	11.9	10.0
3	10	6	21.7	20.8
4	10	6	18.4	16.6
0	11	6	28.2	27.7
1	11	6	18.9	18.1
0	1	7	12.0	2.1
1	1	7	46.4	47.4
2	1	7	64.0	63.7
3	1	7	27.3	26.4
5	1	7	46.1	47.6
6	1	7	47.6	47.7
8	1	7	15.6	16.4
9	1	7	15.8	17.9
0	2	7	81.9	79.8
1	2	7	28.4	28.3
2	2	7	17.7	17.3
3	2	7	51.3	50.7
4	2	7	53.4	53.6
5	2	7	25.5	24.7
6	2	7	15.3	15.7
7	2	7	31.3	30.7
8	2	7	12.4	13.1
1	3	7	24.8	23.6
2	3	7	23.5	21.6
3	3	7	13.4	13.5
4	3	7	8.9	9.0
8	3	7	17.4	15.9
0	4	7	94.0	80.5
1	4	7	68.0	64.2
3	4	7	69.7	68.3
4	4	7	63.4	61.9
5	4	7	8.8	6.0
6	4	7	46.7	45.4
7	4	7	39.4	39.1
8	4	7	15.1	13.4
1	5	7	17.8	18.5
2	5	7	16.8	17.4
3	5	7	8.8	11.3
4	5	7	32.6	31.4
5	5	7	9.7	9.1
6	5	7	40.7	39.6
8	5	7	23.2	22.9
0	6	7	47.6	45.5
3	6	7	16.0	15.4
4	6	7	14.1	15.4
5	6	7	10.8	9.8
6	6	7	20.5	20.1
7	6	7	17.7	16.3
0	7	7	13.7	13.3
1	7	7	14.7	13.8
2	7	7	43.5	45.6
4	7	7	31.4	30.7
5	7	7	15.4	14.8
0	8	7	18.4	18.3
1	8	7	8.0	6.3
3	8	7	34.3	34.1
5	8	7	22.7	20.9
6	8	7	13.3	13.2
1	9	7	17.4	16.3
2	9	7	42.3	42.0
3	9	7	14.3	16.2
4	9	7	8.8	1.0
5	9	7	21.5	21.3
0	10	7	24.0	24.6
1	10	7	25.1	24.2
3	10	7	38.9	38.2
0	0	8	71.6	72.8
1	0	8	45.6	45.1
2	0	8	47.5	46.7
3	0	8	34.0	34.6
4	0	8	19.3	19.4
0	0	8	33.5	34.0
4	1	8	36.0	35.4
2	1	8	14.3	12.0
3	1	8	25.0	24.6
4	1	8	9.3	8.8
5	1	8	11.7	12.8
6	1	8	11.1	10.0
7	1	8	11.5	9.8
0	2	8	80.5	86.1
1	2	8	35.6	34.9
2	2	8	61.9	58.9
3	2	8	31.0	29.8
4	2	8	29.0	28.8
5	2	8	27.9	29.1
6	2	8	40.3	41.2
7	2	8	36.9	31.5
0	3	8	42.0	39.9
1	3	8	48.3	48.9
2	3	8	69.2	67.7
4	3	8	50.3	49.5
5	3	8	57.5	58.0
6	3	8	21.5	21.2
7	3	8	36.4	38.6
8	3	8	45.8	46.5
0	4	8	18.3	17.1
1	4	8	22.6	22.0
2	4	8	17.5	15.8
4	4	8	22.5	21.6
5	4	8	32.3	32.6
6	4	8	26.1	24.7
7	4	8	15.5	13.7
0	5	8	30.5	30.6
1	5	8	35.0	34.1
2	5	8	11.2	11.8
3	5	8	10.2	5.7
4	5	8	38.0	37.4
5	5	8	21.6	22.8
6	5	8	12.9	12.9
7	5	8	16.5	14.3
0	6	8	45.9	43.7
2	6	8	39.7	39.5
3	6	8	27.2	25.8
7	6	8	24.9	24.4
0	7	8	29.0	28.6
4	7	8	8.8	7.4
0	8	8	33.5	32.0
2	8	8	16.8	15.8
3	8	8	35.2	34.6
4	6	8	22.9	21.0
1	9	8	24.6	21.7
2	9	8	24.6	25.5
4	9	8	22.3	24.1
0	1	9	67.2	65.7
1	1	9	53.6	53.0
2	1	9	28.2	27.1
3	1	9	35.4	36.5
4	1	9	24.9	24.3
6	1	9	10.7	11.4
7	1	9	19.6	19.0
8	1	9	17.4	13.9
0	2	9	55.7	54.1
1	2	9	15.7	14.9
2	2	9	50.1	51.4
3	2	9	73.5	73.1
4	2	9	10.8	8.9
6	2	9	38.3	38.3
8	2	9	14.6	19.3
0	3	9	12.4	12.6
1	3	9	26.9	27.3
2	3	9	13.9	13.5
4	3	9	8.8	6.5
7	3	9	10.0	10.4
0	4	9	24.9	25.8
2	4	9	31.7	31.7
3	4	9	64.3	62.8
4	4	9	20.0	19.8
5	4	9	34.2	33.1
6	4	9	57.7	56.0
7	4	9	26.6	27.1
0	5	9	39.9	41.2
1	5	9	9.0	7.3
2	5	9	13.1	12.1
3	5	9	32.5	31.6
4	5	9	43.1	42.7
5	5	0	22.1	19.2
6	5	9	10.3	10.2
7	5	9	29.4	28.4
1	6	9	10.3	9.9
2	6	9	11.3	10.2
5	6	9	19.1	17.2
6	6	9	15.5	14.8
0	7	9	20.4	17.8
5	7	9	10.0	10.1
4	7	9	44.4	44.4
5	7	9	25.5	25.6
0	8	9	13.1	11.0
0	9	9	37.5	36.8
1	9	9	28.5	28.4
2	9	9	15.4	13.1
3	9	9	12.0	11.3
0	10	9	17.3	18.7
1	10	9	13.2	13.2
2	10	9	32.0	30.8
0	0	10	71.2	70.0
1	0	10	30.1	30.7
2	0	10	104.1	110.0
3	0	10	40.2	40.0
4	0	10	10.1	10.0
6	0	10	18.9	20.6
7	0	10	37.5	38.5
0	1	10	32.0	30.5
1	1	10	34.3	34.9
2	1	10	9.1	9.0
7	1	10	19.3	19.2
0	2	10	36.9	36.3
1	2	10	41.2	41.0
2	2	10	75.7	76.1
3	2	10	30.5	31.9
4	2	10	48.4	47.6
5	2	10	30.5	31.0
6	2	10	21.7	21.4
0	3	10	60.0	61.0
1	3	10	67.5	68.5
2	3	10	25.3	25.6
3	3	10	44.9	44.6
4	3	10	41.6	42.7
6	3	10	23.6	23.7
7	3	10	44.5	43.5
0	4	10	21.4	23.7
1	4	10	27.7	29.0
3	4	10	16.2	15.6
0	5	10	19.8	19.0
1	5	10	24.3	25.2
2	5	10	9.8	3.1
3	5	10	18.1	17.3
4	5	10	40.0	39.3
5	5	10	13.5	15.7
0	6	10	9.7	7.7
1	6	10	12.6	10.6
2	6	10	10.5	10.4
3	6	10	21.6	21.2
4	6	10	10.6	9.4
5	6	10	27.8	28.4
0	7	10	18.5	17.6
1	7	10	12.8	11.2
2	7	10	16.4	15.8
3	7	10	12.0	12.1
0	8	10	14.1	12.4
1	8	10	14.9	14.6
2	8	10	16.1	15.0
3	8	10	18.2	18.2
4	8	10	11.7	12.1
0	9	10	21.1	22.3
1	9	10	13.7	13.2
3	9	10	14.1	15.3
0	1	11	44.9	45.5
2	1	11	23.7	24.4
3	1	11	25.5	24.7
4	1	11	27.9	29.0
6	1	11	19.5	18.1
7	1	11	28.9	29.4
1	2	11	40.3	39.6
2	2	11	34.0	34.5
3	2	11	26.8	26.0
4	2	11	9.5	8.6
5	2	11	25.1	25.5
6	2	11	31.9	32.3
1	3	11	16.2	15.7
2	3	11	32.2	32.1
3	3	11	17.4	15.9
4	3	11	10.1	9.1
5	3	11	14.4	13.3
7	3	11	11.3	11.3
0	4	11	34.9	34.8
1	4	11	56.9	57.2
2	4	11	40.3	40.4
4	4	11	30.2	31.5
5	4	11	41.1	41.5
6	4	11	16.3	17.4
2	5	11	16.2	16.6
3	5	11	25.1	24.5
4	5	11	31.3	30.7
6	5	11	27.3	27.1
0	6	11	16.9	17.8
2	6	11	19.2	18.6
3	6	11	16.5	17.3
4	6	11	15.0	17.1
5	6	11	24.9	26.9
0	7	11	40.5	39.2
1	7	11	20.5	20.0
3	7	11	48.2	47.6
4	7	11	46.9	48.1
6	8	11	10.4	7.0
1	8	11	13.1	11.4
2	8	11	10.0	11.5
3	8	11	12.0	8.8
0	9	11	26.8	26.2
1	9	11	17.9	17.4

Table 4. (Continued)

H	K	L	F_o	F_c
2	4	11	14.5	13.2
1	0	12	94.0	97.2
2	0	12	39.2	40.6
3	0	12	32.5	32.7
4	0	12	47.6	48.0
5	0	12	44.7	44.3
6	0	12	17.1	17.4
0	1	12	27.3	26.5
2	1	12	14.5	14.8
3	1	12	15.3	18.3
5	1	12	0.3	4.3
6	1	12	21.7	21.2
0	2	12	43.6	44.9
1	2	12	24.3	25.5
2	2	12	21.8	22.9
5	2	12	23.5	24.3
0	3	12	37.0	37.3
2	3	12	26.8	26.1
3	3	12	32.4	31.9
5	3	12	32.7	32.3
6	3	12	17.5	16.8
1	4	12	9.5	9.8
2	4	12	10.8	9.2
3	4	12	13.6	14.9
4	4	12	18.0	18.5
0	5	12	36.0	35.9
1	5	12	14.9	16.0
2	5	12	23.7	25.6
3	5	12	52.2	51.6
4	5	12	29.5	29.1
1	6	12	32.2	32.7
2	6	12	19.3	18.1
4	6	12	32.7	32.9
5	6	12	28.9	27.4
0	8	12	13.7	9.3
1	8	12	29.6	29.0
3	8	12	20.5	19.8
0	9	12	21.0	20.3
1	1	13	38.2	38.4
2	1	13	26.9	26.7
3	1	13	15.3	13.5
5	1	13	38.7	38.8
6	1	13	31.1	31.5
0	2	13	24.8	25.6
1	2	13	67.5	70.3
2	2	13	19.3	18.8
3	2	13	28.2	28.3
4	2	13	37.5	37.8
5	2	13	20.7	20.2
0	3	13	38.3	38.9
1	3	13	50.7	53.6
5	3	13	10.5	8.1
0	4	13	34.1	34.1
1	4	13	39.2	39.5
2	4	13	19.5	18.7
3	4	13	29.7	30.2
4	4	13	22.4	22.2
5	4	13	18.5	20.0
0	5	13	23.9	23.8
2	5	13	21.3	21.4
0	6	13	15.5	17.2
1	6	13	14.4	15.1
4	6	13	20.1	19.9
0	7	13	27.5	28.0
1	7	13	16.4	15.6
2	7	13	43.4	43.6
3	7	13	26.6	25.0
0	8	13	14.9	14.8
1	8	13	16.9	16.6
0	0	14	57.2	57.4
1	0	14	21.3	21.1
2	0	14	10.2	6.8
3	0	14	23.6	23.0
4	0	14	51.6	52.9
5	0	14	8.7	8.4
0	1	14	29.3	29.7
1	1	14	11.9	10.7
2	1	14	19.5	19.3
4	1	14	10.3	8.7
5	1	14	14.2	14.3
0	2	14	22.4	21.4
2	2	14	15.3	13.6
4	2	14	24.5	23.5
0	3	14	20.1	20.2
1	3	14	18.7	19.3
2	3	14	19.8	19.4
3	3	14	16.3	14.4
5	3	14	20.2	20.8
2	4	14	24.9	23.3
3	4	14	16.5	15.9
4	5	14	13.3	13.4
1	5	14	35.1	35.2
2	5	14	37.4	38.2
3	5	14	13.2	14.0

H	K	L	F_o	F_c
0	6	14	60.2	60.5
1	6	14	17.6	16.6
2	6	14	15.3	15.2
3	6	14	37.4	36.2
0	7	14	10.6	5.6
0	8	14	22.0	22.2
0	1	15	13.3	9.1
1	1	15	50.3	50.8
2	1	15	37.8	36.9
3	1	15	13.0	12.5
4	1	15	25.2	25.3
0	2	15	28.1	28.6
1	2	15	19.9	19.0
2	2	15	42.3	42.3
3	2	15	29.7	29.9
4	2	15	14.3	14.0
0	3	15	18.5	17.5
1	3	15	14.6	13.3
2	3	15	22.9	23.5
3	3	15	14.4	15.9
0	4	15	34.6	35.6
1	4	15	28.6	27.5
2	4	15	10.4	8.8
3	4	15	25.5	26.2
4	4	15	31.4	30.3
0	5	15	10.5	10.0
1	5	15	12.1	13.4
2	5	15	15.2	13.6
3	5	15	15.4	14.6
0	6	15	28.1	27.9
1	7	15	25.9	26.2
0	0	16	22.7	23.0
1	0	16	14.4	14.8
2	0	16	63.2	64.5
3	0	16	23.1	23.5
1	1	16	18.2	19.3
3	1	16	11.5	8.3
4	1	16	15.3	15.2
0	2	16	29.6	29.7
1	2	16	11.7	7.8
2	2	16	24.1	23.2
3	2	16	19.8	19.9
0	3	16	22.4	23.9
1	3	16	21.5	22.1
2	3	16	11.2	12.7
3	3	16	18.5	14.6
0	4	16	13.6	14.1
1	4	16	9.8	10.5
2	4	16	15.4	14.6
0	5	16	29.8	29.9
1	5	16	22.3	20.8
0	6	16	34.9	35.2
0	1	17	19.4	19.3
1	1	17	45.6	46.9
3	1	17	26.4	24.9
0	2	17	15.4	12.5
2	2	17	23.5	23.8
0	3	17	15.9	16.3
1	3	17	14.6	15.7
0	4	17	16.8	15.1
1	4	17	16.2	14.9
1	0	18	22.4	22.1
2	0	18	58.3	59.8
0	1	18	6.7	5.8
1	2	18	19.2	19.4
0	3	18	18.4	21.2
1	3	18	16.4	17.4
0	1	19	15.2	16.3

A crystal measuring 0.10 mm x 0.15 mm x 0.49 mm was selected and mounted along its prismatic axis (0.49 mm) on a goniometer head. Zero level precession photographs revealed two zones 90° apart. The zero and upper level pictures at these two settings possessed vertical and horizontal mirror symmetry. For zero level pictures the odd reflections (2n + 1) were systematically absent along the horizontal axis. These findings indicated an orthorhombic crystal with a two fold screw axis along the mounting axis. Moreover for the (0kℓ) and (2kℓ) pictures the odd rows of reflections, (k = 2n + 1), were systematically absent while for the (1kℓ) the even rows of reflections, (k = 2n), were systematically absent. For the (h0ℓ) and (h2ℓ) pictures the odd rows of reflections, (h = 2n + 1), were systematically absent.

A second crystal of the same material was mounted with its long prismatic axis parallel to the direction of the incident x-ray beam. The zero level picture at that orientation possessed vertical and horizontal mirror symmetry and odd reflections (2n + 1) along the vertical and horizontal axes were systematically absent. Moreover the even reflections, (h = 2n), were systematically absent on odd rows of reflections, (k = 2n + 1), and the odd reflections, (h = 2n + 1), were systematically absent on the even rows, (k = 2n). Similar systematic absences were observed if columns, instead of rows, of reflections were considered.

The systematic absence may be summarized as follows,

(0, 0, ℓ): ℓ = 2n + 1, (0, k, 0): k = 2n + 1, (h, 0, 0): h = 2n + 1, (h, 0, ℓ): h = 2n + 1, (0, k, ℓ): k = 2n + 1, (h, k, 0): (h + k) = 2n + 1, and (h, k, ℓ): (h + k) = 2n + 1.

Since the crystal was of an optically active material the possibilities of a centro-symmetric space group or a glide plane were eliminated. The space group of the crystal was therefore identified, on the basis of symmetry, systematic absences and optical activity, as $C222_1$, #20 (46).

The unit cell parameters from film data were: a = 14.36(4)Å, b = 18.92(5)Å, c = 15.63(4)Å. The density of the material, determined by flotation, was found to be: d_{exp} = 1.93(3) g/cc. z was therefore calculated as 8. (An accurate value of d_{calc} is presented later.)

The crystal was then transferred to a Picker four-circle diffractometer and a working set of unit cell parameters was obtained by the refinement of fourteen individually centered reflections. The values obtained for the cell parameters* were: a = 14.334(3)Å, b = 18.880(4)Å and c =

*The crystal was mounted along its long axis (0.49 mm) and during data collection that axis had been arbitrarily called the b-axis. At that stage the crystal axes were referred to as a = 14.36Å, b = 15.63Å and c = 18.92Å based on a right-handed cartesian system. That nomenclature would have implied a b-centered orthorhombic lattice. Just after locating the Co and the Br atoms the order of the (k) and (ℓ) indices for all reflections, the (y) and (z) coordinates for all atoms and the (b) and (c) axes, were reversed to obtain the conventional C-centered orthorhombic lattice. Reversal of the order (i.e., exchange) of two axes implies a change to a left-handed cartesian coordinate system. Another reversal, or exchange, is necessary to keep the absolute configuration of the molecule unchanged with respect to the original right-handed cartesian

15.466(3)Å.

The optimum value for the takeoff angle was found to be 2.0° and ω-scans for three low angle reflections gave 0.05°, 0.07° and 0.06° for full widths at half maxima. These values, though a bit small, were still in the range for ideally imperfect mosaic crystals (40). Reflections were collected in one octant of reciprocal space between the limits: h = 0 to 16, k = 0 to 22 and ℓ = 0 to 18. Three axial reflections (2, 0, 0), (0, 6, 0) and (0, 0, 4) were scanned every 200 reflections to check for crystal orientation and systematic changes in intensity. Intensities for a total of 2205 reflections were collected. A plot of the net intensities of each of the standard reflections versus their ordinal numbers gave a 1% drop over the entire collection period. The intensitites for all reflections were corrected for background. They were then linearly scaled such that the intensity for the last collected reflection was increased by 1% while the intensity for the reflection measured first was left unchanged. Reflections were omitted if their corrected intensities were less than three times their corresponding standard deviations.

A total of 1265 reflections were retained after the

---

coordinate system. This was achieved by reversing the signs of the Miller indices for all reflections.

The exchange of two unit cell axes followed by a reversal of the signs of the Miller indices, (h, k, ℓ) to (-h, -k, -ℓ), would have no net effect on the absolute configuration of the molecule.

above screening. Lorentz and polarization corrections were then applied to those reflections and a three dimensional Patterson map was calculated, using all 1265 reflections. Solution of the Patterson yielded the coordinates of the heavy atoms, three of which were in general positions; one bromine was disordered and occupied two special positions, with half occupancy in each position. A difference Fourier electron density map, phased on the coordinates of the cobalt and bromine atoms, yielded the positions of the ligand atoms and the oxygen of a disordered water molecule.

Absorption corrections were then applied. The linear absorption coefficient was calculated to be 69.57 cm^{-1}. The crystal faces exposed were:(0,0,1), (0,0,$\bar{1}$), (1,1,0), ($\bar{1}$,$\bar{1}$,0) (1, $\bar{1}$, 0), and ($\bar{1}$, 1, 0). The diagram below illustrates the appearance of the crystal. The (0, 0, 16) reflection had

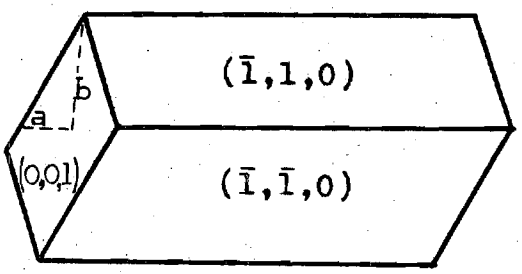

Figure 7. Crystal of $(-)_{589}$ $Co(C_2N_5H_7)_3Br_3 \cdot H_2O$.

the largest value of A* (Eq. 5), 2.7159 while the (1, 5, 6) reflection had the smallest value of A*, 1.840. The structure

was then given full matrix least squares refinement, isotropically and then anistropically, until shifts for all variables became small, $(\Delta/\sigma) << 0.5$. The values for the conventional R-factor and the weighted R-factor were 0.068 and 0.047 respectively. At this stage there were three ligand atoms that had negative anisotropic temperature factors.

A three dimensional model of the molecule was then constructed on a right-handed cartesian coordinate system. The configuration of the model was, Λ (lambda) or, a left-handed helix when viewed along its three fold axis.

In order to test the absolute configuration of the molecule, the signs of all the coordinates of the atoms were then reversed. The structure was given full matrix refinement, isotropically and then anisotropically, until the shifts of all variables became small $(\Delta/\sigma) << 0.5$. The values for the conventional R-factor and the weighted R-factor were 0.079 and 0.055 respectively. At that stage there were five ligand atoms with negative anisotropic temperature factors.

Application of the Hamilton (15) test to the results of the above refinements to determine the absolute configuration favored the Λ (lambda) isomer with a better-than-(99.5%) confidence level.

Therefore the absolute configurations of the (-) $(\text{negative})_{589}$ $Co(C_2N_5H_7)_3$ $Br_3 \cdot H_20$ isomer is, Λ (lambda) or, a left-handed helix, when viewed along the molecular three-

fold axis. These results are consistent with the findings of Snow (30) that the other enantiomer, $(+)_{589}Co(C_2N_5H_7)_3Cl_3 \cdot H_2O$ had a delta, (Δ), configuration when viewed along the molecular three-fold axis.

One suspected cause for negative anisotropic temperature factors was extinction. An investigation of the calculated (F_c) and observed (F_o) structure factors showed that forty-one low order and fairly intense reflections had consistently lower (F_o) values as compared with the corresponding (F_c) values. As pointed out before in this section the ω-scans for this crystal though in the range acceptable for ideally imperfect crystals, were low. Those reflections were therefore removed and isotropic refinement with the remaining 1193 reflections gave well behaved temperature factors for all atoms.

A third peak at special position (0, .16, .25) appeared to be an oxygen of the disordered water molecule. A refinement of the occupancy factors of the other two oxygen positions resulted in a 0.9 occupancy for both positions combined. The peak at (0, 0.16, 0.25) was therefore assigned a 0.1 occupancy, and an invariant isotropic temperature factor of 4.0; its y-coordinate was refined. The hydrogen atoms, except those for water, were then put in and given isotropic temperature factors of 4.0 or 5.0 as shown in the final list. Anisotropic refinement for the two stronger oxygen peaks and the non-hydrogen atoms was then performed but two ligand

atoms still had negative temperature factors. At that stage, these two atoms were reassigned their isotropic temperature factors and the structure was given full matrix refinement, varying scale factor, coordinates, and temperature factors, until the shifts of all variables became small, $(\Delta/\sigma) << 0.3$. The hydrogens were not included in those refinements. The resulting R-factors for the refinement were $R = 0.065$ and $R_w = 0.042$. The causes for the large anisotropic temperature factors of the ligand atoms are discussed in Chapter V.

A new crystal was then used on a syntex $P2_1$ automatic diffractometer to obtain a revised, and final, set of unit cell parameters. The same technique was used as described in the previous structure determination. The values obtained for the unit cell parameters were: $a = 14.362(4)\text{Å}$, $b = 18.918(7)\text{Å}$, $c = 15.630(4)\text{Å}$, Volume $= 4247(2)\text{Å}^3$, $d_{calc} = 1.94$ g/cc and $d_{exp} = 1.93(3)$ g/cc, by flotation.

Refinement was continued with those revised unit cell parameters but there was no significant change in the final R-values.

A final difference electron density map gave 1.00 $\bar{e}/\text{Å}^3$ for the height of the largest residual peak. Before the hydrogens were entered into the atoms list the largest peak was 1.37 $e/\text{Å}^3$. The first difference electron density map, phased with the coordinates of the cobalt and bromine atoms from the Patterson, gave 2.16 $e/\text{Å}^3$ for the weakest nonhydrogen

ligand atom.

Tables 5 and 6 give the final values for the coordinates and temperature factors of all atoms for one formula unit of the material. Table 7 lists the final values for the 1193 calculated (F_c) and observed (F_o) structure factors.

Crystallographic calculations were performed on a Univac 1108 computer. The programs, in the approximate order that they were used, are a modified version of Carter's program (47) for refining cell parameters and generating instruction cards for the settings on a Picker four circle diffractometer, Bertrand's program (48) for Lorentz and polarization correction, Zalkin's FORDAP program (49) for Fourier analysis, Busing, Levy and Martin's XFLS crystallographic least squares program (50), and ORFFE functions and errors program (51). The following programs were also used for further computations as needed: a modified version of Stewart's ABSORB, x-ray 70 (45) for x-ray absorption corrections, Johnson's ORTEP (52) for drawing crystal structure illustrations, and Bertrand and Kelley's program (53) for fitting least squares planes through a number of atoms.

Spectroscopic Experiments

General Description and Instrumentation

Three types of spectra were measured for the materials described in the previous sections visible and ultraviolet (Vis - UV), circular dichroism (C.D.) and optical rotatory

Table 5. Final Positional Parameters for $\Lambda Co(C_2N_5H_7)_3Br_3 \cdot H_2O$.

Atom	x	y	z
Br-1	0.2707(2)	0.2796(1)	0.2066(1)
Br-2	0.3544(2)	0.0341(1)	0.3253(2)
Br-3a	0.4355(2)	0.0000	0.0000
Br-3b	0.0000	0.0331(2)	0.2500
Co	0.0455(2)	0.1774(1)	-0.0069(2)
N-1a	-0.0121(10)	0.2367(7)	-0.0891(9)
N-2a	-0.0616(13)	0.3435(8)	-0.1533(11)
C-1a	-0.0132(13)	0.3058(9)	-0.0983(12)
N-3a	0.0374(12)	0.3439(7)	-0.0399(13)
C-2a	0.0929(14)	0.3223(10)	0.0216(12)
N-4a	0.1369(13)	0.3776(7)	0.0658(12)
N-5a	0.1058(9)	0.2574(7)	0.0435(9)
N-1b	-0.0206(11)	0.0982(8)	-0.0573(11)
N-2b	-0.1448(12)	0.0356(8)	-0.1021(11)
C-1b	-0.1053(16)	0.0859(10)	-0.0569(15)
N-3b	-0.1637(9)	0.1192(7)	0.0033(12)
C-2b	-0.1370(15)	0.1630(9)	0.0679(13)
N-4b	-0.2068(11)	0.1747(10)	0.1258(12)
N-5b	-0.0573(12)	0.1967(8)	0.0691(10)
N-1c	0.1515(12)	0.1617(8)	-0.0797(10)
N-2c	0.3031(15)	0.1346(10)	-0.1149(14)
C-1c	0.2299(19)	0.1343(12)	-0.0646(16)
N-3c	0.2467(11)	0.1026(9)	0.0129(12)
C-2c	0.1830(18)	0.0924(11)	0.0809(16)
N-4c	0.2170(14)	0.0492(12)	0.1431(12)
N-5c	0.1038(14)	0.1177(9)	0.0751(11)
O-b1	0.0000	0.2655(14)	0.2500
O-b2	0.0000	0.4128(14)	0.2500
O-b3	0.0000	0.1567(49)	0.2500

Table 5. (Continued)

Atom	x	y	z	B
H-1a	-0.050	0.215	-0.131	4.0
H-2a1	-0.055	0.391	-0.169	5.0
H-2a2	-0.110	0.327	-0.194	5.0
H-3a	0.027	0.392	-0.052	5.0
H-4a1	0.161	0.371	0.116	5.0
H-4a2	0.108	0.422	0.037	5.0
H-5a	0.142	0.247	0.079	4.0
H-1b	0.004	0.080	-0.091	5.0
H-2b1	-0.211	0.024	-0.107	5.0
H-2b2	-0.117	0.012	-0.148	5.0
H-3b	-0.227	0.111	-0.005	5.0
H-4b1	-0.180	0.197	0.170	5.0
H-4b2	-0.224	0.142	0.116	5.0
H-5b	-0.046	0.209	0.113	4.0
H-1c	0.144	0.172	-0.118	4.0
H-2c1	0.348	0.100	-0.113	5.0
H-2c2	0.295	0.140	-0.175	5.0
H-3c	0.294	0.081	0.024	5.0
H-4c1	0.181	0.047	0.195	5.0
H-4c2	0.277	0.037	0.154	5.0
H-5c	0.067	0.110	0.114	4.0

The isotropic temperature factor of an atom, in $\mathring{A}^2$, is given by the expression, $\exp[-\frac{B}{4}(\frac{2\sin\theta_{hk\ell}}{\lambda})^2]$. Values of B are given in Tables 2 and 5.

Table 6. Final Anisotropic Thermal Parameters for $\Lambda Co(C_2N_5H_7)_3Br_3 \cdot H_2O$. (Parameters x 10^4).

Atom	β_{11}	β_{22}	β_{33}	β_{12}	β_{13}	β_{23}
Br-1	44(1)	34(1)	24(1)	6(1)	3(1)	0(1)
Br-2	40(1)	23(1)	57(1)	-1(1)	-7(1)	6(1)
Br-3a	28(2)	22(1)	73(2)	000	000	-1(1)
Br-3b	43(2)	42(1)	30(2)	000	2(2)	000
Co	25(1)	12(1)	22(1)	0(1)	0(1)	0(1)
N-1a	31(9)	12(4)	29(7)	3(5)	-10(7)	10(5)
N-2a	50(10)	24(6)	38(9)	9(67)	-32(9)	4(6)
C-1a	B = 2.13(36)					
N-3a	42(11)	8(4)	69(11)	-1(6)	-34(9)	6(6)
C-2a	39(12)	12(6)	26(11)	-12(7)	20(9)	3(7)
N-4a	44(11)	13(5)	49(10)	-1(6)	7(9)	-9(6)
N-5a	15(8)	11(5)	33(8)	1(4)	-7(6)	7(5)
N-1b	26(11)	16(5)	40(9)	-3(6)	6(8)	-15(6)
N-2b	46(10)	23(5)	47(9)	1(7)	-11(9)	-24(7)
C-1b	37(13)	15(7)	31(11)	-10(8)	-7(11)	6(7)
N-3b	27(8)	24(5)	23(7)	5(5)	3(9)	2(6)
C-2b	B = 2.22(37)					
N-4b	16(9)	41(7)	60(11)	-5(7)	24(8)	-21(7)
N-5b	27(10)	26(6)	40(9)	2(7)	18(8)	-7(6)
N-1c	38(10)	20(6)	27(8)	15(6)	1(9)	9(5)
N-2c	56(14)	36(7)	59(13)	23(8)	29(11)	12(8)
C-1c	37(15)	28(8)	48(14)	5(9)	5(13)	7(9)
N-3c	18(8)	46(8)	42(10)	16(6)	-1(10)	14(8)
C-2c	44(15)	22(8)	40(13)	8(9)	-4(12)	7(8)
N-4c	47(11)	60(9)	52(11)	11(9)	1(10)	33(8)
N-5c	55(13)	24(6)	33(10)	12(7)	-17(9)	7(7)
O-b1	187(35)	25(9)	89(19)	000	19(20)	000
O-b2	174(33)	26(9)	141(28)	000	117(28)	000
O-b3	B = 4.0					

Table 7. List of Structure Factors for $\Lambda Co(C_2N_5H_7)_3Br_3 \cdot H_2O$.

H	K	L	F_o	F_c
-4	0	0	212.8	199.1
-6	0	0	65.3	57.1
-8	0	0	132.4	126.6
-10	0	0	224.0	221.1
-14	0	0	118.2	113.2
-6	0	-1	108.5	103.8
-8	0	-1	122.9	120.3
-10	0	-1	67.4	72.5
-16	0	-1	84.6	64.1
-4	0	-2	203.9	187.3
-6	0	-2	170.9	166.7
-8	0	-2	287.0	281.7
-10	0	-2	124.7	126.4
-12	0	-2	82.2	90.9
-14	0	-2	114.6	118.3
-4	0	-3	161.0	155.6
-6	0	-3	349.9	334.5
-8	0	-3	150.1	145.8
-10	0	-3	151.5	146.4
-12	0	-3	71.7	66.4
-16	0	-3	115.9	119.4
0	0	-4	361.6	310.3
-2	0	-4	327.5	316.2
-4	0	-4	301.8	291.2
-6	0	-4	148.8	139.0
-10	0	-4	85.1	78.1
-4	0	-5	147.9	140.1
-6	0	-5	70.6	62.5
-8	0	-5	265.7	264.0
-12	0	-5	81.2	64.6
-14	0	-5	79.4	74.6
-2	0	-6	92.5	81.1
-4	0	-6	130.1	126.4
-6	0	-6	160.1	158.4
-8	0	-6	184.5	187.4
-10	0	-6	270.0	269.9
-12	0	-6	93.7	82.7
-2	0	-7	64.8	16.5
-4	0	-7	56.6	40.5
-6	0	-7	186.9	184.0
-10	0	-7	179.2	175.5
-12	0	-7	67.5	47.7
-2	0	-8	281.5	275.6
-4	0	-8	214.5	210.6
-8	0	-8	158.5	156.6
-14	0	-8	61.5	10.7
-2	0	-9	170.9	157.8
-4	0	-9	223.4	217.5
-6	0	-9	71.6	66.3
-8	0	-9	64.3	54.8
-12	0	-9	92.8	91.9
-14	0	-9	68.0	70.7
0	0	-10	199.3	190.4
-2	0	-10	124.4	113.8
-4	0	-10	84.9	89.4
-6	0	-10	122.1	122.1
-8	0	-10	73.2	72.8
-10	0	-10	147.9	143.2
-8	0	-11	72.2	62.1
-10	0	-11	68.4	41.4
0	0	-12	162.9	159.8
-2	0	-12	250.0	246.1
-4	0	-12	61.6	59.9
-6	0	-12	156.6	159.5
-10	0	-12	77.4	79.4
-6	0	-13	65.9	70.2
0	0	-14	107.0	106.2
-2	0	-14	77.5	63.9
-4	0	-14	58.8	61.2
-6	0	-14	122.4	131.4
-8	0	-14	87.4	82.1
-10	0	-14	70.5	75.5
-4	0	-15	70.9	69.1
-8	0	-15	67.2	56.5
0	0	-16	99.7	86.6
-2	0	-16	85.1	78.9
-5	-1	0	249.1	253.9
-9	-1	0	189.5	185.6
-11	-1	0	84.7	77.3
-13	-1	0	62.1	45.0
-15	-1	0	73.8	68.4
-7	-1	-1	85.5	83.7
-9	-1	-1	135.4	130.7
-11	-1	-1	130.7	129.8
-13	-1	-1	92.8	95.8
-15	-1	-1	79.7	89.2
-5	-1	-2	130.2	132.9
-7	-1	-2	158.1	155.4
-9	-1	-2	89.9	89.1
-11	-1	-2	111.8	109.1
-13	-1	-2	59.1	73.9
-5	-1	-3	65.0	56.9
-7	-1	-3	183.9	181.0
-9	-1	-3	143.6	144.6
-11	-1	-3	150.1	148.6
-13	-1	-3	91.0	97.4
-3	-1	-4	222.4	219.9
-5	-1	-4	262.8	267.1
-9	-1	-4	50.2	53.1
-13	-1	-4	71.4	66.0
-3	-1	-5	127.0	118.9
-5	-1	-5	294.8	296.1
-7	-1	-5	103.5	92.0
-15	-1	-5	78.9	71.3
-3	-1	-6	229.7	227.0
-5	-1	-6	67.2	65.3
-7	-1	-6	218.8	217.3
-13	-1	-6	109.6	116.4
-15	-1	-6	91.8	77.9
-3	-1	-7	89.5	88.4
-5	-1	-7	229.8	226.8
-7	-1	-7	52.9	53.5
-11	-1	-7	83.2	80.5
-13	-1	-7	66.6	63.4
-1	-1	-8	158.9	159.5
-3	-1	-8	110.3	108.1
-5	-1	-8	131.6	134.9
-7	-1	-8	175.3	173.3
-9	-1	-8	62.5	63.5
-1	-1	-9	103.7	97.9
-3	-1	-9	171.6	169.9
-5	-1	-9	111.8	105.7
-7	-1	-9	69.5	61.2
-9	-1	-9	149.9	153.1
-13	-1	-9	89.1	89.5
-1	-1	-10	93.7	85.0
-3	-1	-10	109.9	103.1
-7	-1	-10	91.3	91.0
-9	-1	-10	59.7	68.3
-11	-1	-10	89.2	82.1
-1	-1	-11	54.2	70.5
-3	-1	-11	52.7	47.7
-5	-1	-11	157.9	158.1
-7	-1	-11	76.7	65.2
-9	-1	-11	56.8	68.8
-11	-1	-11	76.9	83.1
-3	-1	-12	95.7	104.3
-7	-1	-12	56.7	48.3
-1	-1	-13	74.3	63.7
-5	-1	-13	76.5	75.8
-7	-1	-13	59.2	68.9
-9	-1	-13	87.2	82.7
-1	-1	-14	73.3	67.4
-3	-1	-14	95.5	97.0
-1	-1	-15	66.0	56.7
-1	-1	-16	82.2	81.5
-3	-1	-16	99.4	104.0
-5	-1	-17	73.0	58.3
-1	-1	-18	76.9	82.9
-8	-2	0	48.1	37.9
-12	-2	0	96.6	94.3
-14	-2	0	131.4	134.9
-16	-2	0	61.8	52.2
-10	-2	-1	79.9	76.1
-14	-2	-1	70.7	73.5
-4	-2	-2	154.6	154.4
-8	-2	-2	95.0	85.6
-4	-2	-3	94.4	88.8
-6	-2	-3	192.3	189.0
-8	-2	-3	75.0	65.4
-10	-2	-3	79.3	77.9
-12	-2	-3	174.8	176.1
0	-2	-4	66.7	60.6
-4	-2	-4	148.7	146.3
-14	-2	-4	61.7	69.7
-16	-2	-4	73.5	80.6
0	-2	-5	179.7	167.8
-2	-2	-5	44.4	48.2
-6	-2	-5	157.8	157.4
-8	-2	-5	71.4	70.0
-10	-2	-5	133.1	132.5
-12	-2	-5	96.4	94.0
-14	-2	-5	100.5	99.2
0	-2	-6	127.8	118.0
-2	-2	-6	103.9	108.4
-4	-2	-6	170.8	176.6
-10	-2	-6	107.3	107.2
-14	-2	-6	81.1	84.6
-2	-2	-7	126.9	124.7
-4	-2	-7	154.8	149.8
-6	-2	-7	205.8	208.2
-8	-2	-7	49.7	45.4
-10	-2	-7	86.8	85.5
-12	-2	-7	98.1	95.6
0	-2	-8	82.1	79.7
-4	-2	-8	174.4	171.2
-6	-2	-8	115.1	115.1
-8	-2	-8	66.1	68.6
-10	-2	-8	68.6	74.6
-12	-2	-8	82.9	72.6
0	-2	-9	80.2	37.8
-2	-2	-9	156.3	163.8
-4	-2	-9	137.3	132.0
-8	-2	-9	168.6	166.9
-12	-2	-9	84.1	75.7
-14	-2	-9	68.2	63.0
0	-2	-10	193.3	198.5
-2	-2	-10	62.5	46.6
-4	-2	-10	221.1	226.3
-8	-2	-10	86.2	92.9
0	-2	-11	143.2	131.6
-4	-2	-11	62.5	77.4
-6	-2	-11	124.2	121.7
0	-2	-12	195.6	187.1
-2	-2	-12	106.7	115.4
-4	-2	-12	63.2	68.2
-8	-2	-12	99.9	83.2
0	-2	-13	70.6	59.1
-2	-2	-13	74.1	59.6
-4	-2	-13	53.0	46.0
-6	-2	-13	61.1	63.3
-8	-2	-13	69.4	69.7
-12	-2	-13	71.5	52.3
0	-2	-14	164.6	162.4
-6	-2	-14	65.9	55.2
-10	-2	-14	69.7	52.1
0	-2	-15	54.0	43.9
-4	-2	-15	63.6	62.2
-8	-2	-15	77.4	79.7
0	-2	-16	68.4	59.0
-4	-2	-16	63.1	45.6
-8	-2	-16	87.0	73.1
-0	-2	-17	70.3	8.6
-6	-2	-17	81.6	83.1
-5	-3	0	52.7	40.0
-7	-3	0	126.0	131.4
-9	-3	0	195.8	192.9
-11	-3	0	279.0	279.2
-1	-3	-1	45.5	35.1
-7	-3	-1	167.7	170.6
-9	-3	-1	211.4	213.5
-5	-3	-2	49.6	34.1
-7	-3	-2	91.1	94.4
-9	-3	-2	180.0	179.5
-1	-3	-3	105.9	112.3
-3	-3	-3	266.4	278.2
-5	-3	-3	283.0	281.3
-7	-3	-3	49.6	54.4
-9	-3	-3	108.3	109.0
-11	-3	-3	115.9	115.3
-15	-3	-3	78.7	80.8
-7	-3	-4	237.8	234.6
-9	-3	-4	195.4	193.6
-11	-3	-4	143.8	146.3
-13	-3	-4	60.4	54.2
-3	-3	-5	141.2	143.8
-7	-3	-5	161.7	161.4
-9	-3	-5	115.1	120.6
-13	-3	-5	90.3	84.0
-15	-3	-5	66.3	52.0
-3	-3	-6	149.0	150.9
-5	-3	-6	109.4	99.4
-7	-3	-6	116.2	119.7
-9	-3	-6	119.1	120.2
-11	-3	-6	88.8	81.9
-1	-3	-7	179.1	178.1
-5	-3	-7	140.7	138.8
-7	-3	-7	140.9	143.1
-9	-3	-7	109.3	111.2
-15	-3	-7	63.9	44.1
-1	-3	-8	85.1	76.0
-3	-3	-8	197.7	201.6
-5	-3	-8	183.5	186.3
-7	-3	-8	171.5	169.2

Table 7. (Continued)

H	K	L	F_o	F_c
-9	-3	-8	166.3	164.0
-13	-3	-8	98.5	106.3
-3	-3	-9	93.1	82.6
-5	-3	-9	84.4	81.7
-7	-3	-9	110.6	110.5
-11	-3	-9	68.4	62.9
-1	-3	-10	202.0	204.9
-3	-3	-10	110.0	112.2
-5	-3	-10	81.7	83.1
-7	-3	-10	75.5	81.0
-9	-3	-10	55.9	44.6
-11	-3	-10	94.2	87.1
-1	-3	-11	82.1	97.0
-3	-3	-11	91.0	84.7
-7	-3	-11	106.8	103.7
-9	-3	-11	96.3	89.8
-11	-3	-11	84.4	86.3
-1	-3	-12	103.1	105.8
-5	-3	-12	73.9	82.0
-9	-3	-12	142.6	143.9
-11	-3	-12	61.0	58.8
-3	-3	-13	107.7	113.3
-5	-3	-13	74.6	78.3
-11	-3	-13	71.1	81.4
-1	-3	-14	121.8	133.2
-3	-3	-14	97.7	100.1
-5	-3	-14	73.6	84.9
-1	-3	-15	69.7	65.0
-3	-3	-15	64.0	61.0
-1	-3	-16	65.5	57.4
-3	-3	-16	59.0	62.7
-5	-3	-16	73.4	56.3
-1	-3	-18	74.5	75.2
-2	-4	0	37.2	29.5
-4	-4	0	83.6	77.4
-8	-4	0	104.0	106.6
-12	-4	0	63.1	56.9
-14	-4	0	116.8	121.8
0	-4	-1	353.2	345.2
-2	-4	-1	202.8	195.1
-4	-4	-1	191.1	192.3
-6	-4	-1	156.7	159.1
-8	-4	-1	136.3	137.7
-10	-4	-1	57.5	49.1
-12	-4	-1	70.7	81.3
-4	-4	-2	145.3	143.4
-6	-4	-2	124.8	124.8
-8	-4	-2	227.8	234.5
-12	-4	-2	55.5	44.2
-16	-4	-2	69.3	62.1
0	-4	-3	294.3	284.7
-2	-4	-3	195.9	197.5
-4	-4	-3	197.3	200.0
-8	-4	-3	162.8	161.8
-10	-4	-3	65.6	66.8
-12	-4	-3	77.1	77.9
-14	-4	-3	107.3	93.9
0	-4	-4	147.1	138.2
-2	-4	-4	54.0	57.9
-4	-4	-4	87.2	88.2
-6	-4	-4	165.8	163.1
-8	-4	-4	121.2	121.4
-10	-4	-4	65.5	78.0
-14	-4	-4	72.1	65.7
-2	-4	-5	86.3	85.3
-4	-4	-5	168.6	174.8
-6	-4	-5	232.8	236.4
-8	-4	-5	147.0	148.9
-10	-4	-5	69.0	81.7
-16	-4	-5	75.6	46.9
0	-4	-6	115.2	108.7
-2	-4	-6	110.6	107.8
-4	-4	-6	244.5	241.5
-6	-4	-6	111.0	113.0
-8	-4	-6	102.8	105.1
-10	-4	-6	92.1	99.0
-12	-4	-6	59.5	50.5
-14	-4	-6	70.8	62.7
0	-4	-7	144.1	142.0
-2	-4	-7	134.3	131.5
-4	-4	-7	222.7	225.0
-8	-4	-7	78.7	62.8
-10	-4	-7	126.3	129.5
-14	-4	-7	69.6	67.7
-2	-4	-8	197.5	199.0
-6	-4	-8	49.5	57.9
-8	-4	-8	63.8	47.4
-10	-4	-8	86.4	78.6
-2	-4	-9	209.5	214.5
-4	-4	-9	64.8	69.7
-12	-4	-9	66.0	72.6
0	-4	-10	94.6	83.8
-2	-4	-10	114.6	113.9
-4	-4	-10	81.1	90.7
0	-4	-11	70.7	65.6
-2	-4	-11	61.1	52.2
-4	-4	-11	88.5	101.6
-6	-4	-11	140.6	145.7
-8	-4	-11	61.1	49.1
-10	-4	-11	69.8	53.4
-12	-4	-11	66.7	49.2
-2	-4	-12	125.2	129.2
-6	-4	-12	83.0	90.1
-12	-4	-12	60.4	19.5
0	-4	-13	91.1	82.8
-2	-4	-13	121.6	126.1
-4	-4	-13	59.0	66.8
-6	-4	-13	83.2	67.4
0	-4	-14	60.5	53.0
-2	-4	-14	74.5	76.4
-6	-4	-14	86.2	94.3
-8	-4	-14	69.5	37.7
-6	-4	-15	73.2	59.0
-8	-4	-15	65.6	37.1
0	-4	-17	72.6	61.9
-2	-4	-17	56.4	63.8
-5	-5	0	226.2	230.5
-7	-5	0	98.4	98.5
-9	-5	0	78.6	85.5
-11	-5	0	123.2	119.5
-1	-5	-1	110.2	109.6
-7	-5	-1	174.1	174.6
-11	-5	-1	135.6	143.2
-13	-5	-1	61.9	63.8
-15	-5	-1	66.8	37.6
-1	-5	-2	158.3	155.2
-3	-5	-2	167.1	173.6
-5	-5	-2	177.8	178.1
-7	-5	-2	124.8	124.5
-9	-5	-2	158.1	159.4
-11	-5	-2	94.5	99.4
-13	-5	-2	111.0	112.3
-15	-5	-2	57.5	22.3
-1	-5	-3	327.4	331.9
-3	-5	-3	164.4	160.9
-5	-5	-3	143.3	148.5
-7	-5	-3	177.0	180.0
-9	-5	-3	97.2	93.5
-11	-5	-3	110.1	115.3
-13	-5	-3	110.9	99.6
-1	-5	-4	128.4	132.9
-3	-5	-4	258.0	262.3
-5	-5	-4	200.1	205.8
-7	-5	-4	119.6	113.3
-9	-5	-4	112.6	117.3
-11	-5	-4	64.9	64.3
-1	-5	-5	194.6	191.5
-3	-5	-5	268.7	275.8
-5	-5	-5	123.6	122.3
-7	-5	-5	240.2	241.5
-9	-5	-5	82.7	84.8
-13	-5	-5	61.2	58.9
-15	-5	-5	77.8	69.1
-1	-5	-6	88.7	86.0
-3	-5	-6	109.9	111.5
-5	-5	-6	143.1	148.0
-7	-5	-6	92.9	84.1
-9	-5	-6	56.8	32.0
-13	-5	-6	98.5	109.8
-15	-5	-6	76.6	70.7
-1	-5	-7	185.0	188.3
-3	-5	-7	78.9	81.7
-5	-5	-7	209.9	210.3
-7	-5	-7	145.6	149.2
-9	-5	-7	57.4	40.6
-11	-5	-7	57.3	50.0
-13	-5	-7	116.5	117.0
-15	-5	-7	67.3	46.9
-1	-5	-8	171.2	173.5
-3	-5	-8	70.2	75.3
-5	-5	-8	77.4	64.2
-7	-5	-8	103.7	102.8
-9	-5	-8	62.6	56.2
-1	-5	-9	170.2	174.5
-3	-5	-9	178.6	185.4
-5	-5	-9	76.4	71.7
-7	-5	-9	117.4	120.6
-9	-5	-9	79.9	65.8
-11	-5	-9	70.7	70.5
-13	-5	-9	64.8	59.2
-1	-5	-10	105.0	102.2
-7	-5	-10	75.5	79.4
-9	-5	-10	58.1	66.9
-11	-5	-10	92.3	93.7
-13	-5	-10	63.7	45.5
-5	-5	-11	146.4	148.7
-7	-5	-11	75.6	79.9
-9	-5	-11	89.9	88.4
-13	-5	-11	62.6	59.1
-1	-5	-12	53.7	33.6
-3	-5	-12	124.7	127.6
-5	-5	-12	61.6	53.6
-7	-5	-12	83.7	83.2
-1	-5	-13	60.8	66.6
-3	-5	-13	80.0	84.0
-5	-5	-13	86.3	89.8
-11	-5	-13	60.1	21.9
-1	-5	-14	54.4	60.9
-7	-5	-14	58.8	47.7
-3	-5	-15	93.5	98.4
-7	-5	-15	69.8	61.4
-9	-5	-15	66.2	57.6
-3	-5	-16	57.9	51.5
-1	-5	-17	72.2	68.4
-5	-5	-17	75.2	74.5
0	-6	0	275.7	288.3
-4	-6	0	99.6	96.3
-6	-6	0	74.6	18.6
-8	-6	0	203.2	207.3
-10	-6	0	172.3	173.0
-12	-6	0	83.7	90.0
-14	-6	0	72.7	65.5
0	-6	-1	140.0	136.6
-6	-6	-1	282.8	285.8
-8	-6	-1	147.9	154.8
-10	-6	-1	96.6	98.6
-14	-6	-1	72.7	78.9
-16	-6	-1	64.1	45.5
0	-6	-2	268.4	254.2
-2	-6	-2	225.5	218.8
-4	-6	-2	207.5	202.6
-6	-6	-2	165.9	166.7
-8	-6	-2	170.5	173.6
-10	-6	-2	180.7	183.1
-12	-6	-2	160.0	159.6
-2	-6	-3	215.9	212.5
-4	-6	-3	144.4	140.3
-6	-6	-3	179.9	169.3
-8	-6	-3	86.9	90.3
-12	-6	-3	95.3	92.2
0	-6	-4	106.0	104.6
-4	-6	-4	69.7	66.5
-6	-6	-4	47.9	57.4
-8	-6	-4	127.5	127.6
-10	-6	-4	108.0	113.6
-12	-6	-4	103.3	103.9
0	-6	-5	110.8	102.2
-2	-6	-5	202.4	202.9
-4	-6	-5	126.7	132.1
-6	-6	-5	100.1	110.1
-8	-6	-5	56.9	50.0
-10	-6	-5	118.7	120.0
0	-6	-6	233.2	226.7
-2	-6	-6	211.0	215.3
-4	-6	-6	140.4	142.0
-8	-6	-6	149.4	148.0
-10	-6	-6	97.0	105.6
-12	-6	-6	93.9	92.3
-2	-6	-7	58.9	62.4
-4	-6	-7	227.6	235.1
-6	-6	-7	67.9	52.8
-8	-6	-7	96.4	97.1
-10	-6	-7	96.4	98.4
-12	-6	-7	66.9	45.2
-14	-6	-7	62.7	53.8
0	-6	-8	204.1	202.6
-4	-6	-8	100.4	107.2
-6	-6	-8	115.7	109.3
-8	-6	-8	111.1	123.1
-10	-6	-8	61.6	64.3
0	-6	-9	74.1	75.8
-2	-6	-9	56.8	58.7
-4	-6	-9	154.3	158.7
-6	-6	-9	68.5	69.0
-10	-6	-9	84.5	79.5
0	-6	-10	77.3	75.7
-2	-6	-10	151.3	158.4
-8	-6	-10	111.8	118.2
-12	-6	-10	63.0	60.9
0	-6	-11	230.5	229.5
-2	-6	-11	66.1	71.2
-4	-6	-11	98.0	102.2
-8	-6	-11	93.3	94.4
-10	-6	-11	62.4	45.4
0	-6	-12	167.2	167.4
-2	-6	-12	70.5	59.9
-6	-6	-12	67.1	59.5
-10	-6	-12	60.2	76.7
0	-6	-13	116.0	116.7
-2	-6	-13	53.4	47.4
-8	-6	-13	78.8	82.9
-2	-6	-14	78.8	75.1

Table 7. (Continued)

H	K	L	F_o	F_c
-8	-6	-14	70.5	73.7
-10	-6	-14	65.6	48.9
0	-6	-15	125.4	126.9
0	-6	-16	70.4	65.9
-1	-7	0	163.3	166.4
-5	-7	0	72.2	70.6
-7	-7	0	221.7	223.7
-11	-7	0	86.9	98.2
-1	-7	-1	130.3	129.6
-3	-7	-1	249.5	255.8
-5	-7	-1	210.6	208.1
-9	-7	-1	131.5	130.7
-11	-7	-1	97.8	93.6
-1	-7	-2	240.2	238.1
-3	-7	-2	214.6	217.1
-5	-7	-2	138.4	135.3
-7	-7	-2	55.1	30.6
-9	-7	-2	159.1	159.6
-11	-7	-2	83.6	82.6
-13	-7	-2	56.9	40.9
-15	-7	-2	60.7	69.0
-1	-7	-3	128.2	128.4
-3	-7	-3	171.6	171.0
-5	-7	-3	46.3	40.8
-7	-7	-3	77.3	67.3
-9	-7	-3	73.6	63.4
-1	-7	-4	63.8	65.6
-3	-7	-4	96.3	93.3
-5	-7	-4	143.9	146.9
-7	-7	-4	97.9	100.8
-9	-7	-4	81.5	70.0
-11	-7	-4	75.0	88.5
-1	-7	-5	181.1	178.1
-3	-7	-5	74.2	78.0
-5	-7	-5	170.8	173.5
-7	-7	-5	150.6	146.1
-13	-7	-5	87.7	97.2
-1	-7	-6	176.3	177.7
-3	-7	-6	62.4	66.7
-7	-7	-6	55.0	46.3
-9	-7	-6	66.8	87.2
-1	-7	-7	198.8	202.6
-3	-7	-7	189.8	194.3
-5	-7	-7	71.6	63.3
-7	-7	-7	143.9	144.4
-11	-7	-7	67.0	60.7
-13	-7	-7	61.3	50.2
-3	-7	-8	71.6	71.8
-5	-7	-8	92.6	84.4
-7	-7	-8	52.8	50.8
-9	-7	-8	78.1	81.7
-1	-7	-9	93.4	97.3
-3	-7	-9	66.8	67.3
-5	-7	-9	65.6	67.3
-7	-7	-9	97.9	92.7
-11	-7	-9	65.9	60.1
-13	-7	-9	68.9	54.6
-1	-7	-10	84.9	81.6
-3	-7	-10	70.6	72.4
-5	-7	-10	141.3	152.4
-7	-7	-10	65.7	70.5
-11	-7	-10	60.3	49.8
-1	-7	-11	68.8	69.9
-3	-7	-11	127.3	132.7
-3	-7	-12	56.2	41.9
-5	-7	-12	58.7	65.2
-9	-7	-12	70.0	77.8
-3	-7	-13	98.0	99.8
-9	-7	-13	66.7	52.9
-1	-7	-15	71.5	71.4
-3	-7	-15	77.2	71.0
-5	-7	-15	73.5	76.2
-5	-7	-16	68.7	67.3
-3	-7	-17	73.7	50.5
-2	-8	0	91.1	93.4
-4	-8	0	54.2	50.3
-6	-8	0	56.9	59.6
-8	-8	0	83.3	44.4
-12	-8	0	75.0	77.7
-4	-8	-1	185.7	184.7
-6	-8	-1	182.9	183.6
-8	-8	-1	187.1	184.0
-10	-8	-1	71.2	66.2
-12	-8	-1	71.3	67.7
-14	-8	-1	103.5	93.4
-2	-8	-2	114.7	114.7
-4	-8	-2	89.9	94.1
-6	-8	-2	140.5	143.2
-8	-8	-2	120.5	117.6
-12	-8	-2	75.9	72.8
0	-8	-3	243.0	236.0
-2	-8	-3	138.9	142.7
-4	-8	-3	218.8	223.2
-8	-8	-3	95.0	109.2
-12	-8	-3	58.3	64.1
-2	-8	-4	169.9	173.2
-6	-8	-4	175.2	175.4
-8	-8	-4	169.3	170.7
-12	-8	-4	67.3	61.8
-14	-8	-4	60.6	51.9
-2	-8	-5	230.9	230.9
-4	-8	-5	218.7	223.6
-6	-8	-5	126.7	125.8
-8	-8	-5	92.1	91.0
-10	-8	-5	101.4	106.3
-12	-8	-5	83.1	77.1
0	-8	-6	87.8	82.1
-4	-8	-6	56.3	60.1
-6	-8	-6	99.7	106.0
-8	-8	-6	92.1	93.8
-10	-8	-6	82.4	81.7
-12	-8	-6	72.9	70.7
-14	-8	-6	69.6	65.3
0	-8	-7	137.9	139.1
-2	-8	-7	228.8	232.2
-4	-8	-7	210.0	212.8
-6	-8	-7	105.7	98.4
-10	-8	-7	90.2	110.7
-12	-8	-7	74.0	68.2
0	-8	-8	60.7	61.6
-2	-8	-8	96.5	97.2
-4	-8	-8	114.3	114.7
-8	-8	-8	52.7	33.7
-10	-8	-8	67.3	65.4
-12	-8	-8	72.4	84.3
0	-8	-9	55.8	49.6
-2	-8	-9	152.4	155.3
-4	-8	-9	113.8	117.0
-6	-8	-9	122.9	125.7
-8	-8	-9	73.3	31.9
-10	-8	-9	83.6	78.4
-2	-8	-10	77.3	84.7
-12	-8	-10	79.9	80.7
-2	-8	-11	179.6	182.0
-4	-8	-11	89.1	94.8
-6	-8	-11	118.2	120.7
-2	-8	-12	72.2	63.0
0	-8	-13	64.2	56.1
-2	-8	-13	94.9	99.4
-4	-8	-13	79.6	76.0
-6	-8	-13	119.2	116.7
0	-8	-15	60.7	52.0
-2	-8	-15	61.7	70.8
-4	-8	-15	55.3	49.1
-6	-8	-15	74.6	77.9
-2	-8	-16	66.8	72.5
-1	-9	0	118.1	114.0
-3	-9	0	132.5	132.6
-5	-9	0	69.3	65.5
-9	-9	0	154.6	152.6
-13	-9	0	85.3	77.0
-15	-9	0	79.0	76.8
-3	-9	-1	167.9	170.3
-5	-9	-1	94.4	92.8
-7	-9	-1	99.2	103.9
-9	-9	-1	127.0	129.3
-11	-9	-1	109.7	105.6
-1	-9	-2	183.2	182.2
-3	-9	-2	45.1	41.7
-5	-9	-2	97.1	99.1
-7	-9	-2	152.1	151.5
-9	-9	-2	96.5	93.8
-11	-9	-2	169.1	174.4
-1	-9	-3	82.8	79.4
-3	-9	-3	129.4	133.9
-5	-9	-3	176.9	174.5
-7	-9	-3	141.2	142.3
-9	-9	-3	86.0	71.9
-11	-9	-3	57.1	50.8
-13	-9	-3	58.7	40.2
-1	-9	-4	217.0	221.1
-3	-9	-4	205.0	207.9
-5	-9	-4	130.4	130.3
-9	-9	-4	140.3	148.6
-11	-9	-4	57.6	47.3
-3	-9	-4	64.3	69.5
-15	-9	-4	73.6	49.8
-1	-9	-5	201.9	201.8
-3	-9	-5	121.8	124.6
-5	-9	-5	120.0	117.5
-7	-9	-5	123.4	124.1
-9	-9	-5	51.5	56.5
-11	-9	-5	59.9	39.6
-1	-9	-6	91.3	93.6
-3	-9	-6	151.3	149.6
-5	-9	-6	51.8	33.1
-7	-9	-6	144.3	149.4
-9	-9	-6	80.3	60.7
-13	-9	-6	73.3	65.3
-1	-9	-7	145.0	145.2
-3	-9	-7	130.4	125.5
-5	-9	-7	64.4	60.6
-7	-9	-7	143.2	147.8
-1	-9	-8	164.4	162.6
-3	-9	-8	80.5	75.3
-5	-9	-8	94.4	95.5
-7	-9	-8	99.7	97.1
-11	-9	-8	75.5	89.8
-1	-9	-9	126.9	128.2
-5	-9	-9	53.0	52.2
-7	-9	-9	70.6	66.0
-9	-9	-9	64.9	68.4
-1	-9	-10	98.0	96.2
-3	-9	-10	94.6	91.4
-5	-9	-10	89.7	94.3
-9	-9	-10	135.0	137.8
-3	-9	-11	60.8	50.1
-7	-9	-11	80.7	78.2
-1	-9	-12	75.6	75.3
-3	-9	-12	55.5	50.4
-5	-9	-12	59.2	56.8
-7	-9	-12	66.4	78.5
-11	-9	-12	79.8	71.7
-3	-9	-13	102.6	107.8
-7	-9	-13	71.5	68.5
-1	-9	-15	67.8	66.1
-5	-9	-15	59.6	46.3
-2	-10	0	53.7	43.7
-4	-10	0	107.6	102.3
-6	-10	0	147.5	151.7
-8	-10	0	105.3	107.6
-2	-10	-1	204.5	201.0
-4	-10	-1	175.8	178.5
-6	-10	-1	165.3	169.3
0	-10	-2	179.4	176.8
-2	-10	-2	211.0	210.0
-4	-10	-2	83.1	81.0
-8	-10	-2	57.3	50.9
-10	-10	-2	77.1	73.1
-12	-10	-2	83.3	80.0
0	-10	-3	58.5	55.8
-2	-10	-3	110.6	112.2
-4	-10	-3	136.0	136.0
-6	-10	-3	152.8	152.5
-10	-10	-3	73.2	74.3
0	-10	-4	162.4	153.2
-2	-10	-4	117.0	114.8
-4	-10	-4	129.4	126.1
-6	-10	-4	61.5	67.3
-8	-10	-4	59.0	66.8
-10	-10	-4	104.2	110.2
-12	-10	-4	82.2	87.1
-2	-10	-5	151.3	154.2
-4	-10	-5	96.5	95.5
-10	-10	-5	79.8	86.7
-12	-10	-5	64.2	52.1
0	-10	-6	45.5	26.4
-2	-10	-6	69.2	68.2
-4	-10	-6	67.9	64.8
-6	-10	-6	66.4	61.3
-12	-10	-6	73.2	79.0
0	-10	-7	83.9	79.8
-4	-10	-7	114.3	114.7
-6	-10	-7	52.7	57.9
-10	-10	-7	78.7	83.5
-2	-10	-8	47.2	20.2
-4	-10	-8	74.4	76.2
-8	-10	-8	78.8	79.6
-10	-10	-8	85.9	92.3
0	-10	-9	141.1	138.0
-4	-10	-9	146.3	147.0
-6	-10	-9	68.2	50.7
0	-10	-10	127.6	121.8
-6	-10	-10	106.2	105.2
-8	-10	-10	57.4	76.3
-12	-10	-10	59.9	12.9
0	-10	-11	79.9	79.6
-2	-10	-11	87.2	88.5
-4	-10	-11	64.9	64.7
-8	-10	-11	80.7	78.0
-2	-10	-12	72.8	69.9
-8	-10	-12	68.6	58.1
0	-10	-13	167.8	165.2
0	-10	-14	85.6	74.1
-8	-10	-14	59.5	48.8
-6	-10	-15	57.7	34.8
-1	-11	0	89.9	86.6
-3	-11	0	70.7	65.1
-5	-11	0	62.3	50.1
-7	-11	0	107.4	103.7
-9	-11	0	145.6	148.9
-11	-11	0	64.3	62.5

Table 7. (Continued)

H	K	L	F_o	F_c
-13	-11	0	100.3	114.8
-1	-11	-1	119.0	116.7
-3	-11	-1	201.4	204.2
-5	-11	-1	96.4	102.1
-7	-11	-1	112.6	112.6
-9	-11	-1	84.4	86.7
-11	-11	-1	108.1	110.5
-13	-11	-1	78.2	59.1
-1	-11	-2	92.7	94.0
-3	-11	-2	112.8	110.3
-5	-11	-2	134.4	129.5
-7	-11	-2	56.0	48.8
-9	-11	-2	59.6	65.9
-11	-11	-2	81.0	71.1
-1	-11	-3	84.6	77.4
-3	-11	-3	148.3	148.4
-5	-11	-3	176.2	181.6
-7	-11	-3	141.2	143.3
-9	-11	-3	67.9	64.7
-1	-11	-4	68.9	67.4
-3	-11	-4	138.0	138.5
-5	-11	-4	120.3	124.9
-7	-11	-4	51.1	46.4
-9	-11	-4	89.3	102.0
-11	-11	-4	59.3	54.1
-13	-11	-4	95.5	94.4
-1	-11	-5	225.1	224.8
-3	-11	-5	49.4	36.7
-5	-11	-5	186.4	190.0
-7	-11	-5	91.7	87.2
-9	-11	-5	61.7	73.5
-11	-11	-5	58.2	57.6
-13	-11	-5	74.3	80.7
-1	-11	-6	111.5	108.2
-3	-11	-6	71.9	74.2
-5	-11	-6	90.5	96.6
-7	-11	-6	107.0	109.6
-11	-11	-6	65.4	68.9
-13	-11	-6	56.9	13.0
-1	-11	-7	67.3	69.5
-3	-11	-7	197.1	203.6
-5	-11	-7	50.9	52.6
-7	-11	-7	116.4	121.5
-1	-11	-8	105.6	107.5
-5	-11	-8	64.0	67.3
-7	-11	-8	104.3	104.4
-11	-11	-8	63.2	68.7
-1	-11	-9	83.6	81.0
-5	-11	-9	194.2	196.6
-7	-11	-9	60.4	45.5
-3	-11	-10	64.6	69.5
-1	-11	-11	68.6	77.5
-3	-11	-11	78.1	79.3
-7	-11	-11	57.3	70.0
-1	-11	-12	54.7	32.8
-5	-11	-12	55.0	63.6
-3	-11	-13	79.5	70.5
-5	-11	-13	60.6	60.1
-7	-11	-13	64.6	66.7
-3	-11	-14	75.3	75.0
-5	-11	-15	76.2	78.6
-1	-11	-16	69.2	54.2
-2	-12	0	238.4	239.3
-4	-12	0	62.6	31.0
-6	-12	0	123.5	118.5
-8	-12	0	160.6	170.7
-14	-12	0	70.4	68.5
0	-12	-1	216.2	210.7
-2	-12	-1	73.1	69.6
-4	-12	-1	58.7	63.3
-6	-12	-1	86.2	88.0
-8	-12	-1	86.8	93.2
0	-12	-2	332.6	328.5
-2	-12	-2	112.4	108.4
-6	-12	-2	100.4	97.9
-8	-12	-2	63.2	52.9
-10	-12	-2	72.3	69.5
-14	-12	-2	63.2	32.1
0	-12	-3	67.1	72.6
-2	-12	-3	107.1	112.9
-4	-12	-3	52.3	44.8
-6	-12	-3	50.2	39.0
-8	-12	-3	132.4	140.5
0	-12	-4	141.1	140.7
-2	-12	-4	111.9	112.0
-4	-12	-4	81.4	71.7
-6	-12	-4	64.9	70.9
-8	-12	-4	124.7	131.1
-10	-12	-4	79.4	94.3
-2	-12	-5	50.5	22.5
-4	-12	-5	82.4	72.0
-6	-12	-5	105.8	102.4
-8	-12	-5	53.3	57.3
-10	-12	-5	75.5	82.3
0	-12	-6	59.7	53.2
-2	-12	-6	153.8	151.0
-4	-12	-6	106.6	110.9
-6	-12	-6	114.6	117.1
-8	-12	-6	84.5	87.0
-2	-12	-7	107.5	106.6
-4	-12	-7	100.7	95.2
-6	-12	-7	52.9	44.0
-8	-12	-7	68.1	63.8
-10	-12	-7	68.4	54.5
0	-12	-8	113.5	113.2
-6	-12	-8	69.3	68.9
-10	-12	-8	93.2	98.3
0	-12	-9	123.1	116.0
-2	-12	-9	112.5	117.6
-10	-12	-9	85.0	75.8
-2	-12	-10	114.2	119.2
-8	-12	-10	59.4	46.1
-2	-12	-11	97.7	92.1
-4	-12	-12	67.1	73.1
-6	-12	-12	87.2	78.5
-8	-12	-12	65.1	54.3
-6	-12	-13	66.5	77.7
0	-12	-14	92.1	57.1
-2	-12	-14	66.2	63.6
-1	-13	0	91.2	87.2
-3	-13	0	207.2	210.2
-7	-13	0	130.5	127.7
-9	-13	0	80.1	80.5
-11	-13	0	71.2	56.2
-13	-13	0	60.6	59.3
-1	-13	-1	45.9	54.6
-3	-13	-1	67.8	60.9
-5	-13	-1	99.6	101.1
-7	-13	-1	67.5	71.3
-9	-13	-1	71.9	65.4
-11	-13	-1	92.8	90.9
-13	-13	-1	57.8	53.5
-1	-13	-2	113.5	107.7
-3	-13	-2	80.2	74.0
-5	-13	-2	54.1	42.3
-7	-13	-2	85.6	89.5
-9	-13	-2	96.1	94.8
-11	-13	-2	103.8	104.1
-1	-13	-3	64.8	62.8
-3	-13	-3	82.9	85.8
-5	-13	-3	133.2	137.6
-9	-13	-3	96.7	94.6
-1	-13	-4	195.5	195.9
-3	-13	-4	96.3	92.1
-5	-13	-4	55.2	39.6
-7	-13	-4	70.3	64.3
-9	-13	-4	63.7	54.2
-3	-13	-5	113.5	112.7
-5	-13	-5	70.4	72.5
-1	-13	-6	68.0	57.9
-3	-13	-6	67.8	81.0
-7	-13	-6	92.2	91.0
-9	-13	-6	60.4	62.3
-1	-13	-7	89.1	95.0
-1	-13	-8	136.7	139.1
-7	-13	-8	82.9	75.3
-1	-13	-9	67.0	56.8
-7	-13	-9	57.7	69.6
-9	-13	-9	67.6	70.0
-3	-13	-10	54.5	41.1
-5	-13	-10	89.5	88.1
-9	-13	-10	73.2	79.3
-1	-13	-11	70.4	62.0
-3	-13	-11	56.1	48.1
-5	-13	-11	60.3	48.3
-3	-13	-12	66.5	58.7
-7	-13	-12	60.1	62.7
-1	-13	-14	60.5	32.8
-5	-13	-14	58.5	28.8
0	-14	0	196.2	197.5
-2	-14	0	136.7	132.8
-4	-14	0	86.6	93.1
-6	-14	0	161.0	158.9
-8	-14	0	72.6	53.0
-10	-14	0	58.8	56.4
0	-14	-1	54.9	46.5
-2	-14	-1	155.3	155.9
-4	-14	-1	127.2	134.0
-6	-14	-1	72.4	76.7
-12	-14	-1	58.0	60.4
0	-14	-2	86.3	68.6
-2	-14	-2	57.2	31.2
-4	-14	-2	85.2	88.2
-6	-14	-2	83.9	88.4
-12	-14	-2	60.8	59.9
-2	-14	-3	85.3	81.9
-4	-14	-3	204.9	209.0
-6	-14	-3	113.9	113.6
-10	-14	-3	63.8	62.8
-2	-14	-4	115.4	112.8
-4	-14	-4	72.8	66.2
-6	-14	-4	52.3	41.6
-2	-14	-5	163.9	167.3
-4	-14	-5	73.8	68.8
-6	-14	-5	99.1	94.8
-12	-14	-5	101.0	103.4
0	-14	-6	75.2	72.2
-2	-14	-6	64.2	53.5
-4	-14	-6	72.8	69.2
-10	-14	-6	97.2	98.6
-12	-14	-6	65.7	57.1
-2	-14	-7	74.4	75.0
-4	-14	-7	136.4	141.4
-6	-14	-7	69.7	65.7
-8	-14	-7	91.0	98.3
-4	-14	-8	131.6	131.1
-4	-14	-9	101.5	106.2
-6	-14	-9	146.7	147.4
-2	-14	-11	66.6	68.5
-4	-14	-11	60.6	62.2
-8	-14	-11	68.2	58.4
0	-14	-12	140.1	134.2
-4	-14	-12	67.8	56.0
-2	-14	-14	63.1	45.7
-1	-15	0	95.8	95.5
-3	-15	0	125.2	130.7
-5	-15	0	77.9	83.5
-7	-15	0	75.1	65.2
-1	-15	-1	74.2	68.0
-3	-15	-1	56.6	50.9
-7	-15	-1	75.1	65.7
-11	-15	-1	58.3	48.2
-1	-15	-2	118.2	121.2
-3	-15	-2	52.3	44.8
-9	-15	-2	96.6	94.3
-11	-15	-2	76.5	68.0
-1	-15	-3	85.6	89.3
-5	-15	-3	95.9	89.9
-9	-15	-3	99.9	97.2
-1	-15	-4	121.9	122.9
-3	-15	-4	74.4	67.9
-5	-15	-4	49.3	27.2
-7	-15	-4	59.7	52.0
-9	-15	-4	65.3	53.3
-11	-15	-4	59.4	40.3
-1	-15	-5	73.7	70.7
-9	-15	-5	55.4	31.5
-1	-15	-6	64.5	60.6
-3	-15	-6	103.0	109.3
-5	-15	-6	70.9	66.0
-7	-15	-6	148.5	156.5
-9	-15	-6	57.6	42.8
-11	-15	-6	62.1	20.6
-5	-15	-7	57.4	49.1
-7	-15	-7	53.1	10.0
-1	-15	-8	114.9	112.0
-3	-15	-8	69.0	65.5
-1	-15	-10	58.1	56.6
-7	-15	-10	66.5	50.3
-1	-15	-12	56.6	48.8
-3	-15	-12	56.9	65.4
0	-16	0	107.3	101.7
-2	-16	0	112.7	112.2
-6	-16	0	93.5	89.2
-8	-16	0	122.2	122.9
-10	-16	0	55.4	21.0
0	-16	-1	51.7	10.4
-10	-16	-1	58.2	54.2
0	-16	-2	235.4	232.1
-10	-16	-2	63.2	58.2
-2	-16	-3	82.3	76.4
-6	-16	-3	93.6	95.1
-8	-16	-3	72.5	82.9
0	-16	-4	56.6	55.5
-2	-16	-4	77.4	66.5
-4	-16	-4	78.3	92.0
-8	-16	-4	81.3	83.4
-10	-16	-4	84.5	76.0
0	-16	-5	65.2	50.4
-2	-16	-5	57.9	48.5
-6	-16	-5	99.0	99.8
-2	-16	-6	82.2	89.5
-4	-16	-6	73.4	63.3
-8	-16	-6	62.6	54.3
-2	-16	-7	54.6	37.2
-4	-16	-7	54.5	51.6
0	-16	-8	119.3	123.4
0	-16	-10	70.3	36.3
-2	-16	-10	113.9	120.1
-2	-16	-11	66.3	50.7
-4	-16	-12	70.0	62.4
-1	-17	0	43.2	56.2

Table 7. (Continued)

H	K	L	F_o	F_c
-5	-17	0	62.1	30.8
-7	-17	0	65.6	45.4
-9	-17	0	73.6	69.7
-11	-17	0	81.9	77.9
-1	-17	-1	55.4	51.0
-3	-17	-1	124.9	119.7
-5	-17	-1	86.8	89.5
-7	-17	-1	66.3	67.5
-3	-17	-2	115.2	114.8
-5	-17	-2	110.1	107.8
-3	-17	-3	70.3	67.2
-5	-17	-3	173.6	172.9
-7	-17	-3	82.2	79.6
-1	-17	-4	51.6	36.0
-5	-17	-4	54.8	36.2
-9	-17	-4	61.5	50.0
-1	-17	-5	56.5	60.1
-3	-17	-5	101.1	88.1
-5	-17	-5	58.0	57.9
-7	-17	-5	75.0	82.3
-1	-17	-6	93.4	94.5
-3	-17	-6	69.7	65.2
-5	-17	-6	74.8	60.6
-7	-17	-6	78.8	65.4
-5	-17	-7	77.0	76.8
-5	-17	-9	97.2	89.8
-1	-17	-10	92.0	80.5
-5	-17	-10	57.1	37.1
-3	-17	-11	77.1	61.1
0	-18	0	65.5	36.7
-4	-18	0	68.7	64.2
-6	-18	0	103.9	98.1
-8	-18	0	74.3	60.2
0	-18	-1	71.4	61.9
-6	-18	-1	57.7	34.7
0	-18	-2	70.8	65.9
-2	-18	-2	107.0	105.0
-8	-18	-2	62.2	39.8
-10	-18	-2	58.8	48.4
0	-18	-4	78.2	80.1
-2	-18	-5	61.9	76.6
-4	-18	-5	63.4	35.7
-2	-18	-6	66.8	67.1
-4	-18	-6	69.9	70.3
-6	-18	-6	58.3	40.8
-8	-18	-6	64.9	40.7
0	-18	-7	68.3	55.8
-4	-18	-7	61.8	59.6
0	-18	-8	57.3	41.6
-2	-18	-8	59.8	48.3
0	-18	-9	61.7	37.8
0	-18	-10	65.6	62.0
-1	-19	0	68.6	58.3
-3	-19	0	117.4	118.1
-7	-19	0	69.1	64.9
-5	-19	-1	73.4	58.0
-7	-19	-1	66.9	69.2
-1	-19	-2	93.7	94.2
-7	-19	-2	66.4	47.5
-7	-19	-3	56.5	53.9
-1	-19	-4	100.7	101.2
-5	-19	-5	58.2	44.8
-3	-19	-6	57.5	58.3
-1	-19	-8	88.2	71.7
-5	-19	-8	71.3	54.7
-1	-19	-9	58.9	33.6
0	-20	0	84.7	84.4
0	-20	-1	69.4	52.3
-2	-20	-1	66.4	68.7
-4	-20	-1	81.0	86.9
-2	-20	-2	61.6	64.0
-6	-20	-2	67.7	41.5
-4	-20	-3	78.3	68.3
-6	-20	-3	87.4	84.9
-2	-20	-5	64.2	54.2
-4	-20	-5	72.8	79.5
-2	-20	-8	59.4	55.1
-1	-21	0	55.7	30.0
-3	-21	-1	62.7	61.8
-3	-21	-4	62.1	47.4
-1	-21	-5	63.9	38.9
0	-22	0	74.6	72.0
-2	-22	0	61.7	25.9

dispersion (O.R.D.) experiments. Vis-UV spectra were recorded on a Cary-14 recording spectrophotometer. The same machine, fitted with two Nicol prisms from a polarizing microscope, was used to measure plane-polarized single crystal spectra. C.D. and O.R.D. spectra were recorded on a Jasco model (ORD UV 5) machine with a C.D. attachment. The C.D. scale of the machine was calibrated with a standard solution of d-10-camphorsulfonic acid for quantitative measurements. Polarimetric rotations at fixed wavelengths were recorded on a Bendix-Ericsson automatic recording polarimeter, with interference filters as monochromators. It was calibrated with standard sucrose solutions for quantitative measurements.

Single Crystal Spectra

The individual crystals that were used for spectra were grown as described in the preparations sections. The optimum dimensions of crystals suitable for spectral measurements were 3 to 5 mm long and 1 to 3 mm wide. The large crystals that were grown were all too thick and therefore too opaque. Consequently those had to be sliced down to give spectral signals that were within measurable ranges. In general crystals that were about 0.05 mm thick were found quite adequate.

If the desired crystal face developed properly during crystal growth, the crystal specimen required only thinning down to about 0.05 mm. The crystal was set in polystyrene resin with the desired face pressed flat against an optical

glass disc 18 mm in diameter placed at the bottom of a special teflon mold. When the resin had hardened the mold was taken off and the crystal set in the resin was ground down to the desired thickness and polished to a mirror shine as described below.

If the desired crystal face did not develop during crystal growing, the crystal had to be cut to expose it. From crystallographic data, the dihedral angle was computed between the desired face and an identifiable face that was well developed during crystal growth. The crystal, set inside a coaxial disc of resin, was placed on an accurately made template, and carefully cut to expose the desired face. A small fine-toothed saw was used for the cutting and the exposed face was polished by grinding against carborundum paper of progressively finer grain size. The finishing to a mirror shine was done by grinding against grade 4/0 grinding paper and/or against a dry sheet of coarse paper towel. The polished crystal face was then coated with fresh resin mixture and pressed flat against an optical glass disk 18 mm in diameter placed at the bottom of the teflon mold. Care was taken to exclude air bubbles between the glass and the exposed crystal face. When the resin had hardened the mold was taken off and the crystal-in-resin sample was thinned down and polished as described before.

The Vis-U.V. spectrum of the resin was obtained on a sample 1 mm thick cast between two parallel plates of fused

silica. It showed no absorption between 7000Å and 4000Å. Under 4000Å there was a fairly steep rise in absorption. In effect there was no absorption, due to the resin, in the region of the spectrum between 7000Å and 4000Å, that is most pertinent to this work. A negligible amount of absorption existed between 4000Å and 3500 Å due to the very thin layer- 0.05 to 0.01 mm - of resin between the exposed crystal face and the back plate of glass used as support. Between 3500Å and 3000Å spectra were probably less accurate, although identical glass plates were used in the reference beam of the spectrophotometer to compensate for glass absorption.

Single crystal C.D. spectra were taken with the light beam incident, alternately, on either face of the particular crystal. Crystal samples used for C.D. spectra were covered with glass plates on both faces. For plane polarized single spectra it was enough to cover one face only to support the very thin slice of the crystal (0.05 mm). For the latter spectra light was incident on the exposed polished face of the crystal.

The unequivocal identification of exposed crystal faces used for spectra was of prime importance. When the desired crystal faces developed during crystal growth, identification was done geometrically by comparison with small sample crystals which had their faces identified by crystallography. Confirming the identities of those faces, on the larger crystals, was done by measuring the angles

between those faces on the crystal to be used for spectra. The crystal sample was mounted on a spindle with a 360° protractor and light reflections from those faces were observed under a stereo microscope. This technique was used to identify the (ab)-(0, 0, 1) and the (ac)-(0, 1, 0) faces of the racemic $Co(C_5H_7O_2)_3$ crystal and the (ac)-(0, 1, 0) and (ab)-(0, 0, 1) faces of the Λ-$Co(C_2N_5H_7)_3Br_3 \cdot H_2O$.

When the crystal specimen had to be cut and polished to expose the desired face, a more rigorous technique was used to identify the artifically exposed faces. After all desired spectra for that sample were recorded a portion of suitable size was cut from it and mounted on a goniometer head along the same crystal-axis contained in the exposed face of the crystal slice used for spectra. The goniometer head was then set on a Buerger precession camera. The exposed face was made more reflective with mineral oil, oriented via an optical autocollimator and the protractor reading was recorded at that setting. The protractor reading was again noted when a main zone of the crystal was in exact diffracting position, as confirmed by taking precession pictures at that setting. The exact position of the artificially exposed crystal face, in relation to a known main zone and to the naturally grown crystal faces, was thus established. The maximum error in this technique ($\approx 1°$) is due to the orientation by the optical autocollimator. The latter technique for identifying artifically exposed crystal

faces was used to identify the orientations of two artificially exposed faces of the racemic $Co(C_2N_5H_6)_3 \cdot 2H_2O$ crystals and for the (bc)-(1, 0, 0) face of Λ-$Co(C_2N_5H_7)_3Br_3 \cdot H_2O$. The latter face, of the material investigated, does not grow naturally.

The use of one polarizer only, for plane polarized single crystal spectra, was found unsatisfactory because it gave high extraneous peaks superimposed on the spectra. Those peaks were probably due to partial polarization of the light beam of the machine. To avoid that difficulty, two Nicol prism polarizers, from a polarizing microscope, were used in the sample and reference compartments of the spectrophotometer. Each polarizer was set in a stable holder but it could be rotated about its axis and its orientation could be read against a fixed calibrated protractor. The polarizers could thus be turned or rotated in unison (in phase) so that the planes of the polarized beams emerging from them were parallel at any chosen setting. The base lines were recorded for various settings of the polarizers. Those base lines were smooth except for a broad hump of about 0.05 absorbance units between 3600Å and 3400Å. The corresponding base lines were always subtracted from the spectra to give the net spectral readings.

The desired crystal was firmly mounted in the sample compartment of the machine so that the polarized beam from the prism was incident perpendicularly on the polished face.

An identical glass disc was put in the reference beam. The appropriate crystallographic axis of the crystal sample was set parallel to the plane of polarized light. One spectrum was taken at that setting and the other spectrum was taken with the polarizers turned, in phase, 90° away from the initial position. An attenuator was sometimes used, in the reference beam, to lower the level of the base line.

Spectra were scanned at the slow rate of 2.5Å per second and the wavelengths were accurately recorded on the chart paper. The polarized spectra obtained for single crystals were very smooth, like the best solution spectra, and reproducibilities in trace and in reading wavelengths were 10Å or better.

Single crystal C.D. spectra required a special mounting for the crystal. None of the crystals used possessed crystallographic three-fold symmetry and therefore the observed spectra were a function of the rotational orientation of the crystal in a plane perpendicular to the direction of propagation of the incident beam. Spectra were therefore taken for each crystal at a number of different orientations in this plane. Spectra were taken every 10° for one crystal and every 30° for another sample. The reproducibility of these spectra depended very critically on the accuracy of the crystal mounting. The axis about which the crystal was rotated had to be kept carefully fixed and aligned along the direction of propagation of the incident beam. To accomplish

this the following procedure was adopted. The disc bearing the thin crystal slice was firmly mounted on one face of a specially machined cylindrical metal holder. The crystallographic axes of the sample were set at known orientations with respect to accurate 10° markings on the cylindrical surface of the sample holder. The cylindrical sample holder had a coaxial central bore drilled through it for the passage of the light beam. The cylindrical sample holder was set in

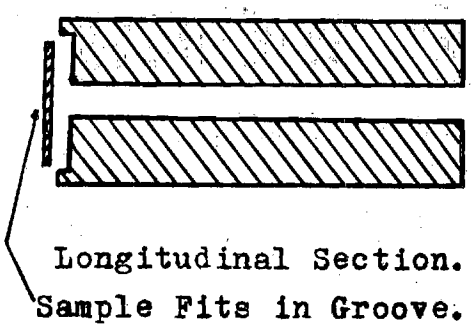

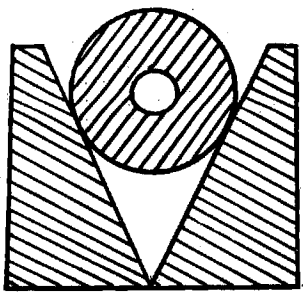

Figure 8. Diagram of Sample Holder for Single Crystal C.D. Spectra.

a channel of V-shaped cross-section in the sample compartment of the machine. The above setup allowed rotation of the crystal, by known angular increments, in the light beam without any wobble.

Single crystal spectra in non-polarized light were attempted but the results were not reliable. The apparent cause for that difficulty was that the light beam in the spectrophotometer was partially polarized. Similarly, O.R.D. single crystal spectra were attempted but the results were

unsatisfactory. The poor quality of the spectra was blamed on light scattering at the faces of the thinned and polished crystal samples and on random stray polarization in the system.

Spectra of Powdered Samples in Pressed Salt Discs

Three types of spectra for powdered samples were attempted, Vis-UV, O.R.D. and C.D. The results from the Vis-U.V. and O.R.D. were not satisfactory. The poor quality of those spectra was due to light scattering by the samples. C.D. spectra however were quite satisfactory. Potassium chloride was the salt used in all cases because it is inert, non-hygroscopic and fairly easy to press into transparent discs.

A sample KCℓ weighing 0.65 g was used to give discs 1 mm thick and 18 mm in diameter. Because pellets pressed in a standard KBr press were not transparent enough a special press was constructed. The press was machined from a 1.5 inch hexagonal bar of grade - 304 stainless steel. A coaxial 0.75 inch cylindrical hole was drilled through it and it was further bored and threaded from both ends to fit 1-inch steel bolts with 14 threads per inch. Two cylindrical plungers each 0.75 inches in diameter and 0.75 inches long went at the center of the press between the bolts, and contained the powdered sample between them. These plungers were machined from a special cobalt-base alloy that was chemically inert and could stand the immense pressures, required to make transparent salt discs, without deforming. The bolt threads

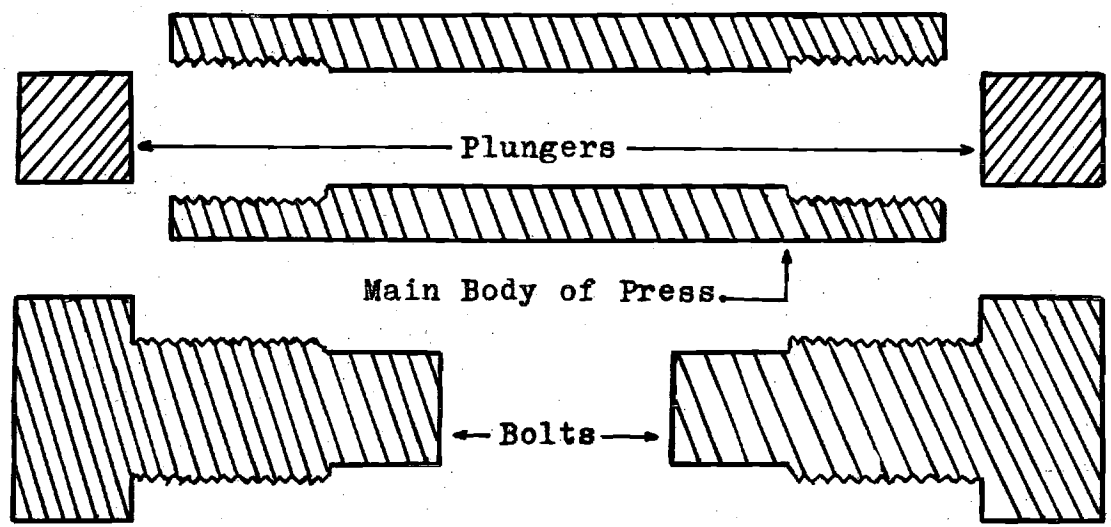

Figure 9. Diagram of Salt Press for Powdered Samples.

and the contacts between the plungers and the bolts were adequately lubricated with graphite. The sample was put in the press and it was torqued to 100 ft-lbs. After 15 minutes the press was retorqued and left for at least 4 hours before the sample was removed for immediate use. The weight of optically active material used varied from 0.001 g to 0.003 g. The sample was mixed with 0.65 g of KCℓ and ground in a mortar until shiny crystallites of the salts could just not be seen any more. Excessive grinding gave pressed discs that fogged too soon. The mixed, ground sample containing Λ-$Co(C_2N_5H_7)_3Br_3 \cdot H_2O$ was dried for 12 to 24 hours at 105°C. The sample with optically active Λ-$Co(C_2N_5H_6)_3$ (free-base complex) was dried at the same temperature under continuous vacuum pumping to prevent interaction with atmospheric CO_2 and moisture. The sample of optically active $\Delta Co(C_5H_7O_2)_3$ was more susceptible to racemization and decomposition. It was therefore dried at 50°C and continuous vacuum pumping for 24 hours.

The dried samples were removed from the oven and immediately transferred, while hot, into the press. The two plungers of the press were heated, like the samples to be pressed, just before use. The salt discs bearing the powdered samples were used, immediately after removal from the press, for recording the C.D. spectra. Those discs stayed transparent for at least three hours, after removal from the press, which was longer than required for recording

their spectra.

The quality of C.D. spectra obtained from those pressed salt discs was quite satisfactory in general. Reproducibilities were also good.

CHAPTER IV

RESULTS

Structural Data

$(-)_{589}$ Tris-(biguanide)cobalt(III) Bromide Monohydrate

There are eight identical symmetry related formula units of this material in each unit cell of the crystal, space group $C222_1$ (46). Four of those are related by a (1/2, 1/2, 0) centering operation to the other four formula units. For the purpose of the following discussion, it is sufficient to consider those four related by the general coordinates (x, y, z), (x, -y, -z), (-x, -y, 1/2 + z), (-x, y, 1/2 -z).

The coordination geometry around the cobalt atom of this complex is very nearly octahedral. The asymmetric unit is the formula unit and the complex, thus occupies a site of C1 symmetry. In all three chelate rings the imine nitrogens are coordinated to the cobalt. The average distance between a coordinated N-atom and the C-atom attached to it is 1.266 (31)Å. The average distance between an N-3 atom and each of the two C-atoms attached to it is 1.374(37)Å. The average distance between an uncoordinated amine-nitrogen and the C-atom attached to it is 1.346(38)Å. The accompanying diagrams, Figures 11 and 12, illustrate the general appearance of one formula unit and the packing of the eight

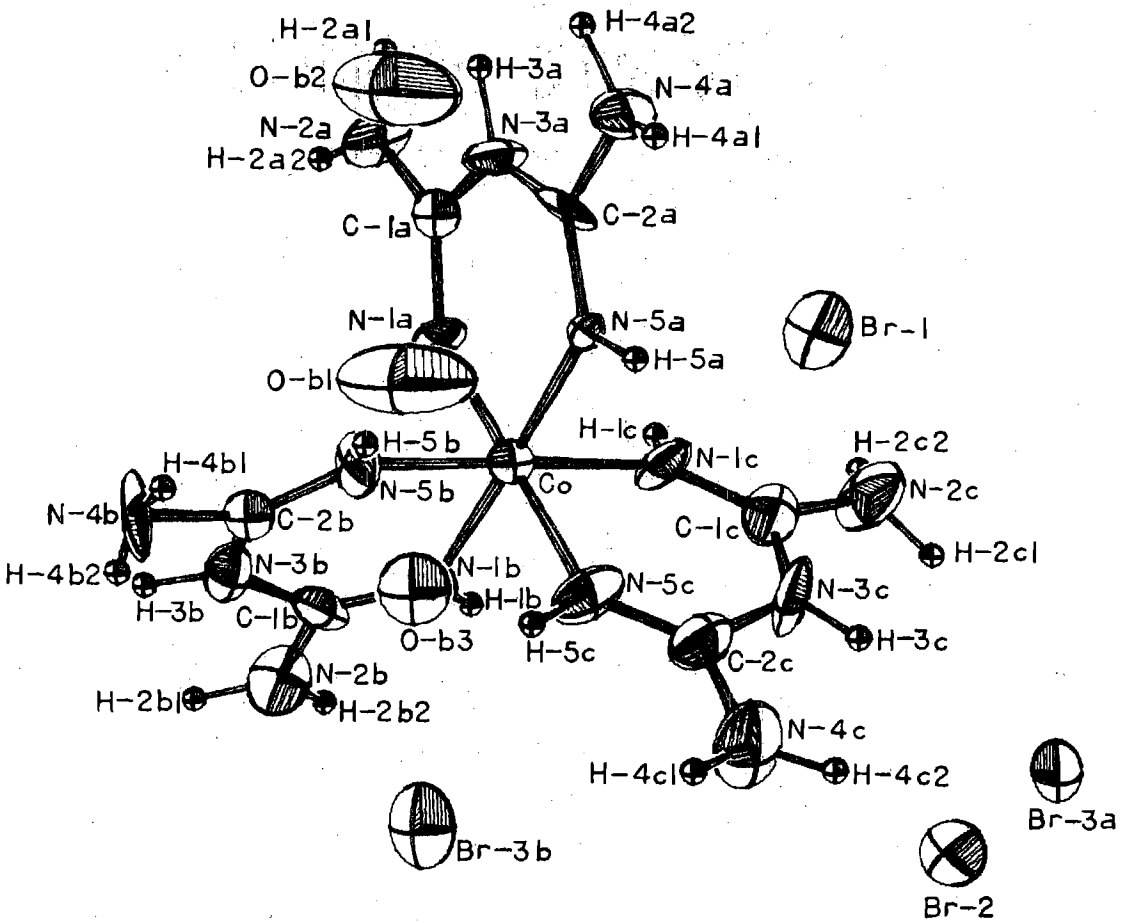

Figure 10. Atomic Labeling Scheme for $\Lambda Co(C_2N_5H_7)_3Br_3 \cdot H_2O$.

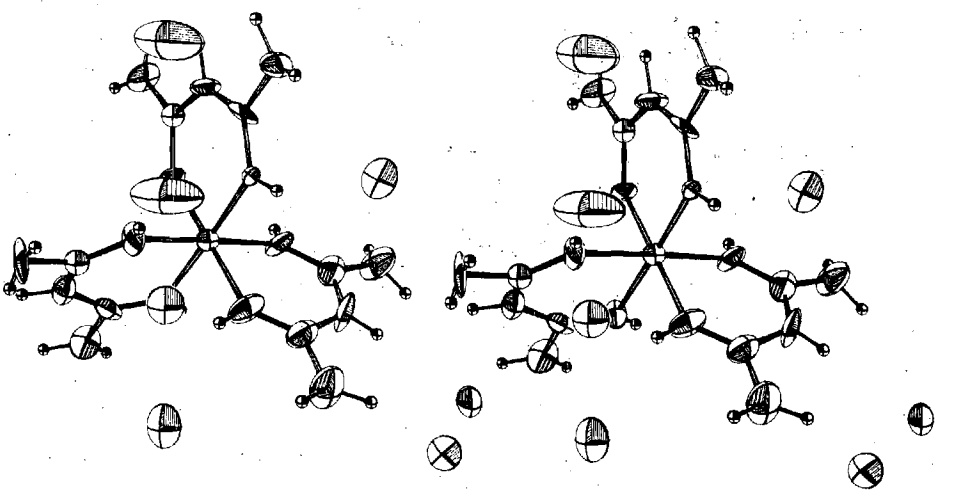

Figure 11. Stereo View of One Molecule of $\Lambda Co(C_2N_5H_7)_3Br_3 \cdot H_2O$.

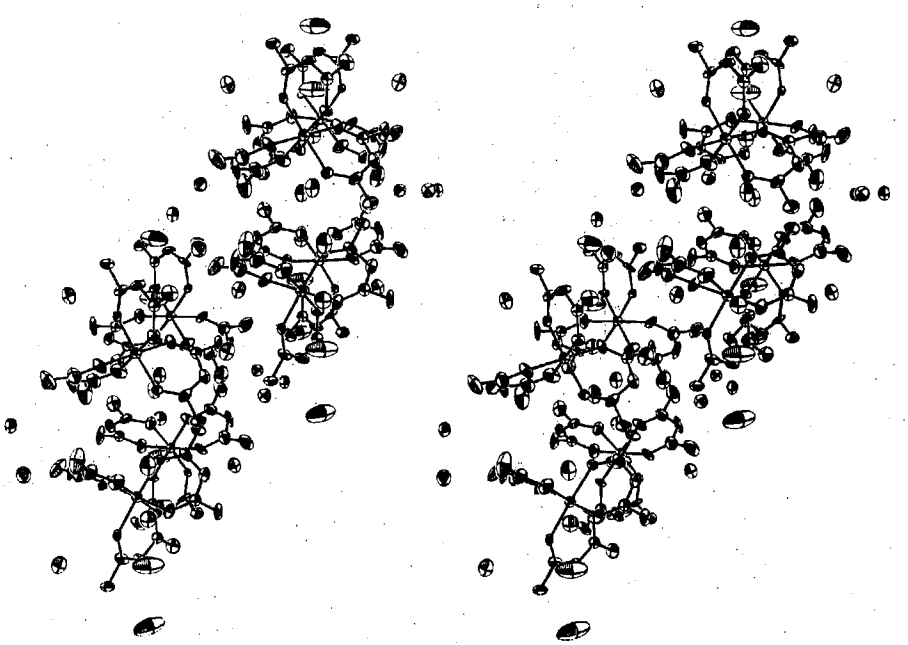

Figure 12. Packing Diagram of Eight Molecules of $\Lambda Co(C_2N_5H_7)_3Br_3 \cdot H_2O$, in a Unit Cell.

Table 8. Interatomic Distances for Λ-$Co(C_2N_5H_7)_3Br_3 \cdot H_2O$(Å)

Co, N-1a	1.895(11)	N-1b, H-1b	0.722(12)
N-1a, C-1a	1.315(16)	N-2b, H-2b1	0.980(15)
C-1a, N-2a	1.317(18)	N-2b, H-2b2	0.934(13)
C-1a, N-3a	1.371(18)	N-3b, H-3b	0.931(11)
N-3a, C-2a	1.314(17)	N-4b, H-4b1	0.896(15)
C-2a, N-4a	1.404(19)	N-4b, H-4b2	0.683(15)
C-2a, N-5a	1.289(17)	N-5b, H-5b	0.785(14)
N-5a, Co	1.913(12)	N-5b, N-1b	2.691(17)
N-1a, H-1a	0.945(12)	Co, N-1c	1.923(14)
N-2a, H-2a1	0.935(13)	N-1c, C-1c	1.262(21)
N-2a, H-2a2	0.992(13)	C-1c, N-2c	1.313(22)
N-3a, H-3a	0.941(12)	C-1c, N-3c	1.373(22)
N-4a, H-4a1	0.867(15)	N-3c, C-2c	1.416(21)
N-4a, H-4a2	1.040(13)	C-2c, C-2c	1.361(22)
N-5a, H-5a	0.785(15)	C-2c, N-5c	1.237(20)
N-5a, N-1a	2.705(16)	N-5c, Co	1.903(13)
Co, N-1b	1.940(12)	N-1c, H-1c	0.639(13)
N-1b, C-1b	1.238(18)	N-2c, H-2c1	0.918(15)
C-1b, N-2b	1.314(19)	N-2c, H-2c2	0.952(18)
C-1b, N-3b	1.410(21)	N-3c, H-3c	0.812(12)
N-3b, C-2b	1.361(19)	N-4c, H-4c1	0.964(16)
C-2b, N-4b	1.369(19)	N-4c, H-4c2	0.908(16)
C-2b, N-5b	1.258(18)	N-5c, H-5c	0.818(16)
N-5b, Co	1.913(13)	N-5c, N-1c	2.649(19)

Table 9. Interatomic Angles for Λ-$Co(C_2N_5H_7)_3Br_3 \cdot H_2O$ (Degrees)

Co, N-1a, C-1a	131.9(1.1)	Co, N-1b, C-1b	128.6(1.2)
N-1a, C-1a, N-3a	116.4(1.3)	N-1b, C-1b, N-3b	120.3(1.5)
N-1a, C-1a, N-2a	128.0(1.4)	N-1b, C-1b, N-2b	123.9(1.7)
N-2a, C-1a, N-3a	115.5(1.2)	N-2b, C-1b, N-3b	115.2(1.4)
C-1a, N-3a, C-2a	130.1(1.2)	C-1b, N-3b, C-2b	126.8(1.3)
N-3a, C-2a, N-5a	125.4(1.4)	N-3b, C-2b, N-5b	121.4(1.5)
N-3a, C-2a, N-4a	113.6(1.3)	N-3b, C-2b, N-4b	112.5(1.3)
N-4a, C-2a, N-5a	120.9(1.4)	N-4b, C-2b, N-5b	126.1(1.5)
C-2a, N-5a, Co	125.4(1.0)	C-2b, N-5b, Co	129.6(1.2)
N-5a, Co, N-1a	90.5(0.5)	N-5b, Co, N-1b	88.6(0.5)
Co, N-1a, H-1a	117.6(0.8)	Co, N-1b, H-1b	115.1(1.1)
H-1a, N-1a, C-1a	110.5(1.2)	H-1b, N-1b, C-1b	113.3(1.6)
C-1a, N-2a, H-2a1	129.6(1.4)	C-1b, N-2b, H-2b1	128.6)1.5)
C-1a, N-2a, H-2a2	128.2(1.3)	C-1b, N-2b, H-2b2	125.1(1.6)
H-2a1, N-2a, H-2a2	101.9(1.1)	H-2b1, N-2b, H-2b2	104.3(1.2)
C-1a, N-3a, H-3a	106.9(1.3)	C-1b, N-3b, H-3b	114.4(1.4)
H-3a, N-3a, C-2a	123.0(1.4)	H-3b, N-3b, C-2b	118.8(1.4)
C-2a, N-4a, H-4a1	121.4(1.3)	C-2b, N-4b, H-4b1	105.8(1.2)
C-2a, N-4a, H-4a2	102.1(1.3)	C-2b, N-4b, H-4b2	88.3(1.4)
H-4a1, N-4a, H-4a2	131.8(1.3)	H-4b1, N-4b, H-4b2	139.1(2.4)
C-2a, N-5a, H-5a	121.4	C-2b, N-5b, H-5b	112.7(1.5)
H-5a, N-5a, Co	113.2	H-5b, N-5b, Co	116.2(1.3)

Table 9. (Continued)

Co, N-1c, C-1c	131.3(1.3)
N-1c, C-1c, N-3c	120.1(1.7)
N-1c, C-1c, N-2c	127.0(1.7)
N-2c, C-1c, N-3c	112.9(1.6)
C-1c, N-3c, C-2c	127.5(1.4)
N-3c, C-2c, N-5c	119.2(1.6)
N-3c, C-2c, N-4c	112.7(1.5)
N-4c, C-2c, N-5c	127.9(1.8)
C-2c, N-5c, Co	133.1(1.4)
N-5c, Co, N-1c	87.6(0.6)
Co, N-1c, H-1c	111.9(1.3)
H-1c, N-1c, C-1c	116.8(1.8)
C-1c, N-2c, H-2c1	122.7(1.8)
C-1c, N-2c, H-2c2	119.5(1.7)
H-2c1, N-2c, H-2c2	101.3(1.6)
C-1c, N-3c, H-3c	123.8(1.6)
H-3c, N-3c, C-2c	108.2(1.5)
C-2c, N-4c, H-4c1	115.8(1.6)
C-2c, N-4c, H-4c2	128.9(1.7)
H-4c1, N-4c, H-4c2	109.9(1.5)
C-2c, N-5c, H-5c	118.1(1.6)
H-5c, N-5c, Co	108.8(1.2)

symmetry related units in a unit cell. Tables 8 and 9 give some values for the distances and angles between various atoms of one formula unit.

The structure consists of tripositive Λ-$Co(C_2N_5H_7)_3$ ions and negative bromide ions linked by hydrogen bonding. Table 11 lists those hydrogen atoms within 3.5Å from the bromide ions, and also the hydrogens within 3.5Å from the disordered oxygens of the water molecule, for one unit cell. The numbers in parentheses refer to the symmetry positions listed in Table 10. The structural data for this material

Table 10. Symmetry Equivalent Positions for Space Group $C222_1$ (46)

Position Number	Coordinates
(1)	x , y , z
(2)	x , -y , -z
(3)	-x , -y , 1/2+z
(4)	-x , y , 1/2-z
(5)	1/2+x , 1/2+y , z
(6)	1/2+x , 1/2-y , -z
(7)	1/2-x , 1/2-y , 1/2+z
(8)	1/2-x , 1/2+y , 1/2-z

are in excellent agreement with Snow's (30) data for the chloride salt of the material with opposite configuration.

Table 11. Hydrogen Bonds and Short Contacts for Λ-$Co(C_2N_5H_7)_3Br_3 \cdot H_2O$.

Atom 1	Atom 2	Dist. (Å)	Atom 1	Atom 2	Dist. (Å)
Br-1	H-2c2(7)	2.574	Br-3b	H-5c (4)	2.750
	H-2a2(6)	2.655		H-4c1(1)	2.751
	H-4a1(1)	2.733		H-4c1(4)	2.751
	H-5a (1)	2.788		H-1b (2)	3.280
	H-4b1(4)	2.804		H-1b (3)	3.280
	H-1a (6)	2.835			
	H-1c (7)	3.140	O-b1	H-5b (1)	2.483
				H-5b (4)	2.483
Br-2	H-2b1(3)	2.564		H-4b1(1)	3.150
	H-4c2(1)	2.899		H-4b1(4)	3.150
	H-4b2(4)	2.919		H-5a (1)	3.380
	H-3a (7)	2.921		H-5a (4)	3.380
	H-2a1(6)	3.109			
	H-2a1(7)	3.211	O-b2	H-2c1(7)	3.067
	H-4c1(1)	3.227		H-4a1(1)	3.218
	H-2a2(6)	3.373		H-4a1(4)	3.218
	H-4a2(7)	3.454		H-2c2(7)	3.323
Br-3a	H-3a (6)	2.562	O-b3	H-5b (1)	2.450
	H-3c (1)	2.572		H-5b (4)	2.450
	H-3c (2)	2.572		H-5c (1)	2.495
	H-2c1(1)	2.877		H-5c (4)	2.495
	H-2c1(2)	2.877		H-4b1(1)	2.971
	H-4a2(6)	2.941		H-4c1(1)	3.436
				H-4c1(4)	3.436
Br-3b	H-2b2(2)	2.468			
	H-2b2(3)	2.468			
	H-5c (1)	2.750			

The three chelate rings are labeled (a), (b) and (c). The labeling of the atoms of one formula unit is illustrated in Figure 10. Each of the chelate rings shows a small deviation from planarity. The two coordinated imine nitrogens and the two carbon atoms of each chelate ring are very nearly planar. The equations of the planes for those four atoms of each chelate ring are given in Table 12.

Table 12. Equations of the L.S. Planes for the Chelates of $\Lambda Co(C_2N_5H_7)_3Br_3 \cdot H_2O$

Equation of plane for atoms N-1a, C-1a, C-2a, N-5a: $-0.77898X + 0.05778Y + 0.62439Z + 0.47683 = 0.0$.
Dihedral angle between above plane and plane (N-1a, Co, N-5a): 4.00°

Atom	Distance From Plane, Å	Atom	Distance From Plane, Å
N-1a	-0.001	Co	-0.094
C-1a	0.001	N-2a	-0.045
C-2a	-0.001	N-3a	0.045
N-5a	0.001	N-4a	0.000
H-1a	0.007	H-3a	-0.096
H-5a	0.071		

Equations are referred to Cartesian axes with the x-axis coincident with (a) and the z axis coincident with (c). Atoms with positive distances are on one side of the plane while those with negative distances are on the other side of it.

Table 12. continued

Equation of plane for atoms N-1b, C-1b, C-2b, N-5b:
0.23052X - 0.72436Y + 0.64973 Z + 2.05081 = 0.0.
Dihedral angle bewteen above plane and plane (N-1b,Co,N-5b):
12.83°

Atom	Distance From Plane, Å	Atom	Distance From Plane, Å
N-1b	-0.054	Co	0.300
C-1b	0.052	N-2b	-0.047
C-2b	-0.053	N-3b	0.091
N-5b	0.050	N-4b	-0.251
H-1b	-0.044	H-3b	0.273
H-5b	-0.182		

Equation of plane for atoms N-1c, C-1c, C-2c, N-5c:
0.32282X + 0.86177Y + 0.39133Z - 2.85520= 0.0.
Dihedral angle between above plane and plane (N-1c, Co, N-5c):
8.55°

Atom	Distance From Plane, Å	Atom	Distance From Plane, Å
N-1c	0.005	Co	-0.205
C-1c	-0.005	N-2c	-0.041
C-2c	0.005	N-3c	-0.040
N-5c	-0.005	N-4c	0.172
H-1c	0.105	H-3c	0.025
H-5c	0.054		

The distances of the cobalt atom from the planes through the chelate atoms are not large compared to interatomic distances. However as can be seen from the figures in Table 12, the corresponding dihedral angles, between the above L.S.-planes and the planes formed by the (N-1, Co, N-5) atoms of every chelate, are not negligible. The N-3 atoms are also close to and on the same side of the respective planes as the cobalt atom. The three chelates are not inclined in the same direction around the cobalt. The inclination of the chelates around the metal is discussed in Chapter V.

Alternatively the chelate rings may be considered to have very shallow boat configurations.

The space group $C222_1$ does not contain crystallographic three-fold symmetry. The "three-fold" axis of the tris-bidentate molecule is defined as the line joining the centroids (T-1) and (T-5) of triangles (N-1a, N-1b, N-1c) and (N-5a, N-5b, N-5c), Figure 15.

The two line segments between the cobalt atom and the centroids (T-1) and (T-5) are very nearly coincident with the line between (T-1) and (T-5). The angle (T-1, Co, T-5) is 179.02°.

The angle between the molecular three-fold axis and the c-axis, θ, is called the lattice polar angle, Figures 3, 4, and 15. The three-fold axes of the eight symmetry related molecules in the unit cell are all equally inclined

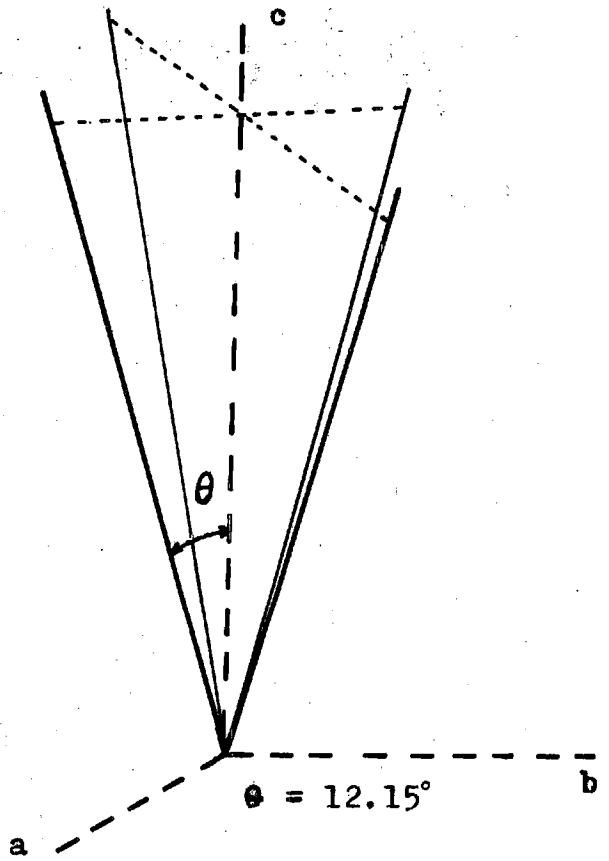

Figure 13. Inclination of the Four Symmetry-Related Three-Fold Axes About the c-Axis Direction.

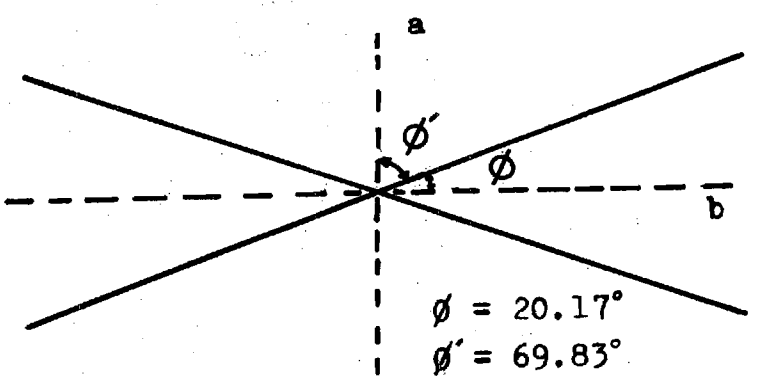

Figure 14. Traces of the Four Symmetry Related Three-Fold Axes on a Plane Parallel to the a and b Axes Directions.

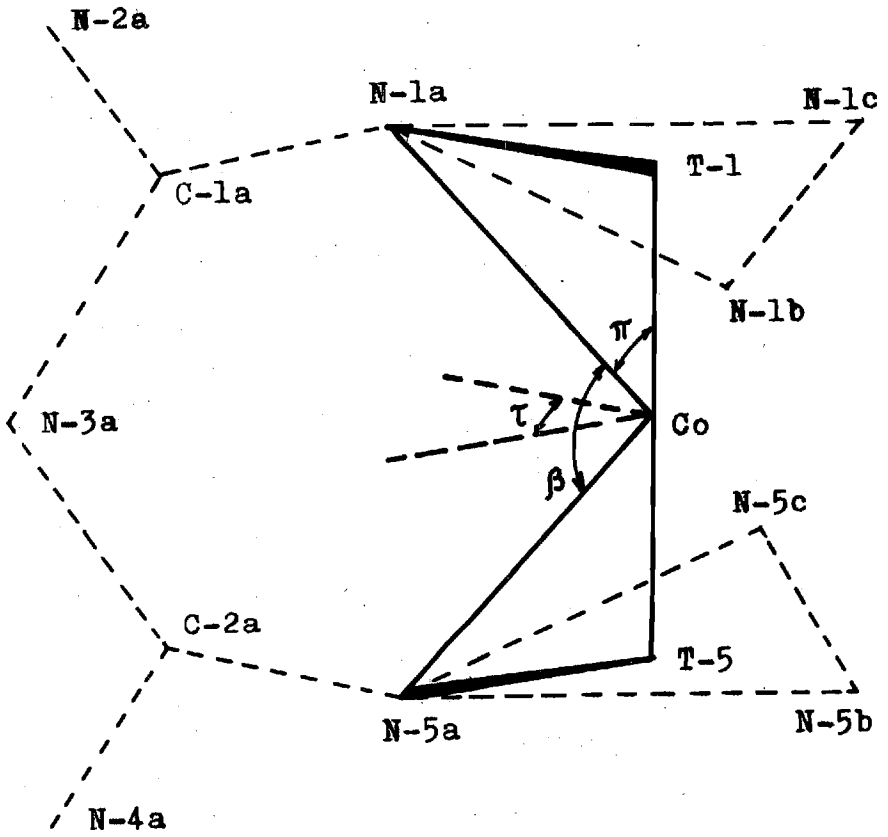

Figure 15. Illustration of Some Molecular Parameters for a Tris-Bidentate.

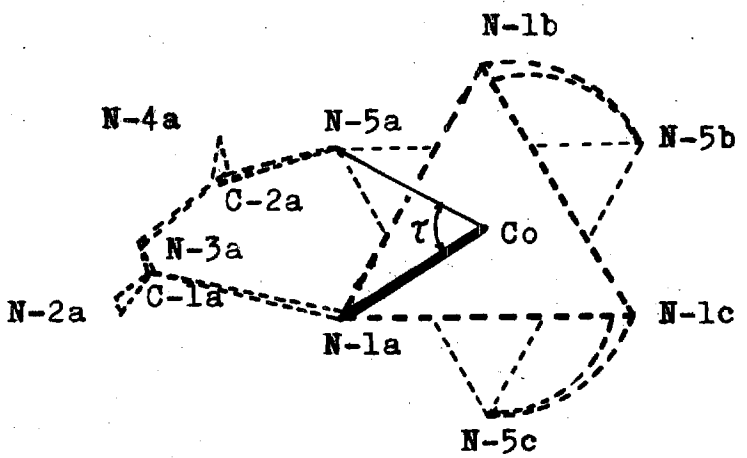

Figure 16. Illustration of Azimuthal Twist Angle for a Tris-Bidentate.

from the c-axis direction, Figure 13. The traces of the three-fold axes on a plane parallel to the a and b axial directions are shown in Figure 14. The angles ϕ and ϕ' between those traces and the a and b axes directions are called the azimuthal angles. Since the crystallographic axes are also two-fold rotation, or screw-axes, the eight symmetry-related molecules have their three-fold axes equally inclined on the lines drawn parallel to the directions of the crystallographic axes.

Figure 15 and 16 illustrate some parameters commonly used in describing tris-bidentate molecules. Table 13 gives the values of those parameters for Λ-$Co(C_2N_5H_7)_3Br_3 \cdot H_2O$. Various authors (54, 55, 56) discuss those parameters for tris-bidentates. In Table 13 and Figures 15 and 16 the symbols represent the following parameters, side, s, refers to the length of the sides of triangle N-1a, N-1b, N-1c or triangle N-5a, N-5b, N-5c. Bite, b, refers to the distance between the two coordinated atoms of a chelate ring. Height, h, refers to the length of the line segment T-1, T-5. Molecular polar angle, π, refers to the angles subtended at the Co atom by a coordinated N-atom and the centroid T-1 (or T-5). Bite angle, β, refers to the angle subtended at the Co atom by the two coordinated atoms of a chelate ring. Twist angle, τ, refers to the dihedral angle between the two planes N-1, Co, T-1 and N-5, Co, T-5 for the three chelates (a), (b), and (c).

Table 13. Values of Some Molecular Parameters for Λ-$Co(C_2N_5H_7)_3Br_3 \cdot H_2O$.

Co, Ligating N-atom (average): 1.915(.016)Å
Bite Angle, (average): 88.91 (1.454)°
Bite, b (average): 2.682(.029)Å
Height, T-1, T-5: 2.206Å
Side/Height: 1.229Å

Sides (s) Å	Molecular Polar Angles (π), Degrees	Twist Angles (τ) Degrees
N-1a, N-1b 2.669(.016)	N-1a, Co, T-1 54.97(.39)	Chelate (a) 59.29(.61)
N-1b, N-1c 2.770(.019)	N-1b, Co, T-1 53.73(.41)	Chelate (b) 57.13(.64)
N-1c, N-1a 2.749(.017)	N-1c, Co, T-1 56.82(.41)	Chelate (c) 58.43(.69)
N-5a, N-5b 2.690(.018)	N-5a, Co, T-5 54.18(.37)	
N-5b, N-5c 2.696(.019)	N-5b, Co, T-5 54.44(.45)	
N-5c, N-5a 2.688(.018)	N-5c, Co, T-5 54.77(.44)	
Average: 2.710(.040)Å	Average: 54.82°(1.074)	Average: 58.28°(1.087)

Racemic Tris-(biguanidato)cobalt(III) Dihydrate

The molecular structure of this compound is very similar to the previously discussed one, except that the N-3 nitrogens on each chelate ring have no hydrogens attached. There are four symmetry-related molecules in every unit cell. Two of those are related by a center of symmetry to the other two. Those molecules related by a center of symmetry are, obviously, of opposite configuration. The material crystallizes in monoclinic space-group $P2_1/c$ #14 (39). The three ligands are labeled (a), (b) and (c). Figures 17, 18 and 19 illustrate the labeling scheme, the molecular structure and the packing of the four symmetry-related molecules in a unit cell. Table 14 gives the values of some parameters commonly used to describe tris-bidentate molecules. Table 15 gives the equations of the least squares planes for the chelates and the distances of various atoms from these planes. The meanings of the various symbols and terms used in Table 14 are the same as in the previous section. Tables 17 and 18 give additional values of distances and angles for the racemic material $Co(C_2N_5H_6)_3 \cdot 2H_2O$.

The structure of the above material consists of individual molecules linked to each other by hydrogen bonding. The two waters of hydration also act as links between the neutral tris-bidentate molecules. Table 19 lists some hydrogen bonding and short contacts. The first parentheses

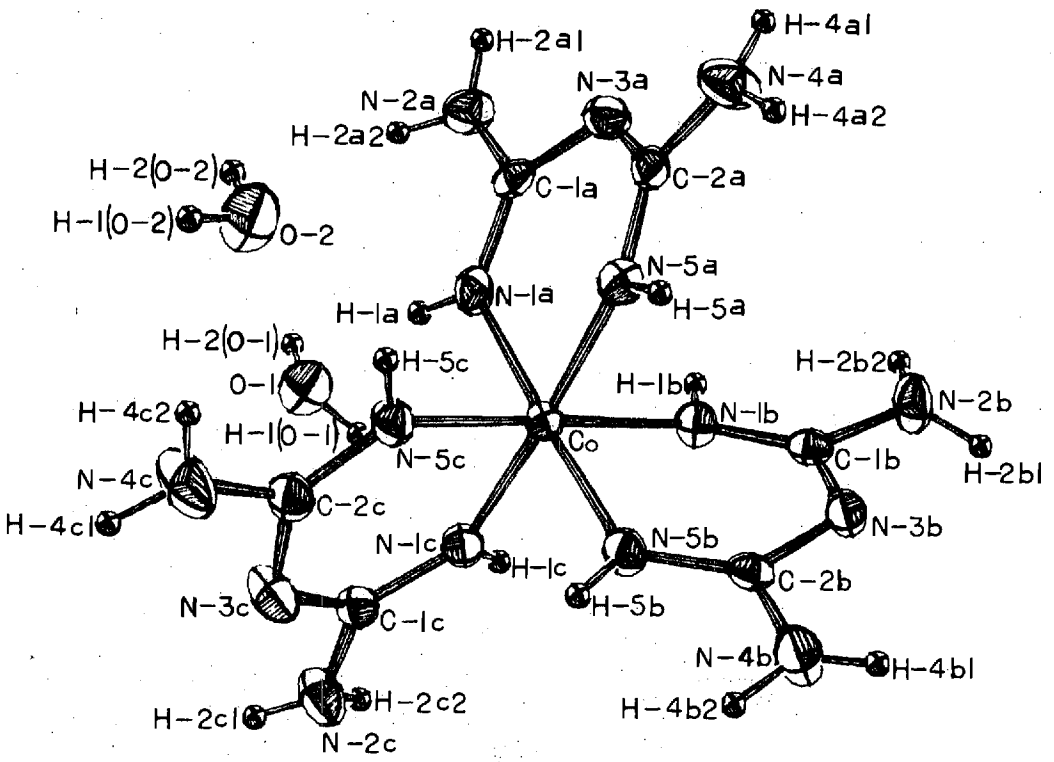

Figure 17. Atomic Labeling Scheme for Racemic $Co(C_2N_5H_6)_3 \cdot 2H_2O$.

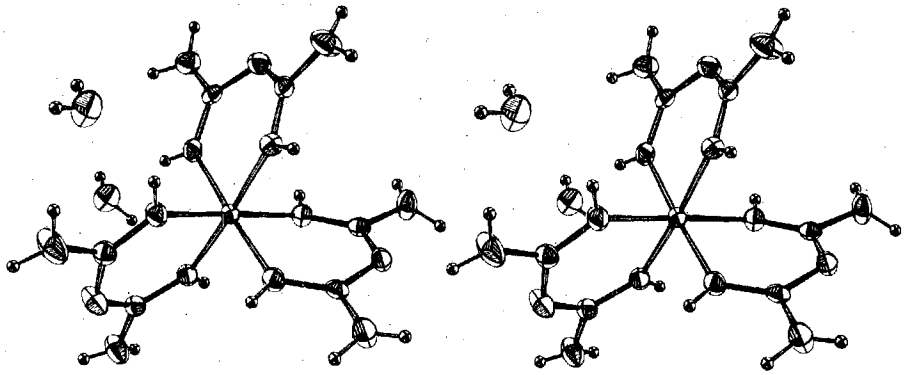

Figure 18. Stereo View of One Molecule of Racemic $Co(C_2N_5H_6)_3 \cdot 2H_2O$.

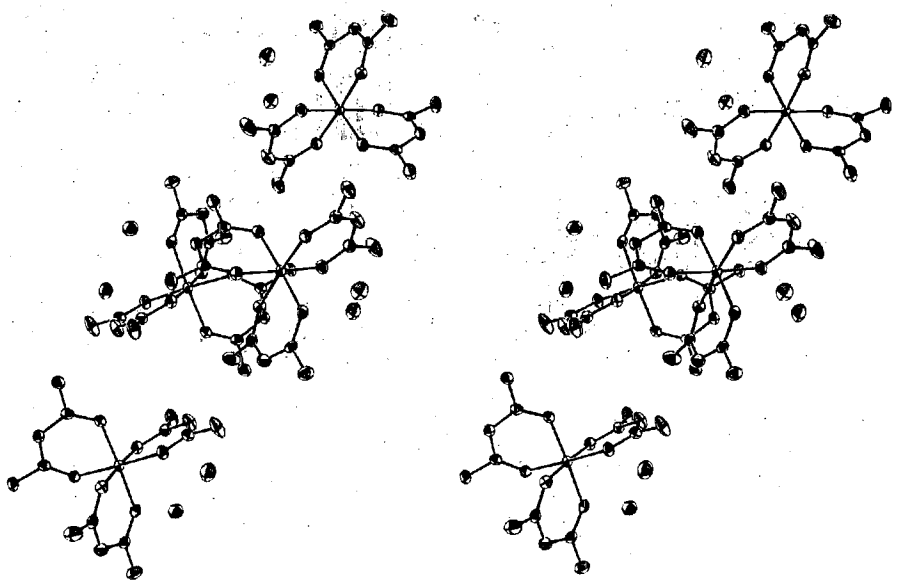

Figure 19. Packing Diagram of Four Molecules of Racemic $Co(C_2N_5H_6)_3 \cdot 2H_2O$, in a Unit Cell.

Table 14. Values of Some Molecular Parameters for Racemic $Co(C_2N_5H_6)_3 \cdot 2H_2O$.

Co, Ligating N-atom (average): 1.920(.009)Å
Bite Angle, (average): 87.04(.76°)
Bite, b (average): 2.644(.015)Å
Height, T-1, T-5: 2.169Å
Side/Height: 1.265Å

Sides (s) Å	Molecular Polar Angles (π), Degrees	Twist Angles (τ) Degrees
N-1a, N-1b 2.756(.005)	N-1a, Co, T-1 55.11(.08)	Chelate (a) 57.14(.14)
N-1b, N-1c 2.794(.005)	N-1b, Co, T-1 56.65(.08)	Chelate (b) 57.87(.14)
N-1c, N-1a 2.714(.004)	N-1c, Co, T-1 55.66(.10)	Chelate (c) 56.06(.08)
N-5a, N-5b 2.754(.004)	N-5a, Co, T-5 55.42(.09)	
N-5b, N-5c 2.722(.005)	N-5b, Co, T-5 55.62(.08)	
N-5c, N-5a 2.723(.004)	N-5c, Co, T-5 55.16(.09)	
Average: 2.744(.030)Å	Average: 55.60°(.56)	Average: 57.02°(.92)

Table 15. Equations of the Least Squares Planes for Racemic $Co(C_2N_5H_6)_3 \cdot 2H_2O$.

Equation of plane for atoms N-1a, C-1a, C-2a, N-5a:
0.58105X - 0.55607Y + 0.59428Z + 0.47098 = 0.0
Dihedral angle between above plane and plane (N-1a, Co, N-5a): 19.51°

Atom	Distance from Plane, Å	Atom	Distance from Plane, Å
N-1a	-0.010	Co	-0.460
C-1a	0.012	N-2a	0.109
C-2a	-0.019	N-3a	-0.114
N-5a	0.019	N-4a	0.101
H-1a	0.077	H-5a	0.162

Equation of plane for atoms N-1b, C-1b, C-2b, N-5b:
-0.54760X + 0.78509Y + 0.28943Z + 0.87550 = 0.0
Dihedral angle between above plane and plane (N-1b, Co, N-5b): 23.86°

Atom	Distance from Plane, Å	Atom	Distance from Plane, Å
N-1b	0.030	Co	-0.563
C-1b	-0.037	N-2b	-0.085
C-2b	0.032	N-3b	-0.075
N-5b	-0.021	N-4b	0.175
H-1b	0.050	H-5b	0.017

Equation of plane for atoms N-1c, C-1c, C-2c, N-5c:
-0.93308X - 0.35170Y + 0.07531Z + 2.54872 = 0.0
Dihedral angle between above plane and plane (N-1c, Co, N-5c): 5.94°

Atom	Distance from Plane, Å	Atom	Distance from Plane, Å
N-1c	-0.007	Co	0.143
C-1c	0.008	N-2c	-0.008
C-2c	-0.008	N-3c	0.060
N-5c	0.008	N-4c	-0.079
H-1c	-0.137	H-5c	-0.123

refer to the symmetry position, as listed in Table 16. The

Table 16. Symmetry Equivalent Positions for Space Group $P2_1/c$ (39).

Position Number	Coordinates
(1)	x , y , z
(2)	-x , -y , -z
(3)	-x , 1/2+y , 1/2-z
(4)	x , 1/2-y , 1/2+z

second parentheses indicate the neighboring unit cell along the a, b, and c crystallographic axes respectively. An atom in the reference molecule would thus be identified with the parentheses, (1)(0, 0, 0).

Because the space group $P2_1/c$ contains no three-fold crystallographic symmetry the three-fold axis is defined as for the previous case. The lattice-polar angle for this substance is defined as the angle between the directions of the crystallographic b-axis and the molecular three-fold axis, Figure 13. Only two molecules and their three-fold axes need to be considered for this material; those that are related by the coordinates x, y, z and -x, 1/2+y, 1/2-z. The other two molecules in the unit-cell are related to those two by a center of inversion and their treatment would offer no additional information to this work. Hence, the two molecular positions represented by the above two sets of

Table 17. Interactomic Distances for Racemic $Co(C_2N_5H_6)_3 \cdot 2H_2O$ (Å)

Co, N-1a	1.911(3)	N-2b, H-2b2	0.883(3)
N-1a, C-1a	1.297(4)	N-4b, H-4b1	0.783(3)
C-1a, N-2a	1.375(4)	N-4b, H-4b2	0.954(3)
C-1a, N-3a	1.362(4)	N-5b, H-5b	0.869(3)
N-3a, C-2a	1.362(4)	N-5b, N-1b	2.638(4)
C-2a, N-4a	1.365(4)	Co, N-1c	1.926(3)
C-2a, N-5a	1.300(4)	N-1c, C-1c	1.313(4)
N-5a, Co	1.924(3)	C-1c, N-2c	1.379(4)
N-1a, H-1a	0.825(3)	C-1c, N-3c	1.346(4)
N-2a, H-2a1	0.809(3)	N-3c, C-2c	1.370(4)
N-2a, H-2a2	0.828(3)	C-2c, N-4c	1.372(4)
N-4a, H-4a1	0.858(3)	C-2c, N-5c	1.292(4)
N-4a, H-4a2	0.825(3)	N-5c, Co	1.908(3)
N-5a, H-5a	0.945(3)	N-1c, H-1c	0.912(3)
N-5a, N-1a	2.634(4)	N-2c, H-2c1	0.756(3)
Co, N-1b	1.932(3)	N-2c, H-2c2	0.843(3)
N-1b, C-1b	1.306(4)	N-4c, H-4c1	0.900(3)
C-1b, N-2b	1.385(4)	N-4c, H-4c2	0.817(3)
C-1b, N-3b	1.350(4)	N-5c, H-5c	0.842(3)
N-3b, C-2b	1.374(4)	N-5c, N-1c	2.661(4)
C-2b, N-4b	1.353(4)	O-1, H-1(O-1)	0.883(3)
C-2b, N-5b	1.298(4)	O-1, H-2(O-1)	0.771(2)
N-5b, Co	1.919(3)	O-2, H-1(O-2)	0.843(3)
N-1b, H-1b	0.857(2)	O-2, H-2(O-2)	0.689(3)
N-2b, H-2b1	0.850(3)		

Table 18. Interatomic Angles for Racemic $Co(C_2N_5H_6)_3 \cdot 2H_2O$ (Degrees)

Co, N-1a, C-1a	128.02(21)	Co, N-1b, C-1b	124.15(19)
N-1a, C-1a, N-3a	125.74(27)	N-1b, C-1b, N-3b	127.26(29)
N-1a, C-1a, N-2a	120.30(27)	N-1b, C-1b, N-2b	120.39(27)
N-2a, C-1a, N-3a	113.90(26)	N-2b, C-1b, N-3b	112.36(28)
C-1a, N-3a, C-2a	119.39(26)	C-1b, N-3b, C-2b	119.32(27)
N-3a, C-2a, N-5a	126.41(26)	N-3b, C-2b, N-5b	125.51(28)
N-3a, C-2a, N-4a	113.64(27)	N-3b, C-2b, N-4b	114.17(29)
N-4a, C-2a, N-5a	119.88(27)	N-4b, C-2b, N-5b	120.30(29)
C-2a, N-5a, Co	126.41(20)	C-2b, N-5b, Co	127.34(22)
N-5a, Co, N-1a	86.76(11)	N-5b, Co, N-1b	86.47(13)
Co, N-1a, H-1a	117.97(23)	Co, N-1b, H-1b	118.65(23)
H-1a, N-1a, C-1a	113.34(27)	H-1b, N-1b, C-1b	112.93(28)
C-1a, N-2a, H-2a1	122.90(29)	C-1b, N-2b, H-2b1	117.34(29)
C-1a, N-2a, H-2a2	111.21(29)	C-1b, N-2b, H-2b2	119.95(31)
H-2a1, N-2a, H-2a2	114.52(33)	H-2b1, N-2b, H-2b2	115.85(32)
C-2a, N-4a, H-4a1	115.69(30)	C-2b, N-4b, H-4b1	118.40(30)
C-2a, N-4a, H-4a2	120.35(31)	C-2b, N-4b, H-4b2	117.88(29)
H-4a1, N-4a, H-4a2	116.24(36)	H-4b1, N-4b, H-4b2	123.72(31)
C-2a, N-5a, H-5a	108.50(24)	C-2b, N-5b, H-5b	112.04(28)
H-5a, N-5a, Co	124.17(20)	H-5b, N-5b, Co	118.90(24)

Table 18. (Continued)

Co, N-1c, C-1c	128.20(21)
N-1c, C-1c, N-3c	127.09(28)
N-1c, C-1c, N-2c	119.72(27)
N-2c, C-1c, N-3c	113.18(27)
C-1c, N-3c, C-2c	119.70(27)
N-3c, C-2c, N-5c	126.67(29)
N-3c, C-2c, N-4c	113.97(29)
N-4c, C-2c, N-5c	119.35(30)
C-2c, N-5c, Co	129.56(23)
N-5c, Co, N-1c	87.90(13)
Co, N-1c, H-1c	116.90(22)
H-1c, N-1c, C-1c	114.86(26)
C-1c, N-2c, H-2c1	119.80(32)
C-1c, N-2c, H-2c2	118.03(30)
H-2c1, N-2c, H-2c2	113.82(34)
C-2c, N-4c, H-4c1	116.48(32)
C-2c, N-4c, H-4c2	113.89(31)
H-4c1, N-4c, H-4c2	122.46(39)
C-2c, N-5c, H-5c	115.04(29)
H-5c, N-5c, Co	115.20(22)
H-1(O-1), O-1, H-2(O-1)	98.74(25)
H-1(O-2), O-2, H-2(O-2)	111.91(34)

Table 19. Hydrogen Bonds and Short Contacts for Racemic $Co(C_2N_5H_6)_3 \cdot 2H_2O$.

Atom 1	Atom 2	Dist. (Å)
N-1a	H-4b1(4)(0,0,-1)	2.888
	H-4c1(2)(1,0,0)	2.959
N-2a	H-4b1(3)(0,0,-1)	2.726
	H-2/O-2(3)(1,0,-1)	2.869
	H-2/O-1(3)(1,-1,-1)	2.923
	H-1/O-1(3)(1,-1,-1)	3.151
N-3a	H-2/O-1(3)(1,-1,-1)	2.024
	H-2c1(4)(0,0,-1)	2.673
N-4a	H-2a2(3)(1,-1,-1)	2.545
	H-2/O-1(3)(1,-1,-1)	2.896
N-1b	H-5a(3)(1,1,-1)	2.400
N-2b	H-2c2(3)(0,-1,-1)	2.577
	H-1/O-1(3)(0,-1,-1)	3.107
N-3b	H-1/O-1(3)(0,-1,-1)	2.207
	H-1c(3)(0,-1,-1)	2.634
	H-2a2(1)(-1,0,0)	2.821
N-4b	H-4c1(2)(0,0,0)	2.517
	H-1b(3)(0,-1,-1)	2.735
	H-1/O-1(3)(0,-1,-1)	2.823
N-5b	H-4a2(3)(0,0,-1)	2.799
N-1c	H-4a2(3)(0,0,-1)	2.674
N-2c	H-2b2(4)(0,0,0)	2.782
	H-2/O-2(2)(1,0,0)	3.098
N-3c	H-4ba(2)(0,0,0)	2.039
	H-2/O-2(2)(1,0,0)	2.502
	H-5b(2)(0,0,0)	2.956
N-4c	H-4b2(2)(0,0,0)	2.681
O-1	H-1/O-2(2)(1,0,0)	1.935
	H-1a(1)(0,0,0)	2.312
	H-4b1(3)(0,0,-1)	2.583
O-2	H-2b1(3)(0,-1,-1)	2.220
	H-4c2(1)(0,0,0)	2.252
	H-2a1(3)(1,-1,-1)	2.533
	H-1/O-1(1)(0,-1,0)	3.109
	H-2/O-1(2)(1,0,0)	3.124
	H-2/O-1(1)(0,-1,0)	3.264

coordinates, will be the ones referred to in all following discussions. The molecules at these positions and their three-fold axes are related by a two-fold screw-axis. The traces of these three-fold axes on a plane parallel to the directions of the a and c crystal axes are collinear. The azimuthal angles ϕ and ϕ' for this structure are defined as the angles between the trace of the exposed crystal face and the trace of the three-fold axes on a plane parallel to the directions of the a and c crystal axes, Figures 38, 39 and 40.

Solution Spectra

Absorption Spectra

Electronic absorption spectra were measured in the visible and ultraviolet (Vis-UV) regions. The spectra for Λ-$Co(C_2N_5H_7)_3Br_3 \cdot H_2O$ and racemic $Co(C_2N_5H_6)_3 \cdot 2H_2O$ were measured in water solution. The corresponding spectra for racemic $Co(C_5H_7O_2)_3$ were measured in cyclohexane solution. Due to the low solubility of the latter material in cyclohexane 10 - cm cells were used to record those spectra. Table 20 gives the values for positions of absorption maxima, the molar extinction coefficients ε-max, the full width at half height and the dipole strength D for the three substances described above.

The expression for D, the dipole strength, for a Gaussian type transition is (11, 57)

Table 20. Data on Molar Absorbances for Solutions.

Compound	ν(kk)	ε_{max}	$\Delta\nu_{1/2}$(kk)	D(cgs)
$\Lambda Co(C_2N_5H_7)_3Br_3 \cdot H_2O$	21.05	191.5	3.635	3240
	28.29	170.8		
	37.37	3596		
Rac. $Co(C_2N_5H_6)_3 \cdot 2H_2O$	20.83	233.1	4.140	4540
	27 shoulder	203		
	34 shoulder			
Rac. $Co(C_5H_7O_2)_3$ (in cyclohexane solution)	16.89	137.5	3.025	2414
	31.16	7356		
	38.94	35760		
	43.54	39040		

The abbreviations in the table above represent the following:

ν : Frequency in kilokaisers
ε_{max} : Extinction coefficient, liter. $mole^{-1}$. cm^{-1}
$\Delta\nu_{1/2}$: Full width at half height, in kilokaisers
D : Dipole strength, 10^{-40} cgs units.
Rac. stands for Racemic.

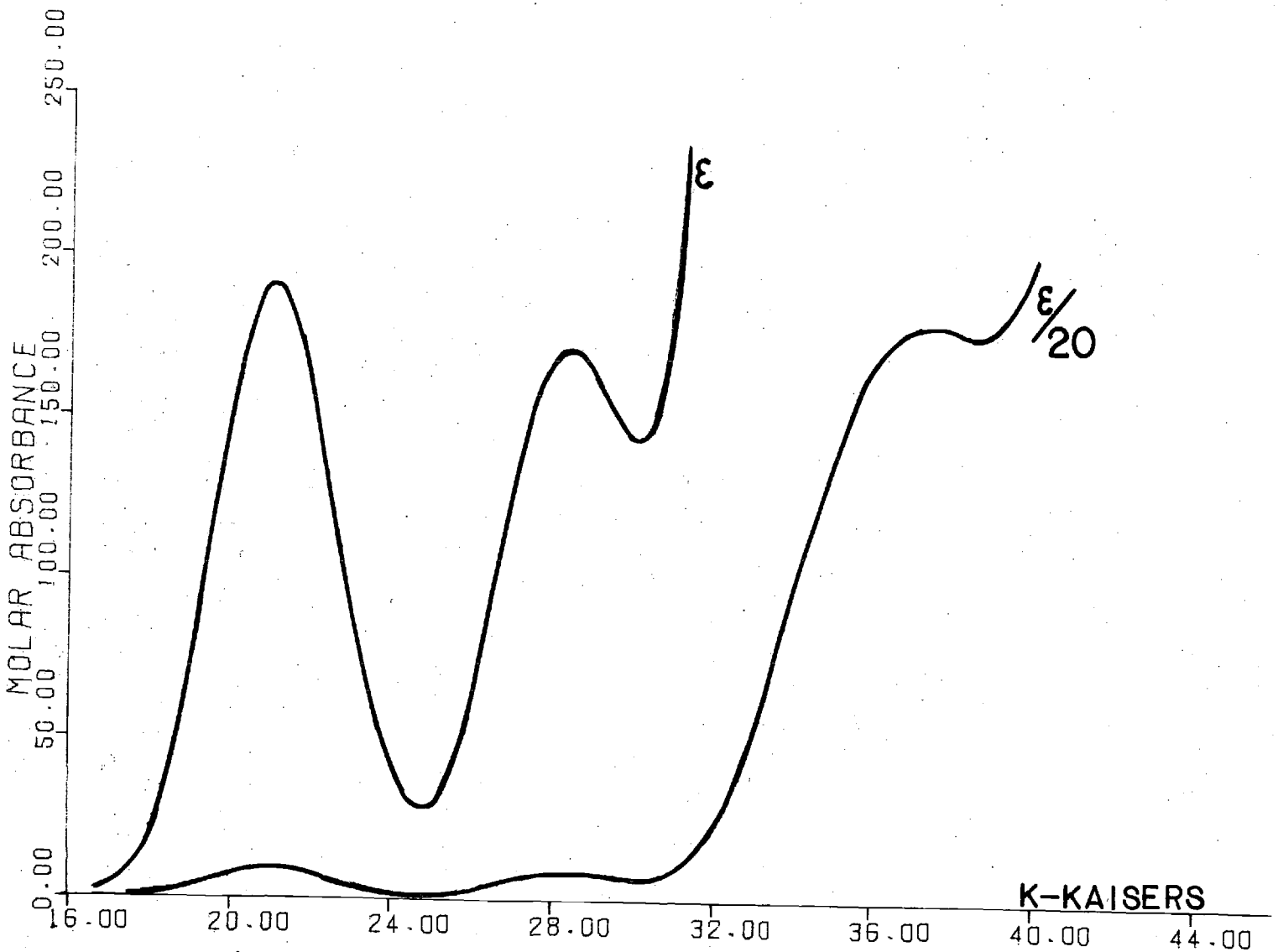

Figure 20. Molar Absorbance of $\Lambda Co(C_2N_5H_7)_3Br_3 \cdot H_2O$ in Water Solution.

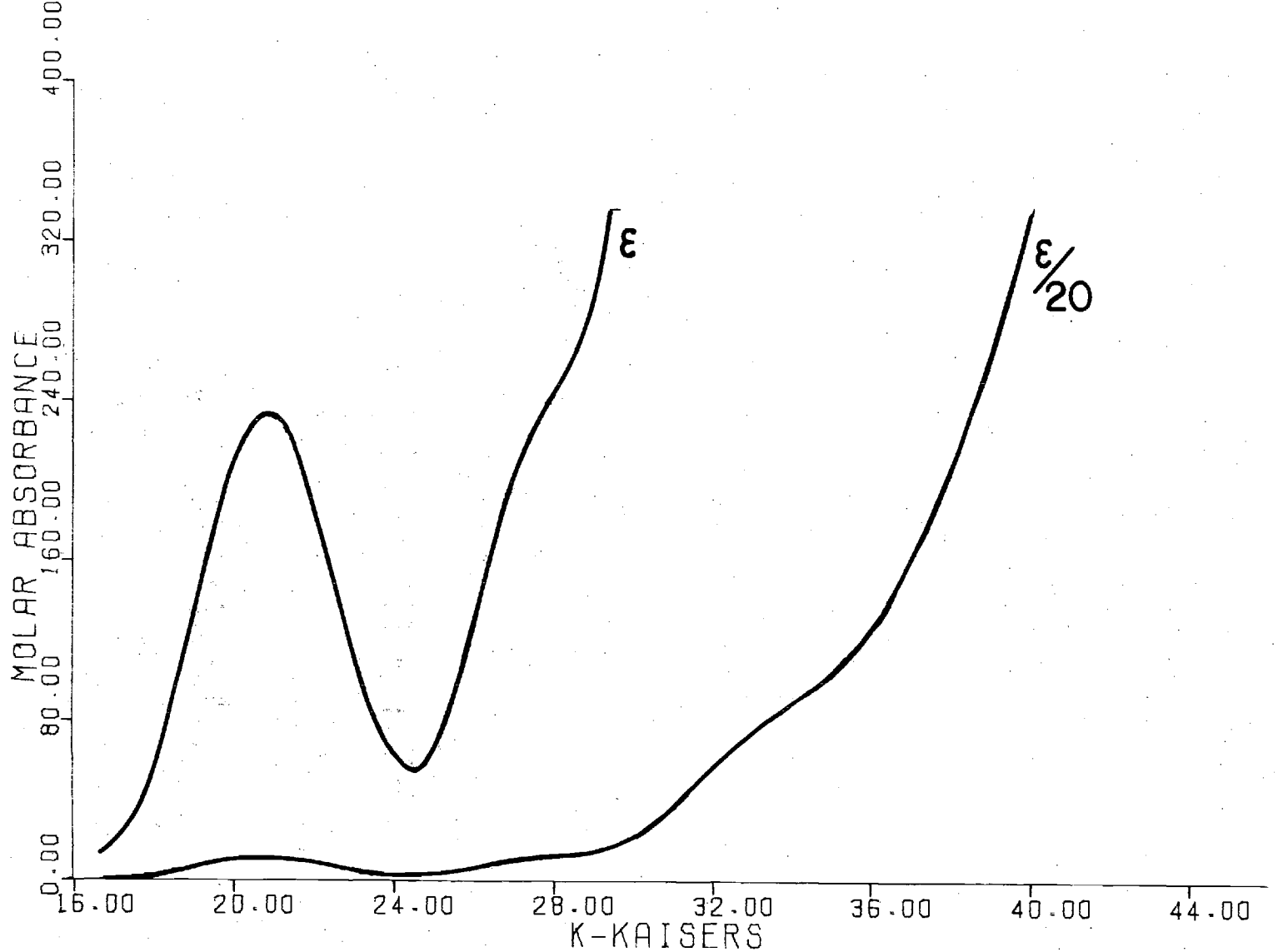

Figure 21. Molar Absorbance of $Co(C_2N_5H_6)_3 \cdot 2H_2O$ in Water Solution.

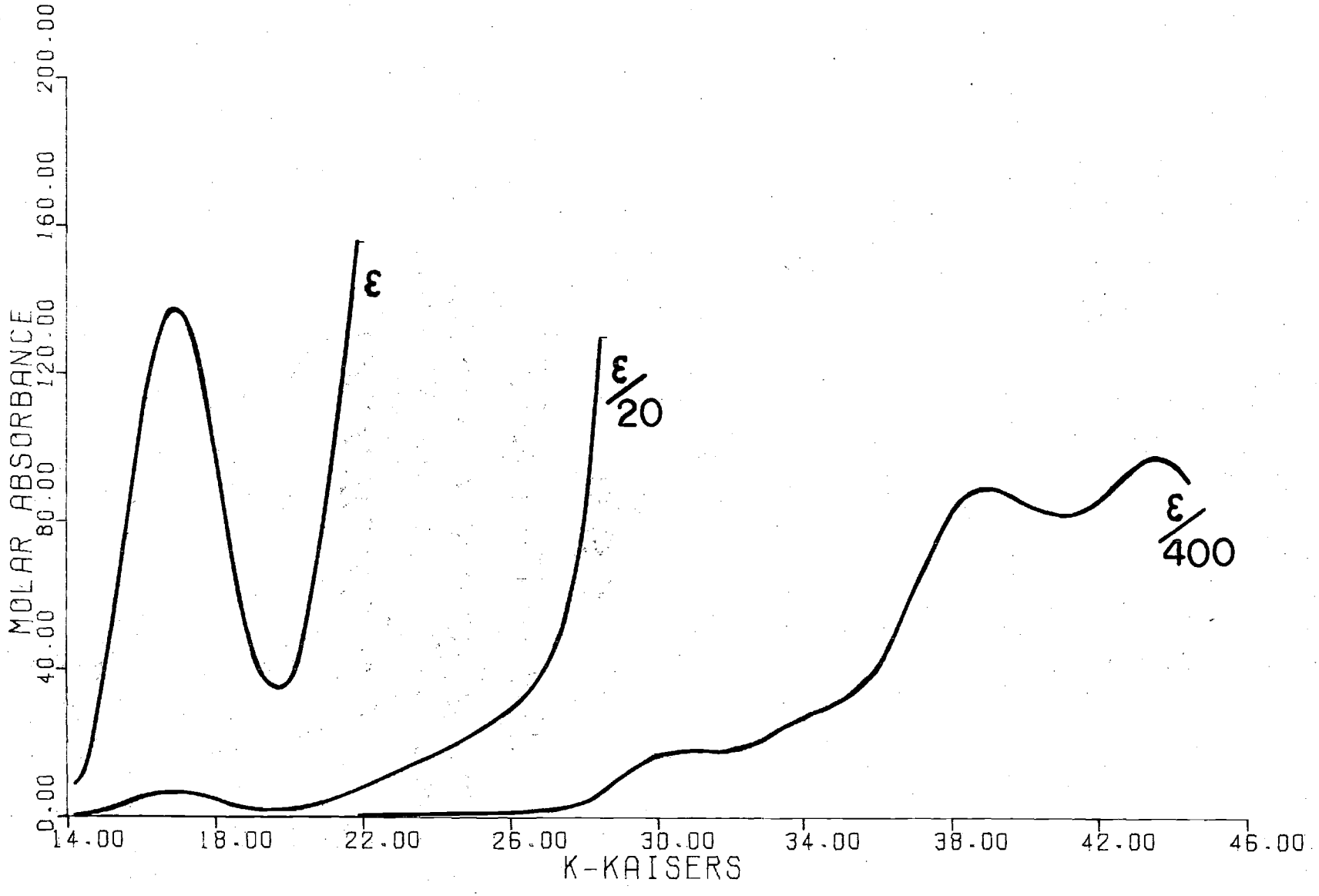

Figure 22. Molar Absorbance of $Co(C_5H_7O_2)_3$ in Cyclohexane Solution.

$$D = \frac{3hc(10^3)\ell n(10)}{8\pi^3 N}\int(\varepsilon/\nu)\ d\nu \simeq \frac{98x10^{-40}\cdot\varepsilon_{max}\cdot\Delta\nu 1/2}{\nu_o}$$

where the various terms have their usual meanings and the frequency ν is measured in KK (KK = $10^5/\lambda$ in Å).

The traces of those in the Vis-UV ranges are graphically illustrated in Figures 20, 21, and 22.

The spectra for those materials given above agree well with data given by other authors (58, 59, 35, 61).

Optical Rotary Dispersion Spectra

The ORD spectra presented here were determined on the same solutions for which CD spectra are presented in the following section. Those ORD spectra are included as an aid for the identification of the particular optical isomers used. No ORD spectrum was measured for $Co(C_2N_5H_6)_3$ but all optically active samples of this material were obtained by deprotonation of Λ-$Co(C_2N_5H_7)_3Br_3\cdot H_2O$ and were therefore assumed to have the same Λ-absolute configuration. The ORD spectrum of Λ-$Co(C_2N_5H_7)_3Br_3\cdot H_2O$ was determined for a water solution of the material while the ORD spectrum of Δ-$Co(C_5H_7O_2)_3$ was determined for a solution of the material in cyclohexane. Figures 23 and 24 show those ORD spectra.

Circular Dichroism Spectra

The CD spectra described here were determined in the Vis-UV ranges. The spectra for Λ-$Co(C_2N_5H_7)_3Br_3\cdot H_2O$ were determined for water solutions and methanol solutions of the

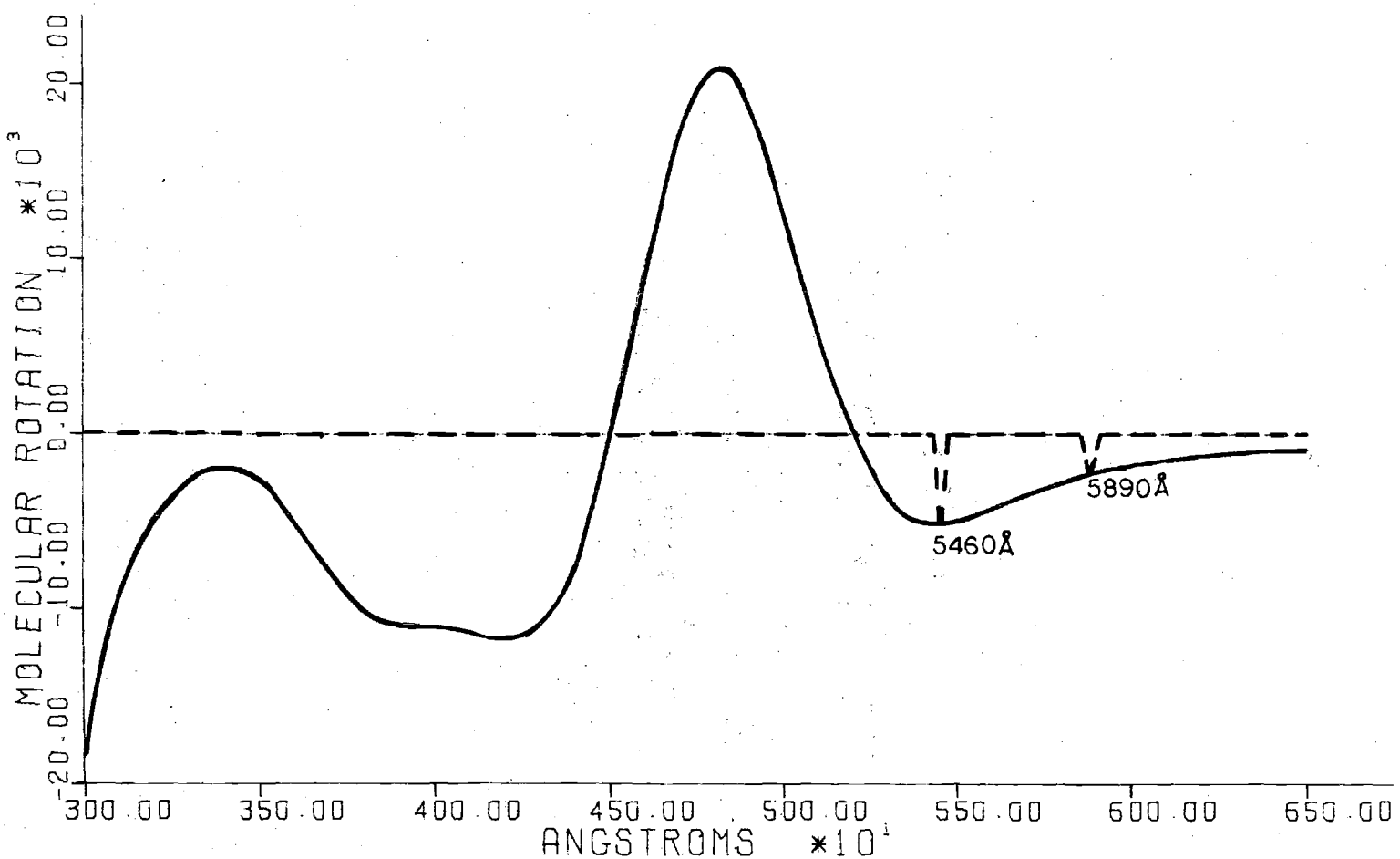

Figure 23. O.R.D. Spectrum of $\Lambda Co(C_2N_5H_7)_3Br_3 \cdot H_2O$ in Water Solution.

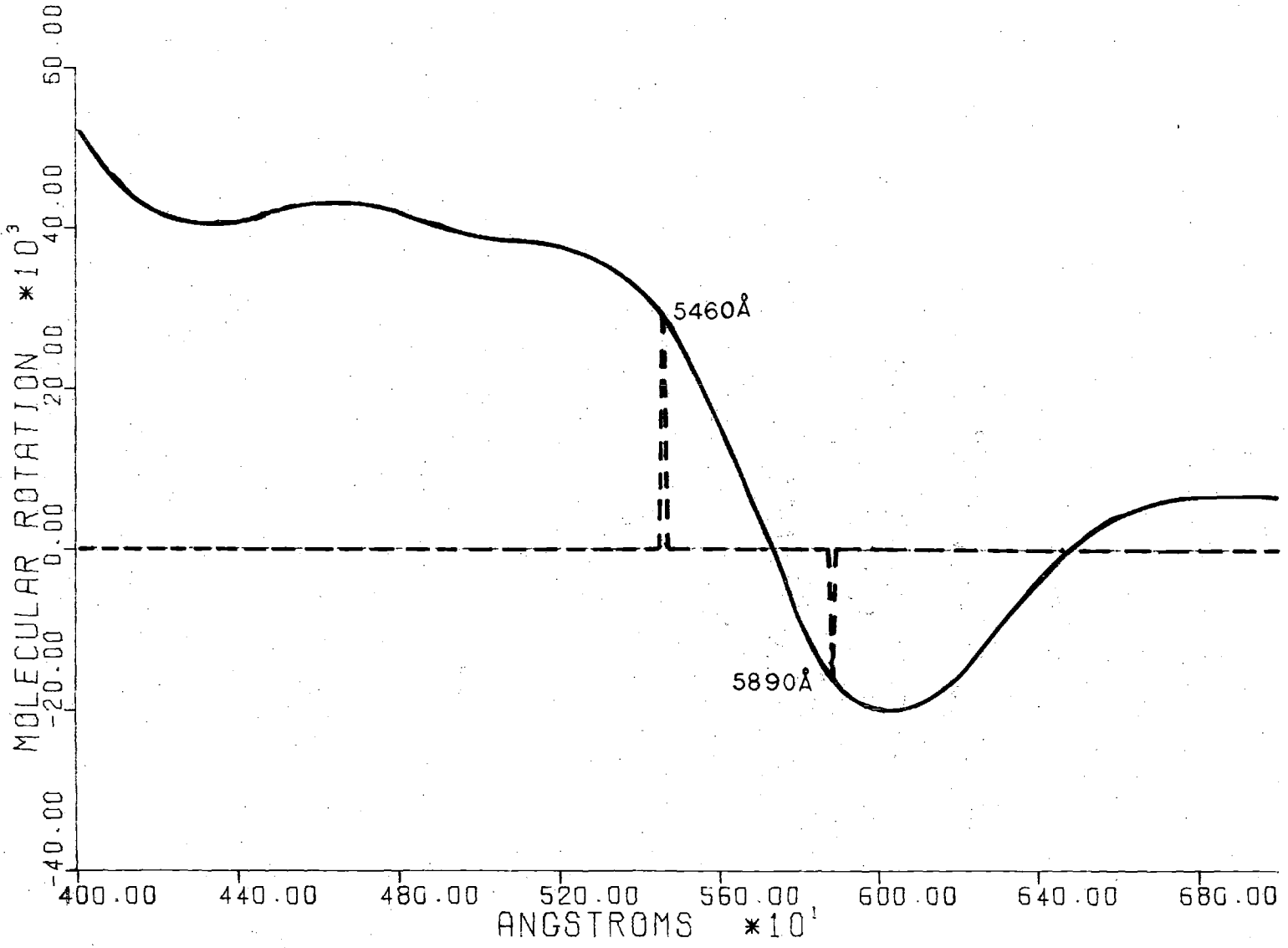

Figure 24. O.R.D. Spectrum of $\Delta Co(C_5H_7O_2)_3$ in Cyclohexane Solution.

material. The spectrum for Λ-$Co(C_2N_5H_6)_3$ was measured in methanol solution. The spectrum for Δ-$Co(C_5H_7O_2)_3$ was measured in cyclohexane solution. The data obtained for those spectra agree well with the corresponding data obtained by other investigators (35, 58, 59, 61).

The CD spectra in this section, and in the following sections, were resolved into Gaussian components to obtain approximate values for frequency separations at the peaks of the various CD transition bands. The resolution into Gaussian components was performed by a computer program written by Schievelbein and Swart (60). The program sought to fit a pre-assigned number of Gaussian components of the form, Component = $\phi_1 \exp(-(\phi_2-KK)^2/(\phi_3)^2))$, to the various peaks of the CD spectrum. The refinement of the fit was stopped when a shift of .002 for any of the variables produced no improvement of the fit. Tables 21 and 22 give the data for the CD spectra and the results of the Gaussian resolution of the three materials discussed above. Figures 25, 26, 27, and 28 illustrate those CD spectra and the corresponding Gaussian components.

The identification of the various bands in solution spectra was based on the results of single crystal spectra for those materials. Those single crystal spectra are discussed in the following sections.

Table 21. C.D. Spectral Data for Solutions.

Compound	ν_o(kk)	$(\varepsilon_\ell - \varepsilon_r)$	Compound	ν_o(kk)	$(\varepsilon_\ell - \varepsilon_r)$
$\Lambda Co(C_2N_5H_7)_3Br_3 \cdot$	46.30	32.52	$\Lambda Co(C_2N_5H_7)_3Br_3 \cdot$	45.	4. (*)
	41.32	-41.51		40.98	-4.81 (*)
H_2O/H_2O Solution	33.67	0.74	H_2O/MeOH solution	33.22	0.055 (*)
	27.93	-1.88		27.78	-0.17 (*)
	22.12	4.74		22.03	0.40 (*)
	19.61	-3.53		19.53	-0.41 (*)
$\Delta Co(C_5H_7O_2)_3$/	43.47	65.77	$Co(C_2N_5H_6)_3$/	45.	3.6 (*)
cyclohexane	37.59	-212.43	MeOH solution	40.16	-4.25 (*)
solution	34.48	15.49		30.12	-0.17 (*)
	30.30	101.25		27.78	-0.21 (*)
	23.47shoulder	6.06		21.93	0.38 (*)
	17.70	-8.38		19.23	-0.47 (*)
	15.53	2.68			

The abbreviations in the table above represent the following:

ν_o : Frequency in kilokaisers

$(\varepsilon_\ell - \varepsilon_r)$: Differential extinction coefficient, liter. mole.$^{-1}$ cm^{-1}

(*) : Relative magnitudes, data not quantitative.

Table 22. Gaussian Components for Solution C.D. Spectra.

Compound	ν_o(kk)	$(\varepsilon_\ell - \varepsilon_r)$	$\nu_{1/2}$(kk)	R(cgs)	#
$\Lambda Co(C_2N_5H_7)_3Br_3 \cdot$	45.62	48.73	5.412	141.6	(1)
	41.97	-51.62	5.987	-180.4	(2)
H_2O/H_2O Solution	33.93	1.108	1.988	1.590	(3)
	28.09	-1.892	2.050	-3.383	(4)
	22.00	4.950	2.781	15.33	(5)
	19.79	-4.313	2.175	-11.61	(6)
σ (bands 4, 5, 6):		0.080 (74 data points)			
σ (bands 1, 2, 3, 4):		0.775			
σ (overall)		0.775 (119 data points)			
$\Lambda Co(C_5H_7O_2)_3$/	43.27	66.50	2.997	112.9	(1)
	37.75	-214.4	3.597	-500.5	(2)
cyclohexane	35.22	43.48	2.131	64.46	(3)
solution	30.23	101.3	3.447	282.9	(4)
	23.50	5.956	4.163	25.85	(5)
	17.62	-8.467	2.097	-24.69	(6)
	15.73	3.431	1.522	8.133	(7)
σ (bands 6, 7):		0.225 (41 data points)			
σ (overall)		6.46 (124 data points)			
$\Lambda Co(C_2N_5H_7)_3Br_3 \cdot$	45.	5.8	3.75	(*)	(1)
	41.23	-5.099	6.305	(*)	(2)
H_2O/MeOH Solution	33.62	0.141	1.881	(*)	(3)
	27.91	-0.174	3.492	(*)	(4)
	21.92	0.419	2.638	(*)	(5)
	19.63	-0.460	2.139	(*)	(6)
σ (bands 4, 5, 6):		0.007 (60 data points)			
σ (bands 1, 2, 3):		0.084 (54 data points)			
σ (overall)		0.063 (94 data points)			

(*): Relative magnitudes, data not quantitative.

Table 22. (Continued)

Compound	ν_o(kk)	$(\varepsilon_\ell - \varepsilon_r)$	$\nu_{1/2}$(kk)	R(cgs)	#
$Co(C_2N_5H_6)_3$	44.4	5.9	4.4	(*)	(1)
	41.11	-5.025	6.843	(*)	(2)
	-	-	-	-	(3)
	28.44	-0.219	4.522	(*)	(4)
	21.77	0.410	2.711	(*)	(5)
	19.36	-0.514	2.414	(*)	(6)

σ (bands 4, 5, 6): 0.012 (100 data points)
σ (bands 1, 2) : < 0.06 (58 data points)
σ (overall) : 0.051 (136 data points)

The abbreviations in the table above represent the following:

ν_o : Frequency in kilokaisers
$(\varepsilon_\ell - \varepsilon_r)$: Differential extinction coefficient, liter. mole.$^{-1}$ cm^{-1}.
$\nu_{1/2}$: Full width at half height, kilokaisers
R : Rotational strength, 10^{-40} cgs units
(*) : Relative magnitudes, data not quantitative.
σ : Standard deviation for fit of Gaussian components.

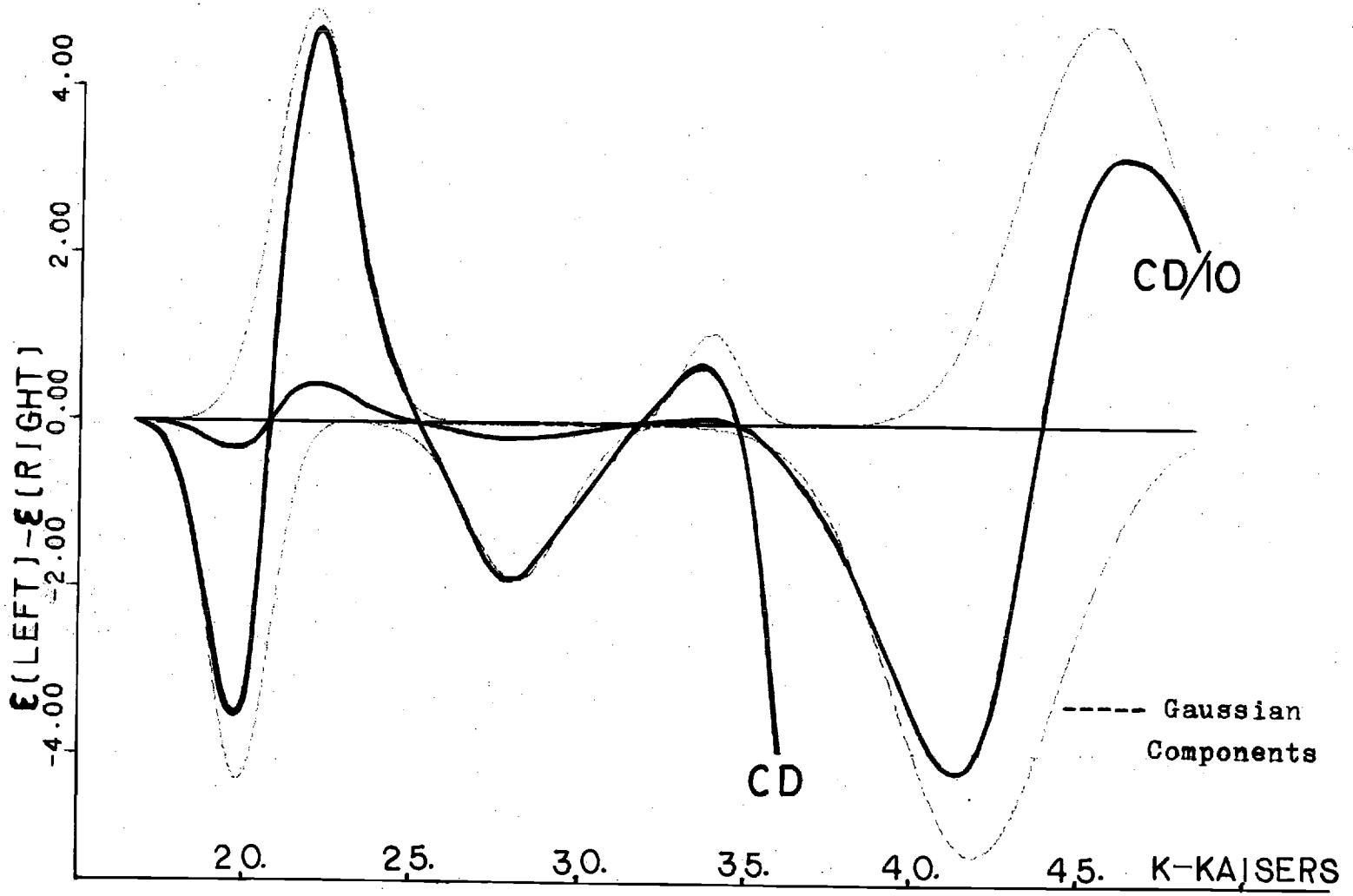

Figure 25. C.D. Spectrum and Gaussian Components of $\Lambda Co(C_2N_5H_7)_3Br_3 \cdot H_2O$ in Water Solution.

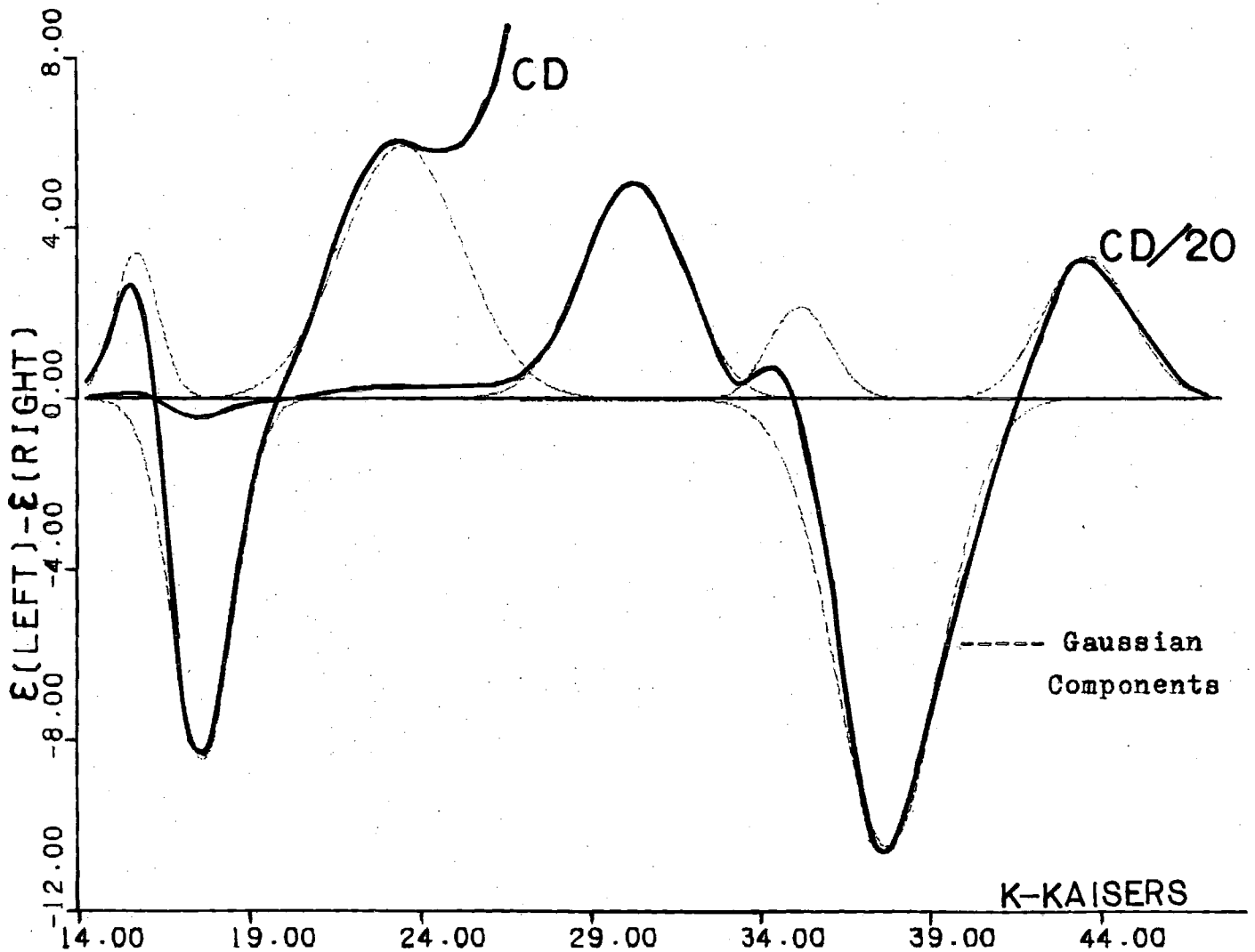

Figure 26. C.D. Spectrum and Gaussian Components of $\Delta Co(C_5H_7O_2)_3$ in Cyclohexane Solution.

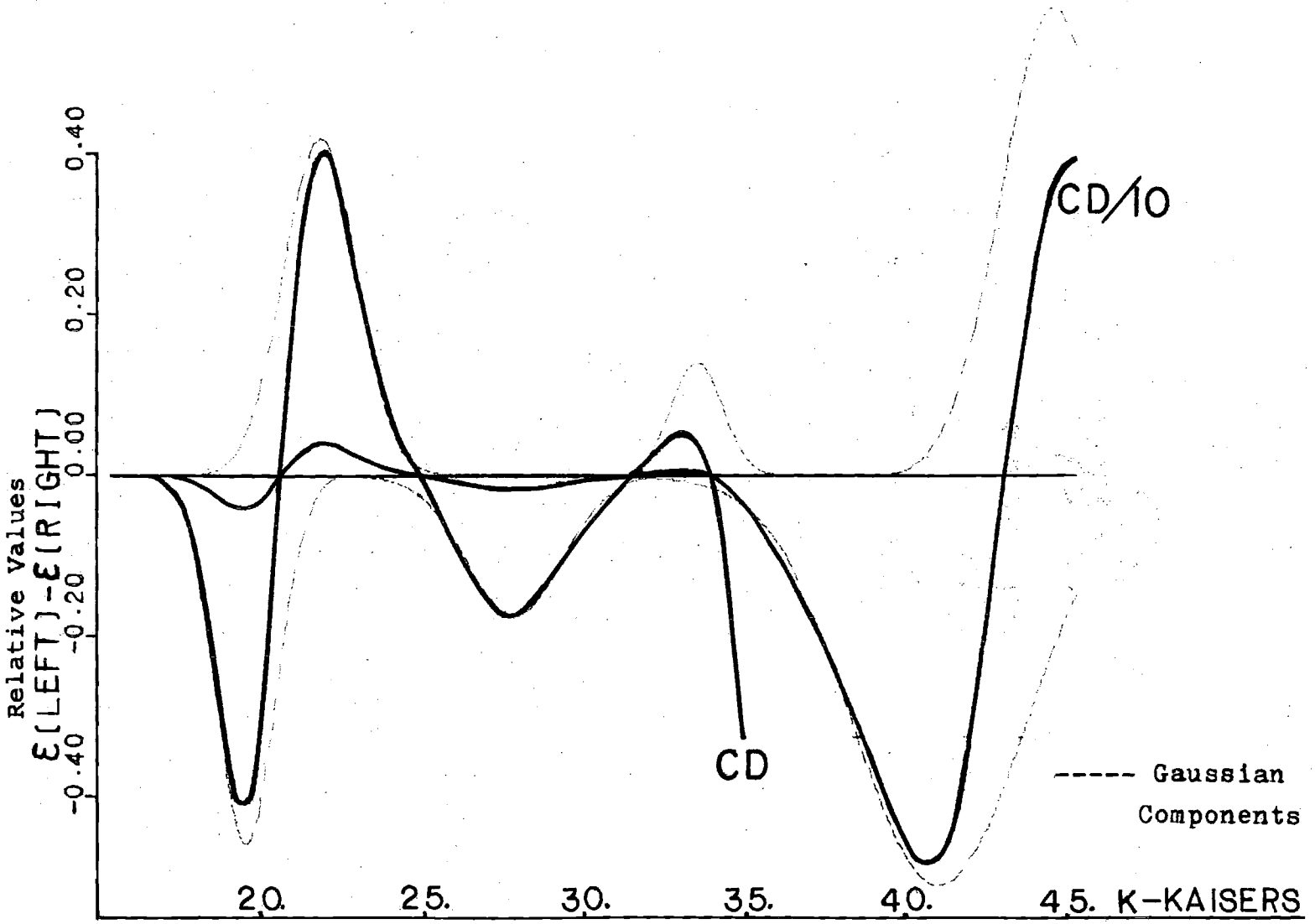

Figure 27. C.D. Spectrum and Gaussian Component of $\Lambda Co(C_2N_5H_7)_3Br_3 \cdot H_2O$ in Methanol Solution.

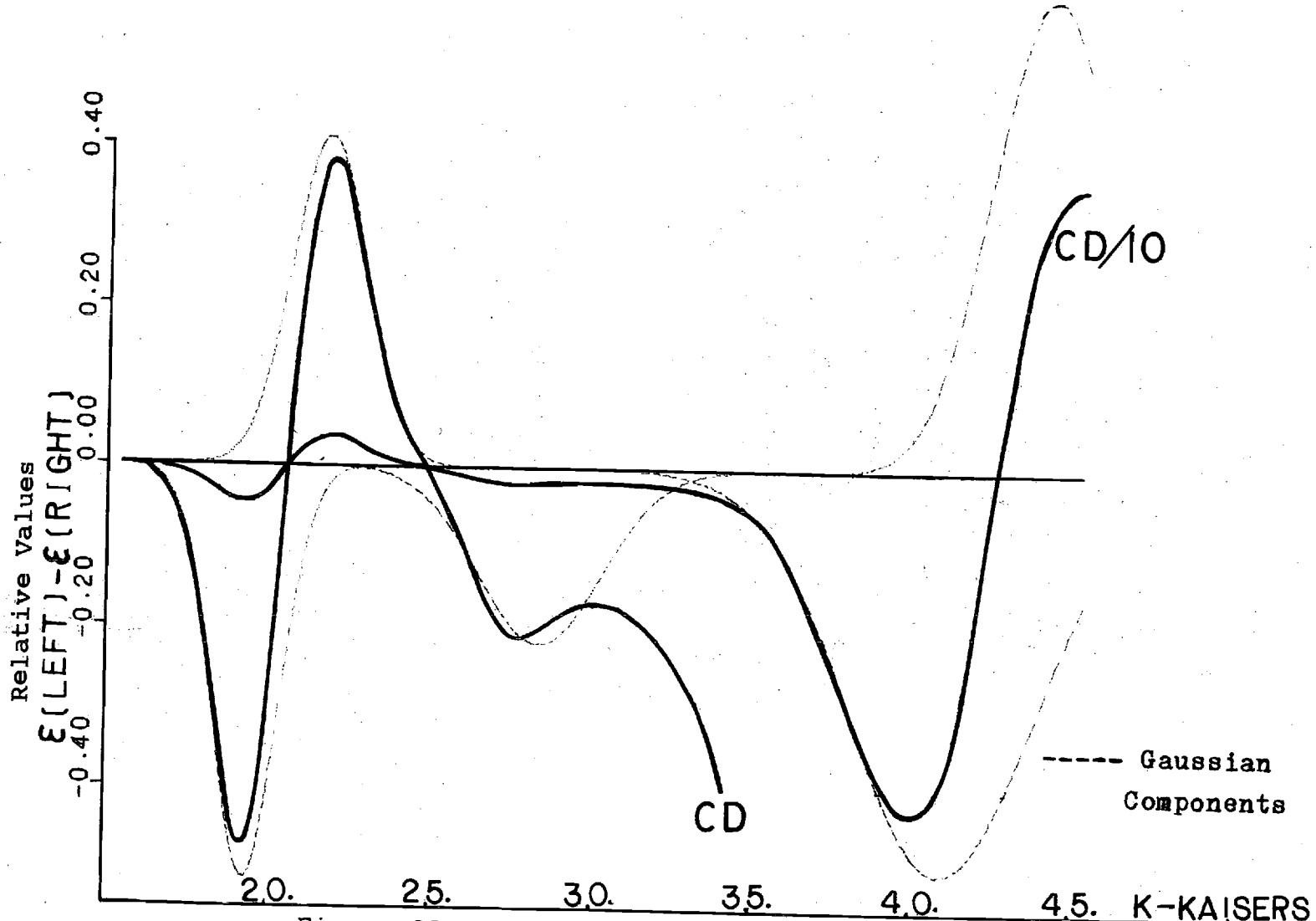

Figure 28. C.D. Spectrum and Gaussian Component of $\Lambda Co(C_2N_5H_6)_3$ in Methanol Solution.

Powder Spectra

The CD spectra of powdered samples in pressed KCℓ discs were measured for Λ-$Co(C_2N_5H_7)_3Br_3 \cdot H_2O$, Λ-$Co(C_2N_5H_6)_3$ and Δ-$Co(C_5H_7O_2)_3$. As mentioned in the previous chapter, electronic absorption spectra and ORD spectra were also attempted for samples of the powdered materials in KCℓ discs but the results were not satisfactory. The poor quality of those spectra was due, probably, to the high degree of light scattering from those powdered samples.

The CD spectra, for powdered samples, were measured in the visible region of the spectrum. These spectra were analyzed into Gaussian components by the same method described for solution CD spectra. Powder CD spectra, in general, show a shift towards the low frequency end of the spectrum when compared with the corresponding solution CD spectra. The ratios of the intensities of the various transitions are different in the powder and in solution spectra.

Table 23 gives the peak positions and the relative intensities of the powder CD spectra while Table 24 gives the results of their resolution into Gaussian components. Figures 29, 30 and 31 illustrate the powder CD spectra for the three substances and their Gaussian components.

The weights of the salt in the discs used for those spectra were 0.65 g. The discs were 1 mm thick, i.e., the length of the light path through them was 1 mm. The weights

of samples used for powder spectra were 2.3 mg of Λ-$Co(C_2N_5H_7)_3Br_3 \cdot H_2O$, 2.0 mg of Λ-$Co(C_2N_5H_6)_3$ and 2.0 mg of Δ-$Co(C_5H_7O_2)_3$. No quantitative data can be given for the intensitites of powder CD spectra. The spectra shown in the following figures are for the entire wavelength regions scanned. However, the data entered into the program for Gaussian resolution were 15.38 KK-31.25 KK (the entire range) for Λ-$Co(C_2N_5H_7)_3Br_3 \cdot H_2O$ and the data were analyzed into three Gaussian components. For Λ-$Co(C_2N_5H_6)_3$ the range entered into the Gaussian resolution was 15.38 KK - 21.74 KK, and the resolution was into two Gaussian components. For Δ-$Co(C_5H_7O_2)_3$ the range of data used for Gaussian resolution was 14.29 KK - 20.00 KK and the resolution was into two Gaussian components. The high frequency portions of those spectra were either less reliable, for Λ-$Co(C_2N_5H_6)_3$, or not pertinent, for Δ-$Co(C_5H_7O_2)_3$.

Table 23. CD Spectra for Powders in KCℓ Discs.

Compound	ν(kk)	Relative Height
Λ$Co(C_2N_5H_7)_3Br_3 \cdot H_2O$	26.67	-0.400
	21.37	0.880
	18.73	-0.130
Λ$Co(C_2N_5H_6)_3$	26.39	0.170
	21.28	1.300
	17.99	-0.140
Δ$Co(C_5H_7O_2)_3$	22.22	0.340
	17.12	-0.858
	14.93	0.280

Table 24. Gaussian Components for Powder C.D. Spectra.

Compound	ν_o(kk)	Relative Height	$\nu_{1/2}$(kk)	#
$\Lambda Co(C_2N_5H_7)_3Br_3 \cdot H_2O$	26.86	-0.403	6.119	(1)
	21.40	0.932	2.310	(2)
	18.91	-0.153	2.092	(3)
σ (bands 1, 2, 3): 0.012 (37 data points)				
$\Lambda Co(C_2N_5H_7)_3Br_3 \cdot H_2O$	21.32	0.890	2.186	(2')
	18.90	-0.149	2.115	(3')
σ (bands 2' and 3' only): 0.006 (22 data points)				
$\Lambda Co(C_2N_5H_6)_3$	21.29	1.315	3.031	
	18.39	-0.215	1.932	
σ (two bands only): 0.009 (25 data points)				
$\Delta Co(C_5H_7O_2)_3$	17.07	-0.895	2.055	
	15.31	0.355	2.167	
σ (two bands only): 0.012 (18 data points)				

In the table above ν_o stands for frequency in kilokaisers and $\nu_{1/2}$ is the full width at half height. The Relative Heights are on the same scale as the corresponding data in the previous Table 23. The standard deviations, σ, are for the fit of the Gaussian components.

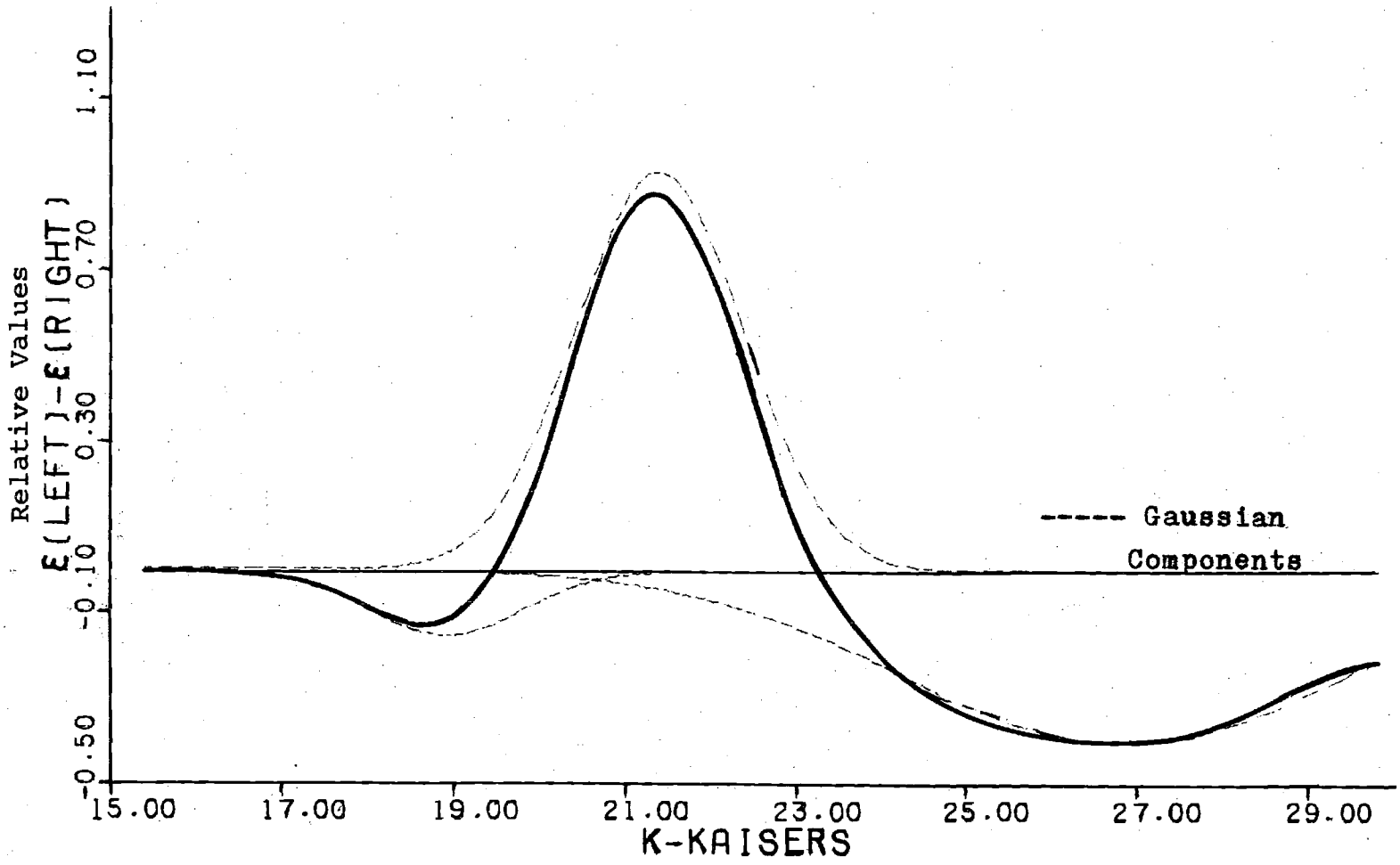

Figure 29. C.D. Spectrum and Gaussian Components of $\Lambda Co(C_2N_5H_7)_3Br_3 \cdot H_2O$ Powder in KCℓ Disc.

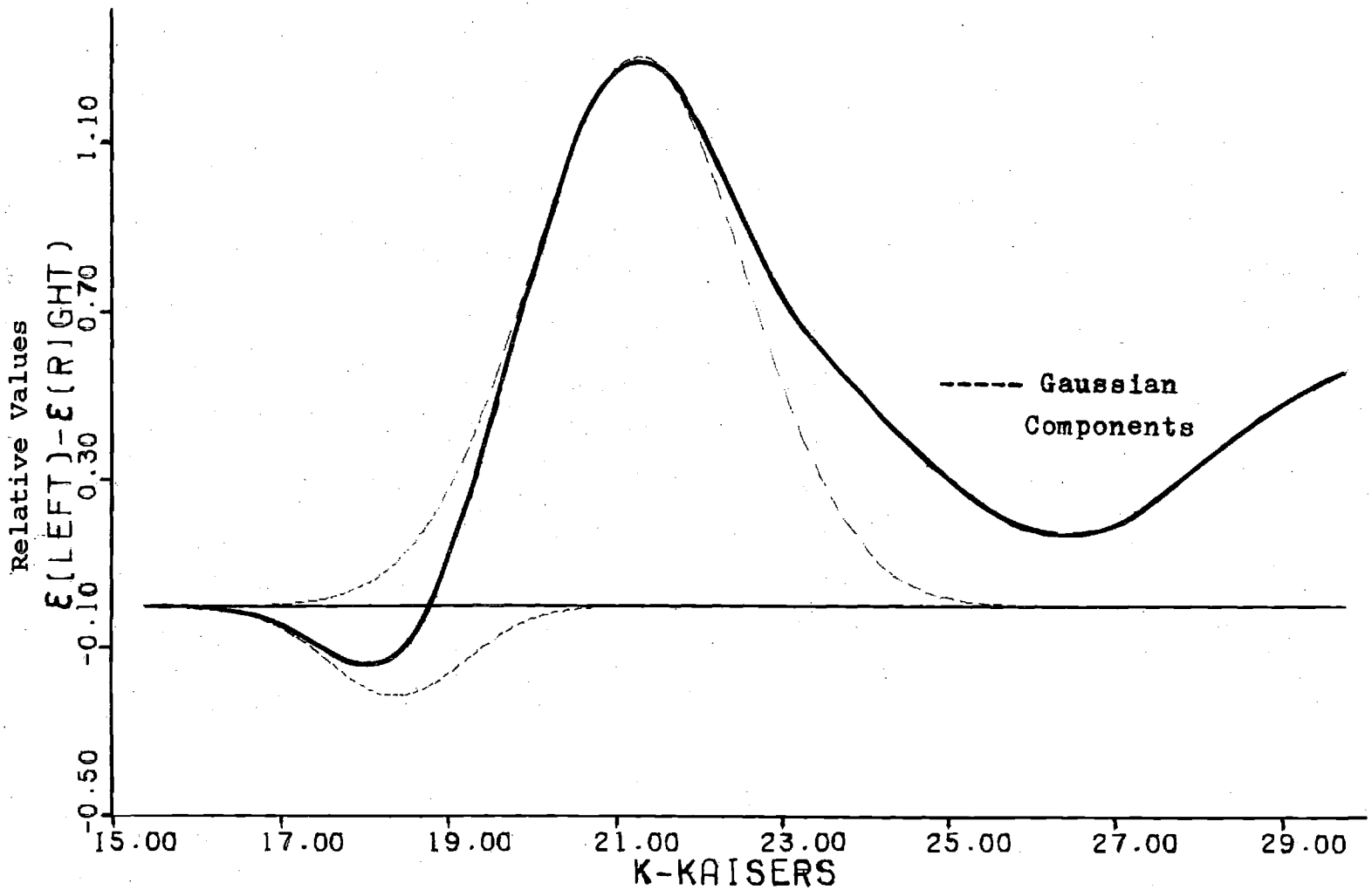

Figure 30. C.D. Spectrum and Gaussian Components of $\Lambda Co(C_2N_5H_6)_3$ Powder in KCℓ Disc.

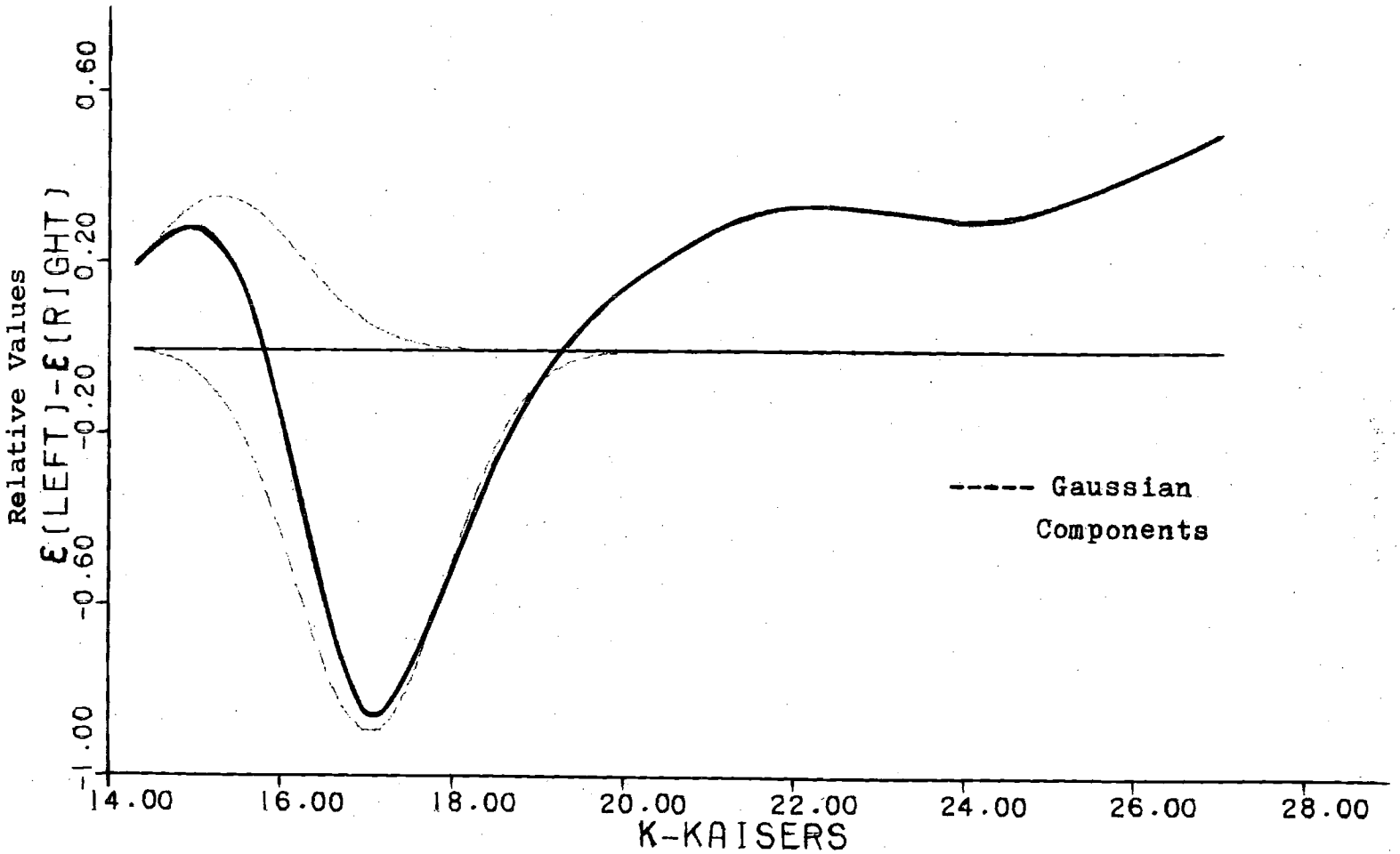

Figure 31. C.D. Spectrum and Gaussian Components of $\Delta Co(C_5H_7O_2)_3$ Powder in KCℓ Disc.

In Table 23 the frequency ν is measured in kilokaisers. Relative heights are reported, rather than $(\varepsilon_\ell - \varepsilon_r)$ because the data for powders are not quantitative.

Single Crystal Spectra

Circular Dichroism Spectra

If circularly polarized light is directed along the three-fold axis of a tris-bidentate molecule of a Co(III) complex (a d-6 electron system) having D-3 or C-3 symmetry only the A → E components of the CD spectrum will be observed. Such an ideal experimental condition is encountered, in a few fortunate cases, in crystals of optically active materials of those substances possessing crystallographic three-fold symmetry, and with the three-fold molecular axes all aligned parallel to the direction of the unique crystal axis. The above conditions were obviously not satisfied for any of the materials investigated here. However the CD spectra for powdered samples in KCℓ discs may be considered as crystal CD spectra, with the tiny crystallites intact but arranged at random orientations in the sample. As described before, those powdered samples gave good CD spectra that were qualitatively very similar to the corresponding solution CD spectra. Therefore, despite the lack of crystallographic three-fold symmetry for all those crystalline samples, the investigation of the CD spectra, for those crystals, was considered worthwhile.

The site symmetries for Λ-$Co(C_2N_5H_7)_3 \cdot H_2O$, racemic $Co(C_2N_5H_6)_3 \cdot 2H_2O$ and racemic $Co(C_5H_7O_2)_3$, though definitely lower than D-3, are nevertheless not far removed from it, as stated earlier in this chapter. Moreover the three-fold axes of the molecules of Λ-$Co(C_2N_5H_7)_3Br_3 \cdot H_2O$ are only slightly inclined (12.15°) from the direction of the crystallographic c-axis. For Δ-$Co(C_5H_7O_2)_3$, single crystal CD spectra may be taken on this material doped into racemic crystals of $Al(C_5H_7O_2)_3$. Good quality single crystals containing one mole-percent Δ-$Co(C_5H_7O_2)_3$ were grown by slow solvent evaporation from a toluene solution. Those crystals contain the cobalt molecules substituted into aluminum sites, since it is known that the racemic Co and Al compounds have crystal structures that are isomorphous (37).

Samples of the mixed crystals containing the active cobalt compound were redissolved in toluene and the CD spectrum of the solution indicated, unequivocally, the presence of the optically active Δ-$Co(C_5H_7O_2)_3$ in those mixed crystals. The lattice polar angle for this material (angle between the b-axis direction and the molecular three-fold axes for the Aℓ compound) is appreciably large, 30°. This was foreseen as an unavoidable difficulty.

The structure of γ-$Al(C_5H_7O_2)_3$ was recently reported (62). In this structure the material crystallizes in an orthorhombic lattice with the three-fold molecular axes all very nearly parallel to the crystallographic c-axis.

Attempts to obtain mixed single crystals of Δ-$Co(C_5H_7O_2)_3$ in $Al(C_5H_7O_2)_3$ having such an orthorhombic structure gave inconclusive results. The only crystals obtained, that were similar in appearance to the orthorhombic material, were of microscopic size. For crystals of that size it is practically impossible to test their content of $Co(C_5H_7O_2)_3$ or whether such material is racemic or optically active.

A JASCO model ORD-UV-5 machine, with CD attachment, was used to record all CD spectra. The machine has a Pockels cell that generates circularly polarized light from an incoming beam of plane-polarized light. To obtain circularly polarized light a sinusoidal electric signal, of value appropriate for the frequency of the incident monochromatic light, is applied to the Pockels cell. At the peak of the sinusoidal modulating signal pure circularly polarized light is obtained. When the modulating signal is zero the incident plane polarized beam goes through the Pockels cell, and emerges from it, unperturbed. When the modulating electric signal is between zero and maximum, elliptically polarized light is produced. The elliptically polarized beam may be considered as the sum of a pure circularly polarized beam and a plane polarized beam. It can be shown that the time-average of the intensity of pure circularly polarized light coming out of the Pockels cell is 12.5% of the intensity of the incident beam, assuming a pure sinusoidal modulating signal. When the modulating signal is zero the

plane polarized beam that emerges from the Pockels cell, vibrates in a vertical plane. For the CD attachment of the machine there is a synchronous detector that is locked in phase with the sinusoidal modulating signal of the Pockels cell. This detector measures the intensity of light absorption as a function of the phase of the modulating signal.

In a solution and in a powdered sample, the molecules are at random orientations. The true CD spectrum will therefore be obtained and the effects of birefringence and polarization are either absent or cancel out. Similarly the CD spectrum of a uniaxial crystal, with light directed along the optic axis, is also straight forward. All interfering optical effects cancel out when the light beam, from the Pockels cell of the machine, is directed along the optic axis of an uniaxial crystal.

The situation is considerably more difficult if the CD spectrum of an anisotropic crystal is to be measured at a random orientation. The CD spectrum will be superimposed upon the plane-polarized spectrum and the birefringence. The latter effects are about one order of magnitude more intense than the desired CD spectrum. Under such conditions special techniques must be used to eliminate the effects of the above undesirable phenomena. These techniques are discussed in the following sections.

$\Lambda Co(C_2N_5H_7)_3Br_3 \cdot H_2O$. Single crystal CD spectra for this material were taken with the light beam incident

perpendicular to the (ab) face of the crystal. The first spectrum was taken with the direction of the a-axis vertical. At that orientation the direction of the a-axis was also parallel to the plane-polarized component of the light beam incident on that crystal face. The next spectrum was taken with the direction of the a-axis inclined at ten degrees to the vertical direction. Subsequent spectra were taken every ten degrees from the preceeding orientation.

Spectra were taken at the 36 different orientations spaced by ten degree increments. Spectra taken with the direction of the a-axis vertical gave a very shallow minimum, around 16.9 kk, then a sharp intense maximum at 20.8 kk followed by another steep minimum at 27.0 kk. Alternatively, spectra taken with the direction of the b-axis parallel to the vertical gave a shallow maximum around 16.9 kk, a sharp minimum at 20.8 kk and a steep maximum at 27.0 kk. The results seemed to be periodical every 180°. Figure 32a illustrates typical spectra at three different orientations of the sample crystal and the resultant spectrum for the nine positions in the third quadrant. These positions are for crystal orientations where the reference a-axis direction was parallel to the vertical up to where the a-axis direction was inclined at 80° to the vertical. Figure 32b shows the resultant of the nine spectra, in the fourth quadrant, for the reference a-axis direction at various inclinations between 90° and 170° to the vertical. The resultant spectra

from the first and second quadrants were combined and their average spectrum is shown in Figure 32c. Figure 32d shows the corresponding spectra, and their average, for the third and fourth quadrants.

The resultant spectra for the first and third quadrants were similar to each other. Those for the second and fourth quadrants were also similar to each other but were different from the previous two resultant spectra. The two average spectra, shown in Figures 32c and 32d, were practically identical except for a small shift in their baselines. In those spectra the region between 16.7 kk and 14.3 kk was a horizontal straight line, within experimental error. The region between 23.7 kk and 16.7 kk has a sharp distinct positive band at 20.4 kk (490 ±10 mμ). The results in the region between 29.4 kk and 23.7 kk were slightly ambiguous and not very reliable because of the absorption by the glass plates and the resin around the crystal slice. The average spectrum for all four quadrants is shown in Figure 33.

The spectra described above were all taken with the light beam incident on the (ab) or (0, 0, 1) face. Additional spectra were taken with the light beam incident on the other face, (0, 0, -1)* of the crystal slice and at various orientations of the reference a-axis direction. The two

*In principle, it is not possible to distinguish between such two faces of a crystal. In practice however they were tagged differently for ease of identification.

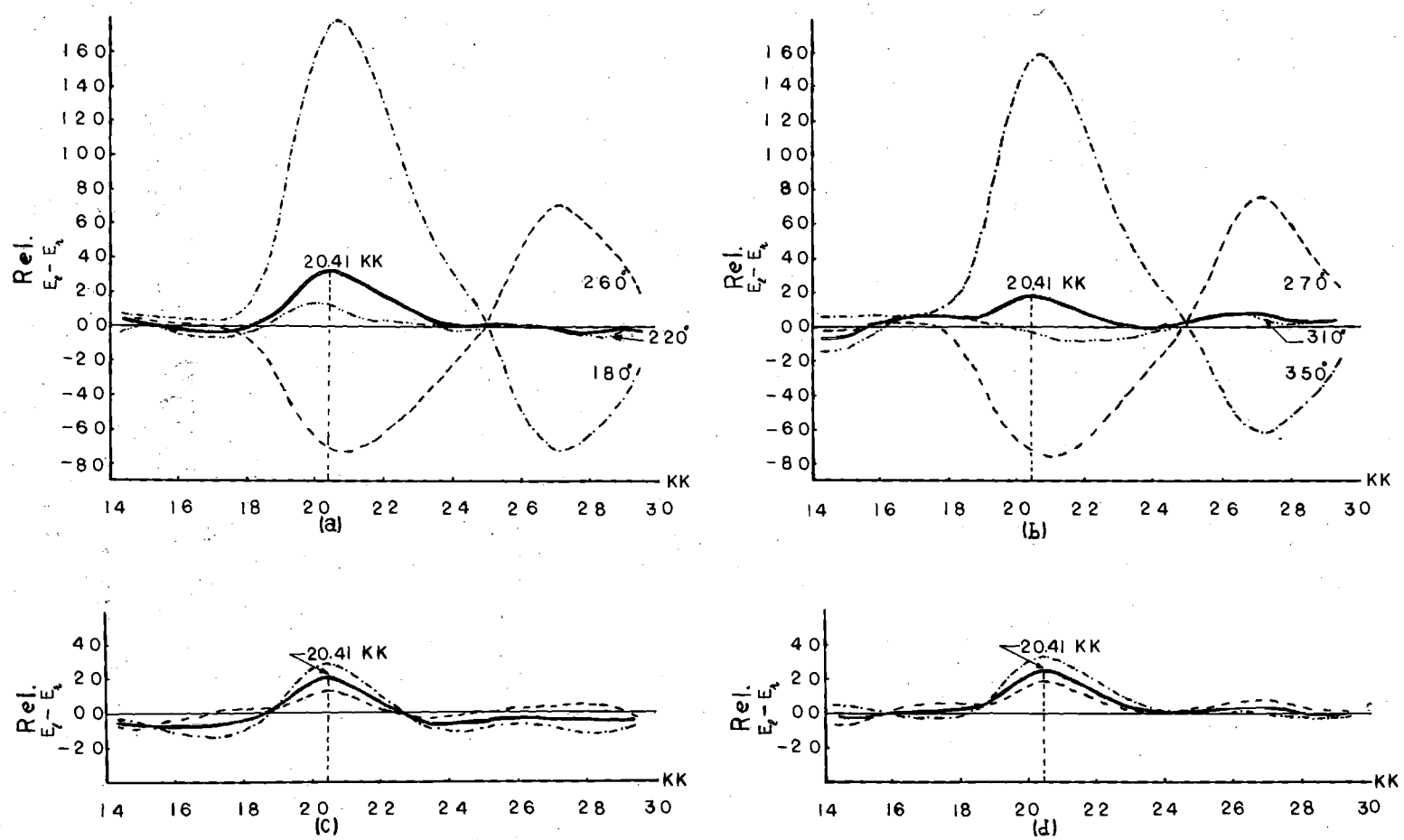

Figure 32. Single Crystal C.D. Spectra for $\Lambda Co(C_2N_5H_7)_3Br_3 \cdot H_2O$.

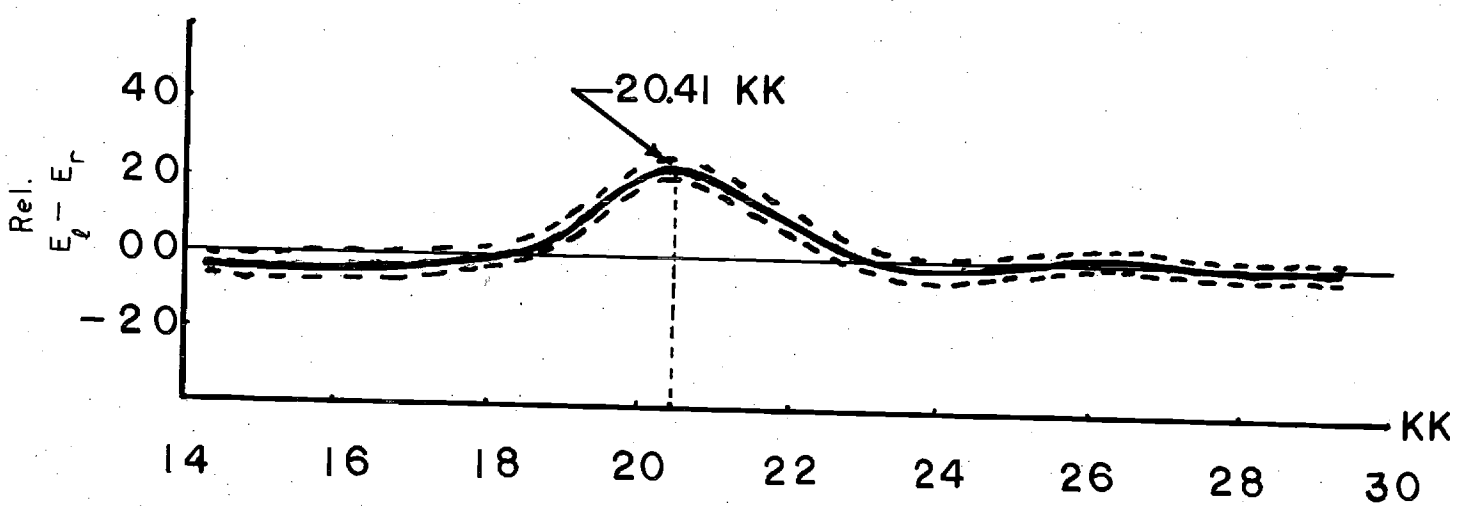

Figure 33. Resultant Single-Crystal C.D. Spectrum of $\Lambda Co(C_2N_5H_7)_3Br_3 \cdot H_2O$.

sets of spectra, through the (0, 0, 1) and (0, 0, -1) faces, were identical to each other for the same orientations of the reference a-axis direction.

Δ-$Co(C_5H_7O_2)_3$. Single crystal CD spectra for this material were attempted on two samples prepared in two different ways. Both samples had the material doped into the racemic $Al(C_5H_7O_2)_3$. The crystals for those samples were grown as described earlier, and in both the (ac) faces were exposed. The first sample had both exposed faces covered with optical glass discs, as for the previous materials, while the other sample had the faces bare. Light was shone through the (ac) face and along the direction of the unique crystal b-axis. The spectra, taken for the various orientations of the reference a-axis direction with respect to the vertical, were very noisy and erratic. No conclusive results could be drawn from those spectra and no satisfactory explanation could be given to those erratic results. However the grinding and polishing of the (ac) face, in particular, of these crystals could not be made as shiny as for other samples.

Racemic $Co(C_2N_5H_6)_3 \cdot 2H_2O$. There are reports in the literature stating that low-symmetry crystals of racemic materials, like $Ni(H_2O)_6SO_4$, do give non-zero CD spectra. Strickland and Richardson (5) have shown that the optical activity of $Ni(H_2O)_6SO_4$ is due to a dissymmetric crystal environment.

It was decided to perform some check on the validity of the net CD spectrum obtained for $\Lambda Co(C_2N_5H_7)_3Br_3 \cdot H_2O$, by performing a similar experiment on a racemic complex, $Co(C_2N_5H_6)_3 \cdot 2H_2O$. This material forms monoclinic crystals of space group $P2_1/c$. The molecular three-fold axes of the two molecules are inclined at 19.73° with respect to the direction of the b-axis. The (ac) faces, (0, 1, 0) and (0, -1, 0), of the crystal slice were exposed and polished as described in the previous chapter. A reference direction was chosen parallel to the direction of the c-axis of that crystal slice. The light beam was incident along the direction of the b-axis of the crystal and spectra were taken in the same manner described for Λ-$Co(C_2N_5H_7)_3Br_3 \cdot H_2O$, but with light incident on the (0, 1, 0) and (0, -1, 0) faces. The first spectrum was taken with the reference c-axis direction in a vertical position. Subsequent spectra were each taken with the reference c-axis direction inclined at 30° with respect to the preceeding position. A total of twelve spectra were taken through each of the (0, 1, 0) and (0, -1, 0) faces. The frequency range spanned for those spectra was from 27.7 kk to 14.3 kk. The pair of spectra taken through the (0, 1, 0) and (0, -1, 0) faces at each setting of the reference c-axis direction were not mirror images about the base line. Figure 34a shows some sample spectra and the resultant spectrum for orientations 0° through 150° of the reference c-axis direction.

Every point on the resultant spectrum was obtained, in the same manner as for the previous material, by algebraic addition of the signal heights at that wavelength for the pairs of spectra through the (0, 1, 0) and (0, -1, 0) faces. The results are shown graphically in Figure 34b. The straight lines in the last two figures are least-squares linear fits through the data points. The resultant spectra were therefore straight lines to a very good approximation. The sloping-down of these straight lines is typical of the base line behavior at these instrumental settings used for running the above spectra.

These results show that crystals of racemic and of optically active tris-bidentates, possessing no three-fold crystallographic symmetry, may be used to measure CD spectra. When the spectra that were taken at various orientations around the optic axis were averaged, at every wavelength value, the crystal of the optically active material gave a resultant spectrum corresponding to one of the components of the solution and powder spectra. That component was thus identified as the one corresponding to the A → E transition. The resultant spectrum for the centro-symmetric racemic material was the base line, as expected (4).

Plane-Polarized Single Crystal Spectra

The first single crystal spectra taken in plane-polarized light were treated in a manner similar to that reported by Piper for racemic $Co(C_5H_7O_2)_3$ in $Al(C_5H_7O_2)_3$, (63).

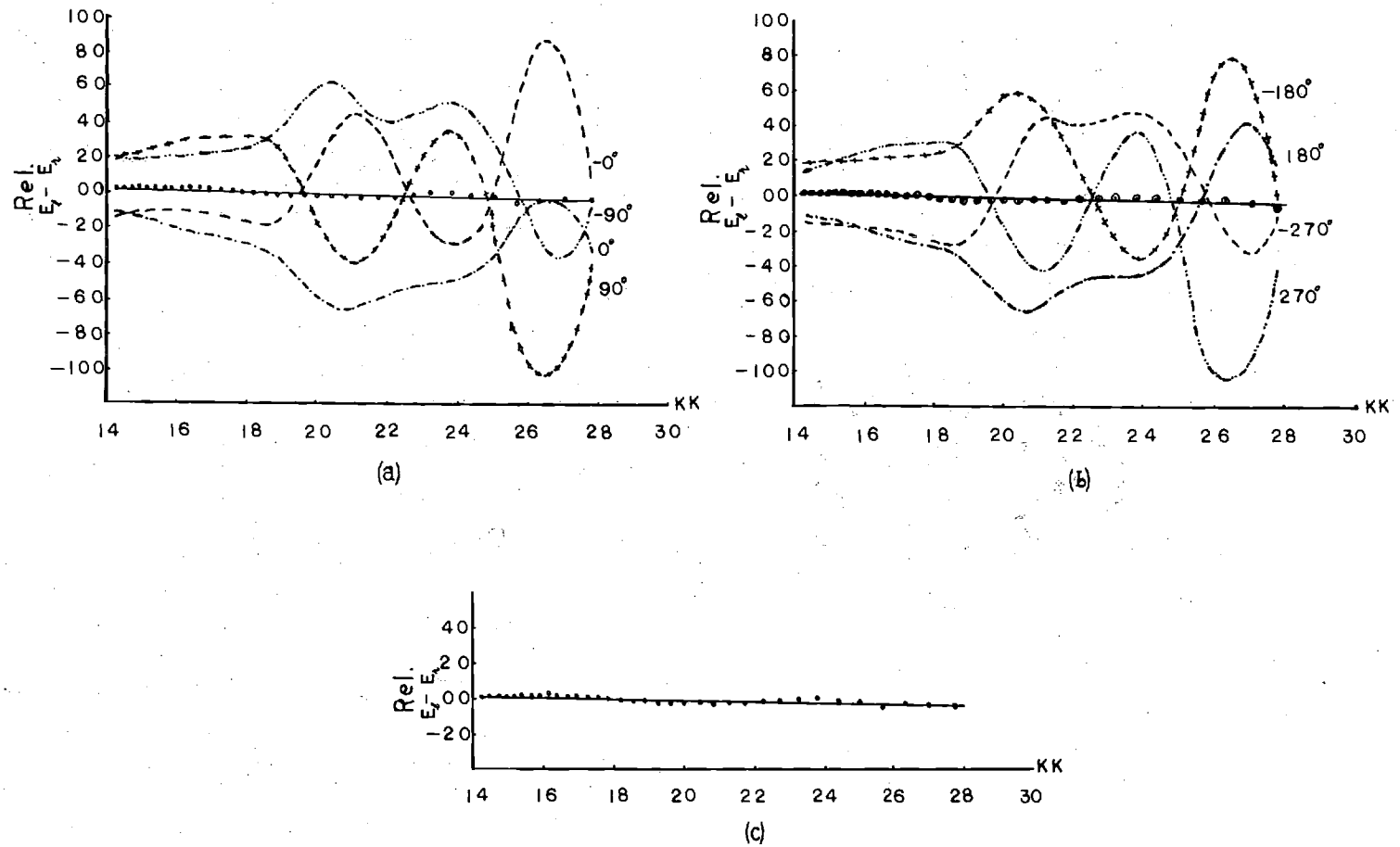

Figure 34. Single Crystal C.D. Spectra for Racemic $Co(C_2N_5H_6)_3 \cdot 2H_2O$.

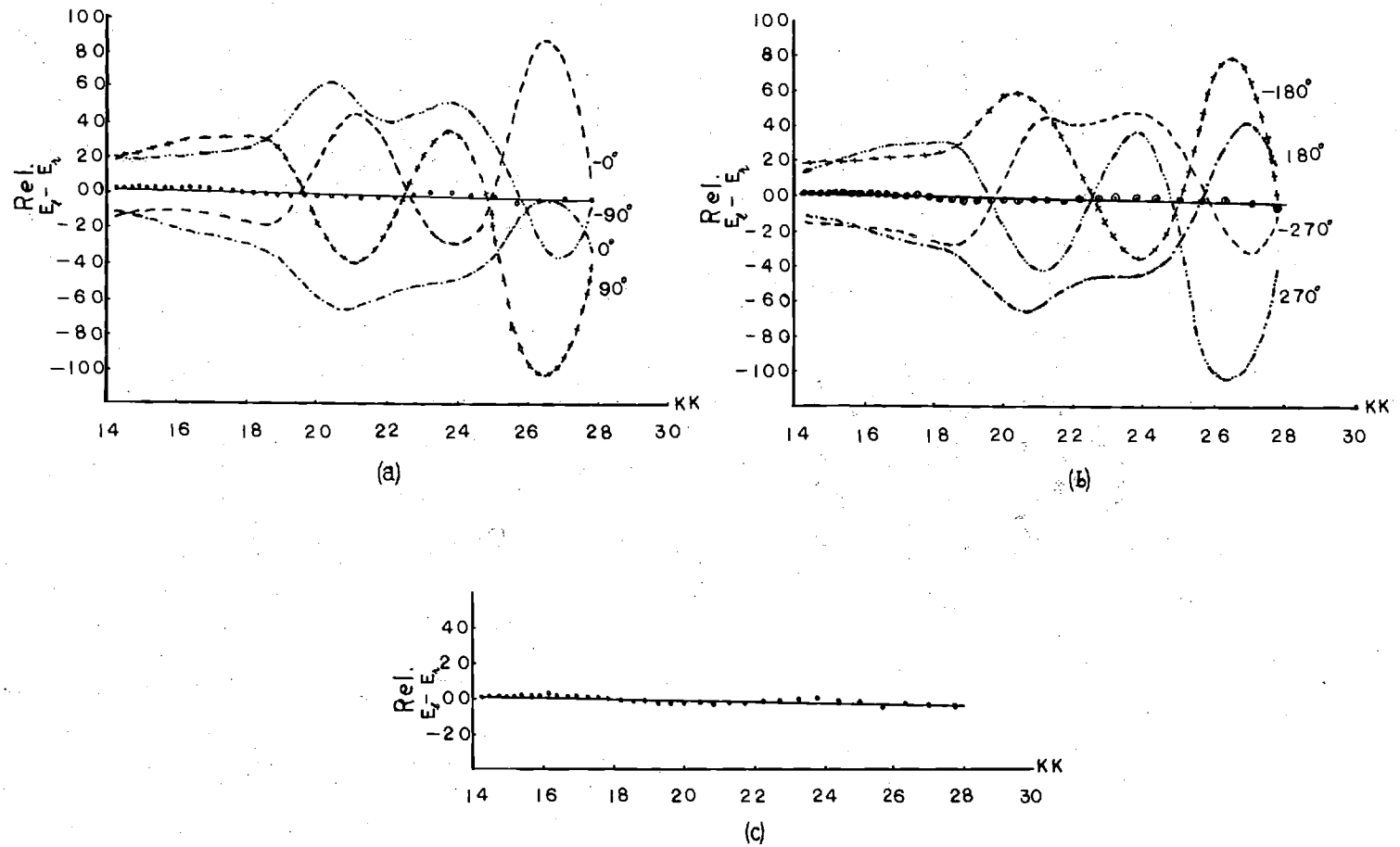

Figure 34. Single Crystal C.D. Spectra for Racemic $Co(C_2N_5H_6)_3 \cdot 2H_2O$.

A serious discrepancy was encountered however when plane-polarized spectra were taken through the (ab) (0, 0, 1) face of a crystal of the orthorhombic Λ-$Co(C_2N_5H_7)_3Br_3 \cdot H_2O$. The spectrum taken with the light polarized parallel to the a-axis direction was markedly different from the one taken with the light polarized parallel to the direction of the b-axis. At either one of those two orientations the spectrum should be almost entirely (about 90% or more as will be shown later in this chapter) due to the A → E transition.

Plane polarized spectra were also taken through the (ac) (0, 1, 0) and the (bc) (1, 0, 0) faces of crystals of the same material, Λ-$Co(C_2N_5H_7)_3Br_3 \cdot H_2O$. The detailed derivation of the mathematical expressions for all of these cases is forthcoming in this chapter. The spectra through the latter two faces, (0, 1, 0) and (1, 0, 0) with light polarized parallel to the c-axis direction were identical. In addition the spectra through the (0, 1, 0) and (1, 0, 0) faces with the light polarized perpendicular to the c-axis direction, were similar to the two spectra taken through the (ab), (0, 0, 1), face.

Based on the above results it was decided to extend the Piper technique and analyze all plane-polarized single crystal spectra into three, rather than two, mutually perpendicular components.

Spectra through two faces of a crystal, e.g., (ac) and (bc) would be needed. Spectra taken through the third

face, (ab), would furnish no extra information.

In the following treatments, mathematical relations will be derived for evaluating the absorbance spectra along the directions of the molecular three-fold axes and at two mutually perpendicular directions orthogonal to them.

Λ-$Co(C_2N_5H_7)_3Br_3 \cdot H_2O$. Plane-polarized spectra through any two of the three crystal faces (0, 0, 1), (0, 1, 0) and (1, 0, 0) would be sufficient. In the following treatment spectra through the (1, 0, 0) and (0, 1, 0) faces will be considered.

With reference to Figure 35, Oc is parallel to the direction of the crystal c-axis. POI represents the plane of polarized light while cOZ represents the plane of the crystal face exposed. OP represents the direction of propagation of light. OS is parallel to the direction of the molecular three-fold axis. OD is the trace, or projection, of OT on the (0, 0, 1) face, plane POZ. Angle cOT = θ, is defined as the lattice polar angle. (θ = 12.15°). Angle BOZ, Figure 36, is defined as the azimuthal angle. For spectra through the (0, 1, 0) face the azimuthal angle, $\phi' = 69.83°$. For spectra through the (1, 0, 0) face the azimuthal angle $\phi = 90.00° - \phi' = 20.17°$, Figures 14, 35 and 36.

From the geometry of Figure 35, OT = OIxcos θ. IT = OIxsin θ. Consider the spectra taken through the faces (1, 0, 0) or (0, 1, 0) with light polarized parallel to the c-axis direction. The component of the amplitude of incident

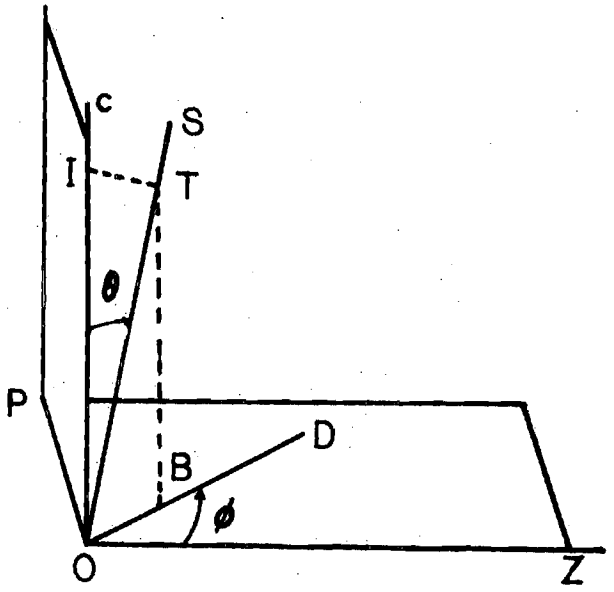

Figure 35. Illustration of Light Polarized Parallel to the Direction of the c-Axis of $\Lambda Co(C_2N_5H_7)_3Br_3 \cdot H_2O$.

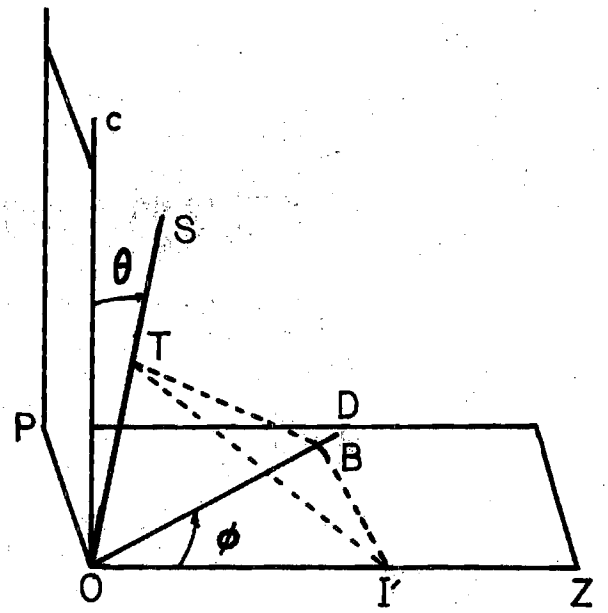

Figure 36. Illustration of Light Polarized Perpendicular to the Direction of the c-Axis of $\Lambda Co(C_2N_5H_7)_3Br_3 \cdot H_2O$.

light parallel to the direction of the molecular three-fold axis is given by OIxcos θ, and the corresponding intensity is $(OIx\cos\theta)^2$. The component of the amplitude perpendicular to the direction of the molecular three-fold axis is given by OIxsin θ, and the corresponding intensity is $(OIx\sin\theta)^2$.

In Figure 36, POI′ represents the plane of polarized light. OI′ represents the amplitude of the incident light beam. OB is the projection of OI′ on OD. OT is the projection of OB on OS. From the geometry of the figure it follows that OT is perpendicular to TI′. In the treatment below the amplitude OI′ of the incident beam is resolved into three mutually perpendicular components OT, TB and BI′. By contrast, Piper's treatment (63) would consider OI′ partitioned to OT and TI′ according to the expression $(TI')^2 = (TB)^2 + (BI')^2$. From the geometry of Figure 36, OB = OI′xcos ϕ. BI′ = OI′xsin ϕ. TB = OBxsin $(90° - \theta)$ = OBxcos θ = OI′xcos ϕ xcos θ. OT = OB xcos $(90° - \theta)$ = OBxsin θ = OI′xcos ϕ xsin θ.

Therefore for spectra taken through the (0, 1, 0) face or through the (1, 0, 0) face, the amplitude of the incident beam of light may be resolved into three mutually perpendicular components along the directions OT, TB and BI′. The intensities along those directions are $(OI'x\cos\phi x\sin\theta)^2$, $(OI'x\cos\phi x\cos\theta)^2$ and $(OI'x\sin\phi)^2$ respectively. Components of the amplitude vector perpendicular to the direction of the three-fold axis and in the plane DOS were called (E_β).

Two such components are present IT (Figure 35) and BT (Figure 36). The component of the amplitude vector perpendicular to the direction of three-fold axis and also to the plane DOS was called (E_α). Only one such component is present, BI´ (Figure 36). The components of the amplitude vector along the direction of the three-fold axis were called (A). Two such components are present OT (Figure 35) and OT (Figure 36).

For spectra taken through the (1, 0, 0) face the following relations can be written for the absorbance readings and their components along the three mutually perpendicular directions above. For light polarized parallel to the c-axis direction, $A\ (1, 0, 0, \perp\!\!\!\perp) = (\cos\theta)^2 A(A) + (\sin\theta)^2 A(E_\beta)$, and for light polarized perpendicular to the c-axis direction, $A\ (1, 0, 0, \perp) = (\cos\phi \cdot \sin\theta)^2 A(A) + (\cos\phi \cdot \cos\theta)^2 A(E_\beta) + (\sin\phi)^2 A(E_\alpha)$.

For spectra taken through the (0, 1, 0) face the following relations can be written for the absorbance readings and their components along the three mutually perpendicular directions above. For light polarized parallel to the c-axis direction, $A(0, 1, 0, \perp\!\!\!\perp) = (\cos\theta)^2 A(A) + (\sin\theta)^2 A(E_\beta)$. For light polarized perpendicular to the c-axis direction, $A\ (0, 1, 0, \perp) = (\cos\phi'\ \sin\theta)^2 A(A) + (\cos\phi' \cdot \cos\theta)^2 A(E_\beta) + (\sin\phi')^2 A(E_\alpha)$.

In the above relationships the terms (A) stand for absorbance readings. The other terms are self-explanatory.

The spectrum through the (0, 1, 0) face with light polarized parallel to the c-axis direction was almost identical to the spectrum through the (1, 0, 0) face with light also polarized parallel to the c-axis direction. The only significant difference was in their amplitudes, since the two crystal slices used to obtain these two sets of spectra were not of identical thicknesses. These results are in accordance with the above relations derived for them. The two absorbance spectra through the (1, 0, 0) face were therefore scaled so that the maximum amplitude of the spectrum through the (0, 1, 0) face with light polarized parallel to the c-axis direction was the same as the maximum amplitude of the spectrum through the (1, 0, 0) face with light polarized also parallel to the c-axis direction. Briefly stated, S.F.xA (0, 1, 0, $\perp\!\!\!\perp$) = A(1, 0, 0, $\perp\!\!\!\perp$). After scaling, the absorbances [at any given wavelength, through the faces (0, 1, 0) and (1, 0, 0,) with polarizations parallel to the c-axis direction] were averaged according to the relationship $A_\lambda(\perp\!\!\!\perp) = 1/2\ [(S.F.)A_\lambda(0, 1, 0, \perp\!\!\!\perp) + A_\lambda(1, 0, 0, \perp\!\!\!\perp)]$*. The numerical values for the trigonometric functions were then substituted and the three relationships for $A(\perp\!\!\!\perp)$,

*After applying the scaling factor S.F. to the (0, 1, 0) spectra the ratio of the maximum heights of $A(1, 0, 0, \perp)$ and $A(0, 1, 0, \perp)$ was equal, within 2%, to the ratio of maximum heights of the two spectra through the (0, 0, 1) face. This test gave a very reassuring result about the validity of this method of analyzing plane-polarized spectra into three mutually perpendicular components, rather than two components, as was the case in the treatment by Piper (63).

A(0, 1, 0, ⊥) and A(1, 0, 0, ⊥) were solved simultaneously to make A(A), A(E_α) and A(E_β) the subjects of the equations. The results were the expressions below,

$$A(A) = 1.0486A(\perp\!\!\!\perp) + 0.0076A(0,1,0,\perp) - 0.0562A(1,0,0,\perp) \quad (1)$$

$$A(E_\alpha) = 1.1560A(0, 1, 0, \perp) - 0.1560A(1, 0, 0, \perp) \quad (2)$$

$$A(E_\beta) = -0.0486A(\perp\!\!\!\perp) - 0.1636A(0,1,0,\perp) + 1.2122A(1,0,0,\perp) \quad (3)$$

A computer program was then used to evaluate those three expressions at various wavelength values between 31.25 kk and 16.67 kk. The data input into the program were the wavelengths and the net absorbance values, corrected for base lines, at the various wavelength values. Four absorbance values were entered at every wavelength, A(1, 0, 0, ⊥⊥), A(1, 0, 0, ⊥), A(0, 1, 0, ⊥⊥), A(0, 1, 0, ⊥). The scaling factor was also supplied. The program applied the scaling factor to the spectra through the (0, 1, 0) face, averaged the scaled A(0, 1, 0, ⊥⊥) with the A(1, 0, 0, ⊥⊥) at every particular wavelength and evaluated the above relationships given by Eq. 1, 2, and 3 at all the given wavelength values. The results of the computer evaluation of those three relationships are presented graphically in Figure 37. Table 25 gives some numeric values for absorption maxima and some other pertinent information from those spectra.

Racemic $Co(C_2N_5H_6)_3 \cdot 2H_2O$. Plane-polarized single crystal spectra for this material were obtained in a manner

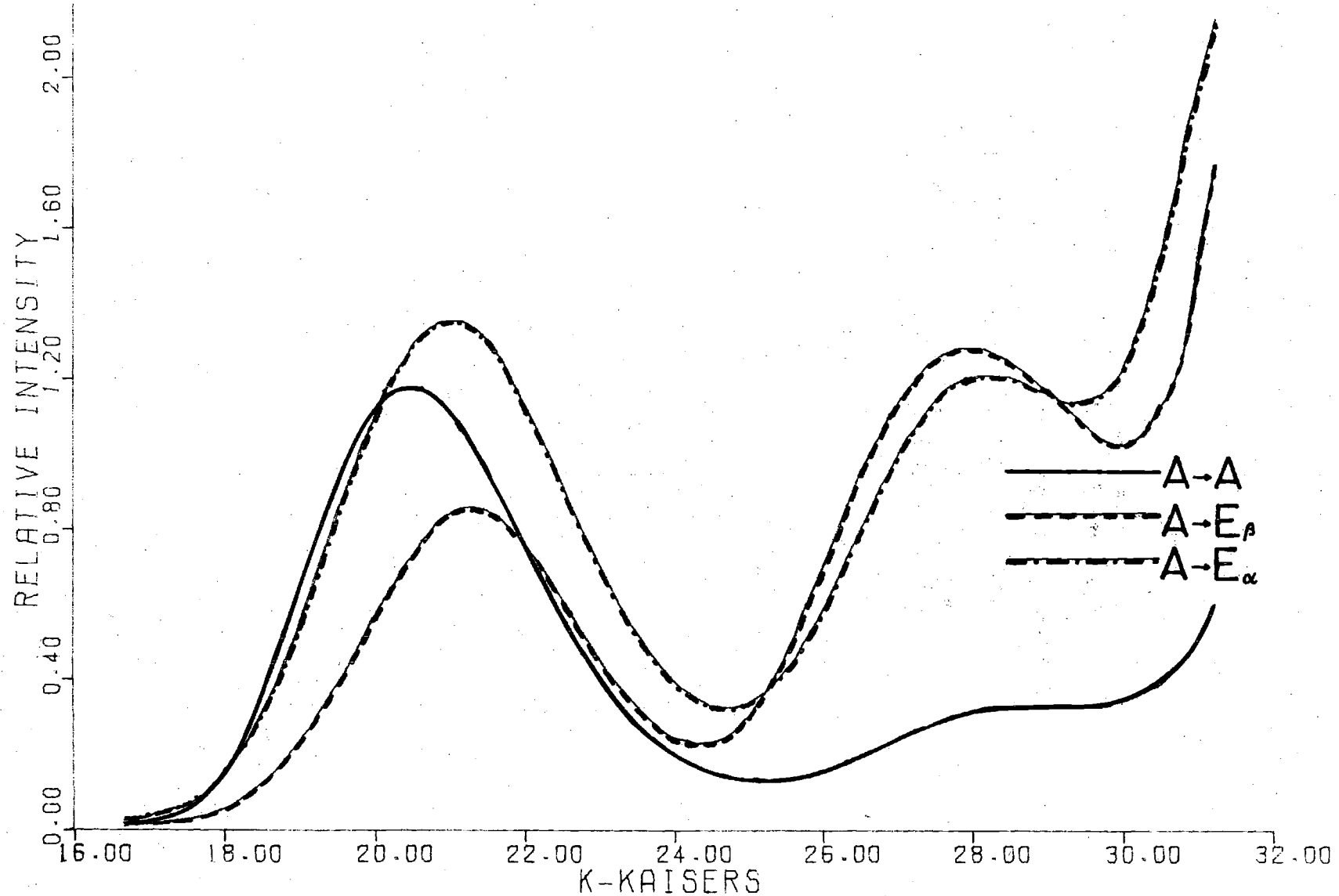

Figure 37. Plane-Polarized Single-Crystal Spectra of $\Lambda Co(C_2N_5H_7)_3Br_3 \cdot H_2O$.

very similar to that described in the previous case. The first crystal face (STO) through which spectra were taken was parallel to the crystal b-axis and to the plane of the two three-fold axes. If the three-fold axes were viewed through the face (STO) they would appear staggered and equally inclined, Figure 38, (lattice polar angle $\theta = 19.74°$) to the direction of the crystal b-axis. The dihedral angle between the face (STO) and the crystal face (0, 0, 1) was 48.67°. Figure 39 shows the trace of the face (STO) on a plane parallel to the direction of the (0, 1, 0) crystal face. For spectra taken through the (STO) face the azimuthal angle ϕ, measured with this (STO) plane as a reference, is obviously zero.

The second face, (ECO), through which spectra were taken was parallel to the direction of the crystal b-axis and approximately at right angles to the previous face, (STO). The dihedral angle between the face (ECO) and the (0, 0, 1) face was 48.7°+ 78.8° = 127.5°. Figure 40 shows the trace of this face on a plane parallel to the direction of the (0, 1, 0) face. If viewed through this face, the three fold axes would appear almost completely eclipsed behind each other. The azimuthal angle ϕ' for spectra measured through this face, (ECO), was 78.8°.

Spectra were measured through faces (STO) and (ECO). Expressions for the absorption spectra through the (ECO) and (STO) faces were derived in the same manner as for

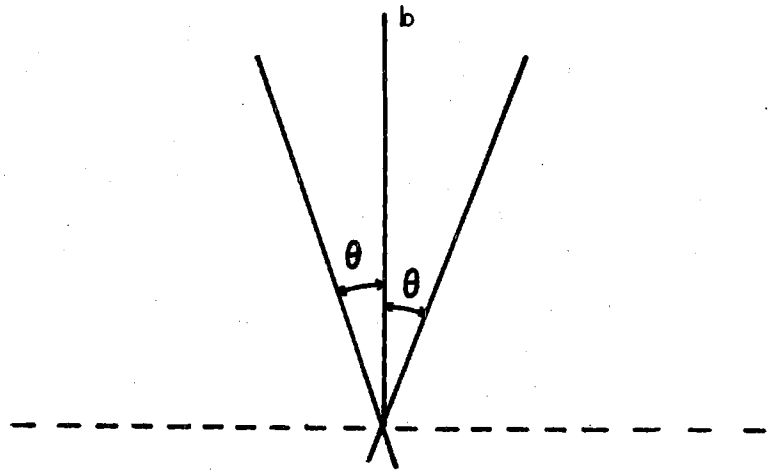

Figure 38. Inclination of the Two Symmetry-Related Three-Fold Axes From the Direction of the b-Axis for Racemic $Co(C_2N_5H_6)_3 \cdot 2H_2O$.

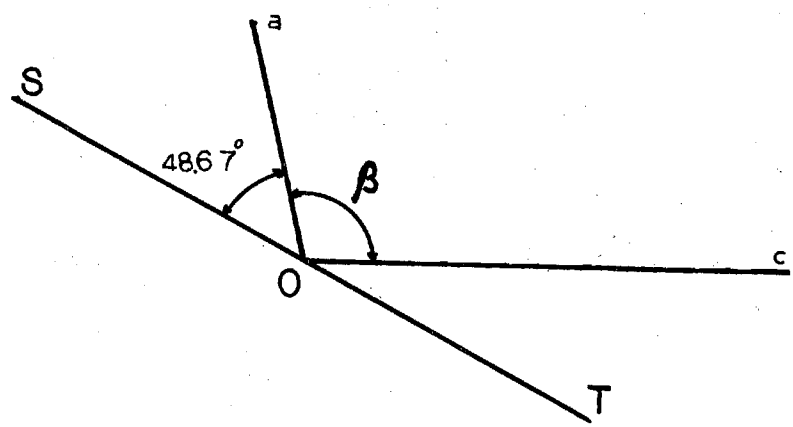

Figure 39. Trace of the Plane of the Three-Fold Axes on a Plane Parallel to the a and c Directions for Racemic $Co(C_2N_5H_6)_3 \cdot 2H_2O$.

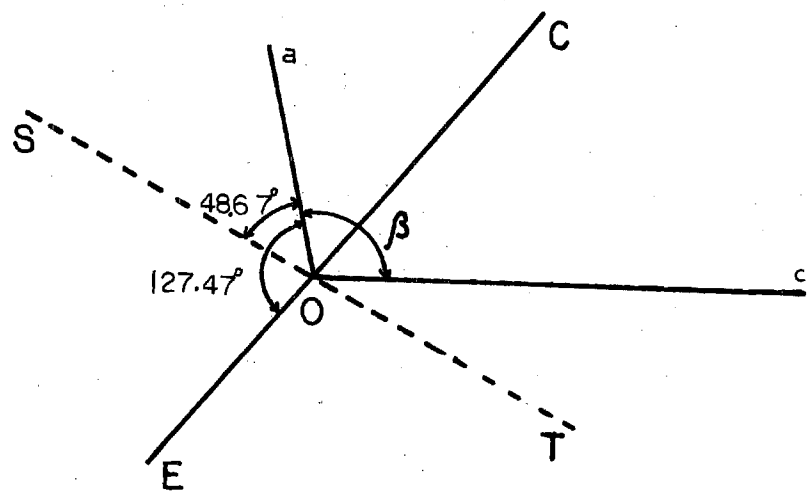

Figure 40. Trace of the Planes ECO and SOT on a Plane Parallel to the a and c Directions for Racemic $Co(C_2N_5H_6)_3 \cdot 2H_2O$.

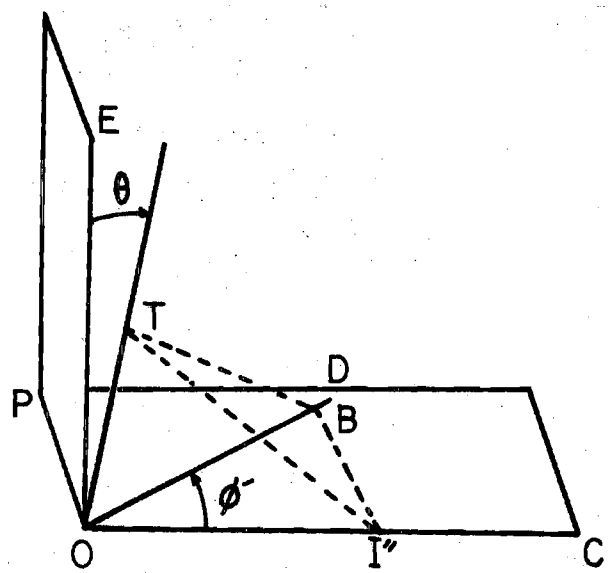

Figure 41. Illustration of Light Polarized Perpendicular to the Direction of the b-Axis for Spectra Through the (1, 0, 0,) Face of Racemic $Co(C_2N_5H_6)_3 \cdot 2H_2O$.

$\Lambda Co(C_2N_5H_7)_3Br_3 \cdot H_2O$.

The numerical values were then substituted for the trigonometric functions in the above expressions and they were solved simultaneously at the various wavelengths. The results were three expressions for A(A), A(E-plane) and A(E-ortho).

$$A(A) = 1.1477A(\perp\perp) - 0.1477A(STO, \perp) \quad (4)$$

$$A(E\text{-plane}) = -0.1477A(\perp\perp) + 1.1477A(STO, \perp) \quad (5)$$

$$A(E\text{-ortho}) = -0.0392A(STO, \perp) + 1.0392A(ECO, \perp) \quad (6)$$

where A(A), A(E-plane) and A(E-ortho) represent the absorbances along OT, TB and BI'' respectively, Figure 41, and the other symbols have been explained before.

The numerical data for absorbances were obtained through a computer program, in the same manner as for the previous example. The results are presented graphically in Figure 42. Table 25 gives some numeric values for the absorbance maxima and some other information pertinent to those spectra.

Racemic $Co(C_5H_7O_2)_3$. Plane polarized single crystal spectra for this material were obtained in a manner very similar to that of the previously discussed two cases. Spectra were determined using two thin slices of the material with the (0, 0, 1) and the (1, 0, 0) faces respectively exposed. From crystallographic data (38) the lattice polar

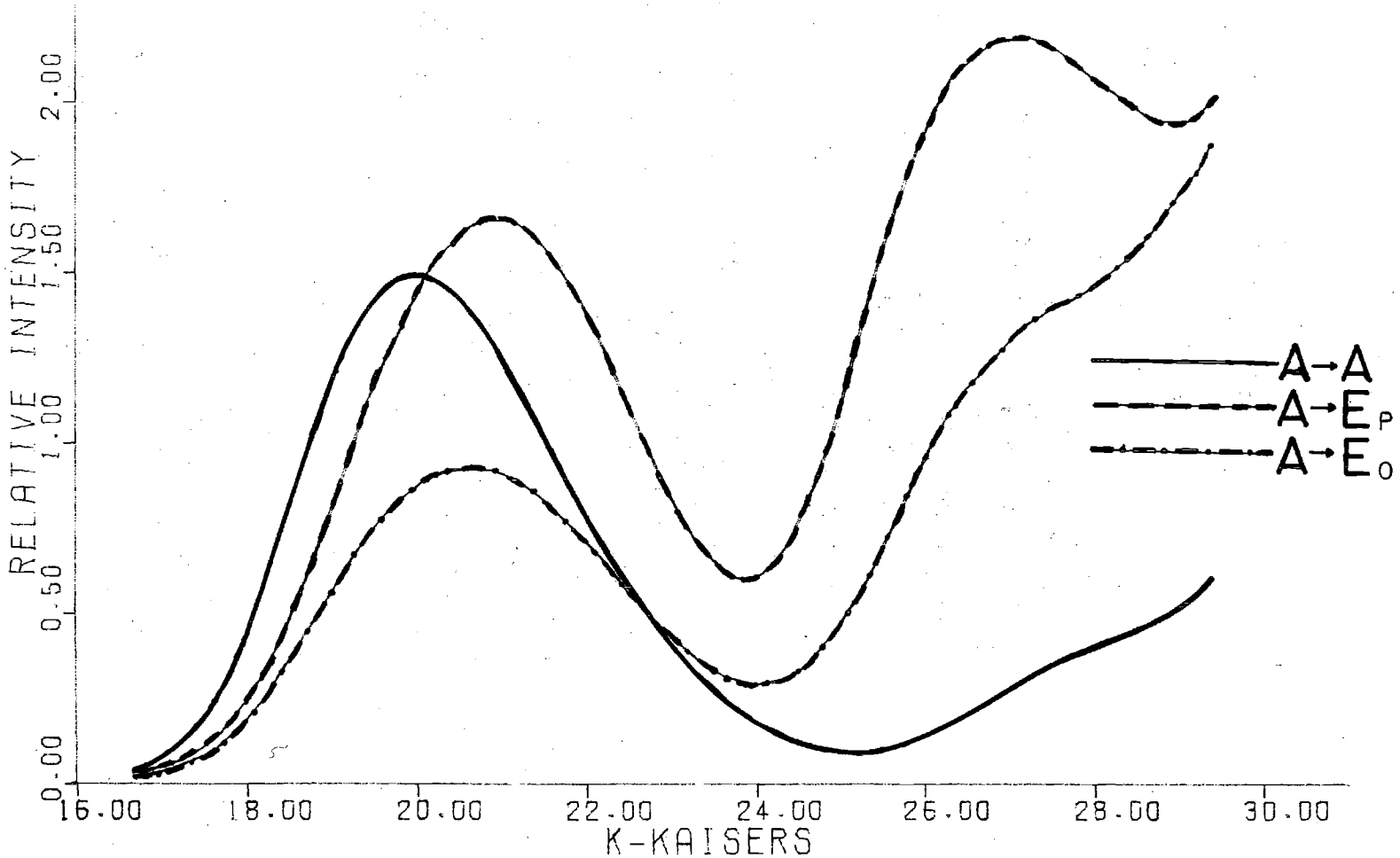

Figure 42. Plane-Polarized Single-Crystal Spectra of Racemic $Co(C_2N_5H_6)_3 \cdot 2H_2O$.

angle, between the three-fold axis direction and that of the b-axis, is $\theta = 30.56°$. The azimuthal angle for spectra through the (0, 0, 1) face is $\phi' = 75.72°$. The azimuthal angle, for spectra through the (1, 0, 0) face, is $\phi = 22.68°$. Figure 43 illustrates the trace of the three-fold axes T'OT on a plane parallel to the (0, 1, 0) face and the two azimuthal angles, ϕ and ϕ'.

Expressions for the absorbance spectra through the (0, 0, 1) and the (1, 0, 0) faces were derived in the same manner as described for $\Lambda Co(C_2N_5H_7)_3Br_3 \cdot H_2O$. The numerical values for the trigonometric functions were then substituted and the three expressions were solved simultaneously to give,

$$A(A) = 1.5353A(\perp\perp) + 0.1007A(0,0,1,\perp) - 0.6360A(1,0,0,\perp) \quad (7)$$

$$A(E\text{-plane}) = -0.5353A(\perp\perp) - 0.2888A(0,0,1,\perp) + 1.8241A(1,0,0,\perp) \quad (8)$$

$$A(E\text{-ortho}) = 1.0770A(0,0,1,\perp) - 0.0770A(1,0,0,\perp) \quad (9)$$

Eq. 7, 8, and 9 are for the absorbances along the directions of OT, TB and BI'' respectively, Figure 44. The absorbance data at the various wavelengths and the scaling factor were then used as input into a computer program and the numerical data for absorbances were obtained through the computer program, in the same manner as for the previous examples. The results are presented graphically in Figure 45. Table 25 gives some numeric values for the absorbance maxima and some other information pertinent to those spectra.

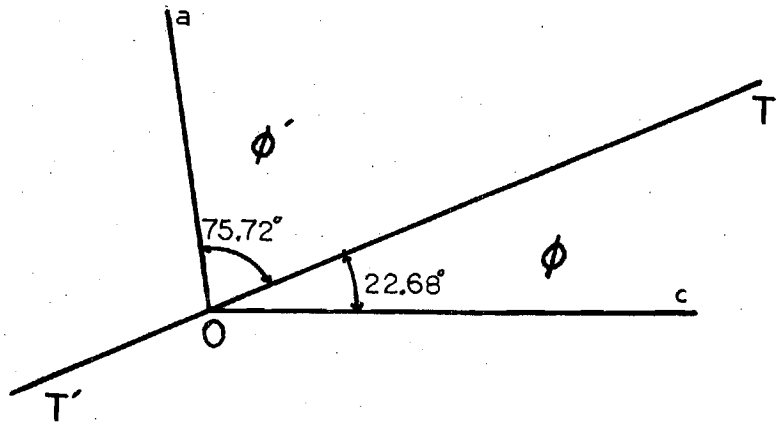

Figure 43. Trace of the Plane of the Three-Fold Axes on a Plane Parallel to the a and c Directions for Racemic $Co(C_5H_7O_2)_3$.

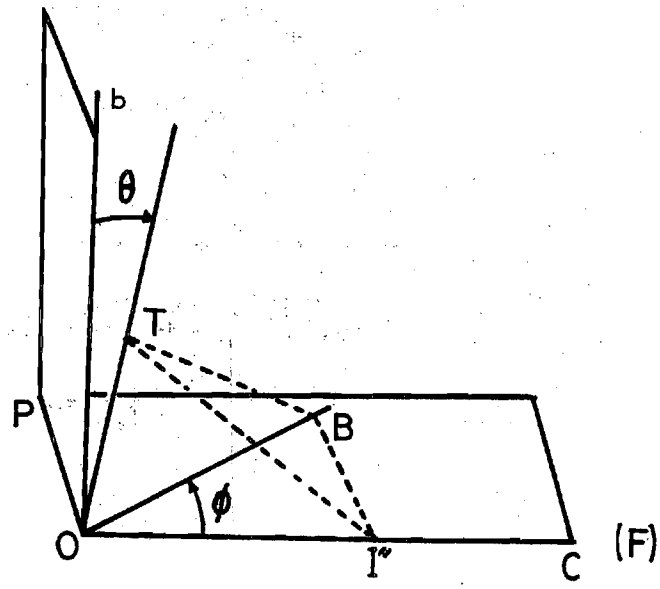

Figure 44. Illustration of Light Polarized Perpendicular to the Direction of the b-Axis for Spectra Through the (1, 0, 0) Face of Racemic $Co(C_5H_7O_2)_3$.

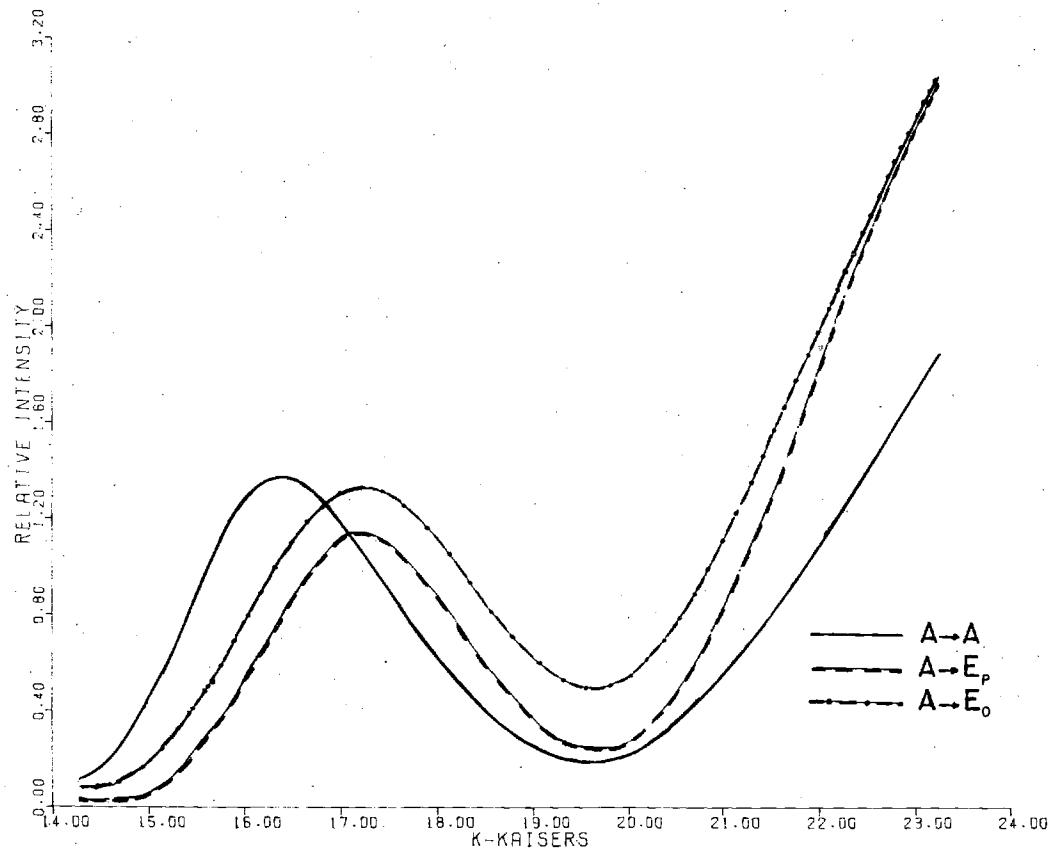

Figure 45. Plane-Polarized Single-Crystal Spectra of Racemic $Co(C_5H_7O_2)_3$.

Table 25. Plane Polarized Single Crystal Spectra.

Compound and Transition	ν_o(kk)	Relative Height	$\nu_{1/2}$(kk)
$\Lambda Co(C_2N_5H_7)_3Br_3 \cdot H_2O$			
(A → A)	20.49	1.180	3.524
(A → E_α)	21.01	1.358	3.844
(A → E_β)	21.28	0.861	3.454
(A → A)	28.91	0.333	
(A → E_α)	28.17	1.212	
(A → E_β)	27.95	1.287	
Rac. $Co(C_2N_5H_6)_3 \cdot 2H_2O$			
(A → A)	20.00	1.497	3.676
(A → E_o)	20.57	0.930	4.120
(A → E_p)	20.89	1.660	3.991
(A → A)	28.	0.4	
(A → E_o)	27.3	1.365	
(A → E_p)	27.2	2.191	
Rac. $Co(C_5H_7O_2)_3$			
(A → A)	16.37	1.370	2.610
(A → E_p)	17.09	1.142	2.502
(A → E_o)	17.24	1.327	3.030

In the above table ν_o is the frequency in kilokaisers and $\nu_{1/2}$ is the full-width at half-height, measured in the same units. E_o and E_p represent E_{ortho} and E_{plane} respectively. E_o, E_p, E_α and E_β are the E-"sublevels" referred to in the text.

Rac. stands for Racemic.

CHAPTER V

DISCUSSION

Structure of $\Lambda Co(C_2N_5H_7)_3Br_3 \cdot H_2O$

A detailed description of the molecular and crystal structure of this material was included in the previous chapter.

In discussing the structural details of the complex cation it is convenient to compare the various angles and distances with some reference figures from other published work. Table 26 lists some averaged values for $\Lambda Co(C_2N_5H_7)_3Br_3 \cdot H_2O$ along with the corresponding values for $\Delta Co(C_2N_5H_7)_3Cl_3 \cdot H_2O$ as determined by Snow (30). The various atoms are identified in Figure 46.

Table 26. Some Molecular Parameters for $\Lambda Co(C_2N_5H_7)_3Br_3 \cdot H_2O$ and $\Delta Co(C_2N_5H_7)_3Cl_3 \cdot H_2O$.

	Λ-Bromide		Δ-Chloride	
Co-N1	1.915	Å	1.912	Å
N1-C1	1.266		1.282	
C1-N2	1.346		1.353	
C1-N3	1.374		1.365	
N1-N5	2.682		2.688	

Angles:

	Λ-Bromide	Δ-Chloride
N1-Co-N5	88.91°	89.3°
Co-N1-C1	129.97°	129.1°
N1-C1-N2	125.62°	124.3°
N1-C1-N3	120.45°	121.5°
N2-C1-N3	113.73°	114.2°
C1-N3-C2	128.11°	127.2°

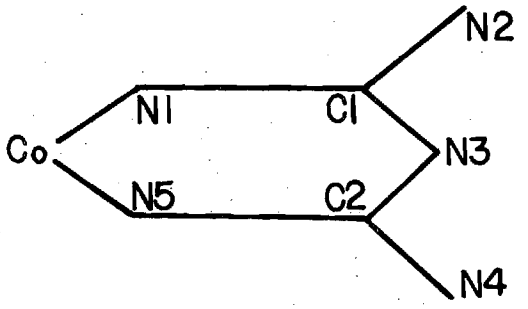

Figure 46. Identification of Atoms in a Chelate Ring.

The distances between the various C and N atoms in the chelate rings may be compared with the following average values for organic compounds, Table 27, (64).

Table 27. Some Values for C-N Bond Lengths*

Methylamine, CH_3NH_2	1.474 ± .005Å
Diazomethane, CH_2N_2	1.32Å
Hydrogen Cyanide, HCN	1.1554Å
Pyridine, C_5H_5N	1.340 ± 0.005Å

The C1-N1 bond is the shortest C-N bond in the chelate, indicating the greatest degree of multiple bond character. Next is the C1-N3 bond which is close to the C-N bond distance in pyridine. Finally the C1-N2 bond is slightly longer than C1-N3. The difference between the last two bond lengths however is not very significant.

*An unambigous C-N double bond distance is difficult to obtain, but it is probably about 1.30Å.

The Co-N bond length (1.915Å) is appreciably shorter than 1.968(1) - 1.972(1)Å the corresponding value (65) in $Co(NH_3)_6^{3+}$.

As mentioned in the previous chapters, the chelates assume a shallow boat configuration. The Co and N3 atoms of every chelate ring are on the same side of the near-perfect plane formed by the N1-C1-C2-N5 atoms. A boat configuration is more favorable than a chair for π-bond delocalization throughout the chelate. The deviation of the chelate rings from planarity may be due to the large size of the Co atom which cannot be accommodated within the chelate bite, N1-N5, and must therefore protrude out of the plane.

The deviation of the N1-Co-N5 angle from 90° may also be ascribed to the large size of the Co. Of the other angles within the chelate ring, the Co-N1-C1 is the most distorted. The ligating atoms N1 and N5 may be assumed to utilize sp2 hybridization, based on the C1-N1 bond length and the C1-N1-H1 angle which is 119°(30). The Co-N1-C1 angle is thus about ten degrees larger than expected for sp2 hybridization. The large value of the C1-N3-C2 angle may also be attributed to the large size of the Co atom. The larger size of the N1-C1-N2 angle may be due to the steric repulsion by the N-2 atoms of the two other chelates of the cation and to a lesser extent by hydrogen bonding to the bromide anions.

Snow (30) reports an apparent concerted deviation from

planarity of the three coordinated N atoms on the same end of the molecular three-fold axis. The same trend was noticed for the isostructural $\Lambda Co(C_2N_5H_7)_3Br_3 \cdot H_2O$. This trend is less prominent for the bromide salt, probably due to different packing forces with the bulkier bromide ion. A similar trend with the same effect, was noticed when two planes were computed for every chelate ring. Thus when planes for N1-C1-N2 and N5-C2-N4 are considered the Co atom is found to lie much closer to planes N5-C2-N4 than to planes N1-C1-N2 for the three chelate rings. The coordinated atoms N1 for the chelates a, b, and c lie on the same end of the three-fold axis. Table 28 illustrates this phenomenon for the Λ-bromide and the Δ-chloride complexes.

Table 28. Distances of the Co Atom from Some Ligand Planes for $\Lambda Co(C_2N_5H_7)_3Br_3 \cdot H_2O$ and $\Delta Co(C_2N_5H_7)_3Cl_3 \cdot H_2O$.

Plane (Λ-Bromide Co-Dist)		Plane (Δ-Chloride Co-Dist)	
N1a, C1a, N2a	.155 Å	N3, C3, N10	-.189 Å
N5a, C2a, N4a	.094	N4, C4, N12	-.086
N1b, C1b, N2b	-.240	N5, C5, N13	.361
N5b, C2b, N4b	.026	N6, C6, N14	.032
N1c, C1c, N2c	.261	N1, C1, N7	-.204
N5c, C2c, N4c	-.017	N2, C2, N9	.050

No concerted trend for the displacement of the Co atom was observed for the deprotonated racemic compounds $Co(C_2N_5H_6)_3 \cdot 2H_2O$ and $Cr(C_2N_5H_6)_3 \cdot H_2O$ (66). For these two materials the

metal atom was found to be almost equidistant from both planar halves of one of the three chelates. The above concerted trend may thus be a consequence of crystal packing in the optically active materials.

Structure of $Co(C_2N_5H_6)_3 \cdot 2H_2O$

A detailed description of the crystal and molecular structure of this material was included in Chapter IV. The structure consists of individual neutral molecules for which the N3 atoms have been deprotonated. The molecules are linked to each other by hydrogen bonding. The two waters of hydration also act as links between the neutral tris-bidentate molecules. To aid in the discussion of the structural details the complex ion may be compared with the corresponding chromium compound (66). Table 29 lists some average values for some molecular parameters. These parameters may also be compared with the data in Tables 27 and 28. The nomenclature scheme in the following table is described in Figure 46.

For the deprotonated molecule $Co(C_2N_5H_6)_3$ the Co-N bond length is shorter than the corresponding length (65) in $Co(NH_3)_6^{3+}$ yet slightly longer than that for $Co(C_2N_5H_7)_3^{3+}$. The N1-C1 bond is still the shortest bond in the chelate ring. The C1-N2 bond for the neutral molecule is insignificantly longer than for the tripositive ion while the C1-N3 bond is slightly shorter.

The chelate bite, N1-N5, is slightly smaller for the

Table 29. Distances and Angles Between Chelate Atoms for $Co(C_2N_5H_6)_3 \cdot 2H_2O$ and $Cr(C_2N_5H_6)_3 \cdot H_2O$.

Distances	Co-Compound	Cr-Compound
M -N1	1.920 Å	2.018 Å
N1-C1	1.301	1.313
C1-N2	1.365	1.370
C1-N3	1.361	1.353
N1-N5	2.644	2.694
Angles		
N1-M -N5	87.04°	83.79°
M-N1-C1	127.28	128.65
N1-C1-N2	119.99	119.70
N1-C1-N3	126.45	126.82
N2-C2-N3	113.54	113.48
C1-N3-C2	119.47	120.73

neutral molecule - this is consistent with the smaller N1-Co-N5 coordination angle. The N2-C1-N3 angle is practically unchanged. The angle C1-N3-C2 at the tail N-atom decreases by about nine degrees upon deprotonation. The decrease of the angle at N3 is due to the presence of the lone electron pair on that atom of the deprotonated chelate, and is consistent with the arguments of Gillespie and Nyholm (67). The distortion of the chelates from planarity is larger for the deprotonated complex. The distances of the Co atom from the planes N1-C1-C2-N5 are given in Tables 12 and 15. These distortions from planarity, as described earlier, result in the chelates taking shallow boat configurations. In the crystalline materials these boats are not all twisted in the same sense. A diagramatic representation

for a view along the three fold axis is shown in Figure 47.

Figure 47. Diagramatic Representation of Twist in Tris-Bidentates.

The larger bromide anion allows more space for thermal motion than the chloride ion (30). This would explain the unusually large anisotropic thermal motions of the chelate atoms for the bromide compound. The energy differences between the (C1) and (C3) forms, Figure 47, is probably very small since the "boats" are very shallow. The dihedral angles (γ) are four, eight and twelve degrees.

The (C1) form has been observed in crystals of five complexes containing six membered chelates with π-bond. Those complexes are $Co(C_2N_5H_6)_3 \cdot 2H_2O$, $Cr(C_2N_5H_6)_3 \cdot H_2O$ (66), $Co(C_5H_7O_2)_3$ (38), Δ-$Co(C_2N_5H_7)_3Cl_3 \cdot H_2O$ (30) and $Cr(C_5H_7O_2)_3$ (68).

That the above (C1) configurations are due to crystal packing forces is supported by proton n.m.r. studies of Λ-$Co(C_2N_5H_7)_3Br_3 \cdot H_2O$ and $Co(C_2N_5H_6)_3 \cdot 2H_2O$ in d6-dimethyl-

sulfoxide solution. At room temperature, proton n.m.r. spectra indicate that for each complex the three chelates are equivalent or that the energy between Cl and C3 is much smaller than their thermal energies, $|E(Cl)-E(C3)| << kT$. Spectra taken on a varian A-60 show three separate peaks in the ratio 4: 2: 1 at τ = 3.31, 4.76 and 6.4 respectively for Λ-$Co(C_2N_5H_7)_3Br_3 \cdot H_2O$. The first two peaks are sharp but the third peak, τ = 6.4, was very broad. For the neutral material only two peaks were observed. The peak maxima were well resolved at τ = 6.43 and 6.60 respectively. The areas of the two peaks however were overlapping. The absence of a third peak from the n.m.r. spectrum of the deprotonated material is consistent with crystallographic data showing that deprotonation occurs at the N-3 sites.

Correlation of Structures and Spectra

The optical activity of transition metal coordination compounds has been extensively investigated. Investigations of particular interest are those that have dealt with accurate determination of crystal structure and absolute configuration (18) of tris-bidentates, the measurement of CD spectra (12, 69), in solution and in the solid state and the correlation (26) of structural properties, absolute configuration and CD spectra.

When plane-polarized single crystal spectra of tris-bidentate metal complexes show substantial energy separations between the components parallel and perpendicular to the

molecular three-fold axis, e.g., for $\Lambda Co(C_2N_5H_7)_3\ Br_3 \cdot H_2O$, $Co(C_2N_5H_6)_3 \cdot 2H_2O$ and $Co(C_5H_7O_2)_3$, these spectra may be safely used for the identification of the (A) and (E) spectral components. This technique has been used by Piper (63, 70) for the crystal spectra of $Co(C_5H_7O_2)_3$ and $Cr(C_5H_7O_2)_3$. If the above energy separations are very small as for $Co(en)_3^{3+}$ and $Cr(en)_3^{3+}$ (109), then the predictions of the nature of transitions, based on plane-polarized spectra, may be questionable. Moreover, as pointed out by Caliga and Richardson (71), other complications will probably be introduced when such energy separations are small.

In this work the results of plane-polarized spectra have been used, along with single crystal CD spectra, for the identification of the transition bands of three tris-bidentate metal complexes. However, as described in Chapter III, during the analysis of the plane-polarized single crystal spectra of $\Lambda Co(C_2N_5H_7)_3Br_3 \cdot H_2O$, the spectra obtained when light was polarized perpendicular to the three-fold molecular axis showed very different intensities at various orientations. In order to better describe the optical behavior of these materials, plane-polarized single crystal spectra were resolved into three, rather than two, mutually perpendicular components. No rigorous theoretical justification was sought for that procedure. However when the symmetry of a tris-bidentate metal complex is lower than D3 or C3, the (E) level will no longer be degenerate.

Moreover in the low-symmetry structures, as were encountered for the above complexes, vibrational effects are not expected to be the same in all directions and these effects may be one cause for the differences in intensities for the (E) "sublevels". The difference in energy between the (E) "sublevels" was small compared with the energy separation between the (A) and either (E) "sublevel."

The energies of the spectral components in plane-polarized single crystal spectra are higher than the energies of the corresponding components of the CD spectra for powdered samples, thus $\nu_{(A)}$ (plane-polarized) > $\nu_{(A)}$ (CD) and $\nu_{(\bar{E})}$ (plane-polarized) > $\nu_{(E)}$ (CD), Tables 23, 24 and 25. The value of $\nu_{(\bar{E})}$ for $\Lambda Co(C_2N_5H_7)_3Br_3 \cdot H_2O$, 21.14 kk, is also higher than the value of ν_E from the single crystal CD spectra, 20.41 kk. These observations are in agreement with the fact that the spectral components in plane-polarized spectra represent the vibronic transitions in which the energies of some vibrational exitations are superimposed upon the energies of the electronic transitions. Alternatively CD spectra represent the energies of the pure electronic transitions.

The following discussion is addressed to the study of a few compounds that have rigid chleate rings and the correlation of their structural properties to their CD spectra. The rigidity of the chelate rings precludes a change of conformation in solution.

The correlation of optical activity with structure will be discussed with reference to the theoretical models outlined in Chapter II. It is appropriate to start this discussion by listing the structural parameters and optical data available for pertinent compounds. This information is presented in Tables 30 and 31 respectively. Various parameters have been used in describing deviations from octahedral symmetry for tris-bidentate metal complexes. The deviations from octahedral values of the polar angle, π, and the ratio of side to height, s/h, have been used to describe (54) polar distortion. According to the first order approximation (14) the polar distortions give rise to the split of the octahedral T_1 level into the A_2 and E_a components of D_3 symmetry. The polar distortion however does not contribute to the rotatory strengths of the A_2 and E_a components. Values of s/h larger than 1.225 and values of the angle π larger than 54.74° indicate a polar compression.

The azimuthal distortion is described by the deviation from 60° of the trigonal twist angle, $\hat{\tau}$. According to the first order approximation (14), the azimuthal distortion, $|\hat{\tau} - 60°|$, gives rise to rotatory strengths but does not contribute to the $(A_2\text{-}E_a)$ energy separation.

An angle, $\hat{\delta}$, may be defined as the angle between the plane N1-Co-N5 and the three-fold axis of the tris-bidentate. The value of $\hat{\delta}$ may be computed by the formula $\hat{\delta} = \sin^{-1}$

Table 30. Structural Data for Complexes.

Compound	a(Å)	b(Å)	s(Å)	h(Å)	s/h	ℓ(Å)	β(deg)	τ(deg)	π(deg)	ψ(deg)	λ(deg)	δ(deg)	Ref
Regular Prism	a	$2a\sqrt{3/7}$	$2a\sqrt{3/7}$	$2a\sqrt{3/7}$	1.000	-	90.00	0.00	49.11	90.00	-	0.00	56
Regular Octahedron	a	$a\sqrt{2}$	$a\sqrt{2}$	$2a\sqrt{3}$	1.225	-	90.00	60.00	54.74	54.74	-	35.26	56
$Co(NH_3)_6^{3+}$	1.972	2.789	2.778	2.282	1.217	-	87.76	60.00	54.57	54.57	-	35.43	65
$\Lambda(+)_{589}Co(en)_3Cl_3\cdot 3H_2O$	1.974	2.678	2.830	2.214	1.278	1.497	85.43	54.90	55.88	55.76	108.4	34.23	72
$\Delta(-)_{589}Co(R,pn)_3Br_3\cdot 2H_2O$	1.976	2.692	2.813	2.250	1.250	1.489	85.88	54.11	55.29	56.71	109.60	33.29	73
$\Lambda(+)_{589}(ob)Co(R,pn)_3Co(CN)_6$	1.971	2.644	2.845	2.178	1.306	1.485	84.22	54.16	56.44	55.55	110.57	34.45	74
$\Lambda(+)_{589}(ob)Co(-,chxn)_3Cl_3\cdot H_2O$	1.982	2.658	2.818	2.265	1.244	1.494	84.19	50.60	55.16	58.45	109.85	31.55	75
(*) $\Lambda(-)_{589}(lel)Co(+,chxn)_3Cl_3\cdot 5H_2O$	2.019	2.771	2.846	2.346	1.213	1.509	86.69	52.98	54.48	58.13	106.37	31.87	76
(*) $\Lambda(-)_{589}Co(trans,cptn)_3Cl_3\cdot 4H_2O$	2.004	2.756	2.827	2.330	1.213	1.488	86.89	54.15	54.62	57.34	104.93	32.66	77
$\Lambda(-)_{589}Co(tn)_3Cl_3\cdot H_2O$	1.979	2.808	2.788	2.303	1.211	1.484	90.38	59.88	54.42	55.11	122.0	34.90	78
(*) $\Lambda(+)_{546}Co(RR,ptn)_3Cl_3\cdot H_2O$	1.988	2.767	2.799	2.314	1.210	1.505	88.20	56.08	54.35	56.66	115.67	33.34	79
$\Delta(-)_{546}Co(RR,ptn)_3Cl_3\cdot 2H_2O$	1.990	2.790	2.799	2.332	1.205	1.520	89.04	57.21	54.31	56.32	118.03	33.68	80
$\Delta(+)_{589}Co(tmd)_3Br_3$	1.991	2.802	2.772	2.371	1.170	1.506	89.44	55.68	53.47	57.77	122.9	32.23	81
$\Lambda(-)_{589}Co(HBgd)_3Br_3\cdot H_2O$	1.915	2.682	2.710	2.206	1.229	1.266	88.91	58.28	54.81	55.37	129.97	34.63	This work
$\Delta(+)_{589}Co(HBgd)_3Cl_3\cdot H_2O$	1.911	2.684	2.699	2.211	1.221	1.282	89.24	58.42	54.64	55.49	129.08	34.51	30
Rac. $Co(Bgd)_3\cdot 2H_2O$	1.920	2.644	2.744	2.169	1.265	1.301	87.04	57.02	55.60	55.11	127.28	34.89	This work
Rac. $Co(Acac)_3$	1.885	2.814	2.611	2.265	1.153	1.267	96.55	67.27	53.08	53.61	123.40	36.39	35, 38
(*) $\Lambda(-)_{589}Co(Ox)_3\Delta KNi(phen)_3$	1.923	2.580	2.772	2.130	1.301	1.19	84.27	54.08	56.37	55.65	111.50	34.35	82
(*) $\Lambda KCa(+)_{589}Co(thiox)_3\cdot 4H_2O$							89.7	57.0	53.8	56.92		33.08	88

Table 30. (Continued)

Compound	a(Å)	b(Å)	s(Å)	h(Å)	s/h	e(Å)	β(deg)	τ(deg)	π(deg)	ψ(deg)	λ(deg)	δ(deg)	Ref
Rac. $Cr(en)_3Co(CN)_6$	2.081	2.73	3.01	2.29	1.31	1.481	81.83	50.4	56.62	57.12	110.27	32.88	83
Rac. $Cr(en)_3Ni(CN)_5$	2.075	2.73	3.00	2.29	1.31	1.490	82.37	51.3	56.51	56.71	109.44	33.29	84
Rac. $Cr(tn)_3Ni(CN)_5 \cdot 2H_2O$	2.097	2.958	2.943	2.455	1.199	1.487	89.73	58.09	54.15	56.09	119.34	33.91	85
Rac. $Cr(Bgd)_3 \cdot H_2O$	2.018	2.694	2.881	2.283	1.262	1.313	83.79	50.94	55.53	57.93	128.65	32.07	66
$(\Delta)K_3Cr(cat)_3 \cdot 1.5H_2O$	1.986	2.646	2.835	2.247	1.262	1.349	83.56	50.34	55.53	58.27	110.72	31.73	86
Rac. $Cr(Acac)_3$	1.955	2.792	2.760	2.267	1.217	1.263	91.10	61.51	54.57	54.29	126.92	35.71	68
(*)Rac. $Cr(Ox)_3^{3-}$	1.964	2.590	2.826	2.182	1.295	1.273	82.37	50.49	56.13	57.39	110.52	32.61	87
(*)$\Lambda(+)_{589}Cr(mal)_c^{3-}$							91.9	60.2	53.5	55.89		34.11	88, 106
(*) $(+)_{589}Cr(trans, atc)_3$	1.97						91.1						89

(*) Poor data set or poor refinement.
Rac. stands for racemic.

The abbreviations and the symbols used in this table are explained on pages 178 and 179.

The structural parameters in this table were calculated from atomic coordinates and unit cell parameters, as given by the authors. In a few cases they may differ slightly from the explicit data given by the authors. Such differences, however, are less than 0.1 degrees for angles and less than 0.01 Å for interatomic distances.

Table 31. Spectral Data for Complexes

Compound	ν(kk)	Abs(ε)	ν(kk)	C. D. (ε_l-ε_r)	Spectral Transition	Ref.	Single Crystal Spectra Plane-Polarized	C.D.
$Co(NH_3)_6^{3+}$	20.9	60	-	-	T_1	(24)		
	29.2	44	-	-	T_2			
$\Lambda(+)_{589}Co(en)_3^{3+}$	21.4	84	20.28	1.89	E_a	(69, 90)	(109)	(90)
			23.36	-0.166	A_2			
	29.4	74	28.49	0.250	E_b			
$\Lambda(+)_{589}Co(d\text{-}pn)_3^{3+}$	24.413	96.5	20.367	1.89	E_a	(12, 91)		(110)
			22.936	-0.49	A_2			
	30.59	90						
$\Lambda(-)_{589}Co(+trans\ cptn)_3^{3+}$	20.41	74	18.70	0.77	E_a	(95)	(95)	(95)
			21.10	-2.50		-		
	28.33	82				-		
$\Lambda Co(cis,\ cptn)_3^{3+}$	21.01	110	20.41	2.9		(95)		
			-	-		-		
	29.16	100	27.03	0.1				
(another conformer)	21.01	110	20.41	2.7	E_a	(95)		
			24.39	-0.05				
	29.16	100	-	-		-		
$?\Lambda(ob_3)Co(-cptn)_3^{3+}$			19.23	-3.0		(95)		-
			21.98	6.0				
$\Lambda(+)_{589}(ob)Co(-chxn)_3^{3+}$	21.14	101	20.88	4.45		(93)		
	29.15	93	28.99	-0.07				
$\Lambda(-)_{589}(lel)Co\text{-}chxn)_3^{3-}$	21.19	101	20.04	2.45		**(77,93,94)**		
			22.62	-0.66				
	29.24	94						
$\Lambda(-)_{589}Co(tn)_3^{3+}$	20.49	79	18.80	0.067		**(96,97)**		(110)
			21.10	-0.140				
	28.57	76	27.80	-0.015				
$?\Delta Co(RS2,4ptn)_3^{3+}$	20.37	91	19.69	-0.548		(97)		
	28.41	89	28.17	-0.013				
$\Lambda(+)_{546}Co(RR2,4ptn)_3^{3+}$	20.53	98	20.83	2.69		(97)		
	28.65	91	28.41	-0.283				

Table 31. (Continued)

Compound	ν̄(kk)	Abs(ε)	ν̄(kk)	C.D. ($\varepsilon_l - \varepsilon_r$)	Spectral Transition	Ref.	Single Crystal Spectra Plane-Polarized	C.D.
$\Lambda(-)_{546}Co(SS2,4ptn)_3^{3+}$	20.75 28.82	76 74	19.61 28.57	0.586 -0.066	E_a	(97)		(12, 69)
$\Lambda(-)_{589}Co(tmd)_3^{3+}$	19.90	77.8	18.20	0.17	E_a	(98, 99)		(98, 99)
			20.50	-1.83				
	27.90	70.4						
$\Lambda(-)_{589}Co(HBgd)_3^{3+}$	21.05	191.5	19.61	-3.54	A_2	This work	This work	This work
			22.12	4.74	E_a			
	28.29	170.8	27.93	-1.87				
			33.67	0.74				
$\Lambda(-)_{546}Co(Bgd)_3$	20.83	233.09	19.23	-4.73(*)	A_2	This work	This work	This work
(C.D. in MeOH)			21.93	3.80(*)	E_a			
	27 shoulder	203	27.78 30.12	-2.12(*) -1.68(*)				
$\Lambda(-)Co(acac)_3$	16.89	137.5	15.53	-2.68	A_2	This work &	This work	
(in cyclohexane)			17.70	8.38	E_a	(35, 61, 63)	This work	
$\Lambda(-)_{589}Co(Ox)_3^{3-}$	16.61	153	16.21	3.30	E_a	(69)	(101)	(69)
			22.42	0.26				
	23.70	204	24.27	-0.26				
			26.53	0.21				
$\Lambda(+)_{589}Co(tart)_3^{3-}$	15.63	168	16.31	4.6		(69)		
	22.42	215	23.26	-0.8				
$\Lambda(+)_{589}Co(hmc)_3^{3-}$	16.39	174	14.29	-0.4		(69)		
			16.39	5.2				
	22.73	530	21.74	-5.5				
$\Lambda(+)_{589}Co(atc)_3^{3-}$			14.56	-2.15		(102)		
			16.84	6.22				
			22.74	-7.01				
$\Lambda(+)_{589}Co(tniox)_3^{3-}$	17.54	450	15.75	-0.2		(69,115)		
			18.52	2.8				
	21.74	1800	26.32	16.2				

Table 31. (Continued)

Compound	ν(kk)	Abs(ε)	ν(kk)	C.D. $(\varepsilon_l-\varepsilon_r)$	Spectral Transition	Ref.	Single Crystal Spectra Plane-Polarized	C.D.
$\Lambda(+)_{589}Cr(en)_3^{3+}$	21.74	74	21.93	1.36		(69)	(109)	
	28.33	65	28.57	-0.05				
$(+)_{589}Cr(+pn)_3^{3+}$	21.74	71	21.28	1.30		(69)		
			24.51	-0.06				
			27.32	0.06				
$Cr(trans, cptn)_3^{3+}$	21.28	78				(95)		
	27.78	70						
$(-)_{589}Cr(tn)_3^{3+}$	21.01	55	20.83 or 21.05	0.38 or 0.28		(103, 104)		
$\Lambda(-)_{589}Cr(HBgd)_3^{3+}$	20.75	103	19.16	-2.73		**(58,105)**		
			21.17	4.14				
	27.17	78	26.67	-1.28				
$\Lambda(+)_{589}Cr(Ox)_3^{3-}$	17.51	74	15.87	-0.58	A_2	(69)	(100)	(69)
			18.12	2.83	E_a			
	27.30	97	24.10	-0.56				
$\Lambda(+)_{589}Cr(mal)_3^{3-}$	17.39	30	16.13	-0.07		(69, 106)		
			18.18	0.20				
	23.36	28	23.81	-0.04				
$\Lambda(+)_{589}Cr(tart)_3^{3-}$	16.81	66	15.09	-0.88		(69)		
			17.12	3.77				
	22.99	81	23.09	-1.24				
$\Lambda(+)_{589}Cr(hmc)_3^{3-}$	17.70	67	15.63	-0.7		(69)		
			18.35	4.2				
	21.28	187	21.19	0.7				
$\Lambda(+)_{589}Cr(atc)_3^{3-}$			16.393	-1.71		(89)		
			18.519	3.63				
			27.5	-19.				

Table 31. (Continued)

Compound	ν(kk)	Abs(ε)	ν(kk)	C.D. ($\epsilon_l - \epsilon_r$)	Spectral Transition	Ref.	Single Crystal Spectra Plane-Polarized C.D.
$\Lambda Cr(cat)_3^{3-}$ (**)	16.89	78	15.08	-0.49		(108)	
			17.18	2.3			
	23.53	104	22.99	-0.91			
$\Lambda(+)_{546}Cr(thiox)_3^{3-}$	17.00	417	---	---		(107)	
			17.60	(-)			
	21.80	1070	21.00	(+)			

(*) Relative numbers. Absolute magnitudes not available.
(**) The assignment, by Raymond, et al., of the E_a transition to the negative band at lower energy may be questioned. The compound is very similar to ΛCr $(Ox)_3$ for which single crystal C.D. spectra (69) confirm the opposite assignment.

The abbreviations used in this table are explained on page 179.

The symbols in the first line of Table 30 for structural data are identified as follows:

Latin letters are used for interatomic distances,

a: Metal-ligand bond length

b: Bite, ligand-ligand distance within a chelate

s: Side of the octahedron

h: Height of the octahedron

s/h: Ratio of side to height

ℓ: Ligand to carbon atom distance, nearest neighbors

Greek letters are used for interatomic angles,

β: Bite angle, at the metal, within a chelate

τ: Twist angle, azimuthal angle

π: Molecular polar angle

ψ: Pitch angle, between the face of the octahedron and the plane L-M-L'

λ: Metal-ligand-carbon angle within a chelate

δ: Angle between the molecular three-fold axis and the plane L-M-L'

The abbreviations in the first column of Tables 30 and 31 represent the following :

en: ethylenediamine; 1,2-diaminoethane

R,pn: propylenediamine; R-1,2-propanediamine

(-chxn): $(-)_d$ trans 1,2-diaminocyclohexane

trans,cptn: trans 1,2-diaminocyclopentane

tn: trimethylenediamine; 1,3-diaminopropane

RRptn: R R 2,4-diaminopentane

tmd: tetramethylenediamine; 1,4-diaminobutane

HBgd: $(C_2N_5H_7)$; biguanide

Bgd: $(C_2N_5H_6)^{3-}$; biguanidato

Acac: acetylacetonato; 2,4-pentanedionato

Ox: oxalato

cat: catecholato

mal: malonato

atc: acetylcamphorato

tart: tartrato

thiox: 1,2-dithiooxalato

hmc: hydroxymethylcamphorato

$[(\tan \frac{\hat{\tau}}{2})/(\tan \frac{\hat{\beta}}{2})]$ where $\hat{\tau}$ and $\hat{\beta}$ are the <u>average values</u> for the azimuthal twist angle and the coordination or bite angle of the chelate at the metal. The "pitch" angle, $\hat{\psi}$, may be defined as $\hat{\psi} = 90° - \hat{\delta}$. The angle ψ represents the inclination of the plane N1-Co-N5 to the octahedral face which is perpendicular to the three fold axis. The information that may be obtained from the angle ψ will be presented below. However it is worthwhile to point out that $\hat{\psi}$ shows the relationship between the bite angle, β, and the azimuthal twist angle, τ. For the perfect octahedron the angle ψ is identical in value to the polar angle, π, 54.74°.

The deviation of the angle ψ from 54.74° describes the departure of the plane L-M-L´ from its octahedral position or orientation. The larger the value of the angle ψ the steeper is the inclination of this plane, L-M-L´, on the octahedral face perpendicular to the three-fold axis.

The <u>deviation</u> of the angle ψ from the octahedral value, 54.74°, resembles the out-of-plane component, $\tilde{\pi}_j$, of Liehr's angle of mismatch-Liehr (22), pp. 669-670 and pp. 673-675.

Consider the structural parameters s/h and $\hat{\pi}$ for the complexes Λ-Co(en)$_3^{3+}$, ΛCo(S-pn)$_3^{3+}$, $\Lambda(\delta\delta\delta)(\ell e\ell)$Co(chxn)$_3^{3+}$, ΛCo(trans cptn)$_3^{3+}$ and ΛCo(tmd)$_3^{3+}$. The last three complexes possess polar elongation according to their values of

s/h and $\hat{\pi}$. All the above complexes have been examined (12) by single crystal CD spectra and all show a positive CD band at low energy and a negative CD band at higher energy in the $A_1 \rightarrow T_1$ region of the octahedral CoN_6 spectrum.

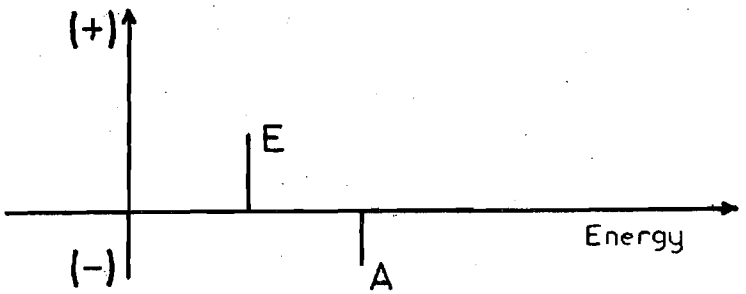

Figure 48. General Pattern of C.D. Spectra of Λ Tris-Bidentates with Saturated Chelates.

The low energy CD bands have been identified, by single crystal CD spectra, as the $A_1 \rightarrow E_a$ while the higher energy bands were identified as the $A_1 \rightarrow A_2$ transitions. The first two of those complexes show a polar compression, $s/h > 1.225$ and $\hat{\pi} > 54.74°$. Since all those complexes show the same pattern of CD spectra, their distortions might be better described by the angle ψ which is larger than 54.74° for all of them. In fact all complexes presented in Table 30, with the exception of $Co(Acac)_3$ and $Cr(Acac)_3$, appear to have $\hat{\psi}$ larger than 54.74°. Besides, all Λ complexes in Table 31 with saturated chelates show a positive CD band at low energy and a negative CD band at higher energy in the $A_1 \rightarrow T_1$ region.

From the spectral (96, 107) and structural (78) data presently available for the complex Λ-$Co(tn)_3^{3+}$, use of the parameter $\hat{\psi}$ would show that it is distorted like all other complexes with saturated chelates, and therefore contradicts the predictions of the ionic model and the Piper, Karipides models (19, 111, 112, 113).

The complex $(ob)_3Co[(-)cptn]_3^{3+}$ has been assigned (95) a Λ absolute configuration. The signs of the components of the CD spectra are reversed in comparison with other ΛCo (III) tris-bidentate complexes with saturated chelates. From the order of chromatographic separation and from the CD spectrum it would seem that the above complex should be the Δ, (delta), enantiomer. No structural data or parameters are available at the present for this material.

Cobalt complexes of Λ configuration with chelates bearing π-bonds have CD spectra that are very similar to each other and different from the spectra for complexes with saturated chelates.

The CD spectra for Co (III) tris-bidentate complexes of Λ configuration with unsaturated chelates have a negative component at low energy and a positive component at higher energy in the region of the first octahedral transition. As shown earlier in this work, the identities of these transitions for Λ-$Co(C_2N_5H_7)_3^{3+}$, Λ$Co(C_2N_5H_6)_3$ and Λ$Co(C_5H_7O_2)_3$ have been assigned, from single crystal spectra, as the $A_1 \rightarrow A_2$ for the low energy and $A_1 \rightarrow E_a$ for the high energy

transitions.

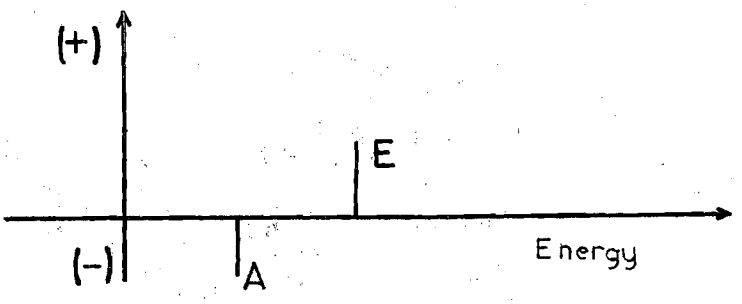

Figure 49. General Pattern of C.D. Spectra of ΛTris-Bidentates with Unsaturated Chelates.

For all other Λ-Co (III) tris-bidentates with unsaturated chelates (and similarly for the corresponding Cr (III) Compounds) shown in Table 31 the low energy transition is negatively rotating while the higher energy transition is positively rotating. The above phenomenon seems to be a general one for all known Λ-tris-bidentate complexes with unsaturated chelates, irrespective of geometric distortions. Thus while the biguanide complexes are axially compressed and azimuthally contracted, the 2, 4-pentanedione complex has a polar elongation and is azimuthally expanded. The CD spectrum for Λ-$Co(Ox)_3^{3-}$ shows no negative peak but the positive E_a has been unambiguously assigned by single crystal CD spectra. It is probable that a weak $^1A_2$ peak is

present yet is covered by a relatively intense ^1E_a peak. The very similar case of $\Lambda Cr(Ox)_3^{3-}$ shows both peaks distinctly. The positive ^4E_a peak for the Cr (III) compound has also been unambiguously assigned by single crystal CD spectra.

A qualitative explanation for the reversal of transition energies, $(\nu_E - \nu_A)$, will be made. A comparative discussion will then be given utilizing the various theoretical models available. A reversal of the order of the energies of the E_a and A_2 transitions is observed for complexes with π-bonds on the ligating atoms of the chelate. For such complexes ν_E is larger than ν_A.

Consider the wave functions for the A_2 and E_a transitions of a trigonally distorted d^6 tris-bidentate. (The same argument is equally applicable to the d^3 complexes of Cr (III)). Liehr (22) (p. 703) gives the following expressions for the A_2 excited state of a d^6 complex, assuming the C3 axis to be the unique axis,

$$^1A_2[\ ^1T_g\ (t_{2g}^5\ e_g^1)]:$$

$$1/2\{|a_1(t_{2g}):(\downarrow\uparrow), e_+(t_{2g}):(\downarrow\uparrow), e_-(t_{2g}):(\uparrow), e_-(e_g):(\downarrow)|$$

$$-|a_1(t_{2g}):(\downarrow\uparrow), e_+(t_{2g}):(\downarrow\uparrow), e_-(t_{2g}):(\downarrow), e_-(e_g):(\uparrow)|$$

$$-|a_1(t_{2g}):(\downarrow\uparrow), e_+(t_{2g}):(\uparrow), e_-(t_{2g}):(\downarrow\uparrow), e_+(e_g):(\downarrow)|$$

$$+|a_1(t_{2g}):(\downarrow\uparrow), e_+(t_{2g}):(\downarrow), e_-(t_{2g}):(\downarrow\uparrow), e_+(e_g):(\uparrow)|\}$$

and for the E_+ excited state,

$$^1E_+ \; [^1T_{1g} \; (t_{2g}^5 \; e_g^1)]$$

$$+1/2\{|a_1(t_{2g}):(\downarrow),e_+(t_{2g}):(\downarrow\uparrow),e_-(t_{2g}):(\downarrow\uparrow),e_+(e_g):(\uparrow)|$$

$$-|a_1(t_{2g}):(\uparrow),e_+(t_{2g}):(\downarrow\uparrow),e_-(t_{2g}):(\downarrow\uparrow),e_+(e_g):(\downarrow)|$$

$$+|a_1(t_{2g}):(\downarrow\uparrow),e_+(t_{2g}):(\downarrow),e_-(t_{2g}):(\downarrow\uparrow),e_-(e_g):(\uparrow)|$$

$$-|a_1(t_{2g}):(\downarrow\uparrow),e_+(t_{2g}):(\uparrow),e_-(t_{2g}):(\downarrow\uparrow),e_-(e_g):(\downarrow)|\}$$

In the above expressions the vertical "arrows" pointing up and down indicate the two possible electron spins. Orbitals containing one "arrow" are those which have only one electron. For the (E_-) "substate" the appropriate expression is obtained by the choice of the other sign from the original text, [22].

From the above wave functions it is noted that for the A_2 transition the electron is promoted, exclusively, from the (e) orbitals of the (t_{2g}) ground state. The "hole" for the A_2 transition is in an (e) orbital. For the E transition the wave function has a combination of (a) and (e) orbitals from which the electron is promoted. The "hole" is therefore in an (a) or in an (e) orbital for the E transition.

Consider next the effect of the π-orbitals present on the chelate rings. Every individual chelate ring,

without the metal, is very nearly planar and has a C_{2v} point group symmetry. If the energies and the symmetries of the filled π-molecular orbitals are determined it is found that the highest occupied ligand π-orbital has B_1 symmetry, in C_{2v}. Table 32 shows the energies and the expressions for the filled π-molecular orbitals of biguanide, obtained from a MINDO/3 calculation (114). A simple Huckel M.O. calculation produces the same order of energy levels for the biguanide and the 2, 4-pentanedione complexes. Figure 50 shows one chelate with the coefficients of the atomic orbitals for the highest occupied π-electron M.O. Figure 51 shows the three chelates, with the proper parities for the highest occupied π-level, arranged in a concerted manner in D_3 symmetry. The ensemble of three chelates in the form described above would have (a_2) and (e) symmetries for the highest occupied π M.O.

For a d^6 metal ion in a D_3 environment the dz^2 orbital forms the basis for the A_1 representation of the ground state (when the C_3 axis of the ion is taken as the reference axis) while a combination of metal d-orbitals form the basis of the (E) ground state representation. The diagramatic scheme, Figure 52, shows the consequence of the interactions between orbitals of the same symmetry, (e), on the metal ion and on the highest filled π-molecular orbital of the ensemble of three chelates. The (a_1) orbital of the metal and the (a_2) orbital of the chelate ensemble do not

Table 32. Data for the π-Orbitals of the Biguanide Ligand.

Wave Function: $\psi = a_1\phi_1 + a_2\phi_2 + a_3\phi_3 + a_4\phi_4 + a_5\phi_5 + a_6\phi_6 + a_7\phi_7$. Energy difference between ψ5 and ψ4 is 0.2748 e.v. or 2.22 kk

	a_1	a_2	a_3	a_4	a_5	a_6	a_7	Symmetry	Energy (e.v.)	ΔEnergy (e.v.)
ψ5	-0.561	-0.561	-0.140	-0.140	0.459	0.245	0.245	B_1	-8.3387	0.2748
ψ4	-0.483	0.483	-0.184	0.184	0.000	0.483	-0.483	A_2	-8.6135	1.0434
ψ3	≈0	≈0	≈0	≈0	-0.588	0.572	0.572	B_1	-9.6569	2.6614
ψ2	0.322	-0.322	0.409	-0.409	0.000	0.478	-0.478	A_2	-12.3183	2.2321
ψ1	-0.256	-0.256	-0.429	-0.429	-0.581	-0.286	-0.286	B_1	-14.5504	

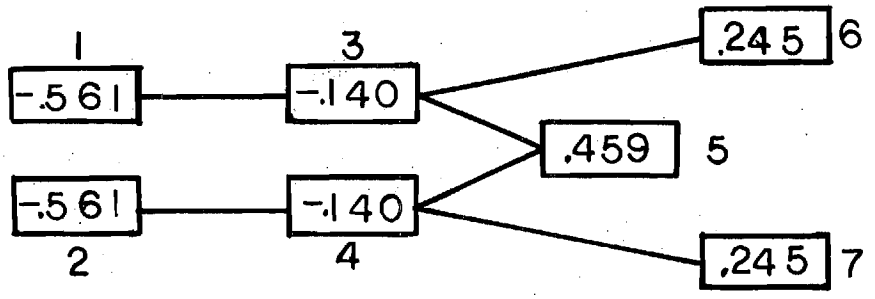

Figure 50. Coefficients of Atomic π-Orbitals in Highest Occupied Level of Biguanide.

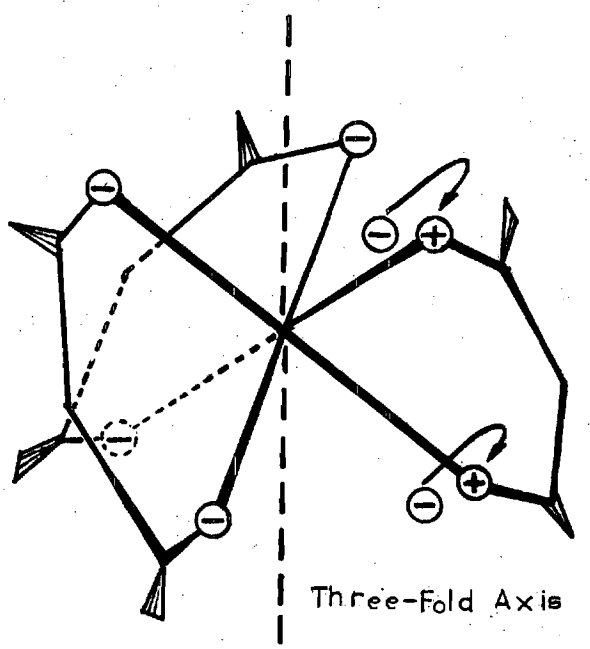

Figure 51. Illustration of a Three-Chelate Ensemble in D3 Symmetry with Parities of Highest Occupied π-Orbital.

have the same symmetry and therefore will not interact.

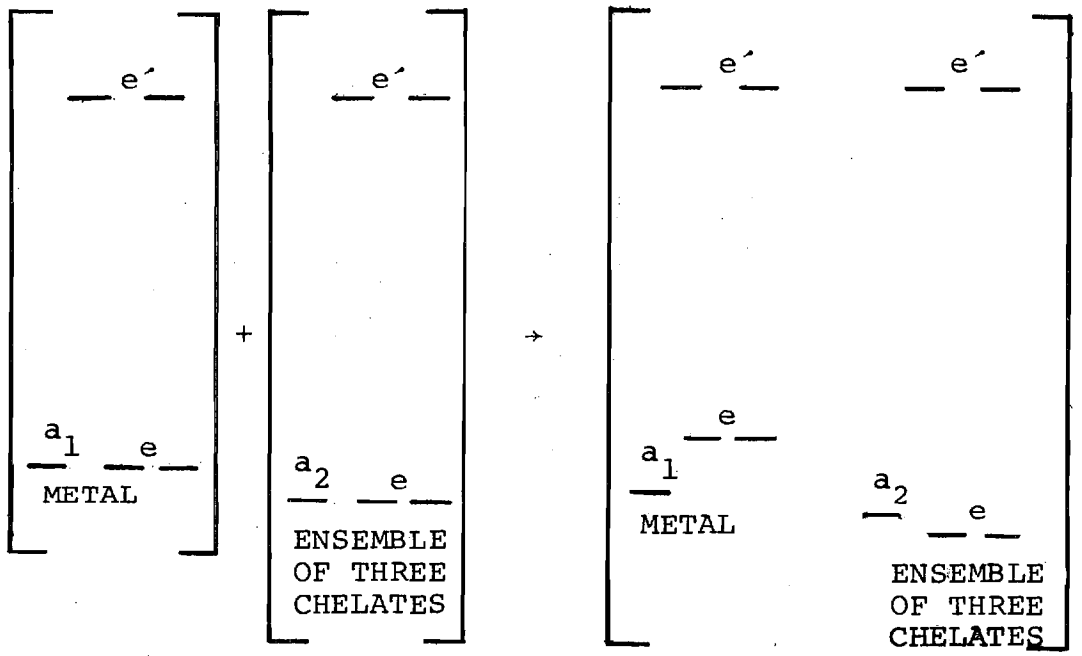

Figure 52. Consequence of Interaction of Highest Filled Ligand π-Orbital with Metal d-Orbitals.

The interaction of the (e) orbitals of the metal with the (e) orbitals of the chelate ensemble results in these two metal (e) orbitals going up in energy, with respect to their corresponding (a) orbital. Remembering that the metal A_2 transition results, exclusively, from electrons promoted from the (e) orbitals, the above interaction makes the A_2 metal transition occur at lower energy than the E transition. This discussion explains qualitatively the reversal of the order of the A_2 and E transitions for complexes with π-bonds on their chelates, compared with complexes having saturated

chelates. From the foregoing discussion it will also be seen that while the energy of the A_2 transition goes down with respect to the energy of the E transition the energy of the latter will also decrease since it occurs, in part, from vacancies on (e) orbitals. The decrease in energy of both transitions explains the fact that despite shorter metal-ligand bonds, the observed spectra for these complexes occur at about the same energy as the spectra of complexes with saturated chelates.

The ionic model of Piper and Karipides (19) and later the more elaborate molecular orbital model by Karipides and Piper (21) make very similar predictions. Both models attribute the optical activity solely to the configuration of the ligating atoms around the metal.

According to these two models a polar compression, where the angle π is larger than the octahedral value of 54.74°, gives an A_2 transition at higher energy and an E_a transition at low energy, $(\nu_E - \nu_A) < 0$. For a complex of Δ configuration and azimuthal expansion, and also for the Λ enantiomer with azimuthal contraction, $\hat{\tau}$ less than 60°, the A_2 component should have a positive rotation while the E_a component should be negative. The two transitions, A_2 and E_a, are predicted to have equal magnitudes and therefore no net rotation results.

The above predictions about $(\nu_E - \nu_A) < 0$ are not in agreement with experimental results for complexes with

π-bonding perpendicular to the chelate rings. The predictions about the signs of rotation of the A_2 and E_a components agree with data for some complexes with saturated chelates. The predictions of the effects of azimuthal distortion could not be tested for complexes with saturated chelates, because none are yet known to have azimuthal expansions. For complexes with unsaturated chelates, the predicted effect of azimuthal distortion does not agree with experimental data for the only available compounds with azimuthal expansion, $Co(Acac)_3$ and $Cr(Acac)_3$.

The molecular orbital model of Liehr (22) allows for σ and π bond contributions in calculating rotational strengths. However since no calculated values for rotational strengths are available for complexes with unsaturated chelates no quantitative comparison can be made. Liehr's model, attributes the optical activity entirely to the angle of orbital mismatch, which is a purely configurational effect of the ligating atoms around the metal.

Qualitatively, this model predicts that the signs of the rotational strengths for the A_2 and E_a components depend upon the chirality of the molecule and upon the sign of the angle of cant, $\hat{\lambda}obs-\hat{\lambda}calc$. The angle of cant, $\hat{\lambda}obs-\hat{\lambda}calc$, has the same sign for the biguanide and the 2, 4-pentanedione complexes. Moreover, for the above complexes with Λ configurations, the CD spectra show a negative $A_1 \rightarrow A_2$ band at lower energy and a positive $A_1 \rightarrow E_a$ band at higher energy,

irrespective of the sign or magnitude of the azimuthal or polar distortions for the cases hitherto observed. For the above complexes it was assumed that the value of $\hat{\lambda}$calc is 120° as in sp^2 hybridization.

For oxalato and malonato complexes, estimation of the value of $\hat{\lambda}$calc is not straight forward, because it depends on the orbital hybridization on the oxygen atoms. It may be possible to infer the values for $\hat{\lambda}$calc from accurate values of the C-O bond lengths. The present values however are not very reliable.

In general it is observed that the absorption and CD spectra are shifted to lower energy, (red shift), when the metal-ligand-carbon angle, $\hat{\lambda}$, is distorted from the expected value. This angle is expected to be 109° 28′ (109.47°), for complexes with no π-bonding on the chelate rings. When π-bonding is present the expected value of $\hat{\lambda}$ is 120°, assuming sp^2 hybridization. The spectra of $Co(tn)_3^{3+}$ and $Co(Bgd)_3$ are examples of the effects of the distortion of $\hat{\lambda}$.

Finally the computed value of the angle of orbital mismatch for the biguanide and the 2, 4-pentanedione complexes is about 10°. This value is a little smaller than the general value proposed by Liehr to explain the magnitude of rotatory strengths. No rotational strengths for the crystalline samples could be determined, therefore no quantitative evaluation of the Liehr model can be made regarding rotational strengths.

Further evidence for appreciable electronic distortion is given in the data of Table 33. The quadrupole coupling constant obtained from broad line ^{59}Co n.m.r., e^2Qq/h, and the energy separations, $\nu_E - \nu_A$, are due to ground-state electronic distortions from octahedral symmetry. The first three values are from CD spectra while the last three values in Table 33 are for plane-polarized single crystal spectra. The last three values are probably of the same order of magnitude as the energy separations obtainable from completely resolved components of solid state CD spectra. The general trend observed in Table 33 is that the two data sets increase in going from top to bottom. This data set indicates an increasing trend of electronic distortion from octahedral symmetry in the ground states.

Table 33. Quadrupole Coupling Constants and Energy Separations for Solid Samples of Complexes.

Compound	e^2Qq/h	Ref.	$\nu_E - \nu_A$	Ref.
$\Lambda[Co(en)_3Cl_3]_2 \cdot NaCl \cdot 6H_2O$	4.1	(110)	-.22	(12)
$\Lambda Co(en)_3Cl_3 \cdot 3H_2O$	3.3	(110)	-.23	(12)
$\Lambda Co(d,pn)_3Cl_3$	4.79	(110)	-.38	(12)
$Co(Acac)_3$	7.8	(110)	+.80	(This work)
$\Lambda Co(HBgd)_3Br_3 \cdot H_2O$	9.4	(116)	+.66	(This work)
$Co(Bgd)_3 \cdot 2H_2O$	13.3	(116)	+.73	(This work)

The model of McCaffery and Mason (24) suggests that the dipole and rotational strengths for transition metal complexes, in the region of d-d´ transitions, is acquired by interaction with the allowed U.V. transitions. This model makes no reference to whether the optical activity originates from conformational or configurational effects. The U.V. transitions are assumed to be charge transfer or ligand transitions with electric moments perpendicular to the planes of the chelate rings. The organic chromophores on the unsaturated chelate rings have intense transitions, in the near U.V., that are very close to the metal d-d´ transitions. The fact that complexes of biguanide and 2, 4-pentanedione have large dipole and rotational strengths lends support to the McCaffery and Mason arguments. Hidaka and Douglas (107) and, later, Butler and Snow (88) have pointed out that the "intensities" or "rotational strength" of the E transitions were enhanced for the CD spectra of complexes with π-bonding on their chelates. The result of this investigation indicate that, in general, all intensities are enhanced for such complexes.

McCaffery and Mason (24) suggest that a complex would have a Λ configuration if its E_a transition has a positive sign, like $\Lambda Co(en)_3^{3+}$. This is in agreement with the results obtained in this work for $\Lambda Co(C_2N_5H_7)_3^{3+}$, $\Lambda Co(C_2N_5H_6)_3$ and $\Delta Co(C_5H_7O_2)_3$. However the above suggestions do not ease the problem of having to assign the E_a transition, for every

complex, by single crystal spectra. If the absolute configuration were known from x-ray crystallography then, for the Λ enantiomer, the positively rotating transition would be the E_a. As mentioned above, this prediction is in agreement with experimental findings.

The McCaffery and Mason model places no restriction on geometric and electronic distortions. This seems to be in agreement with all cases hitherto known for complexes with unsaturated chelates. For complexes with saturated chelates, polar elongation or azimuthal expansion may cause disagreement with the latter prediction. However no complex with saturated chelates and $\hat{\psi} = (90°-\hat{\delta})$ value smaller than 54.74° is yet known.

The very recent theoretical work of Mason and Seal (26) retains the idea of d-d´ spectral interaction with nearby U.V. transitions. In the new model two sources of optical activity are suggested. Conformational optical activity is attributed to the chiral puckering of the chelate rings whereas configurational optical activity is derived from the screw dissymmetry of the entire complex molecule or ion.

The chelate rings for complexes with unsaturated ligands have been shown to have shallow boat forms. Since the boat-forms possess a central plane of symmetry, and therefore lack chirality, there will be no conformational contribution to the optical activity of such complexes with

unsaturated chelates.

Mason and Seal calculate the first order configurational contribution for the A_2 and the E_a transitions of $Co(en)_3^{3+}$. The calculated value, 42 x 10^{-40} cgs, for the E_a transition is close to the experimental value, 53 x 10^{-40} cgs. However the calculated value for the A_2 transition, -43 x 10^{-40} cgs, is almost equal and opposite in sign. The net result of the first order calculation for configurational contribution is almost zero.

The Mason and Seal model however cannot be discounted due to the results for one complex only, $Co(en)_3^{3+}$. Besides the angle λ, Co-N-C, for this complex (108.4°) is very near to the sp^3 value, (109.46°). This complex therefore may be a very special "unfortunate" case where the main contribution to the optical activity is due to the chiral puckering of the chelate rings. The Mason and Seal treatment however does not mention any effect of the special value of the angle λ.

When discussing the optical activity of $\Lambda Co(tn)_3^{3+}$ Mason and Seal remark that the CH_2 and NH_2 groups nearest to the metal have positive contributions to the rotatory strengths for the E_a transition when the coordination angle, β, is smaller than 90°. When the latter angle is larger than 90° the contribution of the CH_2 group stays positive while the NH_2 contribution becomes negative.

The size of the angle β may have a significant effect on the contributions of the NH_2 and CH_2 groups for

complexes with saturated chelates, where the CH_2 and NH_2 groups are far from planarity. For the available complexes with unsaturated planar chelates such effects of the angle β could not be noticed. The values of the angle β for $Co(C_5H_7O_2)_3$ and $\Lambda Co(C_2N_5H_7)_3Br_3 \cdot H_2O$ are 96.55 and 89.91 respectively. The CD spectra for the Λ isomers of these two complexes give a negative A_2 component at low energy and a positive E_a component at higher energy.

The model gives good quantitative rotational strengths for several complexes, in agreement with solid state CD spectra having properly resolved A_2 and E_a components. It would be desirable to see what values the model predicts for complexes with unsaturated chelates, but no such computations were made by the authors.

Finally the model uses several experimental values and empirical parameters. Whereas some experimental data may always be needed for a theoretical model, a multitude of such parameters can lead to a loss of generality.

CHAPTER VI

CONCLUSIONS

In this work the structures and absolute configurations of two complexes were presented along with detailed solution and single crystal spectra. Two comprehensive sets of structural and spectral data were included for reference and discussion. A new dihedral angle ψ is defined that describes the "pitch" of a tris-bidentate; considered as a three-blade propeller or helix. All complexes except $Co(Acac)_3$ and $Cr(Acac)_3$ are found to have a pitch angle $\psi > 54.74°$. The description of the distortion from octahedral symmetry by $\hat{\psi}$ seems to aid in correlations of structural distortion to CD spectra.

Absorption and CD spectra for all complexes with N-ligands, (and with O-ligands when comparison is possible) shift to lower energy when the angles λ at the ligating atoms are distorted. Nevertheless the six ligating atoms may be still very close to octahedral positions.

The shortening of the Co-N (or Co-O) bonds for complexes with π-bonded chelates is accompanied by distortions of the angles at the ligated atoms, but no increase in the energy, ν, is observed for their transitions. However the rotational and dipole strengths are much larger for these complexes than for compounds with saturated chelates. All

the complexes, with saturated chelates, presently available have $\hat{\psi} > 54.74°$. All such complexes with the same absolute configuration show the same pattern of CD spectra, a positive band at lower energy followed by a negative band at higher energy for the Λ configurations. Complexes with unsaturated chelates give CD spectra with a reversed order, a negative band at lower energy followed by a positive band at higher energy for the Λ enantiomer.

A qualitative explanation was offered for the reversal of the pattern of CD spectra. The highest occupied π-electron (e) orbital of the ensemble of three chelates interacts with the (e) orbital, derived from the octahedral (t_{2g}) of the metal. The consequence of this interaction is to raise the energy of the (e) orbital of the metal, relative to the (a) orbital. Since the A_2 transition of the metal results from electrons promoted, exclusively, out of an (e) orbital; the energy of the A_2 transition is decreased relative to the energy of the E transition.

The ionic model of Piper and Karipides (19) and the more elaborate M.O. model of Karipides and Piper (21) give reasonable values for the rotational strengths of the components of the CD spectra for the oxalates. These oxalates resemble the complexes with biguanide and 2,4-pentanedione, by having π-electrons perpendicular to the planes of the chelate rings. However the reversal of the sign of $(\nu_E - \nu_A)$ is not observed, for complexes with

unsaturated chelates, when the angle β becomes larger than 90°, when the angle π becomes smaller than 54.74° or when the azimuthal angle τ passes through 60° and changes sign.

The molecular orbital model of Liehr (22) attributes the optical activity to an electronic distortion or bond mismatch. This model resolves the angle of mismatch into σ , π and $\bar{\pi}_j$ components. It treats the effects of all the σ and π-bonding in a unified manner. The predicted dependence of the sign of rotation on the chirality is generally true but the change of the sign of rotation, when the angle of cant goes through zero to negative, could not be tested for complexes with unsaturated chelates.

The observed values for mismatched bond angles are in agreement with the proposed value of the angle of cant deemed necessary to produce the observed optical activity.

The model of McCaffery and Mason (24) makes an assumption that is particularly useful for complexes with unsaturated chelates. It attributes the d-electron optical activity of transition metals to the interaction with the nearby allowed U.V. transitions. The larger dipole and rotational strengths of such complexes support the McCaffery and Mason suggestion. Their prediction, of the same absolute configuration as $\Lambda Co(en)_3^{3+}$ for complexes with the same sign of E_a as for $\Lambda Co(en)_3^{3+}$, is in agreement with experimental results for the biguanide and 2,4-pentanedione complexes. However no complexes with saturated

chelates and a small pitch angle, $\psi \ll 54.74°$, are yet available to test this model. Neither are complexes, with unsaturated chelates, available that have a very large pitch angle, $\psi \gg 54.74°$.

The McCaffery and Mason model makes no prediction about the relative energies of the A_2 and E_a transitions or the dependence of the sign of $(\nu_E - \nu_A)$ on the geometric or electronic distortions of the complex.

The recent model of Mason and Seal (26), which gave good quantitative predictions for the rotational strengths of some complexes with saturated chelates, is applicable to complexes with unsaturated chelates. The model attributes one source of optical activity to the configurational screw dissymmetry of tris-bidentate molecules. However the example, $\Lambda Co(en)_3^{3+}$, given by the authors for the configurational contribution to the optical activity may be a special "unfortunate choice" that has little contribution to its optical activity from the screw dissymmetry. The applicability of the Mason and Seal model to the complexes of Co (III) with biguanide and with 2,4-pentanedione could not be assessed.

No evaluation of the quantitative predictions of any of the above models could be performed either, as none of those models make any such predictions for complexes of biguanide or 2,4-pentanedione.

Quantitative data for dipole and rotational strengths

of some complexes, in solution, were given in this work. However comparison of solution spectra with theoretical predictions is very difficult. The difficulty arises because theoretical models use geometric data, from the solids, to build their assumptions. Those parameters for the solids may be at variance with the parameters for complexes in solution. Besides the resolution of spectral bands for solutions, as performed by Gaussian analysis, may not be sufficiently accurate due to the severe overlap of those CD bands. The more realistic approach used by Kuroda and Saito (12) is preferred. Their method involves the assignment of the position and intensity of the E_a component from single crystal spectra of a uniaxial crystal. The magnitude and the position of the A_2 component is then obtained by subtracting 2/3 of the E_a component from the CD spectrum of the powdered material in a KBr matrix. The method requires great care to obtain quantitatively valid data.

The above method is very difficult to apply, particularly quantitatively, to biaxial crystals. The materials investigated in this work all form biaxial crystals. The great tedium in obtaining quantitative single crystal CD spectra for biaxial crystals may be reduced by rotating (spinning) the crystal around an axis collinear with the direction of light propagation (117). If special precautions are taken, two CD spectra may be obtained, at optimum

crystal orientations, and can be used to compute the resolved, (pure), A_2 and E_a components quantitatively. The methods of computing the pure A_2 and E_a spectral components would be similar to the methods used in Chapter IV of this thesis for analyzing plane-polarized single crystal spectra.

When such methods are developed and refined enough to obtain accurate quantitative CD spectra, the true magnitudes of the A and E components may be evaluated. Only then can meaningful quantitative comparisons be made with the predictions of any theoretical model.

It is necessary to measure the CD spectra of complexes having all four types of azimuthal and pitch distortions, $\hat{\tau}$ and $\hat{\psi}$ respectively, so that the theoretical correlations between spectra and structures can be properly made. Until the present time, complexes with saturated chelates and pitch angle, ψ, less than 54.74° have not been reported. The following chelating agents represented in Figure 53, may be helpful in producing complexes with various types of distortions. Thus (1) and (2) may be suitable for producing complexes with polar compression and a small pitch angle, while (3) should produce the opposite types of distortions. Chelating agents (4) and (5) would produce the same effects as (1), (2) and (3) respectively, but with π-bonding on the ligating atoms.

The study of complexes with the extremes of geometric and electronic distortions is necessary for the critical

evaluation of the theoretical models of optical activity.

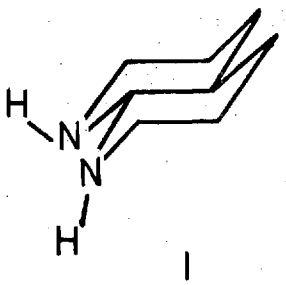

1

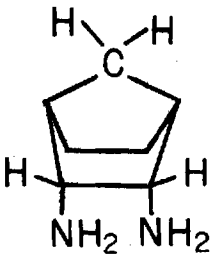

2

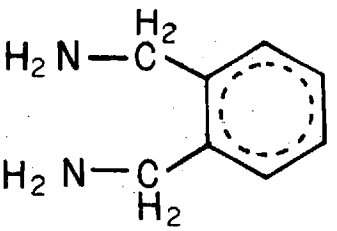

3

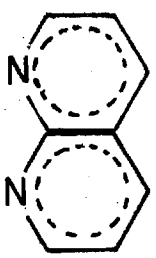

4

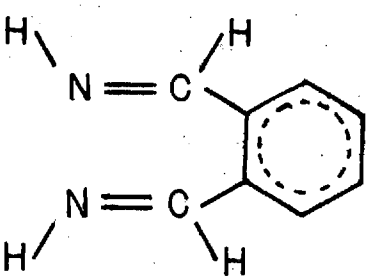

5

Figure 53. Chelating Agents That May Produce Complexes with Large Distortions from O_h Symmetry.

LIST OF REFERENCES*

1. J. B. Biot, Mem. Inst. 1, 1, (1812).

2. A. Werner, Ber. 44, 1887 (1911).

3. A. Cotton, Compt. Rend. 120, 989 and 1044 (1895).

4. G. N. Ramachandran and S. Ramaseshan, Encyclopedia of Physics (Handbuch der Physik)), S. Flugge, Editor, Volume XXV, Part 1, pp. 82-85, Springer-Verlag, Berlin (1961).

5. R. Strickland and F. S. Richardson, J. Chem. Phys. 57, 589 (1972).

6. B. Bosnich, Fundamental Aspects and Recent Developments in Optical Rotary Dispersion and Circular Dichroism. (Ciardelli and Salvadori, editors), Heyden and Son Ltd., London, p. 254, 1973 (Hereafter cited as Fundamental Aspects - O.R.D., C.D.).

7. B. Briat, Fundamental Aspects-O.R.D., C.D., p. 375. P. N. Schatz and A. M. McCaffery, Quart. Rev., Chem. Soc. (London), 23, 552 (1969).

8. P. Salvadori and F. Ciardelli, Fundamental Aspects-O.R.D., C.D., p. 3.

9. S. F. Mason, Fundamental Aspects-O.R.D., C.D., p. 27.

10. S. F. Mason, Fundamental Aspects-O.R.D., C.D., p. 196.

11. S. F. Mason, Quart. Rev. 17, 20 (1963).

12. R. Kuroda and Y. Saito, Bull. Chem. Soc., Japan 49, 433 (1976).

13. E. U. Condon, Rev. Mod. Phys. 9, 432 (1937).

14. W. Moffit, J. Chem. Phys. 25, 1189 (1956).

15. W. C. Hamilton, Acta Cryst. 18, 502 (1965).

16. J. M. Bijvoet, A. F. Peederman and A. J. van Bommel, Nature 168, 271 (1951).

*Journal title abbreviations used are listed in "List of Periodicals" Chemical Abstracts, 1961.

17. Y. Saito, K. Nakatsu, M. Shiro and H. Kuroya, Acta Cryst. 8, 729 (1955).

18. Y. Saito, Coord. Chem. Rev. 13, 305 (1974).

19. T. S. Piper and A. Karipides, Mol. Phys. 5, 475 (1962).

20. S. Sugano, J. Chem. Phys. 33, 1883 (1960).

21. A. G. Karipides and T. S. Piper, J. Chem. Phys. 40, 674 (1964).

22. A. D. Liehr, J. Phys. Chem. 68, 665 (1964).

23. R. W. Strickland and F. S. Richardson, Inorg. Chem. 12, 1025 (1973).

24. A. J. McCaffery and S. F. Mason, Mol. Phys. 6, 359 (1963).

25. F. S. Richardson, J. Phys. Chem. 75, 692 (1971).

26. S. F. Mason and R. H. Seal, Mol. Phys. 31, 755 (1976).

27. D. Karipides and W. Conrad Fernelius, Inorganic Synthesis Vol. VIII, p. 56, Jacob Kleinberg, Editor in Chief, McGraw Hill, N. Y. (1963).

28. P. Ray and N. K. Dutt, J. Indian Chem. Soc. 16, 621 (1939).

29. P. Ray and N. K. Dutt, J. Indian Chem. Soc. 18, 289 (1941).

30. M. R. Snow, Acta Cryst. B30, 1850 (1974).

31. B. E. Bryant and W. Conrad Fernelius, Inorganic Synthesis, Vol. V, p. 188, Therald Moeller, Editor in Chief, McGraw Hill, N. Y. (1957).

32. J. P. Collman, R. P. Blair, A. L. Slade and R. L. Marshall, Chem. Ind. (London) 141 (1962).

33. R. C. Fay, A. Y. Girgis and U. Klabunde, J. Amer. Chem. Soc. 92, 7056 (1970).

34. Jui-Yuan Sun (J. P. Collman, Supervisor), Ph. D., University of North Carolina at Chapel Hill (1967). From Diss. Abs. B28, 4482 (1968).

35. R. B. Von Dreele and R. C. Fay, J. Amer. Chem. Soc. 93, 4936 (1971).

36. International Tables for X-Ray Crystallography, Vol. 1, pp. 78, 79, Kynoch Press, Birmingham, England (1965).

37. P. K. Hon, Ph. D. Dissertation, University of Illinois (1964) from University Microfilms, Ann Arbor, Michigan. Also, P. K. Hon and C. E. Pfluger, J. Coord. Chem. 3, 67 (1973).

38. G. J. Kruger and E. C. Reynhardt, Acta Cryst. B30, 822 (1974).

39. International Tables for X-Ray Crystallography, Vol. 1, p. 99, Kynoch Press, Birmingham, England (1965).

40. U. W. Arndt and B. T. M. Willis, Single Crystal Diffractometry, pp. 243-244, Cambridge University Press, (1966).

41. D. T. Cromer and J. T. Waber, Acta Cryst. 18, 104 (1965).

42. D. T. Cromer, Acta Cryst. 18, 17 (1965).

43. R. F. Stewart, E. R. Davidson and W. T. Simpson, J. Chem. Phys. 42, 3175 (1965).

44. International Tables for X-Ray Crystallography, Vol. III, p. 157, Kynoch Press, Birmingham, England (1965).

45. J. M. Stewart, G. J. Kruger, H. L. Ammon, C. Dickinson and S. R. Hall, X-Ray 70, University of Maryland (1972).

46. International Tables for X-Ray Crystallography, Vol. I, p. 106, Kynoch Press, Birmingham, England (1965).

47. F. Carter, "Master Card Program for the Picker Four Angle Programmer," Picker Instruments, Cleveland, Ohio (1967).

48. J. A. Bertrand, Fortran Program for Calculating Lorentz and Polarization Corrections, Georgia Institute of Technology (1969).

49. A. Zalkin, Fortran Fourier Analysis Program, (FORDAP).

50. W. R. Busing, K. O. Martin and H. A. Levy, FORTRAN Crystallographic Least Squares Program, XFLS (and modified version ORFLS), Oak Ridge National Laboratories.

51. W. R. Busing, K. O. Martin and H. A. Levy, FORTRAN Functions and Errors Program ORFFE, Oak Ridge National Laboratories (1965).

52. C. K. Johnson, A FORTRAN-Ellipsoid Plot Program for Crystal Structure Illustrations (1965).

53. J. A. Kelley, Ph. D. Thesis, Georgia Institute of Technology (1970).

54. E. I. Stiefel and G. F. Brown, Inorg. Chem. 11, 434, (1972).

55. K. R. Dymock and G. J. Palenik, Inorg. Chem. 14, 1220 (1975).

56. A. Avdeef and J. P. Fackler, Jr., Inorg. Chem. 14, 2002, (1975).

57. W. Moffit and A. Moscowitz, J. Chem. Phys. 30, 648 (1959).

58. K. Michelsen, Acta Chem. Scand. 19, 1175 (1965).

59. K. Igi, T. Yasui, J. Hidaka and Y. Shimura, Bull. Chem. Soc., Japan 44, 426 (1971).

60. V. H. Shievelbein, Ph. D. Thesis, Georgia Institute of Technology (1969).

61. I. Jonáš and B. Nordén, Inorg. Nucl. Chem. Letters 12, 43 (1976).

62. B. W. McClelland, Acta Cryst. B31, 2946 (1975).

63. T. S. Piper, J. Chem. Phys. 35, 1240 (1961).

64. Tables of Interatomic Distances and Configurations in Molecules and Ions, The Chemical Society, London, Burlington House, W.1. (1958).

65. M. Iwata and Y. Saito, Acta Cryst. B29, 822 (1973).

66. L. Coghi, M. Nardelli and G. Pelizzi, Acta Cryst. B32, 842 (1976).

67. R. J. Gillespie and R. S. Nyholm, Quart. Rev. Chem. Soc. (London) 11, 339 (1957).

68. B. Morosin, Acta Cryst. 19, 131 (1965).

69. A. J. McCaffery, S. F. Mason and R. E. Ballard, J. Chem. Soc. (London) 2883 (1965).

70. T. S. Piper and R. L. Carlin, J. Chem. Phys. 36, 3330 (1962).

71. D. Caliga and F. S. Richardson, Mol. Phys. 28, 1145 (1974).

72. M. Iwata, K. Nakatzu and Y. Saito, Acta Cryst. B25, 2562 (1969).

73. R. Kuroda, N. Shimanouchi and Y. Saito, Acta Cryst. B31, 931 (1975).

74. R. Kuroda and Y. Saito, Acta Cryst. B30, 2126 (1974).

75. A. Kobayashi, F. Marumo and Y. Saito, Acta Cryst. B28, 2709 (1972).

76. F. Marumo, Y. Utsumi and Y. Saito, Acta Cryst. B26, 1492 (1970).

77. M. Ito, F. Marumo and Y. Saito, Acta Cryst. B27, 2187 (1971).

78. R. Nagao , F. Marumo and Y. Saito, Acta Cryst. B29, 2438 (1973).

79. A. Kobayashi, F. Marumo and Y. Saito, Acta Cryst. B28, 3591 (1972).

80. A. Kobayashi, F. Marumo and Y. Saito, Acta Cryst. B29, 2443 (1973).

81. S. Sato and Y. Saito, Acta Cryst. B31, 1378 (1975).

82. K. R. Butler and M. R. Snow, J. Chem. Soc. (A) (London) 565 (1971).

83. K. N. Raymond and J. A. Ibers, Inorg. Chem. 7, 2333 (1968).

84. K. N. Raymond, P. W. R. Corfield and J. A. Ibers, Inorg. Chem. 7, 1362 (1968).

85. F. A. Jurnak and K. N. Raymond, Inorg. Chem. 13, 2387 (1974).

86. K. N. Raymond, S. S. Isied, L. D. Brown, F. R. Fronczek and J. H. Nibert, J. Amer. Chem. Soc. 98, 1767 (1976).

87. J. N. van Niekerk and F. R. L. Schoening, Acta Cryst. 5, 499 (1952).

88. K. R. Butler and M. R. Snow, Inorg. Nucl. Chem. Lett. 8, 541 (1972).

89. W. D. W. Horrocks, Jr., D. L. Johnston and D. MacInnes, J. Amer. Chem. Soc. 92, 7620 (1970).

90. R. E. Ballard, A. J. McCaffery and S. F. Mason, Proc. Chem. Soc. (London) 331 (1962).

91. K. Ogino, K. Murano and J. Fujita, Inorg. Nucl. Chem. Lett. 4, 351 (1968).

92. S. E. Harnung, B. S. Sørensen, I. Creaser, H. Maegaard, U. Pfenninger and C. E. Schäffer, Inorg. Chem. 15, 2123 (1976)

93. T. S. Piper and A. G. Karipides, J. Amer. Chem. Soc. 86, 5039 (1964).

94. M. Ito, F. Marumo and Y. Saito, Inorg. Nucl. Chem. Lett. 6, 519 (1970).

95. H. Toftlund and E. Pedersen, Acta Chem. Scand. 26, 4019 (1972).

96. F. Mizukami, H. Ito, J. Fujita and K. Saito, Bull. Chem. Soc. Japan 43, 3973 (1970).

97. F. Mizukami , H. Ito, J. Fujita and K. Saito, Bull. Chem. Soc. Japan 45, 2129 (1971).

98. J. Fujita and H. Ogino, Chem. Lett. (Japan) 57 (1974).

99. S. Sato, Y. Saito, J. Fujita and H. Ogino, Inorg. Nucl. Chem. Lett. , 10, 669 (1974).

100. T. S. Piper and R. L. Carlin, J. Chem. Phys. 33, 608 (1960).

101. T. S. Piper and R. L. Carlin, J. Chem. Phys. 35, 1809 (1961).

102. R. M. King and G. W. Everett, Jr., Inorg. Chem. 10, 1237 (1971).

103. F. Woldbye, Rec. Chem. Prog. 24, 197 (1963).

104. P. G. Beddoe and S. F. Mason, Inorg. Nucl. Chem. Lett., 4, 433 (1968).

105. G. R. Brubaker and L. E. Webb, J. Amer. Chem. Soc. 91, 7199 (1969).

106. K. R. Butler and M. R. Snow, Chem. Comm. 550 (1971).

107. J. Hidaka and B. E. Douglass, Inorg. Chem. 3, 1724 (1964).

108. S. S. Isied, G. Kuo and K. N. Raymond, J. Amer. Chem. Soc. 98, 1763 (1976).

109. S. Yamada and R. Tsuchida, Bull. Chem. Soc. Japan 33, 98 (1960).

110. R. R. Judkins and D. J. Royer, Inorg. Chem. 13, 945 (1974).

111. J. R. Gollogly and C. J. Hawkins, Chem. Comm. 689 (1968).

112. P. G. Beddoe, M. J. Harding, S. F. Mason and B. G. Peart, Chem. Comm. 1283 (1971).

113. K. R. Butler and M. R. Snow, Inorg. Chem. 10, 1838 (1971).

114. R. C. Bingham, M. J. S. Dewar and D. H. Lo, J. Amer. Chem. Soc. 97, 1285 (1975).

115. F. P. Dwyer and A. M. Sargeson, J. Amer. Chem. Soc. 81, 2335 (1959)

116. D. J. Royer, Private Communications.

117. D. J. Royer, Private Communications.

VITA

Nadim C. Moucharafieh was born on July 10, 1943, in Beirut, Lebanon, the son of Chamel H. and Najla Kaid-Bey Moucharafieh. He attended high school in Souk-el-Gharb, Lebanon and graduated in June, 1961. During 1961-62, he attended International College in Beirut, Lebanon.

He enrolled at the American University of Beirut, where he received his B. S. in Chemistry, in June 1966 and his M. S. in February 1969. During his last year as an undergraduate he taught mathematics and chemistry for high school, in Beirut; in 1967-68 he was a research assistant and teaching assistant in Chemistry at the American University of Beirut, in Beirut, Lebanon.

He came to the Georgia Institute of Technology in the winter of 1969. His research work in inorganic chemistry was done under the directorship of Dr. D. J. Royer. During part of his stay at Georgia Tech, he was supported by a graduate teaching assistantship in the School of Chemistry.